



UNIVERSITAT DE  
BARCELONA

## Coordination, organometallic and supramolecular chemistry approaches to the design of metal-based cytotoxic agents

Rosa Maria Faustino Brissos

**ADVERTIMENT.** La consulta d'aquesta tesi queda condicionada a l'acceptació de les següents condicions d'ús: La difusió d'aquesta tesi per mitjà del servei TDX ([www.tdx.cat](http://www.tdx.cat)) i a través del Dipòsit Digital de la UB ([diposit.ub.edu](http://diposit.ub.edu)) ha estat autoritzada pels titulars dels drets de propietat intel·lectual únicament per a usos privats emmarcats en activitats d'investigació i docència. No s'autoritza la seva reproducció amb finalitats de lucre ni la seva difusió i posada a disposició des d'un lloc aliè al servei TDX ni al Dipòsit Digital de la UB. No s'autoritza la presentació del seu contingut en una finestra o marc aliè a TDX o al Dipòsit Digital de la UB (framing). Aquesta reserva de drets afecta tant al resum de presentació de la tesi com als seus continguts. En la utilització o cita de parts de la tesi és obligat indicar el nom de la persona autora.

**ADVERTENCIA.** La consulta de esta tesis queda condicionada a la aceptación de las siguientes condiciones de uso: La difusión de esta tesis por medio del servicio TDR ([www.tdx.cat](http://www.tdx.cat)) y a través del Repositorio Digital de la UB ([diposit.ub.edu](http://diposit.ub.edu)) ha sido autorizada por los titulares de los derechos de propiedad intelectual únicamente para usos privados enmarcados en actividades de investigación y docencia. No se autoriza su reproducción con finalidades de lucro ni su difusión y puesta a disposición desde un sitio ajeno al servicio TDR o al Repositorio Digital de la UB. No se autoriza la presentación de su contenido en una ventana o marco ajeno a TDR o al Repositorio Digital de la UB (framing). Esta reserva de derechos afecta tanto al resumen de presentación de la tesis como a sus contenidos. En la utilización o cita de partes de la tesis es obligado indicar el nombre de la persona autora.

**WARNING.** On having consulted this thesis you're accepting the following use conditions: Spreading this thesis by the TDX ([www.tdx.cat](http://www.tdx.cat)) service and by the UB Digital Repository ([diposit.ub.edu](http://diposit.ub.edu)) has been authorized by the titular of the intellectual property rights only for private uses placed in investigation and teaching activities. Reproduction with lucrative aims is not authorized nor its spreading and availability from a site foreign to the TDX service or to the UB Digital Repository. Introducing its content in a window or frame foreign to the TDX service or to the UB Digital Repository is not authorized (framing). Those rights affect to the presentation summary of the thesis as well as to its contents. In the using or citation of parts of the thesis it's obliged to indicate the name of the author.



# UNIVERSITAT DE BARCELONA

Facultat de Química

Departament de Química Inorgànica i Orgànica, Secció de Química Inorgànica

Programa de doctorat en Química Orgànica a la línia de recerca Química biològica i química mèdica

## **Coordination, organometallic and supramolecular chemistry approaches to the design of metal-based cytotoxic agents**

---

**Rosa Maria Faustino Brissos**

2018

Group de Química Bioinorgànica

---

Prof. Patrick Gamez Enamorado

Director i Tutor



Patrick Gamez Enamorado, investigador ICREA Senior i professor associat del Departamento de Química Inorgànica y Orgànica, Secció de Química Inorgànica, de la Universitat de Barcelona,

CERTIFICO que el treball “Coordination, organometallic and supramolecular chemistry approaches to the design of metal-based cytotoxic agents”, que presenta Rosa Maria Faustino Brissos per optar al grau de Doctor, ha estat realitzat sota la meva direcció al Departamento de Química Inorgànica y Orgànica, Secció de Química Inorgànica, de la Universitat de Barcelona.

Barcelona, Febrer de 2018

---

Patrick Gamez Enamorado



"The best scientist is open to experience and begins with romance - the idea  
that anything is possible." ~ Ray Bradbury



*This thesis is dedicated to my family for their constant support and  
unconditional love,  
Obrigada meu Pai, minha mãe e minha irmã.*



# Acknowledgements

---

First, I would like to thank my supervisor Professor Patrick Gamez for the opportunity he has given me. I am grateful for his support and guidance. He gave me the chance, not only to be part of his group and to work on so many interesting projects, but also to be introduced to so many incredible people. This unbelievable experience has been extraordinary, helped me to improve my scientific background, and stimulated my personal growth. Dr. Patrick Gamez was the catalyst of all those changes; he was not “just” my supervisor, he was also someone who taught me valuable lessons and I am profoundly grateful for his patience, guidance and encouragement during this long journey.

I would also like to thank Dr. Guillem Aromí, Dr. Leoní Barrios, Dr. David Aguilá and Dr. Darawsheh for their advice and guidance, and for providing some of the helicates used in this thesis.

I would also like to thank Dr. Olivier Roubeau for the resolution of the crystallographic structures of my precious helicates and Dr. Pau Clavero, Dr. Arnald Grabulosa, and Dr. Guillermo Muller for the series of ruthenium complexes used in this thesis.

I could not forget the technicians who helped me and answered to all my “burning” questions and listened to my crazy ideas, Jordi Diaz and Gerard Oncins (AFM).

I would like to thank Dr. Ricardo Pérez Tomás for providing the research facilities to perform the cell studies and for his guidance. I also would like to thank Dr. Vanessa Soto Cerrato for her valuable advices and for treating me not as a chemist, but as a fellow scientist, one of the group’s students and as part of the Bio family.

As Feynman said, “Study hard what interests you the most in the most undisciplined, irreverent and original manner possible”. This quote always reminds me of the person responsible for my unconditional love for biochemistry and science in general, Professor Aureliano Alves; he inspired me to be curious and made me want to achieve more, be a better scientist and work harder. For that I am grateful!

To Professor Jorge Martins, thank you for being such inspiration you showed me that great scientist can be inspiring professor; and Professor Lídia Po Dionisio, much more than a teacher, a special friend. Someone who I admire and that always was there for me, despite the distance!

As Simon Sinek said, ‘Life is beautiful not because of the things we see or do. Life is beautiful because of the people we meet’ and Barcelona made my life incredible! I could not finish this chapter of my life without thanking the ones from whom I learned a lot and that made me feel home, safe and happy.

Ana Belén Caballero, I am incredibly grateful for all the advices and the support even when I least deserved but most needed. Thank you for being a role model and for inspiring me every day!

Luís Korrodi, my mini boss, I am so grateful to have met you and worked side by side with such an amazing scientist. You were the spark I needed in that hard moment, thank you

for the amazing scientific discussions, for pushing me to be better, to relentlessly question everything and for trusting in me. Most of all, thank you for accepting me as your peer and for all your advices and every nugget of wisdom you shared with me.

To my three sisters, the ones that were my rocks, my safe place, my home, Beltzane, Cristina and Lesly, incredible human beings and bright scientists. Your beauty emanates from inside out. It is incredible how a person can transform our darker days with a hug, a smile or a kind word. ‘Thank you’ feels so small to express my gratitude and for all the things we have endured together.

A special thanks to every single member of this incredible inorganic family, Dr. Virtudes Moreno, Flavia, André, Alejandra, Esther and Ibis for the lessons and advices. To David, the humble and kindest; Gavin, the funny, sarcastic one; MJ and Leo, the amazing dancers; Ivana, the hardest worker with an incredible heart and SASKY, always shining bright like a diamond and setting pretty much everyone on fire.

A special thanks to my superhero Inorganic’s family, thank you for the days you brighten up and for every single Friday, we rocked together. To Alberten, the catalytic guy that made us laugh time and time again; Marta, the amazing mechanistic stressed girl, that made us fall in love with her step by step; Raulito, the young brother; Pau, the big brother who always made us laugh and gave the warmest hugs; El Patito loco, one of the craziest, clumsiest guy, who was here since the beginning. To my biofamily, my tikitikis, for treating me as one of their peers, for accepting me as part of the family, as one of their own. For having my back every step of the way, now and forever! Thank you, Pili, Ananda, Lesly, and David.

To my all of lab mates, a big thank you, I am so glad we have shared time together, you made me learn about so many things, from culture to science. I am really grateful to have met you, Tommy, Im, Ople, Silvia, Ester, Nassim, Annie, James, Niels; I feel blessed to have met you all. Moreover, to my last two old grumpy superheroes: Andreu, the incredibly intelligent grumpy man, so much potential in such a grumpy soul! And Guillermito, the shy intelligent guy that hide behind his pretty eyes, whom I constantly annoy with my theories, questions and stories; thank you for everything, I admire so much, lil’ brother!

I must also express my gratitude to my roommate, Ana for making all the bad moments bearable and the good ones memorable. Amazing 6 years of incredible discussions and enlightening conversations. Thank you for being my closest family here.

André Santos, o meu Mixinha; Marco Correia, o meu Yuppi, Patricia Ramos, my person, the first ones who believed I could do it. The ones that helped me during my hard student days, the best lab mates and the best people I could encountered. If I am here today, we must acknowledge them!

I would also thank FF, for all the support, for all the days you made me fight, despite my despair and for all the incredible scientific discussions.

I would like to acknowledge also my RB co-workers and friends who helped me to have a wonderful time outside science and inside the ‘real world’. Thank you for the last year, you made me smile on the darkest days and you taught me so many lessons.

I could not forget to thank all my “digital mentors” that broke me out of the matrix; my two sisters Annie and Charlie for believing in me and for helping me endure these last and excruciating miles and my MV and RATE tribe, thank you for inspiring me.

Last, but not least, I want to acknowledge the most important people in my life, my incredible family. Luis Brissos, my hero, my dad, my best friend. You always made sure I followed my dreams and you allowed me to become a better person and a better scientist. You made it possible and you made it happen. My mom, Rosa Brissos thank you for the unconditional love. You picked me up, every time I fell down, you lectured me when I made mistakes, but the most important thing, you gave me the best example of all. Your dreams reshaped my reality, you taught me how to fly and you gave me the opportunity to go on and explore the world. Thank you for the support, for the love even when least deserved it, when I was grumpy as hell, thank you for everything!

My baby sister, my shiny diamond. The amazing baby girl that turn out to be one of the incredible women I love and admire. Thank you for being always there for me, lecturing me when I make mistakes and helping me to handle all my blisters and bruises. I cannot thank you enough for being my home, my life, my hero. And a special thanks to Fabinho, a person who I admire and that was there for me every step of the way.

It is exactly as Aristotle once said, 'Pleasure in the job puts perfection in the work'. This is just the beginning of an incredible journey.



# List of publications

---

- (1) Brissos, R.; Ramos, D.; Lima, J. C.; Mihan, F. Y.; Borràs, M.; de Lapuente, J.; Cort, A. D.; Rodríguez, L. *New J. Chem.* **2013**, 37, 1046.
- (2) Brissos, R. F.; Caubet, A.; Gamez, P. *Eur. J. Inorg. Chem.* **2015**, 2015, 2633.
- (3) Brissos, R. F.; García, S.; Presa, A.; Gamez, P. *Comments Inorg. Chem.* **2011**, 32, 219.
- (4) Brissos, R. F.; Torrents, E.; dos Santos Mello, F. M.; Carvalho Pires, W.; Silveira-Lacerda Ede, P.; Caballero, A. B.; Caubet, A.; Massera, C.; Roubeau, O.; Teat, S. J.; Gamez, P. *Metallomics* **2014**, 6, 1853.
- (5) Gamba, I.; Salvado, I.; Brissos, R. F.; Gamez, P.; Brea, J.; Loza, M. I.; Vazquez, M. E.; Lopez, M. V. *Chem. Commun. (Camb.)* **2016**, 52, 1234.
- (6) Gamba, I.; Salvado, I.; Rama, G.; Bertazzon, M.; Sanchez, M. I.; Sanchez-Pedregal, V. M.; Martinez-Costas, J.; Brissos, R. F.; Gamez, P.; Mascarenas, J. L.; Vazquez Lopez, M.; Vazquez, M. E. *Chem. Eur. J.* **2013**, 19, 13369.
- (7) Garcia, S.; Cusco, C.; Brissos, R. F.; Torrents, E.; Caubet, A.; Gamez, P. *J. Inorg. Biochem.* **2012**, 116, 26.
- (8) Giannicchi, I.; Brissos, R.; Ramos, D.; de Lapuente, J.; Lima, J. C.; Dalla Cort, A.; Rodriguez, L. *Inorg. Chem.* **2013**, 52, 9245.
- (9) Grau, J.; Brissos, R. F.; Salinas-Uber, J.; Caballero, A. B.; Caubet, A.; Roubeau, O.; Korrodi-Gregorio, L.; Perez-Tomas, R.; Gamez, P. *Dalton Trans.* **2015**, 44, 16061.
- (10) Machado, I.; Fernández, M.; Becco, L.; Garat, B.; Brissos, R. F.; Zabarska, N.; Gamez, P.; Marques, F.; Correia, I.; Costa Pessoa, J.; Gambino, D. *Inorg. Chim. Acta* **2014**, 420, 39.
- (11) Meenongwa, A.; Brissos, R. F.; Soikum, C.; Chaveerach, P.; Gamez, P.; Trongpanich, Y.; Chaveerach, U. *New J. Chem.* **2015**, 39, 664.
- (12) Meenongwa, A.; Brissos, R. F.; Soikum, C.; Chaveerach, P.; Gamez, P.; Trongpanich, Y.; Chaveerach, U. *New J. Chem.* **2016**, 40, 5861.
- (13) Molas Saborit, J.; Caubet, A.; Brissos, R. F.; Korrodi-Gregorio, L.; Perez-Tomas, R.; Martinez, M.; Gamez, P. *Dalton Trans.* **2017**, 46, 11214.
- (14) Pratumwieng, R.; Meenongwa, A.; Brissos, R. F.; Gamez, P.; Trongpanich, Y.; Chaveerach, U. *Transition Met. Chem.* **2017**, 1.
- (15) Presa, A.; Brissos, R. F.; Caballero, A. B.; Borilovic, I.; Korrodi-Gregorio, L.; Perez-Tomas, R.; Roubeau, O.; Gamez, P. *Angew. Chem. Int. Ed. Engl.* **2015**, 54, 4561.



# Contents

---

## Contents

<b>ACKNOWLEDGEMENTS .....</b>	<b>IX</b>
<b>LIST OF PUBLICATIONS.....</b>	<b>XIII</b>
<b>CONTENTS .....</b>	<b>XV</b>
<b>ABBREVIATION LIST .....</b>	<b>XVII</b>
<b>ABSTRACT .....</b>	<b>XIX</b>
<b>INTRODUCTION .....</b>	<b>21</b>
HALLMARKS OF CANCER .....	2
AN OVERVIEW OF CHEMOTHERAPY – CANCER: WHEN CHEMISTRY FIGHTS BACK .....	4
<i>DNA as a molecular target</i> .....	5
<i>Metal complexes as cytotoxic agents</i> .....	12
FINAL REMARKS AND OBJECTIVES OF THIS THESIS .....	22
REFERENCES .....	23
<b>TARGETING CANCER WITH SMALL MOLECULES: COPPER COMPLEXES .....</b>	<b>29</b>
<i>Schiff bases</i> .....	32
SYNTHESIS .....	34
<i>Preparation of the ligands</i> .....	34
<i>General method for the preparation of the complexes</i> .....	36
DNA-BINDING STUDIES.....	51
<i>UV-Vis Spectroscopy</i> .....	51
<i>ESI-MS and EPR spectroscopy</i> .....	54
<i>Fluorescence-dye displacement</i> .....	56
<i>Agarose-gel electrophoresis</i> .....	60
<i>AFM experiments</i> .....	62
CELL-VIABILITY ASSAYS .....	63
<i>MTT Reduction Assay</i> .....	64
CONCLUSIONS .....	70
REFERENCES .....	72
<b>TARGETING CANCER WITH SMALL MOLECULES: RUTHENIUM COMPLEXES .....</b>	<b>79</b>
PRELIMINARY DNA-INTERACTION STUDIES.....	83
CELL-VIABILITY ASSAYS .....	83
<i>Single-point assays</i> .....	83
<i>MTT Reduction Assay</i> .....	91

<i>Cell migration – Wound-healing assay</i> .....	98
CONCLUSIONS .....	103
REFERENCES .....	104
<b>HELICES AND HELICATES – SUPRAMOLECULAR RATIONAL DESIGN .....</b>	<b>107</b>
SYNTHESIS .....	110
<i>Design of dinucleating organic ligands – Poly-<math>\beta</math>-diketones</i> .....	110
<i>General method for the preparation of the supramolecular complexes</i> .....	115
DNA-BINDING STUDIES.....	119
<i>UV-Vis Spectroscopy</i> .....	119
<i>Fluorescence-dye displacement</i> .....	121
<i>Circular Dichroism</i> .....	124
<i>Agarose-gel electrophoresis</i> .....	125
<i>Polyacrylamide-gel electrophoresis – DNA three-way junction binding</i> .....	126
<i>AFM experiments</i> .....	129
CELL-VIABILITY ASSAYS .....	131
<i>Single-point assays</i> .....	131
<i>MTT Reduction Assay</i> .....	132
<i>Fluorescence spectroscopy assays</i> .....	133
CONCLUSIONS .....	135
REFERENCES .....	137
<b>CONCLUSIONS .....</b>	<b>141</b>
<b>EXPERIMENTAL SECTION .....</b>	<b>CXLV</b>
MATERIALS AND METHODS .....	CXLVII
<i>Synthesis</i> .....	cxlvii
<i>DNA-binding studies</i> .....	cxlvii
<i>Cell Culture</i> .....	clx
CHAPTER I – COPPER COMPLEXES .....	CLXVI
<i>Preparation of the Schiff bases</i> .....	clxvi
<i>Preparation of the complexes</i> .....	clxvii
<i>DNA-Binding Studies</i> .....	clxviii
CHAPTER II - RUTHENIUM COMPLEXES.....	CLXXV
<i>Structure of the complexes</i> .....	clxxv
<i>DNA-Binding Studies</i> .....	clxxvi
CHAPTER III - HELICATES .....	CLXXX
<i>Preparation of the Poly-<math>\beta</math>-diketones</i> .....	clxxx
<i>Preparation of the supramolecular complexes</i> .....	clxxxii
<i>DNA-Binding Studies</i> .....	clxxxiv
<i>Cell Studies</i> .....	cxc
REFERENCES .....	CXCVIII

# Abbreviation List

---

ACN	Acetonitrile
AFM	Atomic force microscopy
Bp	Base pair
BSA	Bovin Serum Albumin
CD	Circular dichroism
CDCl <sub>3</sub>	Deuterated chloroform
ct-DNA	Calf thymus DNA
d	NMR- doublet
DME	Dimethoxyethane
DMEM	Dulbecco's modified eagle medium
DMSO	Dimethylsulfoxide
DNA	Deoxyribonucleic acid
$\epsilon$	Extinction coefficient ( $\text{mol}^{-1} \text{ dm}^{-3} \text{ cm}^{-1}$ )
EA	Elemental analysis
EDTA	Ethylenediaminetetraacetic acid
EI	Mass spectrometry- electron impact
ESI	Electrospray ionization mass spectrometry
EtBr	Ethidium bromide
EtOH	Ethanol
HEPES	2-(4-(2-Hydroxyethyl)-1-piperazinyl)-ethanesulfonic acid
<sup>1</sup> H-NMR	Proton nuclear magnetic resonance spectroscopy
Hoechst 33258	2-(4-hydroxyphenyl)-5-[5-(4-methylpiperazine-1-yl)benzimidazo-2-yl]-benzimidazole
IC	Inhibitory concentration
IR	Infrared spectroscopy
M	Molar ( $\text{mol dm}^{-3}$ )
mL	Milliliter
MTT	3-(4,5-dimethylthiazol-2-yl)-2,5-diphenyltetrazolium bromide

m/z	Mass spectrometry- mass/charge
PBS	Phosphate-buffered saline
PI	Propidium iodide
ppm	Parts per million
RT	Room temperature
THF	Tetrahydrofuran
$\delta$	NMR- chemical shift
TBE Buffer	45 mM Tris base, 45 mM boric acid and 1 mM EDTA
Tris	Tris(hydroxymethyl)aminomethane



# Abstract

---

The discovery of cisplatin and its successful use as chemotherapeutic agent have encouraged the development of metal-based anticancer molecules.

The present doctoral research project includes three different chemistry approaches to design new metal-based cytotoxic compounds. Coordination, organometallic and supramolecular chemistry have been used to successfully develop three families of compounds with highly promising biological properties.

Copper(II) *coordination* compounds of various nuclearities have been prepared from new Schiff-base ligands. The complexes strongly interact with DNA without cleaving it and exhibit notable cytotoxicities against various murine and human cancer cell lines.

*Organometallic* ruthenium(II)-arene compounds containing a monophosphane  $\text{PR}_3$  ligand have been obtained, which show remarkable cytotoxicities against a wide panel of human cancer cells, so as very interesting antimetastatic properties. Structure-activity relationship studies have been carried out, which illustrated the great potential (and versatility) of this family of molecules, whose biological properties can be fine-tuned by the selection of the different ligands bound to the metal.

A new family of *supramolecular* compounds has been developed with the objective to target the DNA major groove or/and stabilize non-conventional DNA structures, for instance the three-way junction (3WJ). The series of iron(III) metallohelicates prepared exhibit groove-binding properties but are not capable of stabilizing the 3WJ. Some of these helical complexes show interesting cytotoxic properties and one of them can even induce cell apoptosis.





# Introduction

---

*Cancer is a widespread disease that represents one of the major causes of death in developed countries. The scientific community is actively trying to unravel the molecular and biochemical basis of cancer, with the objective to develop and implement new strategies, not only for the early detection of cancer, but also to find novel and efficient therapies.*

*In the present chapter, potential therapeutic approaches are presented, with special emphasis on chemotherapeutic drugs; their discovery is briefly described, so as their specific molecular targets and peculiar mechanisms of action. Special attention is paid to DNA as the main molecular target of metal-based drugs, and the different types of DNA-recognition are mentioned.*

## Contents

---

HALLMARKS OF CANCER .....	2
AN OVERVIEW OF CHEMOTHERAPY – CANCER: WHEN CHEMISTRY FIGHTS BACK .....	4
<i>DNA as a molecular target</i> .....	5
<i>Metal complexes as cytotoxic agents</i> .....	12
Coordination Compounds: from highly cytotoxic agents to rational design and directed targeting .....	13
FINAL REMARKS AND OBJECTIVES OF THIS THESIS .....	22
REFERENCES .....	23

---

Cancer is a group of various diseases with divergent phenotype characteristics, sharing the same abnormal growth of cells, rapid and uncontrolled, that ultimately leads to proliferation. Cancer cells have the ability to spread by invading adjacent tissues; furthermore, they can break away from a primary tumour and enter the lymphatic system or bloodstream (i.e. metastasis).<sup>1-4</sup> Nowadays, cancer is considered as one of the major public health problems worldwide, affecting 32.6 million people and causing 8.2 million deaths (statistics from 2012).<sup>5</sup> These numbers are expected to almost double by 2030. These groups of diseases are causing more deaths than all coronary heart diseases or all strokes. There are more than 500 distinct types of cancers found within specific organs. They can be grouped into five main subgroups according to the type of cells they affect: carcinomas (organs, most common, > 85%), sarcomas (skeletal system), leukemia (blood system), lymphomas and myeloma (lymphatic system) and brain and spinal cord cancers (nervous system). Carcinomas are cancers that initiate in a tissue that lines the inner or outer surfaces of the body, and there are a number of subtypes, namely adenocarcinoma, squamous-cell carcinoma, basal-cell carcinoma, and transitional-cell carcinoma.<sup>4,6</sup>

Cancer represents a series of complex and progressive transformations over a protracted period, leading to dysregulation and malfunction of elemental cell mechanisms. The inability to correct these dynamic modifications and their stepwise accumulation increases the genomic instability, resulting in malignant transformation of normal cells. Cancer can have genetic and/or environmental causes, and in most cases, there is a synergistic cooperation between these two factors. Environmental causes are characterized by a stepwise accumulation of successive mutations caused by biologic (virus), chemical (genotoxic and epigenetic agents) and physical (radiation) agents. These carcinogenic agents can alter some proto-oncogenes, activating or inactivating them, in a process known as initiation. The subsequent stage is the promotion, arising from the accumulation of mutations (due to malfunction of the repairing systems). The last step in this malignant cycle is called progression, which is a process that can lead to the proliferation of partially altered cells, becoming highly malignant derivatives. This progression is schematically represented in Figure 1.

### ***Hallmarks of cancer***

Over the years, the molecular mechanisms underlying biological and biochemical processes of normal cells have been thoroughly scrutinized, and the major signalling pathways that are altered during tumorigenesis have been described. The way in which these pathways are linked to dysregulated processes, such as proliferation and survival, has also been





reported.<sup>7-11</sup> However, the overwhelming complexity of these pathways makes difficult to predict the outcome of some treatments.<sup>12</sup>

More than 300 genes implicated in cancer have been described, most of them associated with signalling transduction processes within or between cells, cell-cycle progression, apoptosis, angiogenesis, and tissue invasion.<sup>13,14</sup> Carcinogenesis is characterized by mutations that directly affect these genes, up- or downregulating molecules that play a crucial role in complex signalling networks interfering in cell proliferation and cell death. These types of genes are oncogenes and tumour-suppressor genes, which affect directly or indirectly cellular growth or death, respectively.<sup>15-17</sup> The genes associated with the loss of control of cell proliferation may also be involved in genetic instability and tumour vascularization, leading to a dysregulated proliferation of cells. Consequently, these cells have increased requirements in molecular oxygen, which lead to hypoxia and trigger the angiogenesis process.<sup>18,19</sup> Likewise, genes that are involved in tumour-cell invasion may also be involved in the loss of growth control and evasion of apoptosis. The molecular and genetic alterations of cancer cells enable them to generate their own growth-promoting signals and become less sensitive to cell-cycle checkpoint controls, allowing them to evade apoptosis and exhibit an almost limitless replication potential. According to Douglas Hanahan and Robert Weinberg, the manifestation of six essential hallmarks cooperatively dictates the progression of the neoplastic disease in cell physiology.<sup>3,16,20-23</sup>



**Figure 1: Schematic representations of multistage carcinogenesis, the dynamic modifications that can lead to carcinogenesis and the hallmarks of cancer (from left to right). Left: complex and dynamic interactions between genetic and environmental factors can enhance or inhibit some proto-oncogenes, and consequently can influence cancer initiation and development; middle: essential stages of this process known as initiation, promotion and progression; right: acquired cancer abilities, which are characterized by ten important hallmarks. Adapted from <sup>3,20,24</sup>.**

This group of intricate and complementary acquired abilities include sustaining proliferative signalling, evading growth suppressors, resisting cell death, enabling replicative

immortality, inducing angiogenesis, and activating invasion and metastasis. A recent review expands these hallmarks to ten (see Figure 1, right).<sup>20</sup>

### ***An overview of chemotherapy – Cancer: when chemistry fights back***

Historically, cancer chemotherapy started with the work of Paul Ehrlich, who was also the first to describe the development of resistance to chemotherapy.<sup>25</sup> Notwithstanding, the modern concept of chemotherapy brings us back to the 1940's, when some compounds used in mustard bombs during World War I and World War II, were tested against several tumours. It was observed that mustard gases affected the cell division of certain types of somatic cells, thus suggesting that they might be used to suppress cancer cells division in acute leukaemias and lymphomas. A timeline summarizing the events related to the development of cancer chemotherapy is shown in Figure 2.<sup>26-28</sup>

Nitrogen mustards along with some antifolate drugs hence represented the scientific stimulus for the development of new chemotherapeutic compounds, which has led to a multibillion-dollar-a-year industry, in which for-profit commercial interests have high stakes. A second crucial discovery in this area of research was the description of the helical DNA structure by Watson and Crick,<sup>29</sup> after which a number of important antitumor drugs were reported, *e.g.* actinomycin D, bleomycin, anthracyclines, antimetotics (vinca alkaloids), nucleoside analogues and nucleobases (cytarabine, 6-mercaptopurine, 6-thioguanine and fluoropyrimidines), cisplatin, etoposide or procarbazine.<sup>26,28</sup>

The late 1990's spawned an exciting era in molecular biology and biochemistry of cancerous cells. All the scientific breakthroughs achieved during this period allowed chemotherapy to enter a new stage, namely the targeted therapy revolution. Unwanted side effects and drug resistance are the most important drawbacks of chemotherapy, which represent a challenge for modern scientists. While the side effects fundamentally arise from the lack of specificity and selectivity, drug resistance appears because of genetic and biochemical modifications that allow tumour cells to survive during chemotherapeutic treatment. The primary goal of cancer therapy was to eliminate all malignant cells from the patient. Nowadays, acquired knowledge has led to a different approach where cancer is viewed as a “chronic disease”; therapy now is intended to try to reverse the physiological changes induced by the disease rather than attempting to directly eradicate all malignant cells. A new therapeutic era is emerging where case-by-case diagnostic work-up becomes crucial for the selection of relevant targeted therapeutics and prediction of the subsequent response.<sup>2,27</sup>



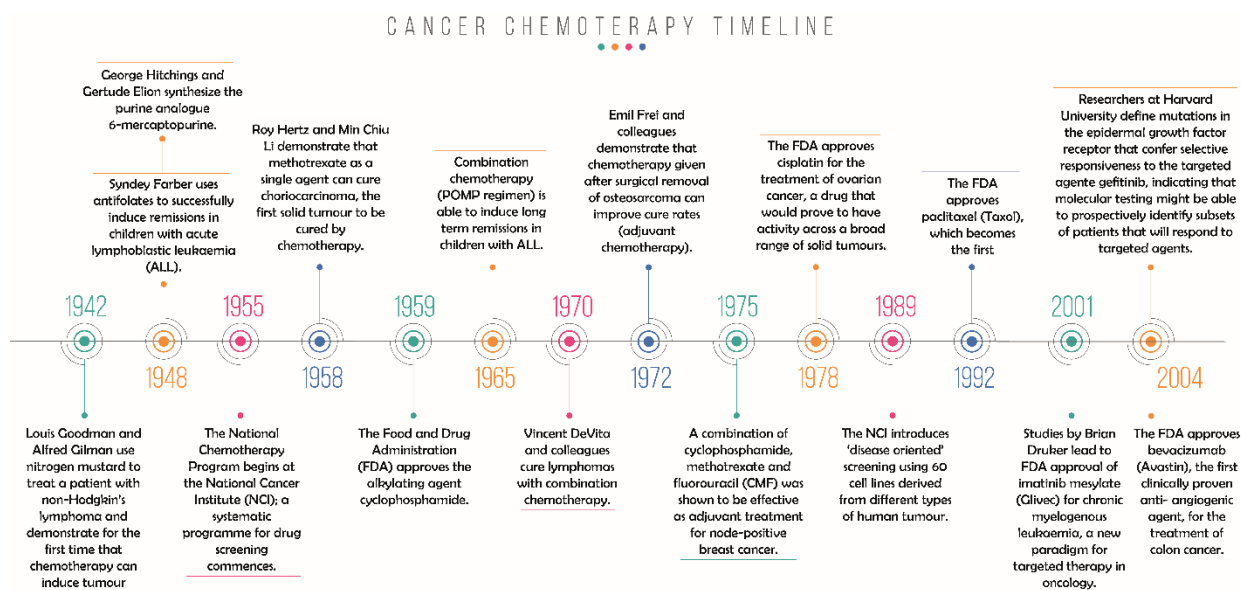


Figure 2: Cancer chemotherapy over years. Adapted from<sup>26-28</sup>

Chemotherapy is an effective treatment against certain types of cancers. However, its lack of specificity and selectivity often have a high impact on patients' health and life expectancy. Therefore, the development of more specific drugs is required, whose mechanism(s) of action, pharmacokinetics and pharmacodynamics should be established in order to achieve a better efficiency.

### *DNA as a molecular target*

In classical chemotherapy, the main targeted structure is the carrier of the genetic information, *i.e.* DNA. Affecting this biomolecule can disturb crucial cellular events such as transcription (gene expression and protein synthesis) or its replication, ultimately triggering cell death.<sup>30</sup> Hence, the design of biologically active agents targeting DNA has been largely explored.<sup>31,32</sup>

Besides the well-known double helix, DNA may exhibit unusual architectures, which have a critical role for reliable protein recognition; the biological significance of these so called non-canonical DNA architectures has been clearly demonstrated.<sup>33-36</sup>

When DNA interacts with gene regulatory proteins, it tends to experience conformational changes; such structural alterations may be induced through interactions with other molecules, which can introduce bends and kinks within the double helix. The ability to recognize other molecules and to be recognized by them is directly correlated with the sequence arrangement, and therefore to the properties of the bases. The most commonly described DNA structure is a double-helix containing complementary anti-parallel polynucleotide strands, stabilized by  $\pi$ - $\pi$  interactions between the stacked hydrophobic aromatic rings of adjacent

bases. These strands are linked by hydrogen bonds and supported by a negatively charged sugar phosphate backbone (commonly referred as B-DNA, Figure 3).<sup>37</sup>

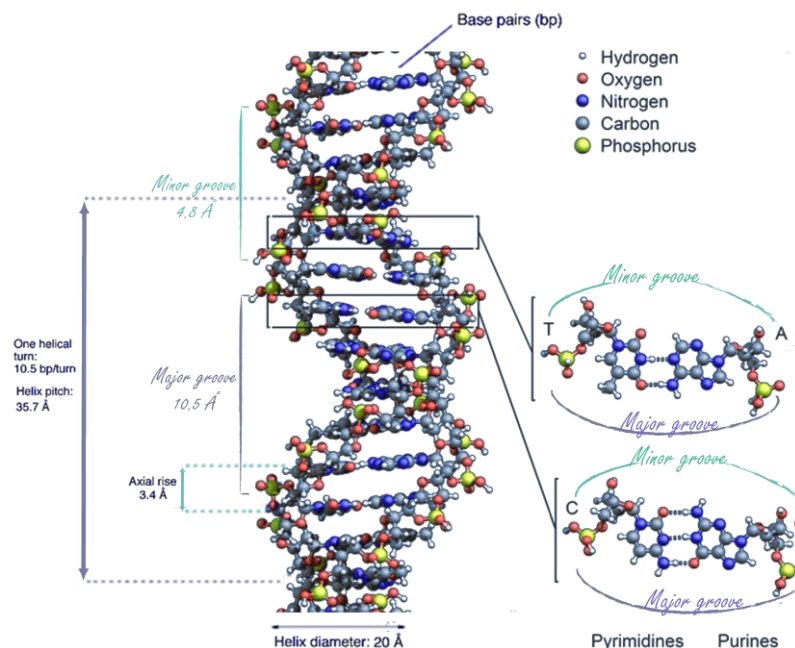


**Figure 3: Structural parameters of the B-form of DNA. Adapted from<sup>38</sup>.**

This B-form of DNA is commonly found in functional cells and the winding of both strands generates two types of hydrophobic grooves within the main structure, *viz.* the major and minor grooves. The minor groove is narrow and deep, with more accessible base edges, providing support for protein recognition. The major groove is wide and shallow, allowing the binding of small molecules. It is important to note that the phosphate backbone plays a role as well; it is not just acting as a linker that holds the bases at their positions. Its natural plasticity underwrites and limits the placement of the bases, so that the local DNA structure results from the interplay between optimal base positions and preferred conformations of the sugar phosphate backbone.<sup>38-40</sup> The overall physical properties of DNA depend not only on its chemical architecture, but also on the contributions from base pairing, base stacking, and ion and water binding. The supramolecule can adapt three major general topologies; according to the handedness of the helix, the pitch (distance between a base and the base obtained after a full 360° turn), the number of nucleotides within one pitch and the distance between consecutive bases, these topologies can be classified as forms A-, B- (right-handed helices) and Z (left-handed helix) (Figure 4). As mentioned previously, under physiological conditions, the B-polymorph is predominant. Any accidental or strategically programmed physiological changes can lead to an alteration of the DNA conformation.<sup>41</sup> It has been demonstrated that small regions of DNA are in an A-like conformation, *in vivo*, thus facilitating its interaction



with specific proteins. This specific conformation is also adopted when DNA is under relative low water-content conditions, and its formation is strongly dependent on base composition and environmental factors like pH, salt concentration, etc. During transcription, when hybrid RNA–DNA helices are generated, the A-conformation is adopted.

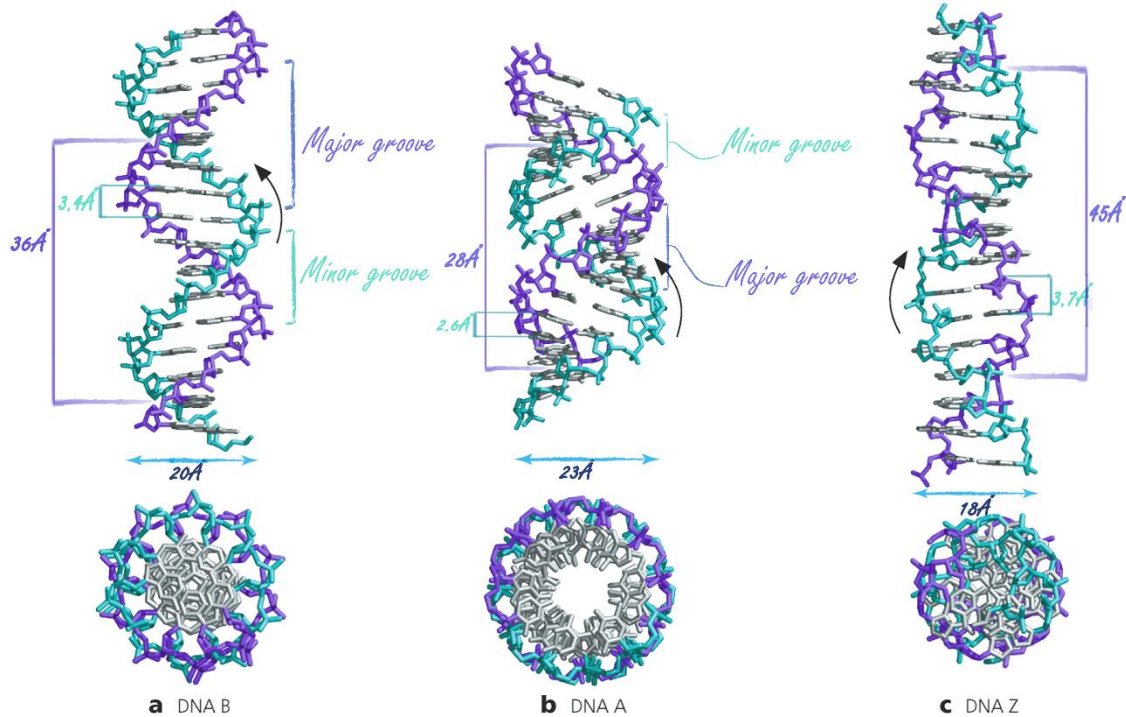


**Figure 4: Duplex DNA conformations with their respective orthogonal representations. Adapted from<sup>42</sup>.**

At high salt concentrations, there is evidence of a left-handed helical geometry form of DNA, namely Z-DNA. This form is highly antigenic and less stable than B-DNA at physiological salt concentrations. However, it can be modulated and stabilized by negative supercoiling or by protein binding. The energy necessary to form and stabilize Z-DNA, *in vivo*, can be generated during the transcription process.<sup>33,43</sup> These conformational changes can also be induced by covalent binding of metal complexes.

Due to its dynamic nature, DNA can also fold into a variety of inter- and intramolecular secondary structures, which are important in the regulation of replication, transcription, and genome stability, both in prokaryotic and eukaryotic cells. Some studies have shown that protein interaction sites exhibit characteristic conformational properties. The broad variety of three-dimensional architectures that deviate from the canonical duplex-DNA can be categorized as i-motifs (four-stranded DNA secondary structures), branched helical species (three- and four-way junctions), bulges (palindromic sequences such as hairpins or cruciforms), RNA:DNA hybrids, Holliday junctions and G-Quadruplex DNA structures (Figure 5).

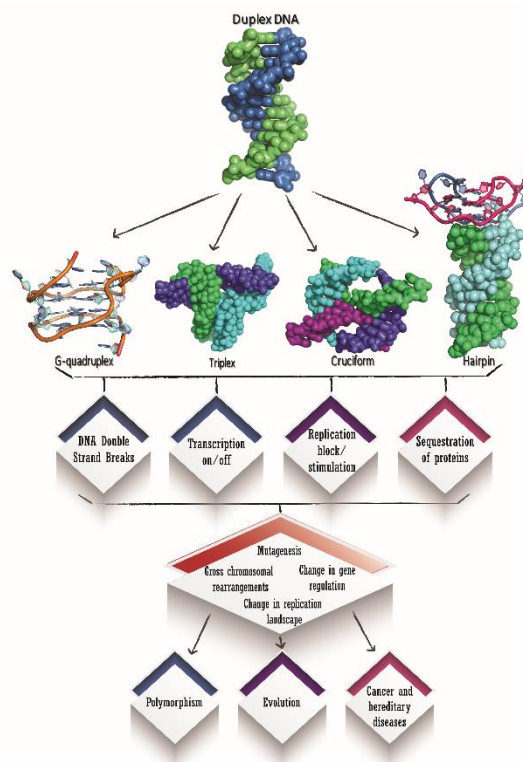


**Figure 5: Different DNA secondary structures and their specific roles in genome function and integrity.** The formation of secondary structures or the occurrence of the sequence motif *per se* can lead to double strand breaks (G-quadruplexes, PDB id: 2N3M, triplexes, PDB id: 1EKW, cruciform, PDB id: 1C7Y, and hairpins, PDB id: 5FHJ); induction (G- quadruplexes and GAA/TTC tracts) or inhibition of transcription (G- quadruplexes and triplexes); initiation (triplexes) or stalling of replication (G- quadruplexes, triplexes, cruciforms and hairpins); and sequestration of cellular proteins (G- quadruplexes, triplexes and r(CUG) hairpins). It is known that such structures are involved in polymorphism, genome evolution and a variety of diseases via gross-chromosomal rearrangements, mutagenesis, dysregulation of gene expression and alteration of the replication landscape. Adapted from<sup>35</sup>

The negative nature of DNA makes it a target for metal ions (and cationic metal complexes). Compounds interacting with DNA can be divided in different classes according to their mechanism of action and their potential binding sites. Metal complexes can bind non-covalently or covalently to DNA duplexes.

Covalent interaction implies the formation of an adduct; thus, the DNA is permanently altered, for instance through alkylation, cross linking or metal-coordination. In contrast, noncovalent interactions are reversible. Covalent binders can produce DNA cross-links, perturbing the structure of the biomolecule, which may result in the inhibition of protein-DNA interactions, hence blocking replication or transcription processes (Figure 6b and c). Covalent binders are usually highly toxic and poorly selective. However, cells have developed a series of repairing tools to overcome such modifications. The identification and repairing of inter- or intrastrand DNA cross-links play one of the key roles in drug resistance.<sup>44-46</sup>

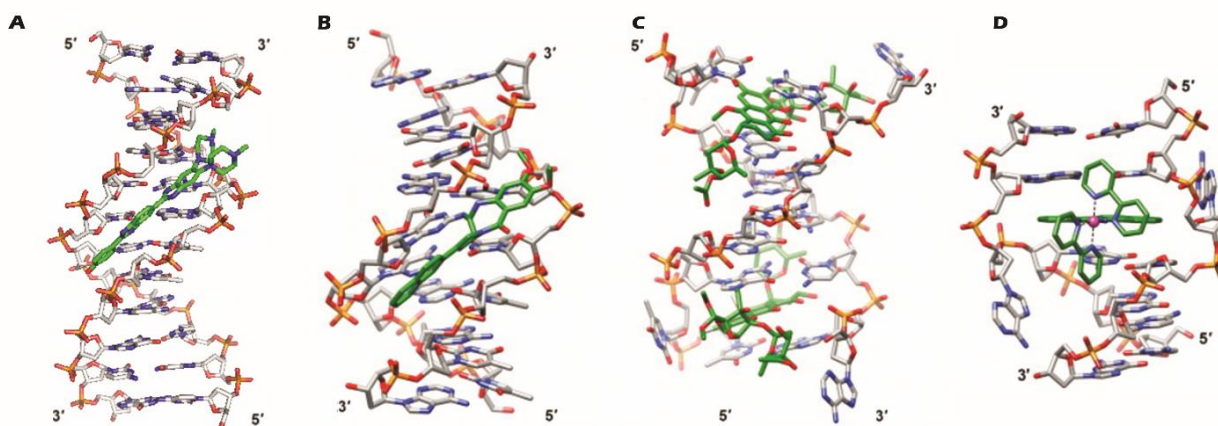


**Figure 6:** Examples of DNA-Drug interactions. **A.** Crystal structure of a DNA:Hoechst 33258 complex, the minor groove binder being highlighted in green (PDB id: 8BNA); **B.** C2-(2-naphthyl)-substituted pyrrolo[2,1-c][1,4]benzodiazepines (highlighted in green) covalently attached to a G base of a duplex (PDB id: 2K4L); **C.** Trioxacarin A molecules (highlighted in green) covalently attached to DNA G bases of a duplex; their intercalation force 3'-adjacent T bases to be located at extra-helical positions (PDB id: 3c2j); **D.** A delta-Rh(bpy)<sub>2</sub>(chrysi)<sup>3+</sup> complex intercalated in a DNA duplex (PDB id: 3GSJ). The metal ion is shown as a pink sphere and the ligands are highlighted in green. The metallo-insertion ejects Adenosine bases to the major groove. Adapted from<sup>47</sup>.

Non-covalent interactions of metal complexes with DNA may occur through coordination bonding, hydrogen bonding or  $\pi$ - $\pi$  stacking. For instance, positively charged molecules can bind along the exterior of the helix; such electrostatic interactions with the anionic sugar-phosphate backbone are commonly non-specific (Figure 7a).

Some coordination compounds bearing planar (aromatic) moieties can intercalate between base-pairs in the major or the minor groove. This type of  $\pi$ -stacking interaction is called classic intercalation and is often combined with hydrogen bonds. The resulting separation of the bases causes an unwinding of the DNA twist. Owing to the lack of flexibility of the DNA backbone, the interacting molecules cannot be consecutively inserted into all gaps. Once one gap is occupied, the adjacent ones remain unfilled, in a maximum of two consecutive gaps per intercalated molecule. This feature is known as the neighbour-group exclusion principle.

An intercalation concomitantly accompanied by a strong interaction with the major and minor grooves is named threading intercalation, which presents a higher DNA-binding affinity and slower dissociation.<sup>50</sup> Aromatic systems have a large polarizability; therefore, both the polarity and charge of a complex containing aromatic ligands play a dominant role in the intercalation and targeting process (Figure 6d). The formation of the “intercalation cavity” requires the unstacking of adjacent base pairs, which induces an unwinding and lengthening of the double helix, with a consequent distortion on the usual helical turn. The unwinding angle depends on the geometry of the ligand–DNA complex. This type of interactions is common

among the drugs currently used for the treatment of ovarian and breast cancers and acute leukaemias.<sup>51-53</sup>

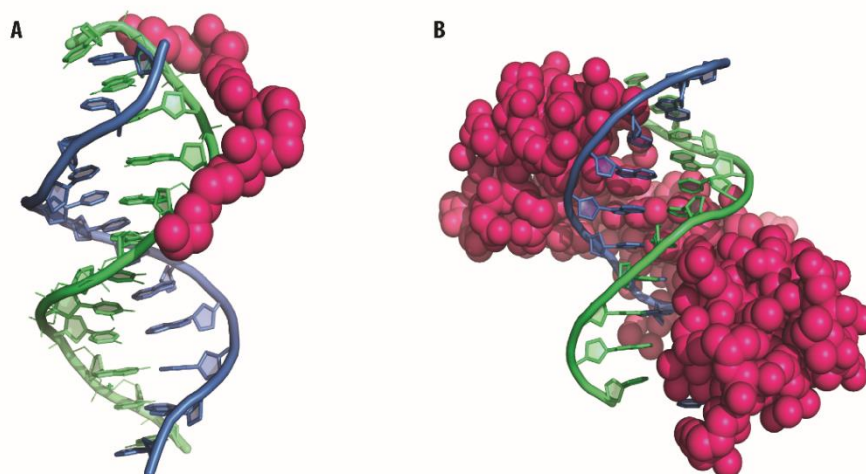


**Figure 7:** Two examples of DNA-Drug interactions. A. Crystallographic structure of a trinuclear platinum drug (in pink) bound to the sugar-phosphate backbone of DNA (PDB id: 2DYW); B. Crystal structure of a zinc finger protein (in pink) bound to the major groove of DNA (PDB id: 1ZAA). Adapted from<sup>48</sup> and<sup>49</sup>.

Some complexes have been described to present sequence specificity and be able to interact with the edges of base pairs from both grooves. Such groove binding produces conformational changes on the DNA double helix. Compounds capable of targeting the DNA grooves usually contain specific features; they often have unfused aromatic ring systems linked by bonds allowing torsional freedom. Hence, such molecules can adopt appropriate conformations to fit the helical curvature of the groove without significant perturbation of the DNA structure. It can be pointed out here that groove targeting allows to disrupt specific gene expression.

DNA minor-groove recognition has been widely explored, for instance using small polyamides or heterocyclic dications targeting AT-rich regions (Figure 6a).<sup>54-56</sup> It has been shown that this type of compounds are able to form specific hydrogen bonding to the minor-groove floor, before and after the turn, and to generate H bonds with water molecules. The resulting, induced conformational pucker minimizes steric interactions with the bases, avoiding a major structural change. Large molecules can affect considerably the minor groove, which can lead to its widening. In such a case, the damage promoted is extended to the major groove, which is narrowed, and therefore becomes too small to accommodate proteins such as transcription factors. This type of compounds can also promote a bent of the helix towards the major groove, resulting in a similar effect (as that described above).

Although the targeting of the major groove would allow to modulate specific gene expressions, only a few molecules have been described so far (Figure 7b). This is due to the





fact that this groove presents a greater diversity, both in size and shape (compared with the minor groove). Bioinspired metallo-supramolecular compounds have been designed to specifically target the major groove of DNA. These molecules are too large to bind in the minor groove and exhibit the perfect shape and size to interact with the major groove, mimicking proteins like zinc fingers proteins. It must be stressed that artificial molecules as highly selective groove binders have not been reported as yet.<sup>57-60</sup>

In addition to their interaction with DNA, metal complexes may act as artificial proteases/nucleases, which can result in the cleavage of the biomolecule. The metal-based compounds may function as oxidative, hydrolytic, and/or photoreactive catalysts, and relatively high specificities towards either DNA or RNA sequences have been reported. Cisplatin derivatives and DNA-alkylating drugs interact with DNA through differing mechanisms of action, *e.g.* strand breakage, base-alkylation/crosslinking etc.<sup>35,46,61,62</sup>

Nowadays, there is a tendency to conjugate functional groups of different properties within the same molecule. The objective of this approach is to synergistically improve not only the cytotoxic behaviour but also the specificity of the multi-functional molecules. Most conjugates reported in the literature contain a non-covalent DNA binding moiety, aimed at driving the molecule towards DNA (sequence specificity), and an active group, such as an alkylating group. Examples of groove binders and intercalators that can be used as DNA-recognition moiety are listed in Table 1, together with their respective association constants.<sup>62</sup>

**Table 1: DNA binding constants ( $K$ ) to calf-Thymus DNA (42% GC)  $[\text{Na}^+] = 50 \text{ mM}$  of known DNA binders<sup>63-65</sup>**

Compound	Binding mode	$K \text{ (M}^{-1}\text{)}$	Sequence selectivity
Hoechst 33258	Minor Groove Binder	$3 \times 10^8$	$(\text{AT})_n$
DAPI	Minor Groove Binder	$1 \times 10^6$	$(\text{AT})_n$
Distamycin A	Minor Groove Binder	$8 \times 10^5$	$(\text{AT})_n$
Methyl Green	Major Groove Binder	$1 \times 10^6$	Insignificant
Ethidium Bromide	Intercalator	$1 \times 10^6$	Insignificant

Another strategy to generate more selective systems consists in targeting higher-order DNA structures such as G-quadruplexes or three-way junctions.<sup>35,36</sup>

Three-way junctions (3WJs) are observed in viruses and in replicating DNAs, particularly during the rapid growth that characterizes cancerous cells. Such DNA secondary structures have also been related to some diseases, like Huntington's disease or myotonic

dystrophy.<sup>66</sup> A 3WJ is formed by three B-type duplex arms that converge towards a single point, named as branch point. This branch point generates a hydrophobic cavity with a diameter of 10 to 15 Å (Figure 8). A 3WJ is thus characterized by its unique geometry, consisting of a well-defined and stable Y-shaped three-dimensional structure. 3WJs resemble the replication fork; therefore, the design of molecules capable of stabilizing them is of therapeutic interest as such molecules may impede cellular replication. Actually, Hannon and co-workers have demonstrated the potential of such strategy.<sup>59,67-69</sup> Selective 3WJ binders may have the ability to stall the replication fork, hence triggering genetic instability in cancer cells. An example of a metal-based compound that stabilizes a 3WJ is depicted in Figure 8. The tetracationic supramolecular complex exhibits helical arms, formed by three ligands wrapped around two central iron atoms, which interact via  $\pi$ - $\pi$  stacking interactions with the DNA bases located in the branch point.

G-Quadruplexes are ubiquitously found in the genome where they are specially clustered in some repetitive regions, named the telomeric 3'-ends. They are also found well distributed in promoter regions such as c-MYC, c-KIT, bcl2 (B cell lymphoma 2), KRAS (Kirsten rat sarcoma viral oncogene homolog), among others. These DNA architectures thus represent non-canonical DNA targets for anticancer drugs.<sup>71,72</sup>

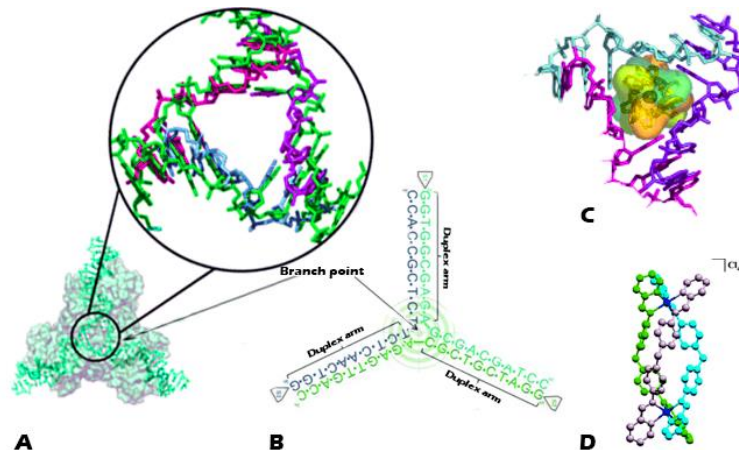


**Figure 8:** A. Side-view of a 3WJ and zoom into the branch point. B. Schematic representation of a 3WJ generated by three DNA single strands (*i.e.* S1, S2 and S3). C. Crystallographic side-view of the complex formed between a 3WJ and a triple helicate complex designed by Hannon and co-workers (PDB Id: 2ET0). D. Molecular structure of the tetracationic triple helical supramolecular complex.<sup>69</sup> Adapted from<sup>70</sup>

### *Metal complexes as cytotoxic agents*

The chemotherapeutic use of metal complexes was stimulated by the serendipitous discovery of the antitumor activity of cisplatin, the inorganic leading anticancer drug.<sup>73</sup> From this pioneering work, the field of “inorganic drug design” has developed exponentially since coordination chemistry offers great potential for the generation of efficient therapeutic and diagnostic agents.<sup>74</sup> Chemists took advantage of the rich coordination chemistry of metal ions,



which provide a wide range of coordination numbers and geometries, various accessible redox states and diverse thermodynamic and kinetic characteristics (*e.g.* ligand-exchange rate, hydrolysis rate, etc.). Also, the intrinsic properties of the cationic metal ion and/or the ligand(s) itself offer a wide spectrum of reactivities that can be exploited, for instance to selectively target unhealthy cells, for *in situ* activation (*e.g.* through the application of light), etc. The use of endobiotic metal-transport pathways, such as the iron-transport protein transferrin, is also an added value to this type of drugs that may be conveyed to specific tumour cells.<sup>30,75</sup>

### **Coordination Compounds: from highly cytotoxic agents to rational design and directed targeting**

As already aforementioned, coordination complexes offer great possibilities to design systems with unique features. According to Alessio and co-workers, anticancer metal complexes can be divided into five classes, based on the role played by the metal centre.<sup>76</sup>

1. The metal has a functional role, *i.e.* the activity arises from its direct interaction with the biological target through coordination or supramolecular bonds. In this case, the compounds behave as prodrugs, which are activated by aquation or/and reduction/oxidation. Cisplatin derivatives (Figure 9) and some Ru(II) compounds (Figure 12) are typical examples for this category of complexes. In this family of compounds, thermodynamic and kinetic parameters of the metal centre are crucial for its binding properties.<sup>77</sup> Additionally, the nature of the non-leaving ligands is extremely important as they may affect the lipophilicity, charge, size, solubility or non-covalent interaction properties of the complex, which in turn will influence its bio-distribution as well as its pharmacokinetics. The activation kinetics is another key factor that influences the reactivity of the compound; in this regard, the nature of the leaving ligand(s) is of paramount importance.

This type of compounds has an important drawback; they exhibit a high toxicity, which is usually related to their uncontrolled reactivity with biomolecules.

2. The metal has a structural role, *i.e.* it acts as a scaffold, organizing the ligands in the three-dimensional space. The resulting geometry of the compound is then essential for its effective interaction with the “active site” of the biological target. The binding occurs predominantly through non-covalent interactions such as Coulombic interactions, hydrogen bonding,  $\pi$ - $\pi$  stacking (intercalation), and the structure of the biomolecule is not significantly altered. An example of such binding is the interaction between ethidium bromide and DNA.<sup>78</sup>

3. The metal is a carrier for active ligands that are delivered *in vivo*. The metal may also protect the ligands before their delivery.

4. The metal complex behaves as a catalyst *in vivo*, *e.g.* through the production of reactive oxygen species (ROS) that cause cell damage. This category is illustrated by a number of copper complexes.<sup>79</sup>

5. The metal compound is photoactive and can act as a photosensitizer. In this category, remarkable examples of ruthenium and rhodium compounds have been described in the literature, where some copper, iron, cobalt, and vanadium complexes can also be found.<sup>80</sup>

The serendipitous discovery of cisplatin, its efficacy and the side effects related to its clinical use, have attracted the interest of a vast number of inorganic chemists. Over the past several decades, it has been proved that metal-containing compounds offer several advantages over conventional, carbon-based (organic) compounds, and that the role played by the metal on the cytotoxic properties of the complexes is very often crucial.<sup>81</sup> The narrow spectrum of action and the induction of resistance (intrinsic or acquired) of the clinically used drugs encouraged researchers to design and synthesize novel complexes from various metals, *viz.* platinum and other transition metals. Some of the coordination compounds developed successfully entered clinical trials.<sup>72</sup> An overview of some of the most efficient/interesting molecules produced is found below.

#### Platinum complexes

After cisplatin discovery, the field was primarily concentrated on the development of analogues, which led to second- and third-generation platinum drugs. Two of them are clinically used worldwide, namely carboplatin and oxaliplatin (Figure 9). Three other compounds, namely nedaplatin, lobaplatin and heptaplatin (Figure 10), are clinically approved in some countries.<sup>82</sup>

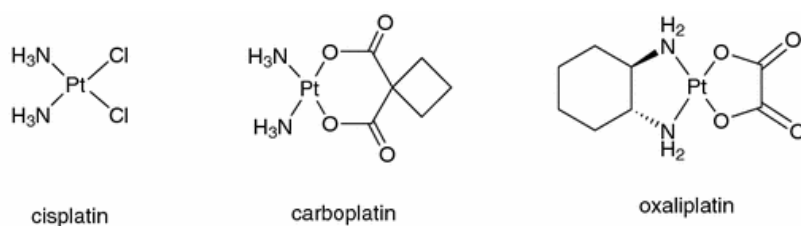


**Figure 9:** Pt(II) compounds used worldwide, *i.e.* cisplatin (*cis*-diamminedichloridoplatinum(II)), carboplatin (*cis*-diammine(1,1-cyclobutanedicarboxylato)platinum(II)), and oxaliplatin (*trans*-R,R-cyclohexane-(1,2-diamine)oxalatoplatinum(II)).

Platinum complexes (particularly cisplatin) are in clinical use for almost 40 years; for instance, cisplatin is used in 50–70% of cancer treatments. It is especially efficient against advanced non-seminomatous germ-cell cancers, testicular, ovarian cancers and other gynaecologic cancers, cervical, and non-small cell lung cancers.<sup>83,84</sup>

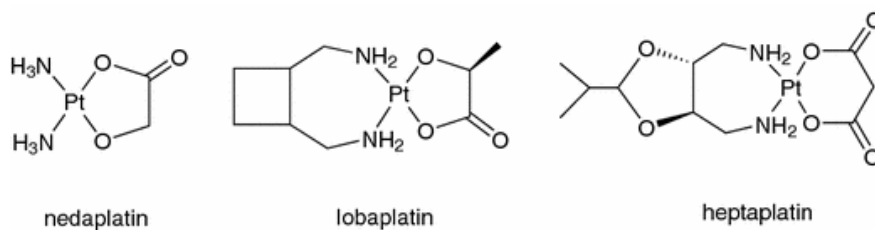


**Figure 10:** Pt(II) compounds clinically approved locally, *i.e.* nedaplatin (*cis*-diammine-glycolatoplatinum(II)) used in Japan, lobaplatin (1,2-diamminomethyl-cyclobutane-platinum(II)-lactate) used in china, and heptaplatin (*cis*-malonato[(4*R*,5*R*)-4,5-bis(aminomethyl)-2-isopropyl-1,3-dioxolane]platinum(II)) used in South Korea.

The mechanism of action and molecular targets of cisplatin are well described; its activity stems from its binding to DNA.

When administrated to the patient, the high concentration of chloride ions in the blood (100 mM) slows down the aquation process. Inside cells, where the [Cl]<sup>−</sup> is significantly lower (around 5 mM), hydrolysis can occur and the aquated species produced can interact with different cell components, such as phospholipids, phosphatidylserine and RNA; it is however widely accepted that the main target is DNA. The platinum complex forms stable adducts, *i.e.* a 1,2-intrastrand cross-link between two adjacent bases (GG or GA), or a 1,3-intrastrand cross-link between two guanines separated by another base (Figure 11). These complex-DNA adducts can hamper or inhibit a series of cellular processes, like the replication and transcription, ultimately leading to cell death.<sup>85</sup> Despite their effectiveness, cisplatin and its analogues have important drawbacks; they often exhibit severe side effects such as neuro, hepato and nephrotoxicity and acquired resistance.

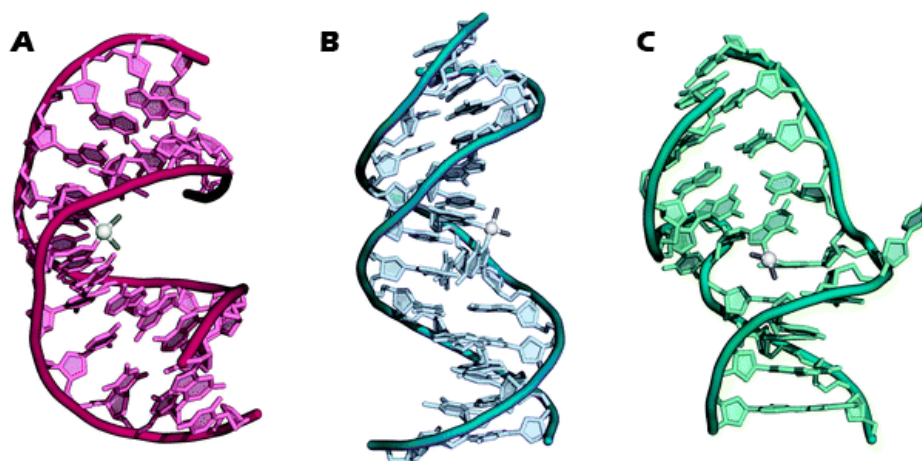


**Figure 11:** X-Ray crystal and NMR structures of double-stranded DNA illustrating different adducts of cisplatin A. Cisplatin 1,2-d(GpG) intrastrand cross-link (PBD Id: 1A1O). B. Cisplatin 1,3-d(GpTpG) intrastrand cross-link (PBD Id: 1DA4). C. Cisplatin interstrand cross-link (PBD Id: 1A2E). Adapted from<sup>86</sup>

The affinity of platinum(II) compounds for the imidazole nitrogen of histidine residues is associated with its inherent toxicity, resulting from a clear inhibitory effect towards the matrix metalloproteinase enzymes. To reduce side effects, kinetically inert platinum(IV)

prodrugs have been developed to overcome some of the problems associated with cisplatin and its analogues. More stable drugs, with reduced aquation rates, have been thus produced through the generation of octahedral Pt(IV) complexes containing two extra ligands at the axial positions. Bioactive ligands may be added at these positions to improve (i) cell targeting and delivery or/and (ii) the pharmacokinetics of the complex.<sup>82</sup> Inside cells, the Pt(IV) compound is reduced to a Pt(II), releasing two ligands and producing the active, DNA-binding species.

### Ruthenium complexes

In 1980, Clarke and co-workers have described the cytotoxic properties of Ru(III) amines, which hence raised interest in the scientific community as potential anticancer-drug candidates. A number of Ru(III) complexes have been designed, *e.g.* *trans*-[RuCl<sub>4</sub>(Im)(DMSO)]ImH (NAMI-A) and *trans*-[RuCl<sub>4</sub>(Ind)<sub>2</sub>]IndH (KP1019) (Figure 12). While KP1019 is cytotoxic, NAMI-A is relatively non-toxic but exhibits interesting metastatic properties. Both compounds underwent clinical trials; these trials terminated for NAMI-A which showed undesirable effects, *viz.* neutropenia, anaemia, elevated liver enzymes, transient creatinine elevation, nausea, vomiting, constipation, diarrhea, fatigue and renal toxicity.<sup>87</sup> Clarke and co-workers have also shown that Ru(III) complexes of the type Ru(η<sup>6</sup>-toluene)Cl<sub>2</sub>(PTA) (RAPTA, PTA = 1,3,5-triaza-7-phosphaadamantane), which are usually relatively inert towards ligand substitution, become active upon *in vivo* reduction to more labile Ru(II) complexes (Figure 12). Consequently, the biological activity of Ru(II) complexes have been studied by the scientific community, and some compounds with interesting anti-metastatic activities have been discovered. It can be stressed that, after more than 15 years of investigation, the mechanism of action of NAMI-A and KP1019 remains unidentified; it is however known that RAPTA compounds have a clear and strong binding preference for proteins (rather than for DNA).<sup>88-90</sup>

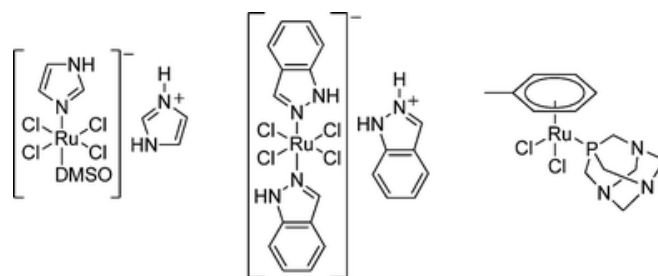


Figure 12: Ru(III) and a Ru(II) complexes that showed promising results against cancer cells, namely *trans*-[RuCl<sub>4</sub>(Im)(DMSO)]ImH (NAMI-A, left), *trans*-[RuCl<sub>4</sub>(Ind)<sub>2</sub>]IndH (KP1019, center) and [Ru(η<sup>6</sup>-toluene)Cl<sub>2</sub>(PTA), PTA = 1,3,5-triaza-7-phosphaadamantane (RAPTA-T, right).

### Rhodium complexes

Some rhodium complexes with interesting biological activities and reduced side effects have been described.<sup>46</sup> The photo-induced DNA cleavage with rhodium compounds has been





reported; upon light irradiation, these new rhodium complexes indeed act as a photonucleases, cleaving the DNA strands.<sup>91-93</sup> For example, the rhodium(III)-polypyridyl complex shown in Figure 6d (and others from the same family) are very cytotoxic against breast and colon cancer cell lines (in the nM range, significantly more efficient than cisplatin). Such Ru compound appears to affect cellular dioxygen consumption, and therefore cell respiration processes; most likely, the activity of mitochondria is inhibited to some extent.<sup>94</sup>

#### *Titanium, Vanadium and Iron complexes*

A number of metallocene halides (Fe, Ti, V) have been reported that show interesting activity against experimental tumours; moreover, they are less toxic than cisplatin. Unlike the model Pt drug, they undergo rapid hydrolysis. Their aqua complexes have a higher affinity for phosphate oxygen atoms than for the heterocyclic bases of DNA. Their mechanism of action is not elucidated but some studies suggest a preference for partial metallo-intercalation and groove binding.<sup>95</sup>

Titanium complexes represent a viable alternative for cancer chemotherapy. It has been shown that titanium-based complexes bind either to macromolecules *via* coordinative (covalent) bonds or *via* intercalation. Titanocene dichloride and budotitane were the first compounds entering clinical trials after platinum ones. Their mechanism of action is not clear, and their poor water solubility and stability represent the major concerns at the clinical level. Current investigation is thus devoted to the development of hydrophilic and water stable Ti(IV) complexes.<sup>96</sup>

Vanadium complexes, with their rich chemistry and usually low toxicity, show potential for the development of chemotherapeutic agents. Several vanadium complexes have been reported that show preventive effects against chemical carcinogenesis and towards the modification of several xenobiotic enzymes, and which reduce the formation of carcinogen-derived active metabolites. Some also inhibit cellular tyrosine phosphatases or/and activate tyrosine phosphorylases, which interfere directly or indirectly with the signal transduction pathways that lead to apoptosis or/and activation of tumour-suppressor genes. Additionally, their potential ability to induce cell-cycle arrest or/and cytotoxic effects through DNA cleavage has been observed; furthermore, plasma-membrane lipoperoxidation mediated by ROS generated through Fenton-like reactions initiated by the intracellular reduction of V(V) to V(IV) has been reported. Inhibitory metastatic effects have also been described for vanadium complexes that can modulate cellular adhesion, and reverse antineoplastic drug resistance.<sup>97</sup>

Iron is a biometal involved in important cell processes like energy metabolism, respiration and DNA synthesis. Ferrocene derivatives have been reported that exhibit anti-

tumour activity, which is ascribed to the redox properties of the metal centre that mediates DNA cleaving.<sup>98</sup> Several Fe(II) compounds have been described that present both *in vitro* and *in vivo* anti-neoplastic properties or promising anticancer activities through apoptotic and necrotic mechanisms.<sup>72</sup>

#### *Cobalt, Nickel and Palladium complexes*

A number of Ni, Pd, Ir and Os complexes have been reported in the literature.<sup>99</sup>

Several Co(II) and Co(III) complexes with interesting activities have been described; they often preferentially interact with non-classical biological targets such as specific proteins and enzymes.<sup>30</sup> For instance, some of them are capable of inhibiting enzymes involved in the metastatic process.<sup>100</sup> Other cobalt complexes have been designed to be photoactivated; hence, remarkable results for potential application in photodynamic therapy (PDT) have been achieved.<sup>101</sup>

Nickel-containing complexes, prepared from active ligands like quercetin<sup>102</sup> or thiosemicarbazones,<sup>103,104</sup> have been reported that show effective cytotoxic activities against a number human cancer cell lines.<sup>105</sup> Their activity mainly results from their interaction with DNA through (i) intercalation, (ii) selective DNA binding, (iii) oxidative DNA damage or (iv) DNA-DNA crosslink formation, which promotes cell apoptosis.<sup>106,107</sup> Ni(II) complexes with salphen-type ligands have been described that show a higher selectivity towards telomeric quadruplex compared with duplex DNA.<sup>108,109</sup> Nickel compounds are also designed for their potential ability to interact with proteins.

Due to its similar chemical and physical properties with platinum, palladium represents one of the possible alternatives to Pt.<sup>110</sup> Thus, Pd(II) complexes with aromatic *N*- and *N,N*-containing ligands such as derivatives of pyridine, quinoline, pyrazole and 1,10-phenanthroline, and with *N,S*-chelating ligands like thiosemicarbazones and dithiocarbamates have shown promising activities against tumour cell lines, in some cases even greater than those of their platinum analogues.<sup>111</sup> It should be pointed out that the design and synthesis of Pd(II)-containing complexes is challenging and that the choice of the ligands is not innocent. The stability of Pd(II) complexes is lower than that of their Pt(II) analogues. They present a faster ligand exchange ( $10^4$ – $10^5$  times faster), which compromises their structural integrity in biological fluids.<sup>112</sup>

#### *Manganese complexes*

Manganese is a redox-active metal that is involved in a number of biochemical and physiological processes of living organisms. Several Mn-based complexes have been prepared that may act as therapeutic agents; however, their efficiency has only been demonstrated with





animals.<sup>113</sup> Manganese complexes with salen- and salphen-type ligands with antitumor activity, attributed to their DNA-binding properties, have been reported. These compounds may inhibit cell proliferation, facilitate programmed cell death *via* a mitochondrial pathway, inhibit proteasome activity or exhibit anti-neoplastic behaviour.<sup>72,114,115</sup>

Recently, a manganese-porphyrin complex has been described that binds strongly to telomeric quadruplex, hence inhibiting telomerase.<sup>116</sup>

### *Copper and Zinc complexes*

Copper and zinc are essential trace elements, which are indispensable to the normal functioning of enzymes and biochemical processes. These two bio-metals represent appealing alternatives to platinum; actually, potential anticancer compounds based on copper and zinc have been reported that are less toxic and more effective than cisplatin.<sup>117</sup>

Copper, which is involved in redox chemical reactions, cellular growth and angiogenesis, has a long history of medical applications.<sup>118</sup> Copper(I) has a clear preference for sulfur ligands, whereas copper(II) is preferentially coordinated by nitrogen-donor atoms (from proteins or DNA) or oxygen donors (specially from proteins).<sup>119</sup> The toxicity of copper-based complexes is a consequence of their ability to change the cellular redox balance, through the production of reactive oxygen species (ROS). ROS can induce lipid peroxidation and/or DNA and RNA cleavage. ROS generation (through Fenton-type chemical reactions) in the presence of superoxide anions or of reducing agents, such as ascorbic acid or glutathione (GSH), leads to the activation of redox-signalling pathways, resulting in apoptosis.<sup>118,120</sup>

After the discovery of the nuclease properties of  $[\text{Cu}(\text{phen})_2]^{2+}$  (phen = 1,10-phenanthroline), new complexes from heterocyclic ligands have been designed.<sup>121,122</sup> The development of copper-based compounds has received great attention from the scientific community since the past two decades.<sup>79</sup>

Zinc(II) ions play a critical role in cellular metabolism regulation. Zn(II) complexes have been used as radioprotective agents, tumour photosensitizers, antidiabetic and insulin-mimetic compounds, or for their antibacterial or antimicrobial activities. Some studies on zinc complexes with cytotoxic properties revealed that their activities were due to their Lewis acid behaviour, mediating the hydrolysis of DNA phosphodiester bonds. Recently, it has been shown that, against all expectations, some zinc complexes can act as nucleases, cleaving oxidatively DNA.<sup>123</sup> Zinc complexes may exhibit fluorescence properties, which can be exploited for imaging or sensing applications. For instance, such probes can be useful tools to study biochemical processes or to investigate the uptake of some drugs and their associated cellular pathway(s).<sup>124-126</sup>

### *Gallium complexes*

Gallium is chemically close to iron, in terms of electrical charge, ion diameter, coordination number and electronic configuration. Recent studies showed that the uptake of gallium is mediated by transferrin receptors; its competitive binding to the protein with iron can cause the inhibition of DNA synthesis.<sup>127</sup> At low gallium concentrations, it is preferentially bound to the phosphates of DNA, with which it forms a stable complex.<sup>128</sup> Gallium may also compete with magnesium for DNA binding, with an affinity 100 times higher. Gallium(III) chloride and gallium(III) nitrate entered clinical trials, but were rapidly discarded due to their low absorption, their nephrotoxicity, optical neuropathy and other severe side effects.<sup>129</sup> Two Ga(III) complexes are currently on clinical trials, with remarkable anti-apoptotic, antimetastatic and antineoplastic properties.<sup>130</sup> The mechanism of action of Gallium(III)-based compounds involves the inhibition of ribonucleotide reductase (RR), which is the enzyme catalysing the conversion of ribonucleotides to deoxyribonucleotides that are highly expressed in tumour cells.<sup>131</sup>

### *Gold complexes*

Gold(I) complexes have entered clinical trials for their immunosuppressive and anti-inflammatory properties.<sup>132</sup> Since there is a reflexive relationship between cancer and inflammation, the design of gold coordination compounds has gained great interest in recent years. Encouraging results have been achieved, especially with gold-dithiocarbamate complexes, which show high stability, interesting antiproliferative activity and selectivity towards cancer cells.<sup>132</sup> In some cases, the gold compounds exhibit higher toxicity than cisplatin, and are capable of overcoming cisplatin resistance.<sup>133</sup> The main targets of this new class of compounds appear to be some proteins/enzymes, *e.g.* cathepsins, tyrosine phosphatases, thioredoxin reductase, deubiquitinases, and some apoptotic proteins, *i.e.* MAPKs and Bcl-2, or cyclooxygenase. Thus, these gold-containing molecules trigger anti-mitochondrial effects and induce apoptotic events, among others.<sup>134</sup> It is also worth mentioning that gold(III) complexes have been exploited for their “switch-on” fluorescent properties. The biological reduction of Au(III) to Au(I) by thiols, such as glutathione or cysteine, turns on the fluorescence, the emission experiencing a 200-times enhancement.<sup>135</sup> Gold-phosphane complexes<sup>136</sup> and Cu(I) and Ag(I) analogues have been reported, which show remarkable cytotoxic activities.





### ***Final remarks and objectives of this thesis***

Most chemotherapeutic drugs that are used clinically present undesirable side effects, which arise from their common lack of specificity and selectivity. The development of more efficient anticancer agents therefore still represents one of the big conundrums faced by the scientific and the medical communities.

The main aim of the present thesis is to use different chemical approaches to design metal-based compounds with great cytotoxic activities or/and selectivity or/and specificity. The rich diversity of research fields in (inorganic) chemistry provides a limitless set of possibilities to achieve these goals.

The research work carried out is divided into three chapters reflecting the different “chemical pathways” employed to generate potential anticancer metallodrugs.

Chapter II is devoted to “*Coordination Chemistry*”; the goal is to design and prepared highly cytotoxic small molecules, namely a series of copper(II) coordination compounds. The idea is to produce simple and very toxic compounds from cheap metal ions (which moreover are of biological relevance), whose mechanism of action originates from DNA cleavage. Selectivity with such highly active metal-based compounds may then be obtained through encapsulation.

Chapter III involves “*Organometallic Chemistry*”; ruthenium(II) piano-stool compounds have shown remarkable properties, particularly as antimetastatic agents. Hence, a new family of half-sandwich ruthenium(II) compounds is investigated, and structure-activity relationships are evaluated (*via in vitro* biological studies). These Ru(II) compounds are based on PR<sub>3</sub> phosphane ligands, whose activity can be fine-tuned through the choice of the R groups (actually, the phosphanes may contain three different R groups, namely R<sup>1</sup>, R<sup>2</sup> and R<sup>3</sup>).

Chapter IV is dedicated to “*Supramolecular Chemistry*”; the supramolecular recognition of DNA (for example by some proteins) is of paramount importance in cellular processes. Thus, artificial molecules that can bind to DNA, hence blocking vital cycles, are of therapeutic interest. The goal is to design supramolecular iron-based structures able to target and recognize specific and noncanonical DNA architectures (*e.g.* three-way junctions). The new iron(III) helicates designed and prepared are thus expected to target not only the major groove of DNA, but also to stabilize non-conventional structures of the biomolecule. The DNA-binding properties of the supramolecules are studied together with their effect of the cell cycle.





## References

- (1) Avendaño, C.; Menéndez, J. C. *Medicinal chemistry of anticancer drugs*; 1st ed.; Elsevier: Amsterdam ; Boston, 2008.
- (2) Cattley, R. C.; Radinsky, R. R. *Toxicol. Pathol.* **2004**, *32 Suppl 1*, 116.
- (3) Hanahan, D.; Weinberg, R. A. *Cell* **2000**, *100*, 57.
- (4) Siegel, R. L.; Miller, K. D.; Jemal, A. *CA Cancer J. Clin.* **2016**, *66*, 7.
- (5) Stewart, B. W.; Wild, C.; International Agency for Research on Cancer; World Health Organization *World cancer report 2014*; International Agency for Research on Cancer WHO Press: Lyon, France Geneva, Switzerland, 2014.
- (6) Ferlay, J.; Soerjomataram, I.; Dikshit, R.; Eser, S.; Mathers, C.; Rebelo, M.; Parkin, D. M.; Forman, D.; Bray, F. *Int. J. Cancer* **2015**, *136*, E359.
- (7) Arya, R.; White, K. *Semin. Cell Dev. Biol.* **2015**, *39*, 12.
- (8) Huangfu, W. C.; Fuchs, S. Y. *Genes Cancer* **2010**, *1*, 725.
- (9) Laplante, M.; Sabatini, D. M. *Cell* **2012**, *149*, 274.
- (10) Martin, G. S. *Cancer Cell* **2003**, *4*, 167.
- (11) Wang, S. Y.; Yu, Q. J.; Zhang, R. D.; Liu, B. *Int. J. Biochem. Cell Biol.* **2011**, *43*, 1263.
- (12) Hornberg, J. J.; Bruggeman, F. J.; Westerhoff, H. V.; Lankelma, J. *BioSyst.* **2006**, *83*, 81.
- (13) Futreal, P. A.; Coin, L.; Marshall, M.; Down, T.; Hubbard, T.; Wooster, R.; Rahman, N.; Stratton, M. R. *Nat. Rev. Cancer* **2004**, *4*, 177.
- (14) Vogelstein, B.; Kinzler, K. W. *Nat. Med.* **2004**, *10*, 789.
- (15) Gabriel, J. *The biology of cancer*; 2nd ed.; John Wiley & Sons: Chichester ; Hoboken, NJ, 2007.
- (16) Bertram, J. S. *Mol. Aspects Med.* **2000**, *21*, 167.
- (17) Weber, G. F. *Cancer Lett.* **2008**, *270*, 181.
- (18) Price, J. T.; Bonovich, M. T.; Kohn, E. C. *Crit. Rev. Biochem. Mol. Biol.* **1997**, *32*, 175.
- (19) Nishida, N.; Yano, H.; Nishida, T.; Kamura, T.; Kojiro, M. *Vasc. Health Risk Manag.* **2006**, *2*, 213.
- (20) Hanahan, D.; Weinberg, R. A. *Cell* **2011**, *144*, 646.
- (21) Weber, G. F. *Molecular mechanisms of cancer*; Springer: Dordrecht, The Netherlands, 2007.
- (22) Benada, J.; Macurek, L. *Biomolecules* **2015**, *5*, 1912.
- (23) Sebolt-Leopold, J. S.; English, J. M. *Nature* **2006**, *441*, 457.
- (24) Weinstein, I. B. *Cancer Res.* **1988**, *48*, 4135.
- (25) Daniel, T. M. *Int. J. Tuberc. Lung Dis.* **2008**, *12*, 113.
- (26) Chabner, B. A.; Roberts, T. G., Jr. *Nat. Rev. Cancer* **2005**, *5*, 65.
- (27) DeVita, V. T., Jr.; Chu, E. *Cancer Res.* **2008**, *68*, 8643.
- (28) Galmarini, D.; Galmarini, C. M.; Galmarini, F. C. *Crit. Rev. Oncol. Hematol.* **2012**, *84*, 181.
- (29) Watson, J. D.; Crick, F. H. *Nature* **1953**, *171*, 737.
- (30) Bruijninx, P. C.; Sadler, P. J. *Curr. Opin. Chem. Biol.* **2008**, *12*, 197.
- (31) Hurley, L. H. *Nat. Rev. Cancer* **2002**, *2*, 188.
- (32) Maiti, M.; Kumar, G. S. *Med. Res. Rev.* **2007**, *27*, 649.
- (33) Ghosh, A.; Bansal, M. *Acta Crystallogr. D. Biol. Crystallogr.* **2003**, *59*, 620.
- (34) Hurley, L. H. *Biochem. Soc. Trans.* **2001**, *29*, 692.

- (35) Saini, N.; Zhang, Y.; Usdin, K.; Lobachev, K. S. *Biochimie* **2013**, *95*, 117.
- (36) Stefan, L.; Bertrand, B.; Richard, P.; Le Gendre, P.; Denat, F.; Picquet, M.; Monchaud, D. *ChemBioChem* **2012**, *13*, 1905.
- (37) Dickerson, R. E.; Drew, H. R.; Conner, B. N.; Wing, R. M.; Fratini, A. V.; Kopka, M. L. *Science* **1982**, *216*, 475.
- (38) Neidle, S. *Nucleic acid structure and recognition*; Oxford University Press: Oxford ; New York, 2002.
- (39) Harteis, S.; Schneider, S. *Int. J. Mol. Sci.* **2014**, *15*, 12335.
- (40) Svozil, D.; Kalina, J.; Omelka, M.; Schneider, B. *Nucleic Acids Res.* **2008**, *36*, 3690.
- (41) Belmont, P.; Constant, J.-F.; Demeunynck, M. *Chem. Soc. Rev.* **2001**, *30*, 70.
- (42) Arnott, S.; Chandrasekaran, R.; Hall, I. H.; Puigjaner, L. C.; Walker, J. K.; Wang, M. *Cold Spring Harb. Symp. Quant. Biol.* **1983**, *47 Pt 1*, 53.
- (43) Wood, B. R. *Chem. Soc. Rev.* **2016**, *45*, 1999.
- (44) Brabec, V. *Prog. Nucleic Acid. Res. Mol. Biol.* **2002**, *71*, 1.
- (45) Rueff, J.; Rodrigues, A. S. *Methods Mol. Biol.* **2016**, *1395*, 1.
- (46) Hadjiladis, N. D.; Sletten, E. *Metal complex - DNA interactions*; 1st ed.; Wiley: Chichester, West Sussex, U.K., 2009.
- (47) Egli, M.; Pallan, P. S. *Curr. Opin. Struct. Biol.* **2010**, *20*, 262.
- (48) Komeda, S.; Moulaei, T.; Woods, K. K.; Chikuma, M.; Farrell, N. P.; Williams, L. D. *J. Am. Chem. Soc.* **2006**, *128*, 16092.
- (49) Pavletich, N. P.; Pabo, C. O. *Science* **1991**, *252*, 809.
- (50) Lokey, R. S.; Kwok, Y.; Guelev, V.; Pursell, C. J.; Hurley, L. H.; Iverson, B. L. *J. Am. Chem. Soc.* **1997**, *119*, 7202.
- (51) Brana, M. F.; Cacho, M.; Gradillas, A.; de Pascual-Teresa, B.; Ramos, A. *Curr. Pharm. Des.* **2001**, *7*, 1745.
- (52) Nelson, S. M.; Ferguson, L. R.; Denny, W. A. *Mutat. Res.* **2007**, *623*, 24.
- (53) Liu, H. K.; Sadler, P. J. *Acc. Chem. Res.* **2011**, *44*, 349.
- (54) Bewley, C. A.; Gronenborn, A. M.; Clore, G. M. *Annu. Rev. Biophys. Biomol. Struct.* **1998**, *27*, 105.
- (55) Cai, X.; Gray, P. J., Jr.; Von Hoff, D. D. *Cancer Treat. Rev.* **2009**, *35*, 437.
- (56) Chaires, J. B. *Arch. Biochem. Biophys.* **2006**, *453*, 26.
- (57) Hamilton, P. L.; Arya, D. P. *Nat. Prod. Rep.* **2012**, *29*, 134.
- (58) Cardo, L.; Hannon, M. J. *Inorg. Chim. Acta* **2009**, *362*, 784.
- (59) Cerasino, L.; Hannon, M. J.; Sletten, E. *Inorg. Chem.* **2007**, *46*, 6245.
- (60) Ducani, C.; Leczkowska, A.; Hodges, N. J.; Hannon, M. J. *Angew. Chem. Int. Ed. Engl.* **2010**, *49*, 8942.
- (61) Nelson, S. M.; Ferguson, L. R.; Denny, W. A. *Cell Chromosome* **2004**, *3*, 2.
- (62) Cardo, L.; Sadovnikova, V.; Phongtongpasuk, S.; Hodges, N. J.; Hannon, M. J. *Chem. Commun. (Camb)* **2011**, *47*, 6575.
- (63) Strekowski, L.; Wilson, B. *Mutat. Res.* **2007**, *623*, 3.
- (64) Albert, F. G.; Eckdahl, T. T.; Fitzgerald, D. J.; Anderson, J. N. *Biochemistry* **1999**, *38*, 10135.
- (65) Tuite, E.; Sehlstedt, U.; Hagmar, P.; Norden, B.; Takahashi, M. *Eur. J. Biochem.* **1997**, *243*, 482.





- (66) Sinden, R. R.; Potaman, V. N.; Oussatcheva, E. A.; Pearson, C. E.; Lyubchenko, Y. L.; Shlyakhtenko, L. S. *J. Biosci.* **2002**, *27*, 53.
- (67) Malina, J.; Hannon, M. J.; Brabec, V. *Chem. Eur. J.* **2008**, *14*, 10408.
- (68) Childs, L. J.; Malina, J.; Rolfsnes, B. E.; Pascu, M.; Prieto, M. J.; Broome, M. J.; Rodger, P. M.; Sletten, E.; Moreno, V.; Rodger, A.; Hannon, M. J. *Chem. Eur. J.* **2006**, *12*, 4919.
- (69) Oleksy, A.; Blanco, A. G.; Boer, R.; Uson, I.; Aymami, J.; Rodger, A.; Hannon, M. J.; Coll, M. *Angew. Chem. Int. Ed. Engl.* **2006**, *45*, 1227.
- (70) Vuong, S.; Stefan, L.; Lejault, P.; Rousselin, Y.; Denat, F.; Monchaud, D. *Biochimie* **2012**, *94*, 442.
- (71) Haq, I.; Ladbury, J. *J. Mol. Recognit.* **2000**, *13*, 188.
- (72) Ali, A.; Bhattacharya, S. *Bioorg. Med. Chem.* **2014**, *22*, 4506.
- (73) Jamieson, E. R.; Lippard, S. J. *Chem. Rev.* **1999**, *99*, 2467.
- (74) Guo, Z.; Sadler, P. J. *Angew. Chem. Int. Ed. Engl.* **1999**, *38*, 1512.
- (75) Sun, H.; Li, H.; Sadler, P. J. *Chem. Rev.* **1999**, *99*, 2817.
- (76) Gianferrara, T.; Bratsos, I.; Alessio, E. *Dalton Trans.* **2009**, 7588.
- (77) Reisner, E.; Arion, V. B.; Keppler, B. K.; Pombeiro, A. J. L. *Inorg. Chim. Acta* **2008**, *361*, 1569.
- (78) Olmsted, J., 3rd; Kearns, D. R. *Biochemistry* **1977**, *16*, 3647.
- (79) Brissos, R. F.; Caubet, A.; Gamez, P. *Eur. J. Inorg. Chem.* **2015**, *2015*, 2633.
- (80) Schatzschneider, U. *Eur. J. Inorg. Chem.* **2010**, *2010*, 1451.
- (81) Allardyce, C. S.; Dyson, P. J. *Dalton Trans.* **2016**, *45*, 3201.
- (82) Johnstone, T. C.; Suntharalingam, K.; Lippard, S. J. *Chem. Rev.* **2016**, *116*, 3436.
- (83) Dyson, P. J.; Sava, G. *Dalton Trans.* **2006**, 1929.
- (84) Bonetti, A. *Platinum and other heavy metal compounds in cancer chemotherapy : molecular mechanisms and clinical applications*; Humana Press: New York, 2009.
- (85) Dilruba, S.; Kalayda, G. V. *Cancer Chemother. Pharmacol.* **2016**, *77*, 1103.
- (86) Todd, R. C.; Lippard, S. J. *Metallomics* **2009**, *1*.
- (87) Leijen, S.; Burgers, S. A.; Baas, P.; Pluim, D.; Tibben, M.; van Werkhoven, E.; Alessio, E.; Sava, G.; Beijnen, J. H.; Schellens, J. H. *Invest. New Drugs* **2015**, *33*, 201.
- (88) Ronconi, L.; Sadler, P. J. *Coord. Chem. Rev.* **2007**, *251*, 1633.
- (89) Scolaro, C.; Bergamo, A.; Brescacin, L.; Delfino, R.; Cocchietto, M.; Laurenczy, G.; Geldbach, T. J.; Sava, G.; Dyson, P. J. *J. Med. Chem.* **2005**, *48*, 4161.
- (90) Babak, M. V.; Meier, S. M.; Huber, K. V. M.; Reynisson, J.; Legin, A. A.; Jakupec, M. A.; Roller, A.; Stukalov, A.; Gridling, M.; Bennett, K. L.; Colinge, J.; Berger, W.; Dyson, P. J.; Superti-Furga, G.; Keppler, B. K.; Hartinger, C. G. *Chem. Sci.* **2015**, *6*, 2449.
- (91) Brunner, J.; Barton, J. K. *J. Am. Chem. Soc.* **2006**, *128*, 6772.
- (92) Copeland, K. D.; Fitzsimons, M. P.; Houser, R. P.; Barton, J. K. *Biochemistry* **2002**, *41*, 343.
- (93) Menon, E. L.; Perera, R.; Navarro, M.; Kuhn, R. J.; Morrison, H. *Inorg. Chem.* **2004**, *43*, 5373.
- (94) Harlos, M.; Ott, I.; Gust, R.; Alborzinia, H.; Wolfl, S.; Kromm, A.; Sheldrick, W. S. *J. Med. Chem.* **2008**, *51*, 3924.
- (95) Dabrowiak, J. C. *Metals in medicine*; Wiley: Hoboken, 2009.
- (96) Melendez, E. *Crit. Rev. Oncol. Hematol.* **2002**, *42*, 309.

- (97) Evangelou, A. M. *Crit. Rev. Oncol. Hematol.* **2002**, *42*, 249.
- (98) van Rijt, S. H.; Sadler, P. J. *Drug Discov. Today* **2009**, *14*, 1089.
- (99) Farrell, N. *Transition metal complexes as drugs and chemotherapeutic agents*; Kluwer Academic Publishers: Dordrecht ; Boston, 1989.
- (100) Failes, T. W.; Cullinane, C.; Diakos, C. I.; Yamamoto, N.; Lyons, J. G.; Hambley, T. W. *Chem. Eur. J.* **2007**, *13*, 2974.
- (101) Garai, A.; Pant, I.; Banerjee, S.; Banik, B.; Kondaiah, P.; Chakravarty, A. R. *Inorg. Chem.* **2016**, *55*, 6027.
- (102) Tan, J.; Zhu, L.; Wang, B. *BioMetals* **2010**, *23*, 1075.
- (103) Chen, J.; Huang, Y. W.; Liu, G.; Afrasiabi, Z.; Sinn, E.; Padhye, S.; Ma, Y. *Toxicol. Appl. Pharmacol.* **2004**, *197*, 40.
- (104) Kalaivani, P.; Saranya, S.; Poornima, P.; Prabhakaran, R.; Dallemer, F.; Vijaya Padma, V.; Natarajan, K. *Eur. J. Med. Chem.* **2014**, *82*, 584.
- (105) Zhao, C.; Chen, X.; Zang, D.; Lan, X.; Liao, S.; Yang, C.; Zhang, P.; Wu, J.; Li, X.; Liu, N.; Liao, Y.; Huang, H.; Shi, X.; Jiang, L.; Liu, X.; He, Z.; Dou, Q. P.; Wang, X.; Liu, J. *Oncogene* **2016**.
- (106) Atasever, B.; Ulkuseven, B.; Bal-Demirci, T.; Erdem-Kuruca, S.; Solakoglu, Z. *Invest. New. Drugs.* **2010**, *28*, 421.
- (107) Lauria, A.; Bonsignore, R.; Terenzi, A.; Spinello, A.; Giannici, F.; Longo, A.; Almerico, A. M.; Barone, G. *Dalton Trans.* **2014**, *43*, 6108.
- (108) Reed, J. E.; Arnal, A. A.; Neidle, S.; Vilar, R. *J. Am. Chem. Soc.* **2006**, *128*, 5992.
- (109) Das, M.; Nasani, R.; Saha, M.; Mobin, S. M.; Mukhopadhyay, S. *Dalton Trans.* **2015**, *44*, 2299.
- (110) Kapdi, A. R.; Fairlamb, I. J. S. *Chem. Soc. Rev.* **2014**, *43*, 4751.
- (111) Jahromi, E. Z.; Divsalar, A.; Saboury, A. A.; Khaleghizadeh, S.; Mansouri-Torshizi, H.; Kostova, I. *J. Iran. Chem. Soc.* **2016**, *13*, 967.
- (112) Ulukaya, E.; Ari, F.; Dimas, K.; Ikitimur, E. I.; Guney, E.; Yilmaz, V. *T. Eur. J. Med. Chem.* **2011**, *46*, 4957.
- (113) Farrell, N.; Royal Society of Chemistry (Great Britain) *Uses of inorganic chemistry in medicine*; Royal Society of Chemistry: Cambridge, 1999.
- (114) Zhang, Z.; Bi, C.; Fan, Y.; Wang, H.; Bao, Y. *Int. J. Mol. Med.* **2015**, *36*, 1143.
- (115) Al-Anbaky, Q.; Al-Karakooly, Z.; Kilaparty, S. P.; Agrawal, M.; Albkuri, Y. M.; RanguMagar, A. B.; Ghosh, A.; Ali, N. *Int. J. Toxicol.* **2016**.
- (116) Dixon, I. M.; Lopez, F.; Tejera, A. M.; Esteve, J. P.; Blasco, M. A.; Pratviel, G.; Meunier, B. *J. Am. Chem. Soc.* **2007**, *129*, 1502.
- (117) Silva, J. J. R. F. d.; Williams, R. J. P. *The biological chemistry of the elements : The inorganic chemistry of life*; 2nd ed.; Oxford University Press: Oxford ; New York, 2001.
- (118) Brissos, R. F.; García, S.; Presa, A.; Gamez, P. *Comments Inorg. Chem.* **2011**, *32*, 219.
- (119) Sava, G.; Bergamo, A.; Dyson, P. J. *Dalton Trans.* **2011**, *40*, 9069.
- (120) Marzano, C.; Pellei, M.; Tisato, F.; Santini, C. *Anticancer Agents Med. Chem.* **2009**, *9*, 185.
- (121) Qiao, X.; Ma, Z. Y.; Xie, C. Z.; Xue, F.; Zhang, Y. W.; Xu, J. Y.; Qiang, Z. Y.; Lou, J. S.; Chen, G. J.; Yan, S. P. *J. Inorg. Biochem.* **2011**, *105*, 728.
- (122) Sigman, D. S. *Acc. Chem. Res.* **1986**, *19*, 180.





- (123) Maheswari, P. U.; Barends, S.; Ozalp-Yaman, S.; de Hoog, P.; Casellas, H.; Teat, S. J.; Massera, C.; Lutz, M.; Spek, A. L.; van Wezel, G. P.; Gamez, P.; Reedijk, J. *Chem. Eur. J.* **2007**, *13*, 5213.
- (124) Storr, T.; Thompson, K. H.; Orvig, C. *Chem. Soc. Rev.* **2006**, *35*, 534.
- (125) Brissos, R.; Ramos, D.; Lima, J. C.; Mihan, F. Y.; Borràs, M.; de Lapuente, J.; Cort, A. D.; Rodríguez, L. *New J. Chem.* **2013**, *37*, 1046.
- (126) Giannicchi, I.; Brissos, R.; Ramos, D.; de Lapuente, J.; Lima, J. C.; Dalla Cort, A.; Rodriguez, L. *Inorg. Chem.* **2013**, *52*, 9245.
- (127) Turel, I.; Kljun, J. *Curr. Top. Med. Chem.* **2011**, *11*, 2661.
- (128) Collery, P.; Keppler, B.; Madoulet, C.; Desoize, B. *Crit. Rev. Oncol. Hematol.* **2002**, *42*, 283.
- (129) Kaluderovic, G. N.; Paschke, R. *Curr. Med. Chem.* **2011**, *18*, 4738.
- (130) Jakupec, M. A.; Keppler, B. K. *Curr. Top. Med. Chem.* **2004**, *4*, 1575.
- (131) Chen, D.; Milacic, V.; Frezza, M.; Dou, Q. P. *Curr. Pharm. Des.* **2009**, *15*, 777.
- (132) Nardon, C.; Boscutti, G.; Fregona, D. *Anticancer Res.* **2014**, *34*, 487.
- (133) Tu, S.; Wai-Yin Sun, R.; Lin, M. C.; Tao Cui, J.; Zou, B.; Gu, Q.; Kung, H. F.; Che, C. M.; Wong, B. C. *Cancer* **2009**, *115*, 4459.
- (134) Casini, A.; Messori, L. *Curr. Top. Med. Chem.* **2011**, *11*, 2647.
- (135) Muhammad, N.; Guo, Z. *Curr. Opin. Chem. Biol.* **2014**, *19*, 144.
- (136) Lima, J. C.; Rodriguez, L. *Anticancer Agents Med. Chem.* **2011**, *11*, 921.





# 1

## Targeting cancer with small molecules: Copper complexes

*Copper is a transition metal and an essential micronutrient involved in critical life processes that are well-preserved throughout all life forms.<sup>1</sup> This ubiquitous element can also have toxic effects in biological systems if not properly regulated.*

*Several aspects of the chemistry and biochemistry of copper make it the perfect ally to develop new compounds for potential medical applications. Among them, we can highlight its different oxidation states and the interesting and rich chemistry of complexes based on this metal. Through the years, several copper(II)-centred compounds have been reported to be promising and/or are being used as viable alternatives to cisplatin, and their mechanism of action, biodistribution and toxicity have been thoroughly studied.<sup>2-7</sup>*

*In this chapter, the design and preparation of a series of unique copper(II) complexes with different Schiff-base ligands inspired by 4-methyl-2-N-(2-pyridylmethylene)aminophenol (Hpyrimol) are reported. The biologic investigation of these new molecules with DNA and different cell lines is subsequently described.*

### Contents

<i>Schiff bases</i> .....	32
SYNTHESIS.....	34
<i>Preparation of the ligands</i> .....	34
Synthesis of 2- <i>tert</i> -butyl-6-(pyridin-2-ylhydrazonomethyl)phenol (HL1).....	34
Synthesis of 2- <i>tert</i> -butyl-6-(quinolin-2-ylhydrazonomethyl)phenol (HL2).....	34
Synthesis of 4- <i>tert</i> -butyl-2,6-bis-(pyridin-2-ylhydrazonomethyl)phenol (HL3).....	35
Synthesis of 4- <i>tert</i> -butyl-2,6-bis-(quinolin-2-ylhydrazonomethyl)phenol (HL4).....	35
<i>General method for the preparation of the complexes</i> .....	36
[Cu(L1)Cl]·CH <sub>3</sub> OH (Cu1).....	36
[Cu(L2)NO <sub>3</sub> ] (Cu2) .....	38

---

Crystallographic and refinement parameters for Cu2 are summarized in Table 5, and selected coordination bond lengths and angles are listed in Table 3. ....	38
[Cu <sub>2</sub> (L3)(ClO <sub>4</sub> ) <sub>2</sub> (CH <sub>3</sub> O)(CH <sub>3</sub> OH)]·CH <sub>3</sub> OH (Cu3).....	39
[Cu <sub>2</sub> (L4)(ClO <sub>4</sub> )(OH)(CH <sub>3</sub> OH)]ClO <sub>4</sub> (Cu4) .....	41
[Cu <sub>8</sub> (L3) <sub>4</sub> (NO <sub>3</sub> ) <sub>4</sub> (OH) <sub>5</sub> ](NO <sub>3</sub> ) <sub>3</sub> ·(CH <sub>3</sub> OH) <sub>5</sub> ·(H <sub>2</sub> O) <sub>8</sub> (Cu5) .....	44
[Cu <sub>3</sub> (HL2') <sub>4</sub> Cl <sub>6</sub> ]·(CH <sub>3</sub> OH) <sub>6</sub> (Cu6).....	47
DNA-BINDING STUDIES .....	51
<i>UV-Vis Spectroscopy</i> .....	51
<i>ESI-MS and EPR spectroscopy</i> .....	54
<i>Fluorescence-dye displacement</i> .....	56
<i>Agarose-gel electrophoresis</i> .....	60
<i>AFM experiments</i> .....	62
CELL-VIABILITY ASSAYS.....	63
<i>MTT Reduction Assay</i> .....	64
CONCLUSIONS.....	70
REFERENCES .....	72

---





Evolution took advantage of the bioavailability of copper as well as its ability to catalyse oxidation–reduction reactions (*i.e.*, redox properties). Hence, this metal is found in the catalytic site of several metallo-proteins and enzymes, as a fundamental co-factor. Thus, copper is one of the most important essential biometals, playing a key role in many biological systems. It is involved in various chemical processes, including electron-transfer reactions, which, for instance, are crucial in biochemical processes that support life such as embryo development, connective tissue formation, temperature control and nerve cell function.<sup>1,2</sup> Therefore, any disruption of copper homeostasis will result in biological failures; this (bio)element can be converted into a toxic agent, leading to numerous types of cell damage and/or metabolism abnormalities.<sup>3,4</sup> In cancer cells, there is a significant imbalance of copper levels, with an increase that reaches several folds its normal concentration. Its increased amount appears to be essential for cancer development and progression, *i.e.* tumour growth, invasion and metastasis, and as a stimulus for angiogenic processes.<sup>5-8</sup> This imbalance, as well as an altered cell metabolism has a strong impact on the transport and distribution of copper and its conversion from copper(II) to copper(I). This reduction can take place in (i) the plasma membrane with plasma-membrane reductases or (ii) directly inside the tumorous cells, where the environment is strongly reductive. The reducing environment is consequence of the lower oxygen concentration in tumour tissues and the increased expression of glutathione (*i.e.* a reducing agent). It can be mentioned here that tumours have a lower pH than normal tissues, due to the excess of lactic acid generated by glycolysis (which represents the principal source of energy for these abnormal cells).<sup>6</sup> Once inside the cell, copper(I) has the potential to generate reactive oxygen species (ROS), like the hydroxyl radical ( $\bullet\text{OH}$ ) or singlet oxygen ( $^1\text{O}_2$ ), *via* Fenton- and Haber–Weiss-type reactions.<sup>9-11</sup> These ROS are able to react with a wide variety of biological molecules including proteins, lipids and DNA, leading to protein oxidation, lipid peroxidation and DNA strand breaks, respectively.<sup>12,13</sup>

The rich chemistry of copper is a versatile tool for the design of potential chemotherapeutic drugs. The cytotoxic properties of several classes of copper coordination compounds have been comprehensively accessed, *in vitro*, but only a limited number of them have been evaluated *in vivo*, *i.e.*, using preclinical animal models.<sup>14-16</sup>

The copper redox activity, and consequently, its ability to produce ROS,<sup>17</sup> the lability of copper complexes, the malleability of the copper centre and its facility to adopt distorted coordination geometries<sup>15</sup> allow the use of a wide variety of ligands, from mono to hexadentate chelates, and to design and obtain molecules with interesting cytotoxic properties.<sup>14</sup> Copper(I), copper(II), copper(III) or even copper(IV) complexes may be generated.<sup>4</sup> Complexes

containing a copper(I) centre can be prepared with halides,<sup>18</sup> amines<sup>19,20</sup> and phosphanes,<sup>21</sup> adopting preferentially a tetrahedral geometry. The most commonly described complexes are copper(II) compounds based on multidentate ligands. A less usual oxidation state is found in complexes containing copper(III) ions, which can be obtained by oxidizing copper(I) or copper(II) compounds using various oxidizing agents. Finally, copper(IV) complexes are very rare and their preparation frequently involves the use of  $F^-$  and  $O^{2-}$ .<sup>5</sup>

Dwyer and co-workers reported the first copper complex with interesting cytotoxic properties regarding cellular-growth inhibition.<sup>22</sup> Some years later, Sigman and co-workers discovered and characterized the first copper chemical nuclease, namely  $[Cu(phen)_2]^{2+}$  (phen = 1,10-phenanthroline).<sup>23-25</sup> This compound strongly interacts with DNA, and its nuclease activity *in vivo* and *in vitro* has been extensively investigated.<sup>26-34</sup> Recent studies report a synergistic effect between this copper complex and *cis*-diammineplatinum(II) dichloride (cisplatin) towards some cancer-cell lines and, most remarkably, their cisplatin-resistant sublines.<sup>35,36</sup> These pioneering studies encouraged bioinorganic chemists to develop new series of copper-based complexes containing heterocyclic ligands. Hence, several new complexes containing thiosemicarbazones, imidazoles and phosphanes were described to exhibit antibacterial, antiviral, antiparasitic, anticancer, or antifungal activity.<sup>25,37,38</sup> Some of these copper compounds present several advantages when compared with platinum-based drugs, like an increased specificity towards cancer cells or their potential ability to bypass the chemoresistance associated with recurrent platinum treatment.<sup>39</sup> Some copper complexes have been reported not only to inhibit DNA synthesis but also to trigger cellular apoptosis *in vitro* and *in vivo*.<sup>40-44</sup> Copper complexes have also been described with the ability to target topoisomerase II, inhibiting the proteasome.<sup>45-47</sup>

One of the main targets of copper complexes is DNA, which they can bind and/or cleave. DNA binding is achieved through supramolecular interactions between the complex and the biomolecule, *viz.* via intercalation, groove binding or electrostatic interaction with the phosphate backbone. The redox activity of copper or its Lewis acid character may lead to a physical alteration of the biomolecule (*i.e.* cleavage). DNA cleavage mainly occurs through two possible mechanisms. The DNA damage may result from oxidative degradation (by ROS) of the sugar or the nucleobase,<sup>48-50</sup> or from hydrolysis of the phosphodiester backbone.<sup>51,52</sup>

### ***Schiff bases***

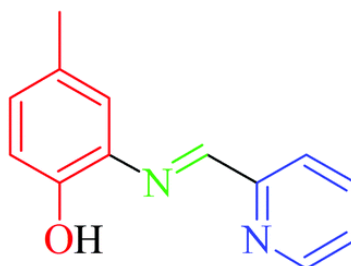
Schiff bases are the products of the condensation reaction between carbonyl compounds and primary amines; this reaction was first described by Hugo Schiff in 1864.<sup>53</sup> Schiff bases





represent a very important class of compounds in medicinal chemistry, which have been used in a plethora of pharmacological applications, for example as antibacterial, anti-fungal, anti-malarial, anti-tuberculosis, insecticidal, antimicrobial and anti-viral agents, as well as anti-inflammatory, antioxidant, anti-cancerous and anticonvulsant drugs.<sup>54-56</sup> Aromatic Schiff bases have been applied in organic degradation, as corrosion inhibitors or optical sensors. Some Schiff-base complexes with unique photoluminescence and electroluminescence have been described.<sup>57,58</sup> Therefore, this family of ligands is very popular, thanks to their easy preparation, extreme versatility and their ability to bind a wide variety of metal ions, even stabilizing various oxidation numbers.

A decade ago, a remarkable and simple Schiff-base ligand, namely 4-methyl-2-*N*-(2-pyridylmethylene)aminophenol (Hpyrimol, Scheme 1), was reported, whose copper(II) complex, *i.e.* [Cu<sup>II</sup>(pyrimol)Cl],<sup>59</sup> was able to catalytically cleave DNA, even in the absence of reductant, moreover showing a high cytotoxicity against several cancer-cell lines.<sup>26,60-62</sup> Since then, a number of Hpyrimol-derived systems have been developed and their DNA-damaging abilities investigated.

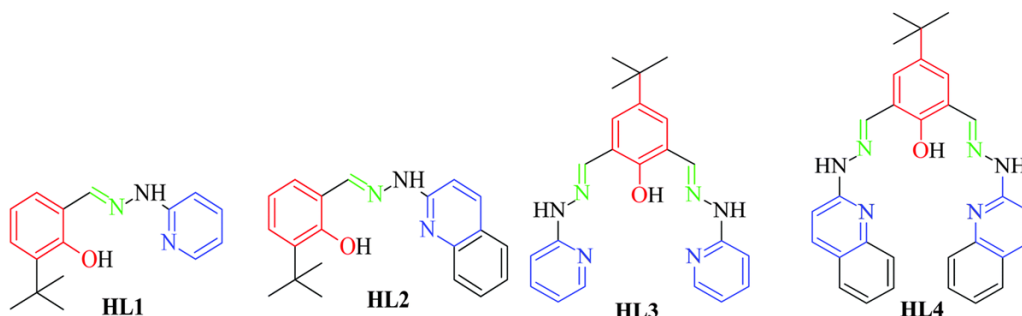


**Scheme 1: Ligand 4-methyl-2-*N*-(2-pyridylmethylene)aminophenol (Hpyrimol) with the three coordinating groups represented in different colours, *i.e.* the phenol in red, the imine in green and the pyridine in blue.<sup>59,63</sup>**

Considering all the interesting data published in the literature, new copper(II) complexes inspired by [Cu<sup>II</sup>(pyrimol)Cl] were designed. Thus, Schiff-base ligands were prepared by condensation of hydrazinopyridinyl reagents with phenol-containing aldehydes. A series of four new ligands were then obtained (Scheme 2), which preserved the three coordinating moieties (illustrated by three distinct colours in Scheme 2) of the original Hpyrimol ligand (Scheme 1).

## Synthesis

### Preparation of the ligands

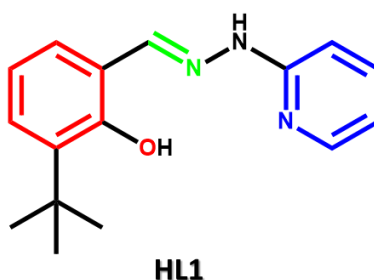


Scheme 2: Representations of the mononucleating ligands 2-*tert*-butyl-6-(pyridin-2-ylhydrazonomethyl)phenol (HL1) and 2-*tert*-butyl-6-(quinolin-2-ylhydrazonomethyl)phenol (HL2), and the dinucleating ligands 4-*tert*-butyl-2,6-bis-(pyridin-2-ylhydrazonomethyl)phenol (HL3) and 4-*tert*-butyl-2,6-bis-(quinolin-2-ylhydrazonomethyl)phenol (HL4). The three different types of coordinating groups, *i.e.* the phenol (red), the imine (green) and the pyridine (blue), are shown in distinct colours.

The ligands (**HL1**–**HL4**; Scheme 2) were synthesized by simple condensation reaction between equimolar amounts of the corresponding hydrazinyl derivatives and aldehydes, in refluxing methanol for four hours. The new N,N,O ligands were obtained in good yields, from 66 to 91%.

### Synthesis of 2-*tert*-butyl-6-(pyridin-2-ylhydrazonomethyl)phenol (HL1)

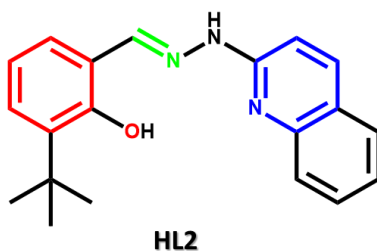
Ligand **HL1** (Scheme 3), obtained by reaction of 2-hydrazinopyridine with 3-*tert*-butyl-2-hydroxybenzaldehyde, includes an electron-donating, bulky substituent (*tert*-butyl) aimed at stabilizing potential phenoxyl radical species that may be produced upon coordination to the metal ion.<sup>64–67</sup> The pure precipitated ligand was collected by filtration and dried under reduced pressure.



Scheme 3: Representation of 2-*tert*-butyl-6-(pyridin-2-ylhydrazonomethyl)phenol (HL1). The three different types of coordinating groups are shown in distinct colours.

### Synthesis of 2-*tert*-butyl-6-(quinolin-2-ylhydrazonomethyl)phenol (HL2)

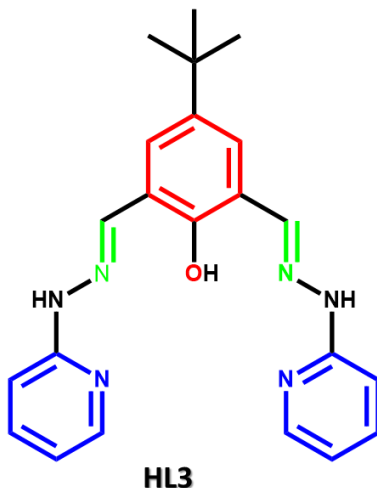
Ligand **HL2** (Scheme 4) was obtained in a similar way, from 2-hydrazinoquinoline and 3-*tert*-butyl-2-hydroxybenzaldehyde. The larger quinoline group (compared with pyridine) is expected to increase the DNA-intercalating properties of the corresponding metal complexes. Pure yellow **HL2** was collected by filtration and dried under reduced pressure.



**Scheme 4:** Representation of 2-*tert*-butyl-6-(quinolin-2-ylhydrazonomethyl)phenol (**HL2**). The three different types of coordinating groups are shown in distinct colours.

#### Synthesis of 4-*tert*-butyl-2,6-bis-(pyridin-2-ylhydrazonomethyl)phenol (**HL3**)

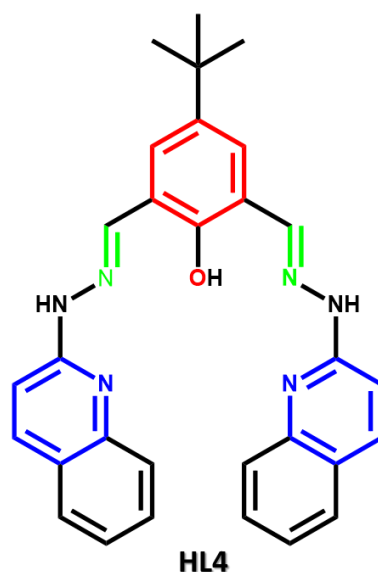
**HL3** (Scheme 5) can be regarded as a dinucleating version of **HL1** (Scheme 3), containing a central phenol group unit connecting two metal-binding pockets. This N,N,O,N,N ligand was prepared by reaction of two equivalents of 2-hydrazinopyridine with one equivalent of 5-*tert*-butyl-2-hydroxyisophthalaldehyde. Pure ligand **HL3** was collected using filtration subsequently dried under reduced pressure.



**Scheme 5:** Representation of 4-*tert*-butyl-2,6-bis-(pyridin-2-ylhydrazonomethyl)phenol (**HL3**). The three different types of coordinating groups are shown in distinct colours.

#### Synthesis of 4-*tert*-butyl-2,6-bis-(quinolin-2-ylhydrazonomethyl)phenol (**HL4**)

**HL4** (Scheme 6) is a dinucleating version of **HL2** (Scheme 4), which was obtained by reaction of two equivalents of 2-hydrazinoquinoline with one equivalent of 5-*tert*-butyl-2-hydroxyisophthalaldehyde. Pure yellow **HL4** was collected by filtration and dried under vacuum.



**Scheme 6:** Representation of 4-*tert*-butyl-2,6-bis-(quinolin-2-ylhydrazonomethyl)phenol (**HL4**). The three different types of coordinating groups are shown in distinct colours.

It can be pointed out here that dinuclear copper(II) compounds from similar phenol-bridging ligands are frequently used to mimic active sites of copper enzymes involved in dioxygen activation.<sup>68,69</sup> Thus, it is expected that dicopper complexes from **HL3** and **HL4** may exhibit oxidative DNA-cleaving abilities, in addition to their potential intercalative behaviour.

#### *General method for the preparation of the complexes*

The metal complexes were prepared by reaction of one equivalent of the ligand with one (for **HL1** and **HL2**) or two equivalents (for **HL3** and **HL4**) of a copper(II) salt in methanol. The corresponding resulting solutions were filtered, and the filtrates were left unperturbed for the slow evaporation of the solvent. After one day, single crystals, suitable for X-ray diffraction studies, of complexes **Cu1–Cu6** were collected.

#### **[Cu(L1)Cl]·CH<sub>3</sub>OH (Cu1)**

Cu1 was obtained by mixing a solution of one equivalent of HL1 in methanol with a solution of one equivalent of copper(II) chloride dihydrate in methanol. Green needles were collected after one day, and the crystallographic structure of Cu1 was determined by single-crystal X-ray diffraction (Figure 13 and Table 4).

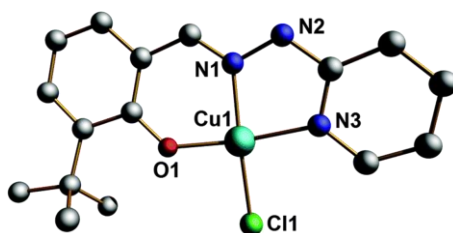


Figure 13: Representation of the crystal structure of Cu1 with the partial atom-numbering scheme. The hydrogen atoms and the lattice methanol molecule are not shown for clarity.

As observed for the similar [Cu(pyrimol)Cl] complex, the copper centre of **Cu1** is in a square-planar geometry.<sup>59,70</sup> The crystal packing of **Cu1** shows that the molecules are associated by means of  $\pi$ – $\pi$  interactions to form supramolecular dimers (Figure 14 and Table 2). The Cu–O, Cu–N and Cu–Cl bond lengths exhibit normal distances, from 1.877(2) to 2.254(1) Å. The coordination angles are similar to those of [Cu<sup>II</sup>(pyrimol)Cl], *viz.* in the range 80.93(9)–97.38(6)°.<sup>59</sup>

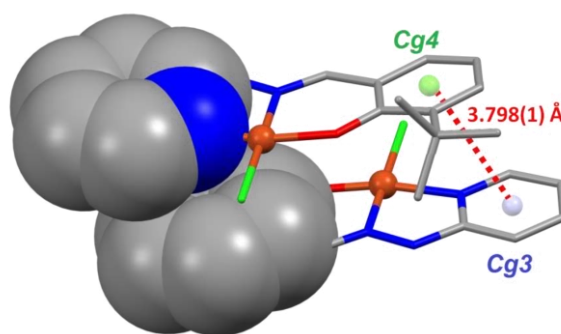


Figure 14: Illustration of the crystal packing of Cu1 showing the formation of  $\pi$ – $\pi$  stacked dimers. The centroid-to-centroid distance Cg3...Cg4 is 3.798(1) Å.

Table 2: Coordination bond lengths (Å) and angles (°), and intermolecular contacts for complex Cu1.

Complex <b>Cu1</b> <sup>a</sup>			
<i>Distances</i>			
Cu1–Cl1	2.254(1)	Cu1–O1	1.877(2)
Cu1–N1	1.950(2)	Cu1–N3	1.983(2)
<i>Angles</i>			
O1–Cu1–Cl1	90.92(6)	Cl1–Cu1–N3	97.38(6)
N3–Cu1–N1	80.93(9)	N1–Cu1–O1	91.28(8)
<i>Hydrogen bonds</i>			
N2–H2A...O1S	2.758(3)	N2–H2A–O1S	160
O1S–H1S...Cl1b	3.124(3)	O1S–H1S–Cl1b	171(4)
<i><math>\pi</math>–<math>\pi</math> interactions</i>			
Cg3...Cg4	3.798(1)	C1a...C14	3.319(4)
		C6a...C14	3.261(3)

<sup>a</sup> Symmetry operations: a = 1–x, 1–y, 1–z; b = –x, 1–y, 1–z.

### [Cu(L2)NO<sub>3</sub>] (Cu2)

Complex **Cu2** was obtained by reaction of one equivalent of **HL2** with one equivalent of copper(II) nitrate trihydrate in methanol. Green single crystals of **Cu2** were obtained, whose X-ray diffraction studies revealed that the compound [Cu(L2)NO<sub>3</sub>] was in a pseudo square-planar geometry, as illustrated in Figure 15.

Crystallographic and refinement parameters for **Cu2** are summarized in Table 5, and selected coordination bond lengths and angles are listed in Table 3.

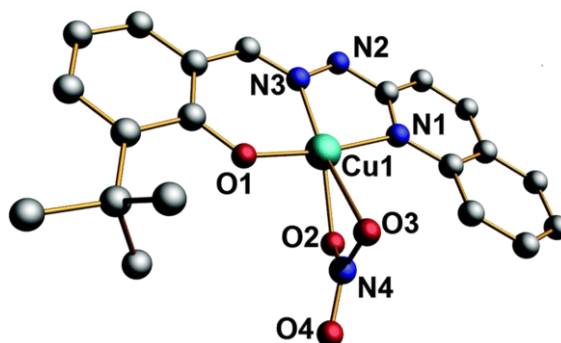


Figure 15: Representation of the molecular structure of Cu2 with the partial atom-numbering scheme. The hydrogen atoms are not shown for clarity.

The pseudo square-planar environment of the metal centre is formed by a N,N,O ligand and a nitrate oxygen atom (O2). The Cu–N and Cu–O bond lengths of respectively 1.924(2)–2.008(2) Å and 1.883(2)–1.964(2) Å can be considered as normal. The copper atom is semi-coordinated by a second oxygen atom (O3) of the bidentate nitrate anion, at a long distance of 2.878(2) Å (Table 4). The coordination angles, within the square plane, are in the range 87.90–99.93(9)°, and are comparable to those of the previously described compound [Cu(pyrimol)Cl].<sup>62</sup>

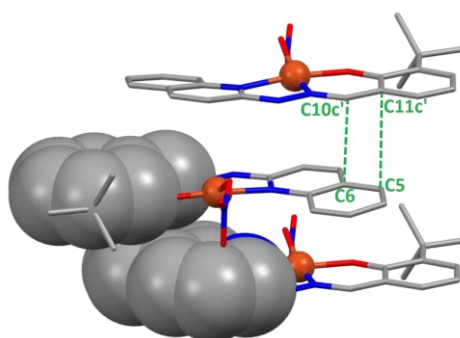


Figure 16: Illustration of the crystal packing of Cu2 showing the formation of  $\pi$ – $\pi$  stacking interactions. The shorter Csp<sup>2</sup>...Csp<sup>2</sup> contact distances are C5...C11c' = 3.344(3) Å and C6...C10c' = 3.354(3) Å. Symmetry operation: c' = 1–x, –y, 1–z.

Similarly to **Cu1**, the crystal packing of **Cu2** shows the supramolecular association of complexes by means of  $\pi$ – $\pi$  interactions (Figure 16 and Table 5).

Table 3: Coordination bond lengths (Å) and angles (°), and intermolecular contacts for Cu2.



Complex <b>Cu2</b> <sup>a</sup>			
<i>Distances</i>			
Cu1–O1	1.883(2)	Cu1–O2	1.964(2)
Cu1–N1	2.008(2)	Cu1–N3	1.924(2)
Cu1–O3	2.878(2)		
<i>Angles</i>			
O1–Cu1–O2	87.90(8)	O2–Cu1–N1	99.93(9)
N1–Cu1–N3	82.22(10)	N3–Cu1–O1	91.46(9)
<i>Hydrogen bond</i>			
N2–H2B...O4b'	2.822(3)	N2–H2B–O4b'	154
<i><math>\pi</math>–<math>\pi</math> interactions</i>			
C5...C11c'	3.344(3)	C6...C10c'	3.354(3)

<sup>a</sup> Symmetry operations: b' = 1–x, –1/2+y, 1/2–z; c' = 1–x, –y, 1–z

### [Cu<sub>2</sub>(**L3**)(ClO<sub>4</sub>)<sub>2</sub>(CH<sub>3</sub>O)(CH<sub>3</sub>OH)]·CH<sub>3</sub>OH (**Cu3**)

**Cu3** was obtained by reaction of one equivalent of the dinucleating ligand **HL3** and two equivalents of copper(II) perchlorate hexahydrate in methanol. After one day, dark-green needles were collected and analysed by single-crystal X-ray diffraction. The analysis of the crystallographic data revealed that **Cu3** is a dicopper species of formula [Cu<sub>2</sub>(**L3**)(ClO<sub>4</sub>)<sub>2</sub>(CH<sub>3</sub>O)(CH<sub>3</sub>OH)]·CH<sub>3</sub>OH, and whose structure is depicted in Figure 17. Crystallographic and refinement parameters for **Cu3** are summarized in Table 5.

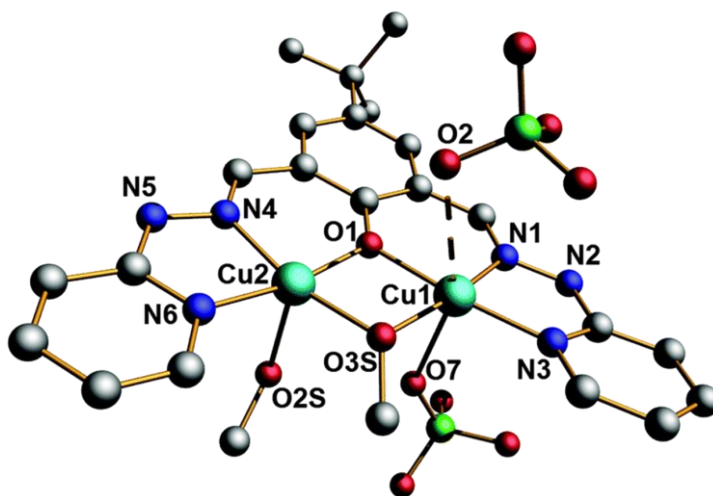


Figure 17: Representation of the molecular structure of **Cu3** with the partial atom-numbering scheme. The hydrogen atoms and the lattice methanol molecule are not shown for clarity.

**Table 4:** Selected bond lengths (Å) and angles (°), and intermolecular bonds for Cu3.

Complex Cu3 <sup>a</sup>			
<i>Distances</i>			
Cu1–O1	1.937(4)	Cu1–O2	2.913(8)
Cu1–O3S	1.930(4)	Cu1–O7	2.612(7)
Cu1–N1	1.932(5)	Cu1–N3	1.949(6)
Cu2–O1	1.939(4)	Cu2–O3S	1.907(4)
Cu2–N4	1.933(5)	Cu2–N6	1.973(5)
Cu2–O2s	2.365(5)	Cu1...Cu2	2.943(2)
<i>Angles</i>			
O1–Cu1–O3S	80.2(2)	O3S–Cu1–N3	106.6(2)
N3–Cu1–N1	82.1(2)	N1–Cu1–O1	91.1(2)
O7–Cu1–O2	158.5(2)		
O1–Cu2–O3S	80.8(2)	O3S–Cu2–N6	105.7(2)
N6–Cu2–N4	82.3(2)	N4–Cu2–O1	90.1(2)
<i>Hydrogen bonds</i>			
O2S–H2S...O7	2.949(8)	O2S–H5–O7	173.6(4)
N2–H2N...O6b	2.824(8)	N2–H2N–O6b	145.4(4)
N5–H5N...O1Sc	2.844(8)	N5–H5N–O1Sc	173.3(4)
O1S–H1S...O3S	3.020(7)	O1S–H1S–O3S	144.7(4)

<sup>a</sup> Symmetry operations: b = –1/2+x, 1/2–y, –1/2+z; c = –x, –y, 2–z.

Compound Cu3 exhibits two copper(II) ions with distinct coordination geometries (see selected coordination bond lengths and angles are listed in Table 4). The Cu1 ion has a pseudo-octahedral environment and is surrounded by the ligand donor atoms N1, N3 and O1 in the equatorial plane, completed by a methoxide oxygen atom (O3S). The axial positions are occupied by two perchlorate anions; one coordinated at a distance of 2.612(7) Å (O7), the other one been semi-coordinated, as shown by the Cu1–O2 bond length of 2.913(8) Å (Table 4).

The equatorial angles varying from 80.2(2) to 106.6(2)° are indicative of a strong distortion of the octahedron. This distortion can be explained by the phenoxide and methoxide bridges, and the small N–Cu–N bite angle imposed by the anionic ligand L3. The atom Cu1 is doubly bridged to the Cu2 ion through the phenoxide unit of L3 (oxygen atom O1) and a methoxide ligand (O3S). Both atoms form part of the basal plane of the square-pyramidal geometry observed for Cu2, which is completed by the ligand nitrogen atoms N4 and N6. The Cu–O and Cu–N bond distances are in normal ranges. The axial position is occupied by a methanol molecule (O2S), at a normal Cu–O distance (Table 4). The tau-factor of 0.05 for the Cu2 ion characterises a square-pyramidal coordination environment.<sup>62</sup> The basal angles, varying from 80.8(2) to 105.7(2)°, are comparable to those found in the equatorial plane of the Cu1 ion, and the deviations from the ideal angle of 90° are a consequence of the two bridges (O1 and O3S), and the small N–Cu–N bite angle of L3. The distance between Cu1 and Cu2 is





short (2.943(2) Å). In the crystal packing, molecules of **Cu3** are interacting *via* an intricate network of hydrogen bonds involving both lattice and coordinated solvents molecules (O2S and O3S), and the nitrogen atoms N2 and N5 (Table 4)



**Cu4** was obtained by mixing a methanolic solution of one equivalent of the dinucleating ligand **HL4** with a methanolic solution containing two equivalents of copper(II) perchlorate hexahydrate. Dark-green plates of **Cu4** were obtained and single-crystal X-ray diffraction analysis revealed that it is a dicopper compound of formula  $[\text{Cu}_2(\text{L4})(\text{ClO}_4)(\text{OH})(\text{CH}_3\text{OH})]\text{ClO}_4$ . A representation of the molecular structure of **Cu4** is shown in Figure 18. Crystallographic and refinement parameters for **Cu4** are given in Table 6.

The solid-state structure of **Cu4** resembles that of **Cu3**, with copper(II) centres exhibiting distinct coordination geometries.

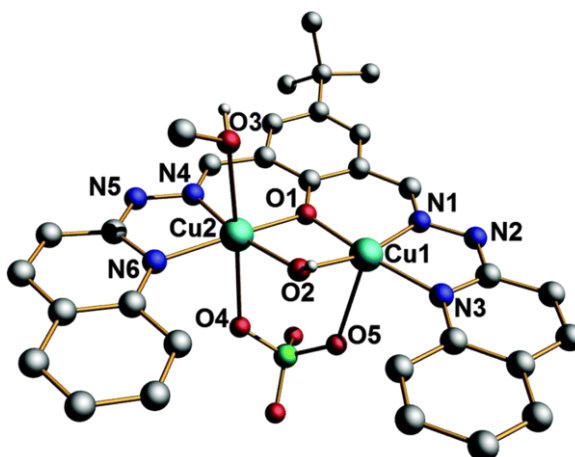
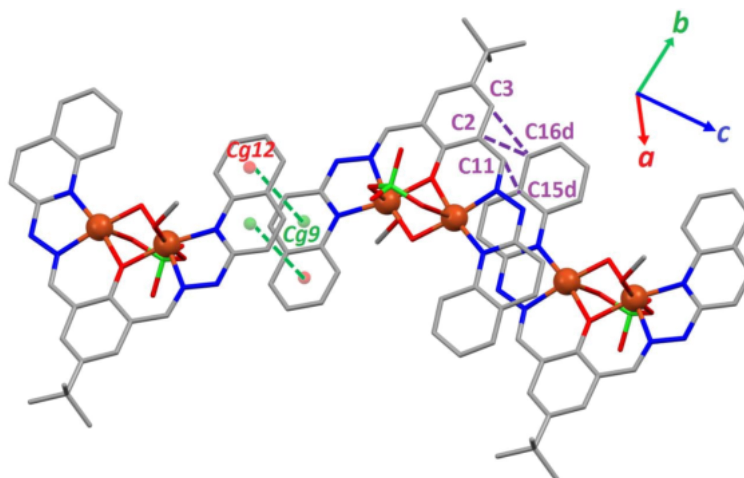


Figure 18: Representation of the molecular structure of **Cu4** with the partial atom-numbering scheme. The hydrogen atoms (except the two OH hydrogens; oxygen atoms O2 and O3) and the lattice perchlorate anion are not shown for clarity.

The pentacoordinated Cu1 ion presents a square-pyramidal environment (with a tau value of 0.10), formed by the nitrogen atoms N1 and N3, the oxygen atom O1 belonging to the anionic ligand **L4**, the hydroxide oxygen atom O2 and the perchlorate oxygen atom O5. The basal plane of the square pyramid is formed by the donor atoms N1, N3, O1 and O2, the apical position being occupied by O5. The bond distances and angles are comparable to those observed for the Cu2 ion in **Cu3** (see Table 6). The Cu1 ion is triply bridged to Cu2, resulting in an octahedral geometry. The equatorial plane of the octahedron is formed by the atoms N4, N6 and O1 (bridging phenoxide) from the ligand **L4**, and the bridging hydroxide atom O2. The axial positions are occupied by a methanol molecule (O3) and the oxygen atom O4 from the

perchlorate anion that bridges the Cu2 and Cu1 ions. The Cu–N and Cu–O bond distances are in normal ranges.



**Figure 19:** Illustration of the crystal packing of Cu4 showing the  $\pi$ - $\pi$  interactions that generate a 1D supramolecular chain, characterized by a centroid-to-centroid distance  $\text{Cg9} \cdots \text{Cg12}$  of 3.607(4) Å and short Csp<sup>2</sup>...Csp<sup>2</sup> contact distances of 3.400(9) ( $\text{C2} \cdots \text{C16d}$ ), 3.281(9) ( $\text{C3} \cdots \text{C16d}$ ) and 3.320(9) ( $\text{C11} \cdots \text{C15d}$ ) Å. Symmetry operation:  $d = 2-x, 1-y, 2-z$ .



Table 5: Crystal data and structure refinement for complexes Cu1, Cu2 and Cu3.

Compound	Cu1	Cu2	Cu3
Empirical formula	C <sub>16</sub> H <sub>18</sub> ClCuN <sub>3</sub> O, CH <sub>4</sub> O	C <sub>20</sub> H <sub>20</sub> CuN <sub>4</sub> O <sub>4</sub>	C <sub>25</sub> H <sub>34</sub> Cl <sub>2</sub> Cu <sub>2</sub> N <sub>6</sub> O <sub>12</sub>
Formula weight (g mol <sup>-1</sup> )	399.37	443.94	808.56
Temperature (K)	100(2)	100(2)	293(2)
Crystal system	triclinic	monoclinic	monoclinic
Space group	<i>P</i> -1	<i>P</i> 2 <sub>1</sub> /c	<i>P</i> 2 <sub>1</sub> /n
Crystal size (mm <sup>3</sup> )	0.08 × 0.06 × 0.02	0.10 × 0.03 × 0.01	0.14 × 0.10 × 0.09
<i>a</i> (Å)	7.9513(4)	17.2957(12)	11.893(9)
<i>b</i> (Å)	10.1551(5)	6.6675(5)	21.582(9)
<i>c</i> (Å)	11.4377(5)	18.3318(9)	12.732(5)
$\alpha$ (°)	103.3680(10)	90	90
$\beta$ (°)	96.2100(10)	119.727(5)	92.466(9)
$\gamma$ (°)	100.2460(10)	90	90
<i>V</i> (Å <sup>3</sup> )	873.38(7)	1835.8(2)	3265(3)
<i>Z</i>	2	4	4
$\rho_{\text{calcd}}$	1.519	1.606	1.645
$\mu$ (mm <sup>-1</sup> )	1.791	1.549	1.535
<i>F</i> (000)	414	916	1656
$\vartheta$ for data collection (°)	2.87–31.10	3.64–32.42	1.86–26.35
Reflections collected / unique	8951 / 4258	15267 / 5093	19288 / 6441
Completeness to theta	97.8	98.9	96.9
Data / restraints / parameters	4258 / 1 / 221	5093 / 0 / 265	6441 / 0 / 424
Goodness-of-fit on <i>F</i> <sup>2</sup>	1.115	1.001	1.004
Final <i>R</i> indices [ <i>I</i> > 2 $\sigma$ ( <i>I</i> )]	<i>R</i> 1 = 0.0515, <i>wR</i> 2 = 0.1601	<i>R</i> 1 = 0.0414, <i>wR</i> 2 = 0.1044	<i>R</i> 1 = 0.0626, <i>wR</i> 2 = 0.1175
<i>R</i> indices (all data)	<i>R</i> 1 = 0.0534, <i>wR</i> 2 = 0.1622	<i>R</i> 1 = 0.0713, <i>wR</i> 2 = 0.1199	<i>R</i> 1 = 0.1700, <i>wR</i> 2 = 0.1479
largest diff. peak and hole (e Å <sup>-3</sup> )	0.749 and -0.896	0.525 and -0.583	0.497 and -0.512

The equatorial angles, varying from 79.28(17) to 108.8(2)°, indicate a strong distortion of the octahedron. The bond distances and angles are comparable to those found in complex

**Cu3**, and the two copper(II) ions are separated by a distance of 2.981(2) Å. The crystal packing of **Cu4** reveals the occurrence of  $\pi$ – $\pi$  interactions between dinuclear molecules, giving rise to the formation of a 1D supramolecular chain (Figure 19 and Table 6). The observation of these  $\pi$ – $\pi$  stacks supports our ligand design, since the quinoline groups were included to further favour  $\pi$ – $\pi$  interactions (compared to the pyridine-containing ligands), which would be beneficial regarding potential (improved) intercalation between DNA base pairs.

Table 6: Selected bond lengths (Å) and angles (°), and intermolecular bonds for **Cu4**

Complex <b>Cu4</b> <sup>a</sup>			
<i>Distances</i>			
Cu1–O1	1.964(4)	Cu1–O2	1.909(4)
Cu1–O5	2.526(5)	Cu1–N1	1.948(5)
Cu1–N3	2.002(5)		
Cu2–O1	1.996(4)	Cu2–O2	1.918(4)
Cu2–O3	2.402(5)	Cu2–O4	2.603(5)
Cu2–N4	1.951(5)	Cu2–N6	2.000(5)
		Cu1...Cu2	2.981(2)
<i>Angles</i>			
O1–Cu1–O2	80.33(17)	O2–Cu1–N3	108.5(2)
N3–Cu1–N1	82.4(2)	N1–Cu1–O1	88.89(19)
O1–Cu2–O2	79.28(17)	O2–Cu2–N6	108.8(2)
N6–Cu2–N4	83.2(2)	N4–Cu2–O1	89.04(19)
O3–Cu2–O4	175.09(18)		
<i>Hydrogen bonds</i>			
N2–H2A...O6a	2.854(7)	N2–H2A–O6a	157
N5–H5B...O11	2.877(7)	N5–H5B–O11	168
O2–H2...O6d	2.934(7)	O2–H2–O6d	161(6)
O3–H3...O10e	2.793(8)	O3–H3–O10e	165(7)
<i><math>\pi</math>–<math>\pi</math> interactions</i>			
C2...C16d	3.400(9)	C3...C16d	3.281(9)
C11...C15d	3.320(9)	Cg9...Cg12	3.607(4)

<sup>a</sup> Symmetry operations: a = 1–x, 1–y, 2–z; d = 2–x, 1–y, 2–z; e = 1–x, –y, 1–z

### [Cu<sub>8</sub>(L3)<sub>4</sub>(NO<sub>3</sub>)<sub>4</sub>(OH)<sub>5</sub>](NO<sub>3</sub>)<sub>3</sub>·(CH<sub>3</sub>OH)<sub>5</sub>·(H<sub>2</sub>O)<sub>8</sub> (**Cu5**)

Reaction of one equivalent of **HL3** with two equivalents of copper(II) nitrate trihydrate in methanol generated an unexpected octanuclear coordination compound of formula [Cu<sub>8</sub>(L3)<sub>4</sub>(NO<sub>3</sub>)<sub>4</sub>(OH)<sub>5</sub>](NO<sub>3</sub>)<sub>3</sub>·(CH<sub>3</sub>OH)<sub>5</sub>·(H<sub>2</sub>O)<sub>8</sub> (**Cu5**), as revealed by X-ray diffraction. The reaction conditions to produce **Cu5** and to obtain single crystals were comparable to those previously described. The crystal structure of **Cu5** and its bis-open-cubane core are depicted in Figure 20A and B, respectively. Crystallographic and refinement parameters are summarized in Table 9.

The solid-state structure of **Cu5** can be considered as the association of four dinuclear [Cu<sub>2</sub>(L3)] units (each of these units being similar to compound **Cu3**, represented in Figure 17),





bridged by hydroxide ligands. This assembly produces two open-cubane-like structures, connected by a single hydroxide bridge (oxygen atom O1E), generating the octanuclear complex **Cu5** (Figure 20B).

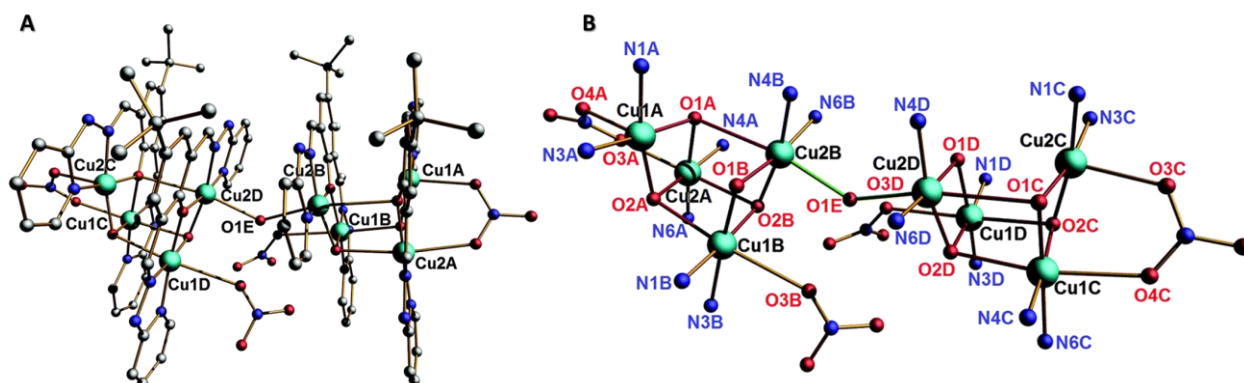


Figure 20: (A) Representation of the molecular structure of Cu5 with the partial atom-numbering scheme. The hydrogen atoms and the lattice nitrate anions, methanol and water molecules are not shown for clarity. (B) Octanuclear core with the atom-numbering scheme.

This cluster compound is formed by six octahedral copper(II) ions (Cu1B, Cu1C, Cu1D, Cu2A, Cu2B and Cu1D) and two square-pyramidal copper(II) ions (Cu1A and Cu2C). The equatorial plane of all octahedra is constituted of a deprotonated ligand **L3** (N, N, O donor atoms) and a bridging hydroxide anion. The metal centres differ only by the axial ligands. The axial positions are occupied by a monodentate nitrate anion and a bridging hydroxide for Cu1B and Cu1D. Cu1C and Cu2A ions are coordinated by a bridging nitrate anion (connecting the metal ions to Cu2C and Cu1A, respectively) and a bridging hydroxide. Finally, in the case of the Cu2B and Cu2D ions, the axial positions are occupied by two bridging hydroxide anions. The basal plane of the pentacoordinated Cu1A and Cu2C cations is constituted of a ligand **L3**<sup>−</sup> and a hydroxide anion. The apical position of the perfect square pyramid (with tau values of 0.00 for Cu2C and 0.01 for Cu1A) is occupied by a bridging nitrate anion. This nitrate is connecting the metal ions to Cu2A and Cu1C, respectively. All Cu–N and Cu–O bond lengths (Table 7) can be regarded as normal for the four different coordination environments observed in **Cu5**.

**Table 7: Coordination bond lengths (Å) and angles (°), and intermolecular contacts for Cu5**

<i>Distances</i>			
Cu1A–O1A	1.954(2)	Cu1A–O2A	1.931(2)
Cu1A–O4A	2.338(2)	Cu1A–N1A	1.948(2)
Cu1A–N3A	1.955(2)		
Cu1B–O1B	1.954(2)	Cu1B–O2A	2.442(2)
Cu1B–O2B	1.941(2)	Cu1B–O3B	2.734(1)
Cu1B–N1B	1.936(2)	Cu1B–N3B	1.953(2)
Cu1C–O1C	1.9702(1)	Cu1C–O2C	1.936(2)
Cu1C–O2D	2.484(2)	Cu1C–O4C	2.494(1)
Cu1C–N4C	1.939(2)	Cu1C–N6C	1.972(2)
Cu1D–O1D	1.959(2)	Cu1D–O2C	2.420(1)
Cu1D–O2D	1.943(2)	Cu1D–O3D	2.643(1)
Cu1D–N1D	1.939(2)	Cu1D–N3D	1.962(2)
Cu2A–O1A	1.972(2)	Cu2A–O2A	1.939(2)
Cu2A–O2B	2.555(1)	Cu2A–O3A	2.407(2)
Cu2A–N4A	1.940(2)	Cu2A–N6A	1.961(2)
Cu2B–O1A	2.794(2)	Cu2B–O1B	1.943(1)
Cu2B–O1E	2.328(2)	Cu2B–O2B	1.940(1)
Cu2B–N4B	1.943(2)	Cu2B–N6B	1.967(2)
Cu2C–O1C	1.944 (2)	Cu2C–O2C	1.927(1)
Cu2C–O3C	2.375(2)	Cu2C–N1C	1.946(2)
Cu2C–N3C	1.952(2)		
Cu1D–O1C	3.780(2)	Cu1D–O1D	1.959(2)
Cu1D–O1E	3.683(1)	Cu1D–O2D	1.943(2)
Cu1D–N1D	1.939(2)	Cu1D–N3D	1.962(2)
Cu1A...Cu2A	2.869(4)	Cu1A...Cu2B	3.733(5)
Cu1A...Cu1B	3.603(1)	Cu1B...Cu2A	3.367(1)
Cu1B...Cu2B	2.930(4)	Cu2A...Cu2B	3.532(1)
Cu1C...Cu2C	2.885(2)	Cu1C...Cu1D	3.327(2)
Cu1C...Cu2D	3.501(2)	Cu1D...Cu2C	3.545(1)
Cu1D...Cu2D	2.942(4)	Cu2B...Cu2D	4.342(2)
<i>Angles</i>			
O1A–Cu1A–O2A	82.69(6)	O2A–Cu1A–N3A	103.45(8)
N3A–Cu1A–N1A	82.43(8)	N1A–Cu1A–O1A	89.91(7)
O1B–Cu1B–O2B	81.66(6)	O2B–Cu1B–N3B	105.48(8)
N3B–Cu1B–N1B	82.77(9)	N1B–Cu1B–O1B	90.09(7)
O2A–Cu1B–O3B	174.68(8)		
O1A–Cu2A–O2A	82.01(6)	O2A–Cu2A–N6A	105.22(8)
N6A–Cu2A–N4A	82.50(8)	N4A–Cu2A–O1A	90.11(7)
O3A–Cu2A–O2B	171.19(8)		
O1B–Cu2B–O2B	81.95(6)	O2B–Cu2B–N6B	104.70(7)
N6B–Cu2B–N4B	82.55(8)	N4B–Cu2B–O1B	90.06(7)
O1A–Cu2B–O1E	168.91(7)		
O1C–Cu1C–O2C	81.49(6)	O2C–Cu1C–N6C	106.42(7)
N6C–Cu1C–N4C	82.42(8)	N4C–Cu1C–O1C	89.69(7)
O4C–Cu1C–O2D	168.31(9)		





O1C–Cu2C–O2C	82.39(6)	O2C–Cu2C–N3C	103.39(8)
N3C–Cu2C–N1C	82.54(8)	N1C–Cu2C–O1C	90.44(7)
O1D–Cu1D–O2D	81.45(6)	O2D–Cu1D–N3D	106.16(7)
N3D–Cu1D–N1D	82.59(8)	N1D–Cu1D–O1D	89.81(7)
O2C–Cu1D–O3D	174.35(8)		
O1D–Cu2D–O2D	81.64(6)	O2D–Cu2D–N6D	105.07(7)
N6D–Cu2D–N4D	82.52(8)	N4D–Cu2D–O1D	89.98(7)
<i>Hydrogen bonds</i>			
O1S...O2C	2.775(1)	O1E...O3D	2.690(2)
O1E...O3B	2.701(2)	O2A...O2	2.869(1)

The equatorial (octahedral geometry) and basal (square-pyramidal geometry) angles are very similar to those observed for complexes **Cu3** and **Cu4**. The Cu...Cu distances within the octanuclear complex vary from 2.869(4) to 4.342(2) Å, the longest one corresponding to that of Cu2B...Cu2D, which are the metal centres through which the two cubane units are connected *via* the hydroxide bridge O1E. Finally, an intricate network of strong hydrogen bonds involving the lattice nitrate anions, methanol and water molecules is observed in the solid-state structure of **Cu5**.

#### [Cu<sub>3</sub>(HL2')<sub>4</sub>Cl<sub>6</sub>]·(CH<sub>3</sub>OH)<sub>6</sub> (**Cu6**)

The slow addition of a methanolic solution of 1.33 equivalent of **HL2** to a solution containing one equivalent of copper(II) chloride dihydrate in methanol generated complex **Cu6**, identified as the trinuclear compound [Cu<sub>3</sub>(HL2')<sub>4</sub>Cl<sub>6</sub>]·(CH<sub>3</sub>OH)<sub>6</sub>, by single-crystal X-ray diffraction studies. The solid-state structure of **Cu6** shows an unexpected but interesting modification of the original ligand **HL2**. Indeed, **HL2** suffered a cyclization reaction generating the 1,2,4-triazolo[4,3,a]quinoline derivative **HL2'**, whose structure is visible in Figure 21. Selected coordination bond lengths and angles are listed in Table 8.

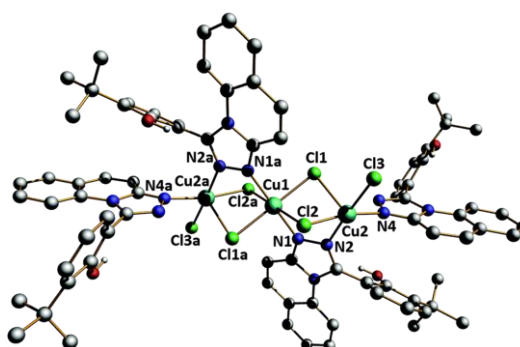
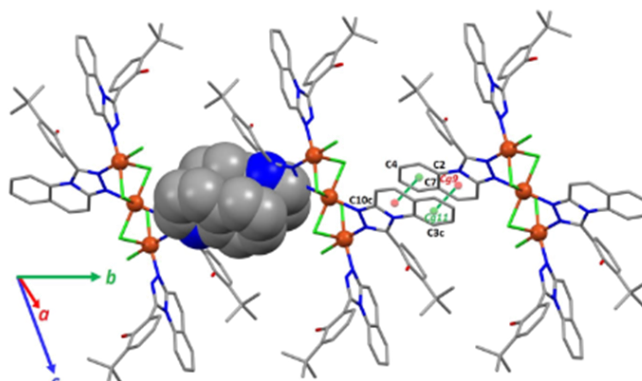


Figure 21: Representation of the molecular structure of **Cu6** with the partial atom-numbering scheme. Only the phenolic hydrogen atoms are shown, and the lattice methanol molecules are omitted for clarity. Symmetry operation:  $a = 1 - x, 1 - y, 1 - z$ .

As evidenced in Figure 21, the trinuclear core of **Cu6** contains a central octahedral copper(II) ion. This Cu1 ion is bridged to two symmetry-related external copper(II) ions, namely Cu2 and Cu2a, which exhibit a square-pyramidal geometry. The equatorial plane of

the Cu1 ion encloses the nitrogen atoms N1 and N1a from two ligands **HL2'** and the chloride atoms Cl1 and Cl1a.



**Figure 22:** Illustration of the crystal packing of Cu6 showing the  $\pi$ - $\pi$  interactions that generate a 1D supramolecular chain along the crystallographic  $b$  axis, characterized by a centroid-to-centroid distance Cg9...Cg11 of 3.883(2) Å and short Csp2...Csp2 contact distances of 3.595(5) (C7...C3c), 3.533(5) (C2...C3c) and 3.456(5) (C4...C10c) Å. Symmetry operation:  $c = 1-x, 2-y, 1-z$ .

The axial positions of the octahedron are occupied by the chloride atoms Cl12 and Cl12a. The Cu-N and Cu-Cl bond lengths are in normal ranges for this type of chromophore, and the equatorial coordination angles varying from 89.37(10) to 90.63(10)° are indicative of an almost perfect octahedral geometry (in Table 8). The Cu2 ion (and Cu2a; symmetry operation:  $a = 1-x, 1-y, 1-z$ ), is in a square-pyramidal environment (with a tau value of 0.12), with a basal plane that is composed of two nitrogen atoms, namely N2 and N4 belonging to two different **HL2'** ligands, and two chlorides, *i.e.* Cl2 and Cl3. The apical position is occupied by the chloride anion Cl1. The Cu-N and Cu-Cl bond distances and the angles can be considered as normal for this type of coordination environment (Table 8). The Cu2 and Cu2a ions are triply connected to the central Cu1 ion, by means of two chloride bridges and one N,N-bridging triazolo ligand **HL2'**, giving rise to a Cu...Cu separation distance of 3.292(1) Å. In the crystal packing of **Cu6**, the neutral complex is interacting with lattice methanol molecules *via* hydrogen bonds with coordinated chlorides and the phenolic hydrogen atoms. Furthermore, the trinuclear units are involved in  $\pi$ -stacking interactions through two of their fused heteroaromatic rings, generating a 1D supramolecular chain (Figure 22).



Table 8: Coordination bond lengths (Å) and angles (°), and intermolecular contacts for Cu6

<i>Distances</i>			
Cu1–N1	1.989(3)	Cu1–Cl1	2.303(1)
Cu1–Cl2	2.793(1)		
Cu2–Cl2	2.287(1)	Cu2–Cl3	2.259(1)
Cu2–N2	2.041(4)	Cu2–N4	2.005(3)
Cu2–Cl1	2.591(1)	Cu1...Cu2	3.292(1)
<i>Angles</i>			
Cl1–Cu1–N1	90.63(10)	N1–Cu1–Cl1a	89.37(10)
Cl1a–Cu1–N1a	90.63(10)	N1a–Cu1–Cl1	89.37(10)
Cl2–Cu1–Cl2a	180		
Cl2–Cu2–Cl3	93.46(4)	Cl3–Cu2–N4	90.35(10)
N4–Cu2–N2	88.92(13)	N2–Cu2–Cl2	86.74(9)
<i>Hydrogen bonds</i>			
O1–H1...O1S	2.664(6)	O1–H1–O1S	145
O1S–H1S...O3S	2.754(8)	O1S–H1S–O3S	161
O3S–H3S...Cl1	3.087(4)	O3S–H3S–Cl1	152
O2–H2...O2S	2.689(4)	O2–H2–O2S	139
O2S–H2S...Cl3	3.184(3)	O2S–H2S–Cl3	156
<i><math>\pi</math>–<math>\pi</math> interactions</i>			
C7...C3c	3.595(5)	C2...C3c	3.533(5)
C4...C10c	3.456(5)	Cg...Cg	3.883(2)

<sup>a</sup> Symmetry operations: a = 1–x, 1–y, 1–z; c = 1–x, 2–y, 1–z

It can be mentioned here that the synthesis of 1,2,4-triazolo[4,3,a]pyridine and 1,2,4-triazolo[4,3,a]quinoline derivatives is commonly achieved by oxidative cyclization of hydrazones (of the type of ligand **HL2**), using iodobenzene diacetate (*i.e.* PhI(OAc)<sub>2</sub>) as the oxidant,<sup>71,72</sup> or other oxidants.<sup>73–75</sup> In the present case, copper(II) ions most likely act as oxidation agents, catalysing the formation of modified ligand **HL2'**. Actually, the generation of such 1,2,4-triazolo compounds by cyclization reaction of hydrazones in the presence of atmospheric dioxygen and catalytic amounts of copper dichloride has been already described in the literature.<sup>76</sup>

**Table 9: Crystal data and structure refinement for Cu4, Cu5 and Cu6**

Compound	Cu4	Cu5	Cu6
Empirical formula	C <sub>31</sub> H <sub>32</sub> ClCu <sub>2</sub> N <sub>6</sub> O <sub>7</sub> , ClO <sub>4</sub>	C <sub>93</sub> H <sub>125</sub> Cu <sub>8</sub> N <sub>31</sub> O <sub>43</sub>	C <sub>80</sub> H <sub>76</sub> Cl <sub>6</sub> Cu <sub>3</sub> N <sub>12</sub> O <sub>4</sub> , 6(C H <sub>4</sub> O)
Formula weight (g mol <sup>-1</sup> )	862.61	2873.56	1865.10
Temperature (K)	100(2)	190(2)	100(2)
Crystal system	triclinic	triclinic	triclinic
Space group	<i>P</i> -1	<i>P</i> -1	<i>P</i> -1
Crystal size (mm <sup>3</sup> )	0.09 × 0.05 × 0.01	0.20 × 0.10 × 0.08	0.06 × 0.06 × 0.05
<i>a</i> (Å)	7.629(3)	15.8661(5)	10.9272(10)
<i>b</i> (Å)	13.448(4)	15.9224(5)	11.8160(11)
<i>c</i> (Å)	17.723(5)	26.4434(9)	18.887(2)
$\alpha$ (°)	110.693(4)	76.076(1)	73.7590(10)
$\beta$ (°)	97.801(4)	87.396(1)	81.8970(10)
$\gamma$ (°)	94.246(4)	68.366(1)	72.6210(10)
<i>V</i> (Å <sup>3</sup> )	1670.6(9)	6020.3(3)	2230.0(4)
<i>Z</i>	2	2	1
$\rho_{\text{calcd}}$	1.715	1.585	1.389
$\mu$ (mm <sup>-1</sup> )	1.901	1.481	1.201
<i>F</i> (000)	880	2952	969
$\vartheta$ for data collection (°)	3.31–28.95	1.42–31.88	3.03–27.11
Reflections collected / unique	13570 / 6721	100899 / 38648	16072 / 7548
Completeness to theta	98.3	99.7	99.3
Data / restraints / parameters	6721 / 0 / 475	38648 / 0 / 1537	7548 / 74 / 535
Goodness-of-fit on <i>F</i> <sup>2</sup>	1.098	1.028	1.033
Final R indices [ <i>I</i> > 2 $\sigma$ ( <i>I</i> )]	R1 = 0.0721, wR2 = 0.2024	R1 = 0.0445, wR2 = 0.1316	R1 = 0.0478, wR2 = 0.1168
R indices (all data)	R1 = 0.0874, wR2 = 0.2123	R1 = 0.0652, wR2 = 0.1316	R1 = 0.0586, wR2 = 0.1233
largest diff. peak and hole (e Å <sup>-3</sup> )	1.587 and -1.513	1.503 and -0.770	1.456 and -0.957

After full characterization of all complexes, their biological activities were subsequently assessed. Hence, several techniques were used to investigate their potential





interaction with DNA and their cytotoxicity behaviour was evaluated with different murine and human cell lines.

### ***DNA-binding studies***

The interaction of copper complexes with DNA has long been described in the literature.<sup>77-82</sup> Their cytotoxicity is often associated with their ability to degrade DNA, for instance through the generation of harmful oxygen species (ROS). Hence, the interaction of copper compounds **Cu1–Cu6** with DNA has been investigated using various complementary techniques, with the objective of assessing their possible mode(s) of action.

### ***UV-Vis Spectroscopy***

UV-Vis spectroscopy is a recurrent technique in biochemistry. This effective tool allows to evaluate and quantify the binding strength of metal complexes to DNA.<sup>83,84</sup> In the present study, titration experiments were carried out to compare quantitatively the binding strength of the copper(II) complexes. The potential binding of complexes **Cu1** to **Cu6** to *calf thymus* DNA (ct-DNA) was investigated, recording absorption spectra at a constant complex concentration, *i.e.* 25  $\mu\text{M}$  in a buffer, in the absence of DNA, and in the presence of increasing amounts of ct-DNA (*i.e.* 0–50  $\mu\text{M}$ ). The corresponding spectra obtained for **Cu1** are shown in Figure 23A; these are representative of the other compounds (*i.e.* complexes **Cu2–Cu6**, see Experimental section, Figure 86). The absorption bands observed in the region 250–300 nm are assigned to  $\pi\text{--}\pi^*$  transitions of the ligands. The bands found around 350–450 nm are attributed to metal-to-ligand charge-transfer (MLCT) absorptions. The latter ones were used to analyze the respective binding affinities of the metal compounds. The spectroscopic data could be fitted to equation (1), and the intrinsic binding constants  $K_b$  could then be determined.<sup>85,86</sup>

$$\frac{[\text{DNA}]}{(\epsilon_a - \epsilon_f)} = \frac{[\text{DNA}]}{(\epsilon_b - \epsilon_f)} + \frac{1}{K_b(\epsilon_b - \epsilon_f)} \quad (1)$$

In this equation, [DNA] is the concentration of DNA in base pairs,  $\epsilon_a$  is the apparent extinction coefficient obtained by calculating  $A_{\text{obs}}/[\text{complex}]$ ,  $\epsilon_f$  corresponds to the extinction coefficient of the DNA-free complex solution, and  $\epsilon_b$  refers to the extinction coefficient of the DNA-bound complex solution.

Upon each DNA addition to the metal complex, the resulting solution was allowed to equilibrate for 5 min at 25 °C. Subsequently, the absorption spectra were recorded and the data obtained were fitted to equation (1) to determine the intrinsic binding constant  $K_b$ .<sup>87-89</sup> Each set of data (namely for each complex) was plotted as  $[\text{DNA}] / (\epsilon_a - \epsilon_f)$  vs. [DNA], giving a slope equal to  $1 / (\epsilon_b - \epsilon_f)$  and a y-intercept corresponding to  $1 / K_b (\epsilon_b - \epsilon_f)$ . Thus, the intrinsic binding

constant  $K_b$  is the ratio of the slope to the intercept.<sup>90</sup> As an example, the  $[DNA] / (\epsilon_a - \epsilon_f)$  vs.  $[DNA]$  plot obtained for **Cu1** is depicted in Figure 23B.

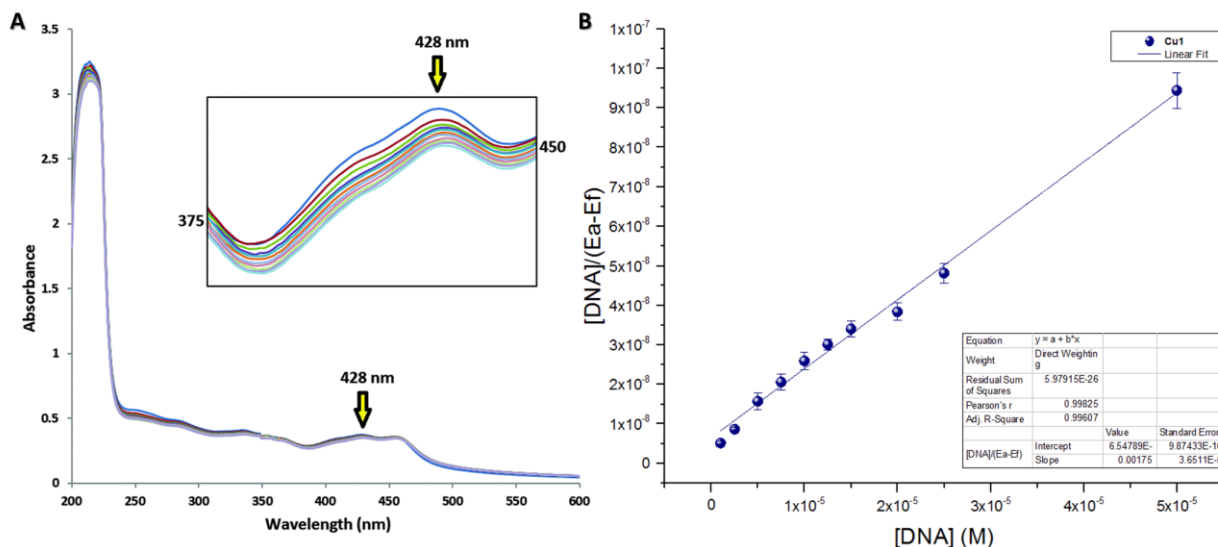


Figure 23: A. Absorption spectra for Cu1 in Tris-HCl buffer (pH = 7.2) upon addition of ct-DNA. The inset shows an enlargement of the region 375–450 nm where the metal-to-ligand charge-transfer (MLCT) absorption is located. Concentration of complex: 25  $\mu$ M; [ct-DNA]: 0–50  $\mu$ M. The [ct-DNA] in base pairs was determined from its absorption intensity at 260 nm with a molar extinction coefficient of 6600  $M^{-1}cm^{-1}$ ; B. Plot of  $[DNA] / \epsilon_a - \epsilon_f$  vs.  $[DNA]$  for the titration of ct-DNA with Cu1 at 428 nm, linear fitting of the data. Concentration of complex: 25  $\mu$ M; [DNA]: 0–50  $\mu$ M.

For **Cu1–Cu6**, the spectroscopic data reveal a hypochromic effect without red shift (Figure 23A and Experimental section, Figure 86). These data suggest that the compounds bind to DNA by means of electrostatic interactions or groove binding;<sup>91,92</sup> a red shift of the absorptions associated to hypochromism would have indicated an interaction through ligand intercalation.<sup>93-97</sup> Therefore, complexes **Cu1–Cu6** may act as DNA-groove binders.<sup>98</sup>

For comparison, the  $[DNA] / (\epsilon_a - \epsilon_f)$  vs.  $[DNA]$  plots for **Cu1–Cu6** are shown in Figure 24; the corresponding  $K_b$  constants are listed in Table 10.

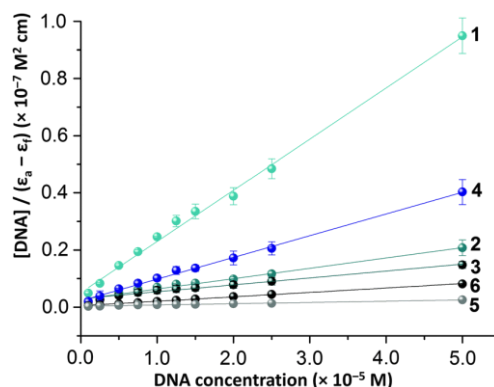


Figure 24: Plots of  $[DNA] / (\epsilon_a - \epsilon_f)$  vs.  $[DNA]$  for the titration of ct-DNA with Cu1-Cu6 at 428 nm: experimental data points and linear fitting of the data. Concentration of complex: 25  $\mu$ M; [DNA]: 0–50  $\mu$ M. For Cu5, a concentration of 10  $\mu$ M was used.



The  $K_b$  values range from 0.80 to  $3.41 \times 10^5 \text{ M}^{-1}$  (Table 10), which are indicative of strong DNA affinities of the copper compounds.

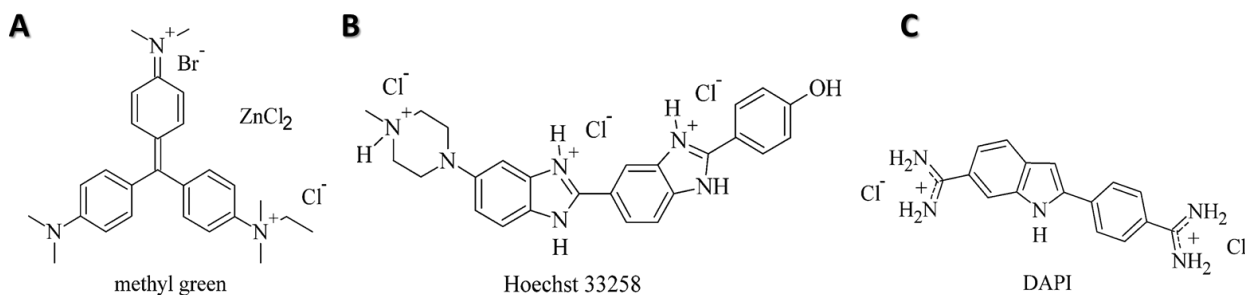
Table 10: Intrinsic binding constants  $K_b$  determined for Cu1-Cu6

Complex	Slope ( $10^{-3}$ )	Intercept ( $10^{-9}$ )	$K_b^{[a]}$ ( $10^{-9} \text{ M}^{-1}$ )	Log $K_b$
<b>Cu1</b>	1.75	6.55	$2.67 \pm 0.15$	5.43
<b>Cu2</b>	0.36	2.75	$1.31 \pm 0.11$	5.12
<b>Cu3</b>	0.24	3.00	$0.80 \pm 0.01$	4.91
<b>Cu4</b>	0.76	2.23	$3.41 \pm 0.13$	5.53
<b>Cu5</b>	0.04	0.35	$1.26 \pm 0.09$	5.1
<b>Cu6</b>	0.15	0.53	$2.93 \pm 0.12$	5.47

<sup>[a]</sup> The uncertainties were determined from measurements in triplicate.

Based on the  $K_b$  constants, the compounds can be divided into two groups. The first group, includes complexes **Cu1**, **Cu4** and **Cu6**, exhibiting the highest binding strengths with  $K_b$  values of respectively  $2.67 \times 10^5 \text{ M}^{-1}$ ,  $3.41 \times 10^5 \text{ M}^{-1}$  and  $2.93 \times 10^5 \text{ M}^{-1}$ . The second group, represented by compounds **Cu2**, **Cu3** and **Cu5**, shows lower DNA-binding efficiency with  $K_b$  values in the range  $0.80$ – $1.31 \times 10^5 \text{ M}^{-1}$ .

It can be noticed that the structurally distinct complex, *i.e.* **Cu6**, shows a relatively strong DNA-binding affinity ( $K_b = 2.93 \times 10^5 \text{ M}^{-1}$ ), comparable to **Cu1** and **Cu4**. Furthermore, comparison of the  $K_b$  values with those of well-known compounds, suggest that **Cu1**–**Cu4** may act as groove binders. Indeed, the major-groove binder methyl green has a  $K_b$  around  $10^6 \text{ M}^{-1}$ ,<sup>99</sup> and those of the minor groove binders Hoechst 33258 and DAPI are in the order of  $10^8$  and  $10^6$ , respectively.<sup>100-103</sup>



Scheme 7: Schematic representations of the structures of well-known, planar groove binders: A. 4-[[4-(dimethylamino)phenyl][4-(dimethyliminiumyl)cyclohexa-2,5-dien-1-ylidene]methyl]-N-ethyl-N,N-dimethylanilinium bromide chloride, zinc chloride salt (methyl green), B. 2'-(4-hydroxyphenyl)-5-(4-methyl-1-piperazinyl)-2,5'-bi-1H-benzimidazole trihydrochloride (Hoechst 33258) and C. 4',6-diamino-2-phenylindole dihydrochloride (DAPI).

These efficient DNA-interacting molecules are aromatic cations that exhibit a planar structure (Scheme 7). It can be stressed that the cationic moieties of **Cu1** and **Cu4** present planar structures as well. This feature may be crucial for their potential groove-binding activity, their size and/or shape defining their target(s), namely the major and/or minor grooves.

### ESI-MS and EPR spectroscopy

In order to corroborate that the planar cationic moieties are present in solution under the experimental conditions applied, electrospray-ionization mass-spectrometry (ESI-MS; positive mode) measurements have been carried out. These experiments demonstrate that compounds **Cu1**, **Cu3** and **Cu4** are stable in solution. However, compounds **Cu2** and **Cu6** do not appear to be stable under the mass-spectrometry conditions. For **Cu2**, the mass data suggest the presence of a nitrate-bridged dicopper species, containing a planar **L2**/Cu unit (Figure 25). The trinuclear complex **Cu6** is clearly unstable under the MS conditions; the free ligand **HL2'** is detected predominantly (Figure 26). The bulky  $(\text{HL2'})_2\text{-Cu}$  complex, originating from the external copper centres of **Cu6**, is found (Figure 14).

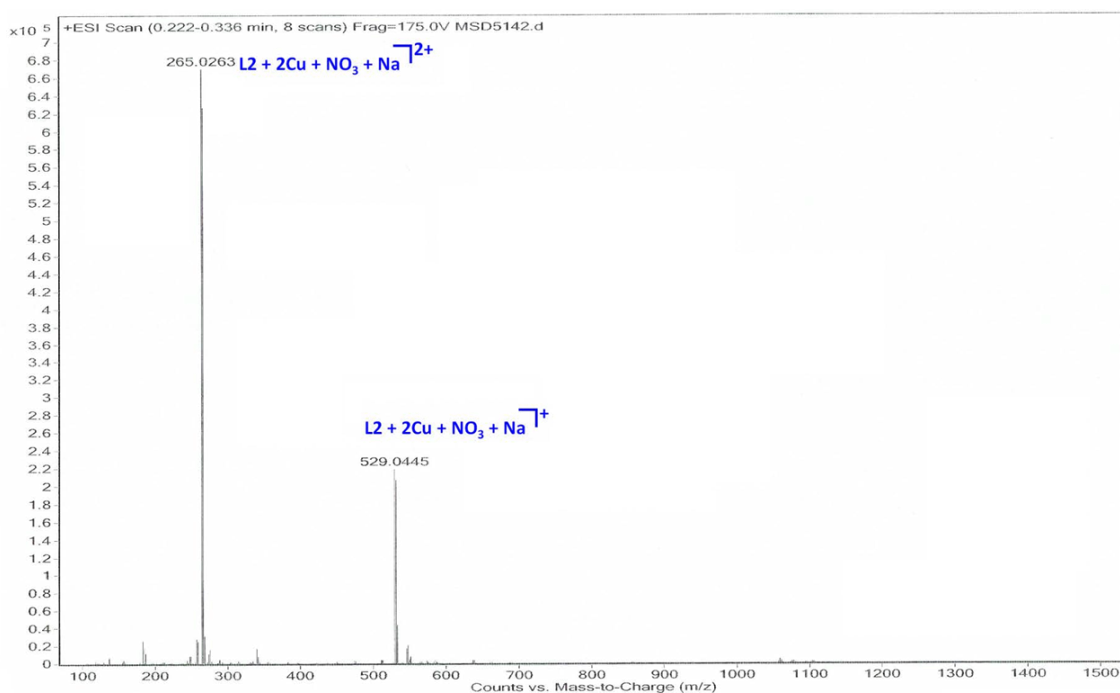


Figure 25: ESI-MS spectrum for Cu2.

It can be emphasised here that the copper species arising from either **Cu2** and **Cu6** in solution (like for instance the  $(\text{HL2'})_2\text{-Cu}$  species in the case of **Cu6**) may function as DNA binders; the MS data cannot discard it.



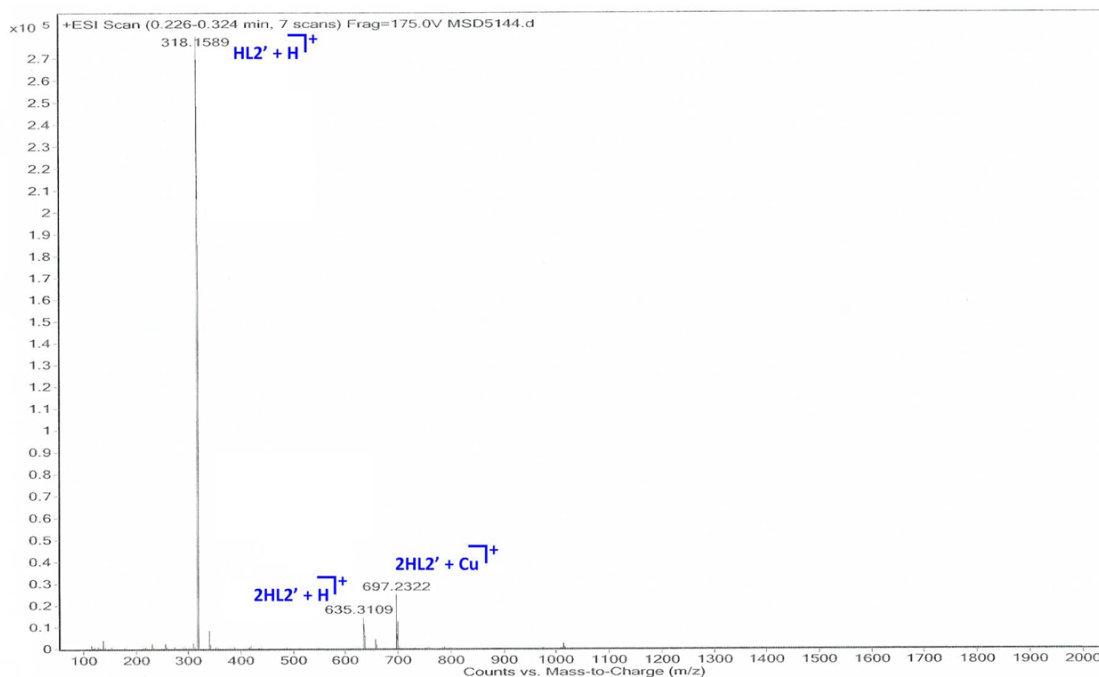


Figure 26: ESI-MS spectrum for compound **Cu6**.

Finally, for **Cu5**, the hydroxy-bridged bis-cubane unit is not observed; nonetheless, the cubane moieties obtained by cleavage of the weak hydroxide bridge  $\text{Cu2B-O1E-Cu2D}$  were detected (Experimental section, Figure 88 and Figure 89).

It has been described that the Tris-HCl buffer can bind copper(II) ions.<sup>104,105</sup> Since most biological studies (DNA-interaction studies) have been performed in this buffer, EPR experiments were performed to verify whether Tris-HCl was competing with the ligands. For this purpose, copper(II) chloride was dissolved in two different solvent mixtures, namely Tris-HCl /DMSO (3:1) and Tris-HCl/DMSO (1:1). The use of DMSO was necessary, because the copper complexes were not soluble in pure buffer. The results corresponding to the frozen-solution EPR spectra evidenced that Tris-HCl binds to copper(II) ions, generating an EPR spectrum with a high  $g_{\parallel}$  value and a low  $A_{\parallel}$  value. These values are characteristic of copper(II) complexes in a tetrahedral geometry; the EPR spectrum obtained is similar to that of  $\text{CuCl}_2$  dissolved in pure Tris-HCl (hence, DMSO does not affect the binding).<sup>106</sup> The frozen-solution spectra of the mononuclear complexes **Cu1** and **Cu2** dissolved in Tris-HCl–DMSO solvent mixtures (1:1 for **Cu1** and 3:1 for **Cu2**) were then recorded. The EPR spectrum of **Cu1** displays a rhombic spectrum with  $g_1$ ,  $g_2$  and  $g_3$  values that are in agreement with a square-planar geometry.<sup>107</sup> Dinuclear **Cu2** is EPR silent, thus suggesting a strong antiferromagnetic interaction between the copper(II) ions. In both cases, the EPR spectrum is different to that of copper-Tris, therefore indicating that the buffer is not competing with ligands **L1** and **L2**.

### Fluorescence-dye displacement

Fluorescence spectroscopy is a valuable technique for the determination and study of the mode of interaction of a molecule with DNA. DNA intercalation and groove binding can be followed through competitive binding studies with well-known fluorescent probes.<sup>108,109</sup> The ability of compounds to displace a particular dye, like for instance a minor groove binder or a DNA intercalator, can be evaluated through the variations of the fluorescence intensity (of the selected dye) upon their addition. In the present study, ethidium bromide (EB) and Hoechst 33258 were used as probes.

EB is a well-known DNA-intercalating agent, which is strongly fluorescent (a 20-fold fluorescence increase is observed) when it is intercalated between DNA base pairs.<sup>110,111</sup> It should be stressed that the quenching of EB fluorescence does not necessarily imply that the studied molecules act as intercalators (like EB). In fact, electrostatic interactions or groove binding may be sufficient to alter significantly the conformation of the DNA double helix, inducing the release of EB.<sup>112,113</sup> Nonetheless, such measurements are useful to better understand the type of DNA interactions that are taking place.

Fluorescence spectra were recorded at constant concentrations of *ct*-DNA and EB (*i.e.* 25 and 125  $\mu$ M, respectively), in the presence of increasing amounts of the complex investigated. Representative emission spectra for DNA-EB in the presence of increasing quantities of **Cu1** are shown in Figure 27.

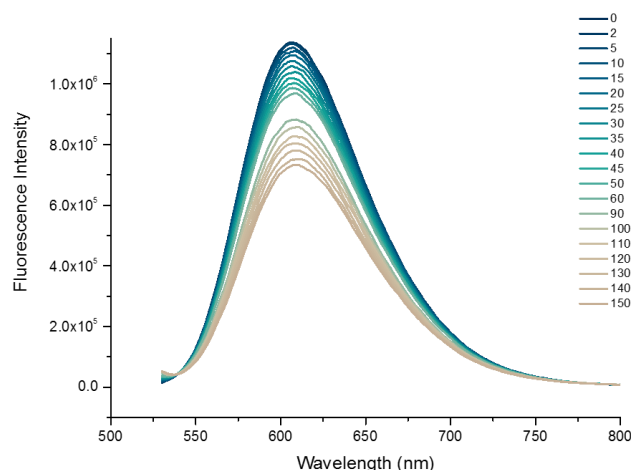


**Figure 27:** Emission spectra of the DNA–EB complex (obtained using [DNA] and [EB] of 25 and 125  $\mu$ M, respectively) in 5 mM Tris-HCl–50 mM NaCl buffer at pH = 7.2,  $\lambda_{\text{exc}}$  = 514 nm,  $\lambda_{\text{em}}$  = 610 nm, upon addition of increasing amounts of Cu1 (2.5–50  $\mu$ M; to a maximum of 2% DMSO).

The fluorescence data (Figure 27 and Experimental section, Figure 90) revealed that all the complexes were able to promote a significant decrease in the emission intensity of DNA-EB, therefore suggesting the occurrence of strong interactions between the different complexes





and *ct*-DNA. To compare the respective affinity of the complexes for *ct*-DNA, their “quenching” efficiency was estimated using the classical Stern-Volmer equation (2), determining the quenching constant,  $K_{SV}$ , by plotting  $I_0/I$  versus [complex], where  $I_0$  is the fluorescence intensity of the DNA bound to ethidium bromide and  $I$  is the fluorescence intensity upon the addition of each concentration.<sup>114</sup>

$$I_0/I = 1 + K[Q] \quad (2)$$

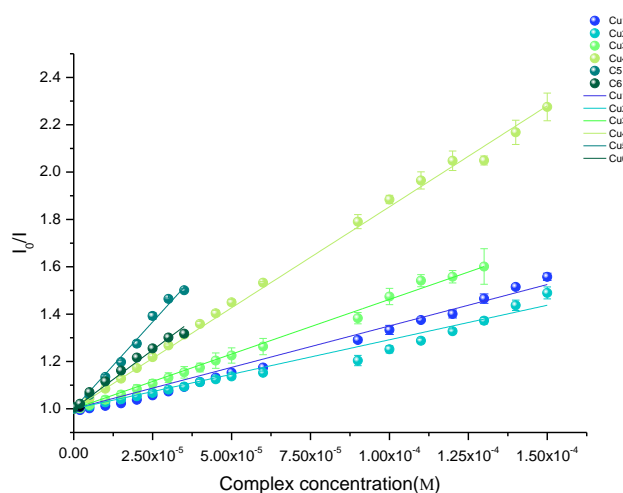


**Figure 28:** Plots of  $I_0/I$  vs. [complex] for the titration of DNA–EB with complexes Cu1–Cu6, in 5 mM Tris-HCl–50 mM NaCl buffer at pH = 7.2,  $\lambda_{em}$  = 610 nm. Experimental data points and linear fitting of the data. [Copper Complex]: 0–150  $\mu$ M; [DNA]: 25  $\mu$ M; [EB]: 125  $\mu$ M.

The  $K_{SV}$  constants determined from the plots depicted in Figure 28 are listed in Table 11. The  $K_{SV}$  values, varying from 2.9 to  $15 \times 10^3 \text{ M}^{-1}$  (Table 11), illustrate the ability of the complexes to displace EB. **Cu5** has the highest  $K_{SV}$  value, which can be explained by its size. As described earlier (see ESI-MS studies), **Cu5** act as a mono-open-cubane in solution, where the hydroxide bridge Cu2B–O1E–Cu2D is broken. Most likely, this bulky species induces a strong distortion of the biomolecule, resulting in the release of EB. The results obtained for the remaining complexes corroborate this assumption. The trinuclear complex **Cu6**, which is the second bulkier compound, and the dinuclear complex **Cu4**, which is sterically hindered, possess the next highest  $K_{SV}$  values. Finally, the data for **Cu1–Cu3** agree with the results obtained by UV-Vis spectroscopy (see Table 10), with **Cu2** showing the lowest affinity for DNA.

**Table 11:** Stern-Volmer constants  $K_{SV}$  determined for complexes Cu1-Cu6 using EB.

Complex	$K_{SV}^{[a]} (10^3 \text{ M}^{-1})$	$\text{Log } K_{SV}$
<b>Cu1</b>	$3.50 \pm 0.01$	3.54
<b>Cu2</b>	$2.92 \pm 0.01$	3.46
<b>Cu3</b>	$4.62 \pm 0.01$	3.66
<b>Cu4</b>	$8.53 \pm 0.01$	3.93
<b>Cu5</b>	$14.69 \pm 0.35$	4.17
<b>Cu6</b>	$9.94 \pm 0.28$	4.00

<sup>[a]</sup>  $K_{SV}$  is obtained from the slope of the straight line. The  $K_{SV}$  errors have been determined from measurements in quadruplicate for each complex.

It is believed that the observed release of EB is due to electrostatic interactions of the complexes with DNA, strongly disturbing its conformation (through a non-intercalative mechanism).<sup>115-118</sup>

Minor-groove binding drugs usually have a crescent and elongated shape and contain several aromatic rings, (such as pyrrole, pyridine or benzene), connected by bonds that allow torsional freedom allowing the molecule to freely shape and adapt to the groove.<sup>119-123</sup>

Hoechst 33258 is a well-known minor-groove binder, which can form hydrogen bonds with particular DNA bases, namely with adenine/thymine (AT) rich sequences fitting neatly into the minor groove; Hoechst 33258 is thus capable of displacing the hydration layer (Scheme 7B and Figure 29).<sup>124</sup> The interaction induces relatively low alterations of the DNA structure. Typically, one of the bases rotates to allow the formation of hydrogen bonding with the drug. When bound to AT-rich sequences, Hoechst 33258 fluoresces at  $\lambda_{em} = 458 \text{ nm}$  when excited at  $\lambda_{exc} = 349 \text{ nm}$  (for free Hoechst 33258,  $\lambda_{exc} = 337$  and  $\lambda_{em} = 508 \text{ nm}$ ). Moreover, the quantum yield of the fluorescence increases from 0.015 (free Hoechst 33258) to 0.42 (Hoechst 33258-bound DNA).<sup>125</sup>

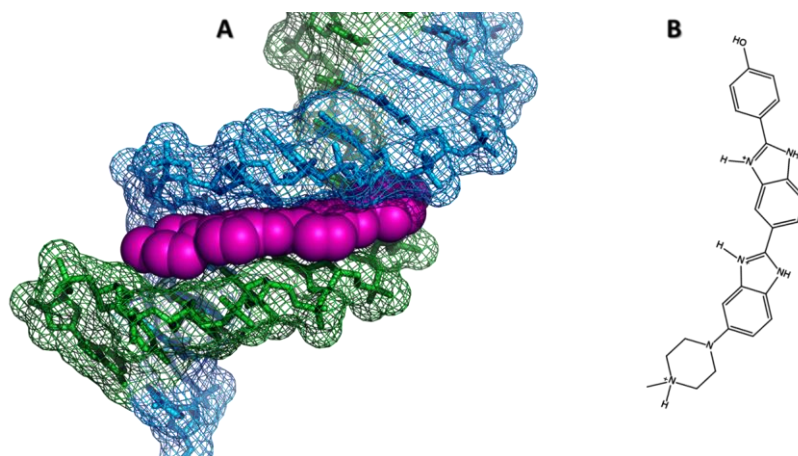




**Figure 29: A. Molecular structure of the DNA A-tract dodecamer d(CGCAAATTTGCG) interacting with Hoechst 33258, as determined by X-ray diffraction analysis B. Representation of the structure of dicationic Hoechst 33258.**<sup>124,126</sup>

The interaction of **Cu1–Cu6** with Hoechst 33258-bound DNA triggers a decrease of the fluorescence intensity, which is indicative of the complex-induced displacement of the dye. Such a fluorescence quenching suggests that the compounds are able to interact with the minor groove of the double helix.

Using the classical Stern-Volmer equation (2), linear regression lines were calculated (Figure 30), which allowed to determine the corresponding  $K_{SV}$  constants (Table 12).

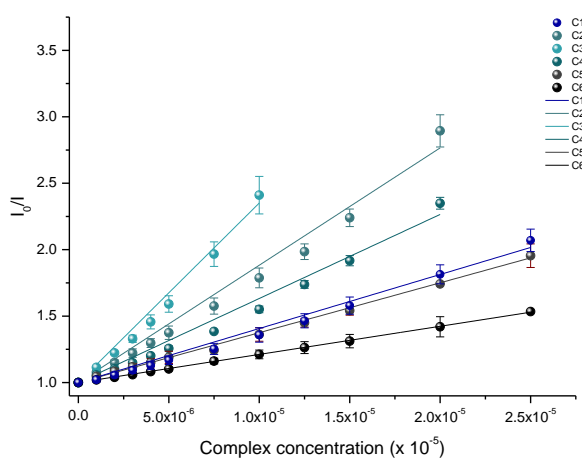


**Figure 30: Plots of  $I_0/I$  vs. [complex] for the titration of DNA–Hoechst 33258 with complexes Cu1–Cu6, at  $\lambda_{exc} = 350$  nm and  $\lambda_{em} = 450$  nm: experimental data points and linear fitting of the data. Concentration of complex: 2–150  $\mu$ M; [DNA]: 0.19  $\mu$ M; [Hoechst 33258]: 15  $\mu$ M.**

The  $K_{SV}$  values varying from 2.1 to  $14 \times 10^4 \text{ M}^{-1}$ , are one order of magnitude higher than those obtained with EB (see above). These features indicate that **Cu1–Cu6** may have a higher propensity to interact in the DNA grooves, rather than to act as intercalators, corroborating the UV-Vis data (see above).

**Table 12: Stern-Volmer  $K_{SV}$  constants determined for complexes Cu1-Cu6 using the minor-groove binder Hoechst 33258.**

Complex	$K_{sv}^{[a]} (10^4 \text{ M}^{-1})$	Log $K_{sv}$
<b>Cu1</b>	$4.07 \pm 0.08$	4.61
<b>Cu2</b>	$8.83 \pm 0.25$	4.95
<b>Cu3</b>	$13.51 \pm 0.36$	5.13
<b>Cu4</b>	$6.33 \pm 0.16$	4.8
<b>Cu5</b>	$3.75 \pm 0.03$	4.57
<b>Cu6</b>	$2.12 \pm 0.01$	4.33

<sup>[a]</sup>  $K_{SV}$  is obtained from the slope of the straight line. The  $K_{SV}$  errors have been determined from measurements in quadruplicate for each complex.

The complexes exhibiting the highest values are **Cu3** and **Cu2**, namely  $13.5$  and  $8.83 \times 10^4 \text{ M}^{-1}$ , respectively. These outcomes could be anticipated; indeed, the size of the complexes is an important factor when considering the DNA minor groove as a target. It is therefore not surprising that compounds **Cu1–Cu4** are those showing certain ability to displace Hoechst 33258 (with the following sequence **Cu3**  $\gg$  **Cu2**  $>$  **Cu4**  $\gg$  **Cu1**; Table 12). With a  $K_{SV}$  value in the range of  $10^{-5} \text{ M}$  range, **Cu3** appears to present the adequate size/structure to fit in the minor groove of DNA.

### Agarose-gel electrophoresis

Agarose-gel electrophoresis is a straightforward technique, commonly used to analyse biomolecules such as DNA, RNA and proteins, based on their size, charge or conformation.<sup>127</sup> In bioinorganic chemistry, this technique is used to evaluate the potential interaction of a coordination compound with plasmid DNA, a double-stranded circular DNA that can be found in bacteria. Plasmid DNA exhibits various forms, which are shown in Figure 31. Hence, plasmid DNA may exist in the normal supercoiled form (form I), the circular nicked form (form II, obtained after the cleavage of one of the double strands) and the linear form (form III, generated when both strands are cleaved). Form I migrates faster than form III, followed by form II (which presents the largest size).

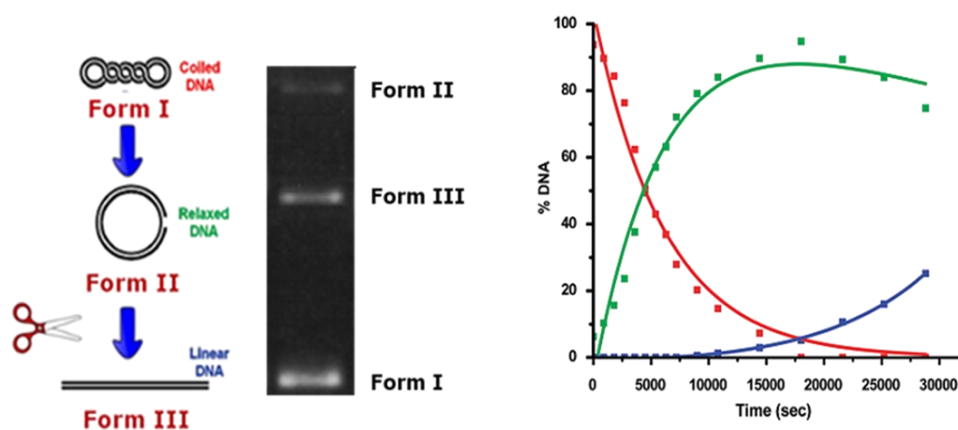


Figure 31: Illustration of the different forms of plasmid DNA upon interaction with a compound that is able to cleave DNA (forming forms II and II). In the left image, the different forms are schematically represented. The right image illustrates the respective appearance/disappearance of the different DNA forms (represented by the % of DNA form, using the different bands intensities) vs different incubation times.<sup>52,128</sup>

The potential cleaving properties of complexes **Cu1–Cu6** were investigated using pBR322 plasmid DNA and a reducing agent, namely ascorbic acid, mimicking the reducing



environment found inside cells.<sup>129</sup> Reduction of copper(II) to copper(I) species can initiate the formation of reactive oxygen species (ROS) that are capable of cleaving DNA.<sup>130-132</sup>

The six copper complexes show a similar behaviour (Figure 32). No linear form III is observed, thus suggesting that the compounds, surprisingly, are not capable of inducing double-strand cleavage of DNA, unlike their parent Hpyrimol-based complex.<sup>62</sup> These distinct properties may be due to the presence of the additional nitrogen atom in the linker connecting the phenol group to the pyridine unit. This nitrogen atom is  $sp^3$ -hybridized, thus causing a disruption of the  $\pi$ -conjugation between the two ligand parts (in contrast to the Hpyrimol ligand).

Figure 32 shows that, upon complex addition, the conversion of form I into form II takes place, associated with a decrease of the intensity of the bands of both form I and form II, at high complex concentrations.

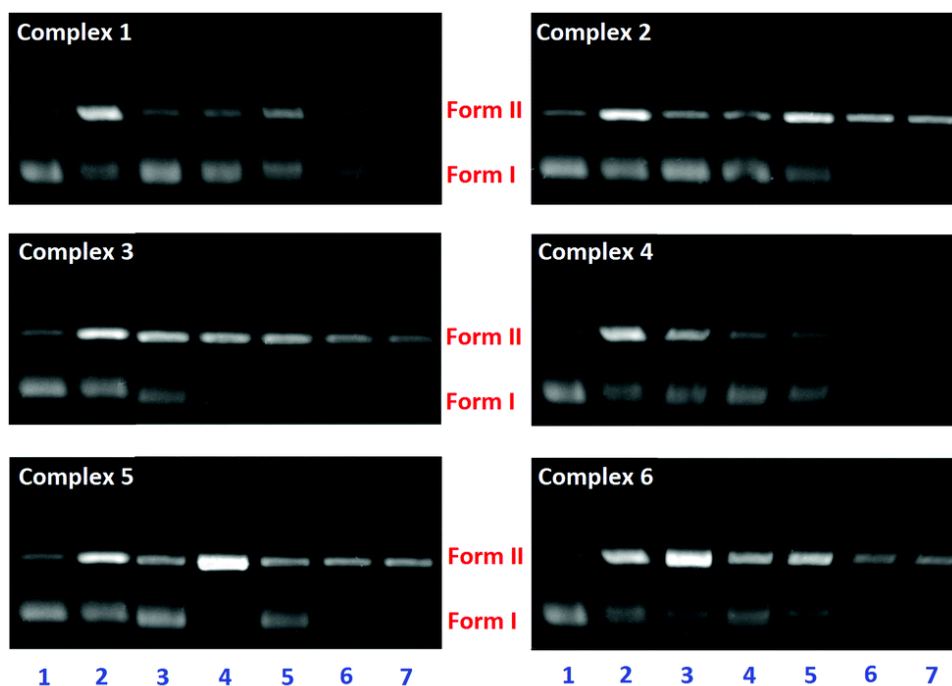


Figure 32: Agarose-gel electrophoresis images of pBR322 plasmid DNA incubated for 24 h at 37 °C with increasing concentrations of complexes Cu1–Cu6, in the presence of a reducing agent, *i.e.* ascorbic acid, during an additional incubation time of 1 h (lanes 3–7). Lane 1: pure plasmid DNA; lane 2: plasmid DNA + ascorbic acid (100  $\mu$ M); lane 3: [complex] = 5  $\mu$ M; lane 4: [complex] = 25  $\mu$ M; lane 5: [complex] = 50  $\mu$ M; lane 6: [complex] = 100  $\mu$ M; lane 7: [complex] = 200  $\mu$ M. Each sample contains 200 ng of plasmid DNA.

Complete disappearance of the bands is observed for **Cu1** and **Cu4**, corroborating earlier spectroscopic data illustrating the existence of strong interactions between the complexes and DNA. As mentioned above, these compounds most likely act as groove binders; the electrophoretic results clearly show that they are not efficient DNA cleavers, in contrast to the copper-pyrimol complex used as model compound. It is thus believed that their interaction with the biomolecule produces large DNA-complex species, destabilizing the usual DNA

coiling, lately forming DNA dimers, trimers, etc., which precipitate (justifying the observed vanishing of the bands). The structurally distinct octanuclear complex **Cu5** (lane 4 in Figure 32) and trinuclear complex **Cu6** (lane 3 in Figure 32) behave differently (compared with **Cu1**–**Cu4**). For instance, form II is the major compound at a concentration of 25  $\mu\text{M}$  for **Cu5** and of 5  $\mu\text{M}$  for **Cu6**, confirming that supercoiled DNA (form I) is affected by these compounds (as observed in the fluorescence experiments). At higher concentrations, a gradual decrease of the intensity of both is noticed, again ascribed to the formation of precipitated DNA-complex species.

Taking into account that all data collected so far suggest that the complexes may act as groove binders, electrophoresis studies have been carried out with the well-known minor-groove binder Hoechst 33258 and the major-groove binder methyl green to compare their electrophoretic bands with those of **Cu1**–**Cu6** (Figure 33). Increasing amounts of the different groove binders were therefore incubated with pBR322 DNA at 37 °C for 24 hours, and the corresponding gels are shown in Figure 33. The electrophoretic patterns for these two groove binders are distinct. With the minor-groove binder Hoechst 33258 (Figure 33, left), both forms I and II gradually disappear upon concentration increase. In the case of the major-groove binder methyl green (Figure 33, right), the bands are not affected by the molecule. **Cu1**–**Cu4** (Figure 32 and Figure 33) appear to behave as Hoechst 33258, thus suggesting that they are acting as DNA minor-groove binders. **Cu5** and **Cu6** may present a different type of interaction, possibly in the major groove, which may be explained by their greater steric bulk.

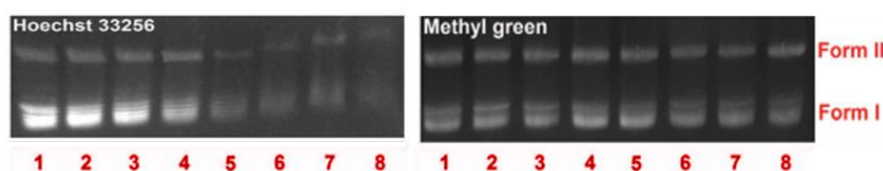


Figure 33: Agarose-gel electrophoresis images of pBR322 plasmid DNA incubated for 24 h at 37 °C with increasing concentrations of Hoechst 33258 (left) and methyl green (right). Hoechst 33258, lane 1: pure plasmid DNA; lane 2: [Hoechst] = 5  $\mu\text{M}$ ; lane 3: [Hoechst] = 10  $\mu\text{M}$ ; lane 4: [Hoechst] = 20  $\mu\text{M}$ ; lane 5: [Hoechst] = 40  $\mu\text{M}$ ; lane 6: [Hoechst] = 60  $\mu\text{M}$ ; lane 7: [Hoechst] = 80  $\mu\text{M}$ ; lane 8: [Hoechst] = 100  $\mu\text{M}$ . Methyl green, lane 1: pure plasmid DNA; lane 2: [methyl green] = 30  $\mu\text{M}$ ; lane 3: [methyl green] = 60  $\mu\text{M}$ ; lane 4: [methyl green] = 100  $\mu\text{M}$ ; lane 5: [methyl green] = 150  $\mu\text{M}$ ; lane 6: [methyl green] = 200  $\mu\text{M}$ ; lane 7: [methyl green] = 300  $\mu\text{M}$ ; lane 8: [methyl green] = 400  $\mu\text{M}$ . Each sample contains 200 ng of plasmid DNA.

### AFM experiments

Atomic force microscopy (AFM) is becoming a valuable tool for biological studies, as the result of its high resolution associated with simple sample preparation. For instance, this technique allows to visualize the DNA structure as well as its dynamics.<sup>133-136</sup> Using AFM, DNA-structural changes induced upon interaction with metal complexes can be detected.<sup>137-139</sup> The interaction of **Cu1**–**Cu6** with pBR322 plasmid DNA has been investigated by AFM





(Figure 34), using experimental conditions comparable to those applied for the agarose-gel electrophoresis studies, for a direct comparison of the results.

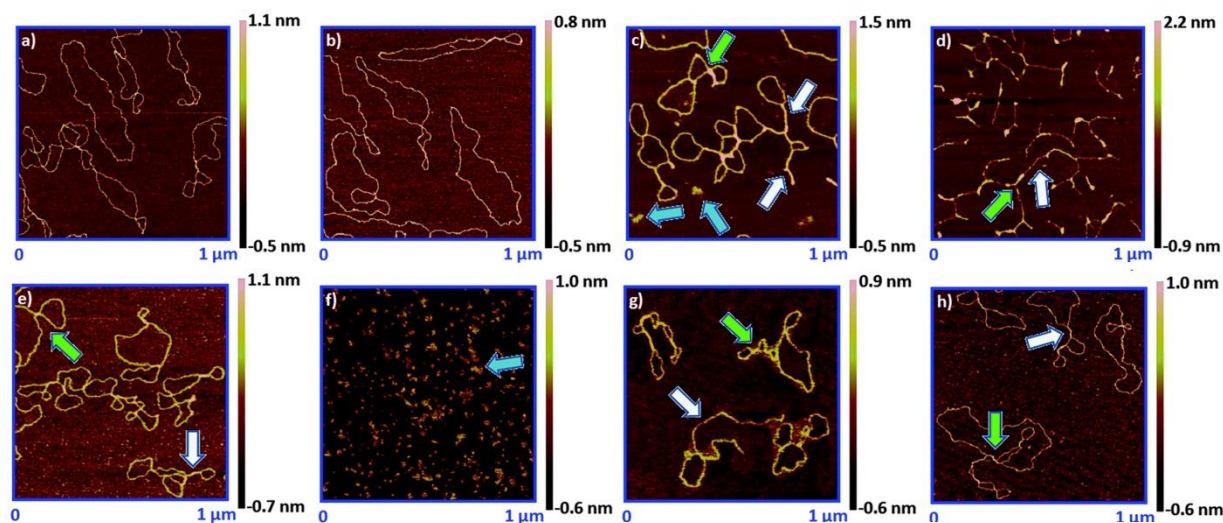


**Figure 34:** AFM images of (a) free pBR322 plasmid DNA; (b) plasmid DNA + ascorbic acid; (c–h) plasmid DNA in the presence of complexes Cu1 to Cu6, respectively. 200 ng DNA per sample; [complex] = 100  $\mu$ M. The white arrows show supercoiling, the green arrows indicate crossing points, and the blue arrows show the initial formation of DNA globular aggregates.

Plasmid DNA is in a dynamic equilibrium between open circular and supercoiled structures, as evidenced in Figure 34a.

DNA was incubated at 37  $^{\circ}$ C for 24 h with the different complexes ([complex] = 100  $\mu$ M) in 40 mM HEPES, 10 mM  $\text{MgCl}_2$  buffer (conditions used in electrophoresis, corresponding at lane 6 in Figure 32). The samples were subsequently incubated for one more hour after addition of ascorbic acid (100  $\mu$ M). The AFM images (Figure 34c–h) show that compounds **Cu1–Cu6** induce some morphological changes of the biomolecule. All the complexes can promote intramolecular DNA supercoiling (see white arrows in Figure 34), confirming the results achieved by UV-Vis, fluorescence and gel electrophoresis (see above). This complex-induced supercoiling of DNA further generates crossing points between strands (green arrows); besides, the formation of DNA-complex aggregates (blue arrows) is detected, which is indicative of a strong interaction between the biomolecule and the coordination compounds. The absence of DNA form III is in agreement with the previous data, which revealed that **Cu1–Cu6** were not DNA-cleaving agents.

### *Cell-viability assays*

The biological activity of the compounds was then examined *in-vitro* (see Experimental section),<sup>140</sup> using three different murine cell lines.

### MTT Reduction Assay

A common method to evaluate the cytotoxicity of a compound is the reduction of tetrazolium salts, measuring mitochondrial activity. The yellow hydrogen acceptor tetrazolium MTT (3-(4, 5-dimethylthiazolyl-2)-2,5-diphenyltetrazolium bromide) is metabolically reduced by active cells, through the action of dehydrogenase enzymes.<sup>141</sup> As a consequence, MTT is converted to its purple metabolite, formazan, which can be solubilized and quantified spectrophotometrically.<sup>140-143</sup> This technique measures the cell-proliferation rate; therefore, when metabolic events lead to apoptosis or necrosis, cell death is perceived. For each cell type, the linear relationship between cell number and signal produced is established, thus allowing an accurate quantification of any alteration of the cell-proliferation rate.<sup>144-146</sup>

IC<sub>50</sub> values for complexes **Cu1–Cu6** and cisplatin (used as reference) were determined with three different murine cell lines, namely mouse fibroblasts (L929), mouse sarcoma cells (S180) and Ehrlich ascites tumour cells (EAT). The IC<sub>50</sub> values (in  $\mu\text{M}$ ) were calculated from the dose–response curves using GraphPad Prism V5.0 for windows (Graphpad Software, San Diego, CA, USA). All the data are shown as the mean values  $\pm$  S.D. of three independent experiments (Figure 35 and Table 13).

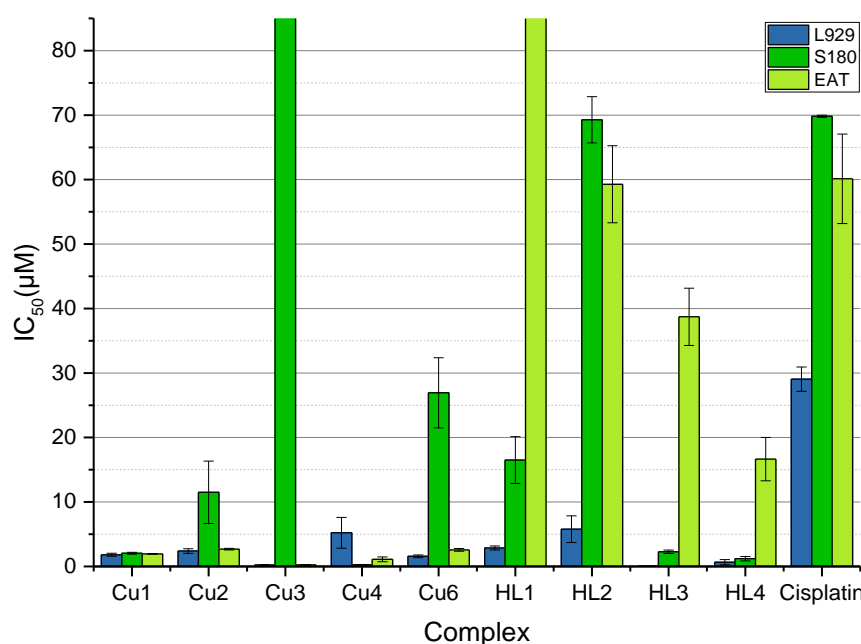


Figure 35: IC<sub>50</sub> values ( $\mu\text{M}$ ) of **Cu1–Cu6**, the ligands **HL1–HL4** and cisplatin against three murine cell lines, after 48 h of incubation. The values for **Cu5** were omitted for graphical clarity. The data shown are means  $\pm$  SD of three independent experiments.

Except **Cu5**, all other compounds exhibit high cytotoxicity against the three cell lines investigated, significantly better than cisplatin. Dinuclear **Cu3** and **Cu4** are greatly cytotoxic, as reflected by their IC<sub>50</sub> values, which are significantly smaller than those of the mononuclear





complexes **Cu1** and **Cu2** (Figure 35 and Table 13). The non-cytotoxic behaviour noticed for octanuclear complex **Cu5** may be due to its voluminous size that can affect its cell internalization. Moreover, **Cu5** is less soluble than the other compounds. Finally, **Cu6** is active against two cell lines, namely L929 and EAT, with IC<sub>50</sub> values in the range of those of **Cu1** and **Cu2** (Table 13).

The free ligands **HL1**–**HL4** were tested as well. Once inside the cell, the ligands may be toxic by themselves, but they may also bind intracellular metal ions (like copper or zinc), thus generating cytotoxic complexes that will lead to cell death.

**Table 13:** IC<sub>50</sub> values (μM) of copper complexes **Cu1**–**Cu6**, the ligands **HL1**–**HL4** and cisplatin against three murine cell lines, after 48 h of incubation. The data shown are means ± SD of three independent experiments.

Compound	L929 <sup>[a]</sup>	S180 <sup>[b]</sup>	EAT <sup>[c]</sup>
<b>Cu1</b>	1.81 ± 0.23	2.05 ± 0.14	1.95 ± 0.06
<b>Cu2</b>	2.39 ± 0.36	11.50 ± 4.84	2.68 ± 0.12
<b>Cu3</b>	0.23 ± 0.01 <sup>[d]</sup>	N.D. <sup>[e]</sup>	0.24 ± 0.02 <sup>[d]</sup>
<b>Cu4</b>	5.22 ± 2.39 <sup>[f]</sup>	0.27 ± 0.03 <sup>[g]</sup>	1.11 ± 0.37 <sup>[h]</sup>
<b>Cu5</b>	— <sup>[i]</sup>	>200	— <sup>[i]</sup>
<b>Cu6</b>	1.57 ± 0.21 <sup>[j]</sup>	26.93 ± 5.45 <sup>[k]</sup>	2.57 ± 0.21 <sup>[l]</sup>
<b>HL1</b>	2.87 ± 0.30	16.50 ± 3.63	142.70 ± 4.65
<b>HL2</b>	5.79 ± 2.07	69.27 ± 3.59	59.28 ± 5.97
<b>HL3</b>	0.04 ± 0.01	2.27 ± 0.27	38.72 ± 4.44
<b>HL4</b>	0.66 ± 0.4	1.20 ± 0.34	16.64 ± 3.36
<b>Cisplatin</b>	29.05 ± 1.88	69.83 ± 0.17	60.13 ± 6.94

<sup>[a]</sup> Mouse fibroblasts. <sup>[b]</sup> Mouse sarcoma cells. <sup>[c]</sup> Ehrlich ascites tumour cells. <sup>[d]</sup> 0.46 μM based on Cu. <sup>[e]</sup> Not determined.

<sup>[f]</sup> 10.44 μM based on Cu. <sup>[g]</sup> 0.54 μM based on Cu. <sup>[h]</sup> 2.22 μM based on Cu. <sup>[i]</sup> Too high value. <sup>[j]</sup> 4.71 μM based on Cu.

<sup>[k]</sup> 80.79 μM based on Cu. <sup>[l]</sup> 7.71 μM based on Cu.

Ligands **HL1** and **HL2** are clearly much less cytotoxic than **Cu1** and **Cu2** against EAT and S180 cells. Some significant activity is observed for these ligands against L929 cells, although lower than the corresponding complexes (Table 13). The dinucleating **HL3** and **HL4** are highly cytotoxic against L929 and S180 cells, with IC<sub>50</sub> values in the nano-range in the case of L929 (Table 13). **Cu1** and **Cu4**, and the corresponding ligands **HL1** and **HL4** were investigated further with several human cancer cell lines, namely A549 (lung adenocarcinoma), A375 (melanoma), DMS53 (small cell lung cancer), MCF-7 (breast adenocarcinoma), SW620 (colorectal adenocarcinoma) and SKOV3 (ovary adenocarcinoma). Cisplatin and Cu(phen)<sub>2</sub>, were used as platinum and copper reference compounds.<sup>147</sup> The corresponding IC<sub>25-75</sub> results, after 24 hours incubation, are illustrated in Figure 36 and listed in Table 14.

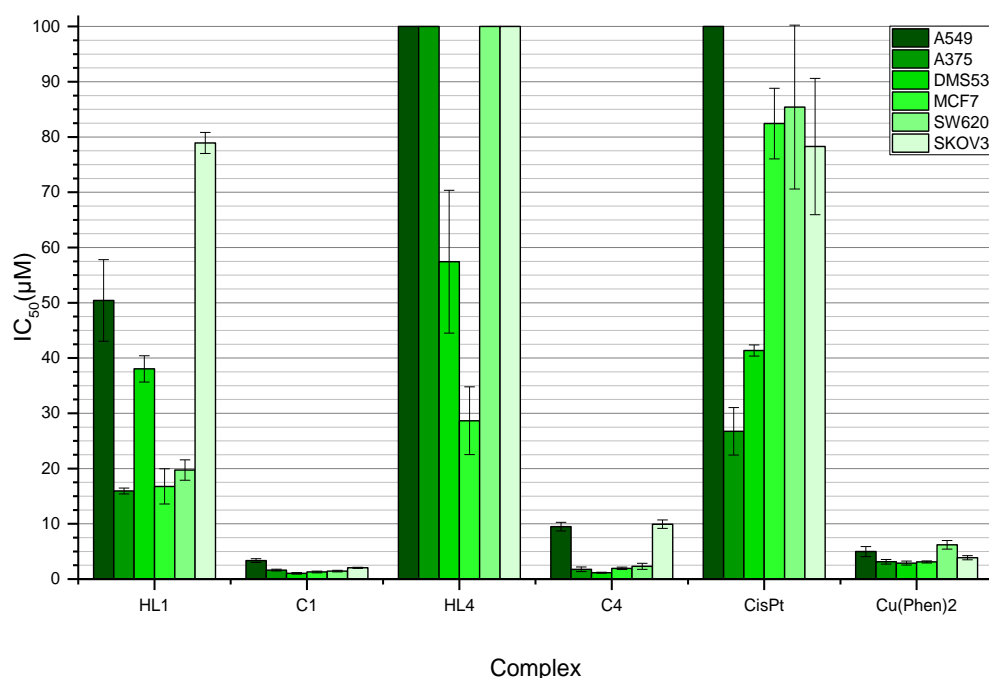


**Figure 36:**  $IC_{50}$  values ( $\mu M$ ) for different cell lines, namely A549 (lung adenocarcinoma), A375 (melanoma), DMS53 (small cell lung carcinoma), MCF-7 (breast adenocarcinoma), SW620 (colorectal adenocarcinoma) and SKOV3 (ovary adenocarcinoma), after 24 incubation with, HL1, Cu1, HL4, Cu4, cisplatin and  $[Cu(phen)_2]Cl_2$ . The results are means  $\pm$  SD of three separate experiments.

The ligands are clearly less toxic than the corresponding complexes. Ligand **HL1** is slightly more toxic than ligand **HL4** and the reference inorganic compound cisplatin. It can also be noticed that ligand **HL1** is more efficient against melanoma, breast and colorectal adenocarcinoma, whereas **HL4** shows some efficiency against small cell lung carcinoma cells, in addition to melanoma. Interestingly, **HL4** appears to be more toxic against lung small cells (*i.e.* DMS53), than against lung normal cells (*i.e.* A549). It should be stressed here that small cell lung carcinoma is one of the most aggressive forms of lung cancer.

The copper complexes are significantly more active than the corresponding free ligands (Figure 36).



**Table 14:** IC<sub>25-75</sub> values (μM) of **Cu1**, **Cu4**, **HL1**, **HL4**, cisplatin and **Cu(phen)<sub>2</sub>** against different cancer cell lines, namely **A549** (lung adenocarcinoma), **A375** (melanoma), **DMS53** (small cell lung carcinoma), **MCF-7** (breast adenocarcinoma), **SW620** (colorectal adenocarcinoma) and **SKOV3** (ovary adenocarcinoma), after an incubation time of 24 h. The results are means ± SD of three separate experiments.

		<b>A549</b>	<b>A375</b>	<b>DMS53</b>	<b>MCF7</b>	<b>SW620</b>	<b>SKOV3</b>
<b>HL1</b>	IC <sub>25</sub>	20.8 ± 1.81	3.56 ± 0.80	15.8 ± 3.19	3.00 ± 0.71	6.97 ± 1.19	31.9 ± 0.31
	IC <sub>50</sub>	50.4 ± 7.38	15.9 ± 0.53	38.0 ± 2.38	16.8 ± 3.20	19.7 ± 1.9	78.9 ± 1.90
	IC <sub>75</sub>	94.0 ± 11.4	45.8 ± 2.78	73.6 ± 1.15	50.0 ± 3.32	48.9 ± 11.8	> 100
<b>Cu1</b>	IC <sub>25</sub>	1.27 ± 0.17	0.96 ± 0.17	0.70 ± 0.09	0.61 ± 0.06	0.61 ± 0.06	0.96 ± 0.07
	IC <sub>50</sub>	3.34 ± 0.34	1.63 ± 0.15	1.04 ± 0.15	1.29 ± 0.17	1.43 ± 0.14	2.04 ± 0.11
	IC <sub>75</sub>	6.90 ± 0.59	3.06 ± 0.29	1.94 ± 0.35	2.81 ± 0.64	3.34 ± 0.44	4.20 ± 0.04
<b>HL4</b>	IC <sub>25</sub>	7.68 ± 0.18	17.1 ± 2.60	5.65 ± 1.35	1.60 ± 0.25	5.39 ± 0.75	42.1 ± 7.6
	IC <sub>50</sub>	> 100	> 100	57.4 ± 12.9	28.7 ± 6.13	> 100	> 100
	IC <sub>75</sub>	> 100	> 100	> 100	> 100	> 100	> 100
<b>Cu4</b>	IC <sub>25</sub>	3.40 ± 0.71	0.96 ± 0.20	0.73 ± 0.08	0.67 ± 0.10	0.80 ± 0.12	2.59 ± 0.64
	IC <sub>50</sub>	9.48 ± 0.78	1.76 ± 0.42	1.14 ± 0.08	1.94 ± 0.21	2.32 ± 0.55	9.94 ± 0.77
	IC <sub>75</sub>	26.3 ± 5.42	4.02 ± 1.01	2.38 ± 0.13	5.59 ± 0.96	6.13 ± 2.32	19.5 ± 0.52
<b>Cisplatin</b>	IC <sub>25</sub>	54.4 ± 12.6	9.45 ± 2.41	12.9 ± 1.10	43.5 ± 4.78	42.9 ± 4.21	35.1 ± 6.4
	IC <sub>50</sub>	> 100	26.7 ± 4.31	41.4 ± 1.00	82.4 ± 6.39	85.4 ± 14.8	78.3 ± 12.3
	IC <sub>75</sub>	> 100	59.0 ± 4.15	174.99	> 100	> 100	> 100
<b>Cu(Phen)<sub>2</sub></b>	IC <sub>25</sub>	2.22 ± 0.33	1.59 ± 0.28	1.55 ± 0.22	1.29 ± 0.20	2.81 ± 0.28	1.90 ± 0.18
	IC <sub>50</sub>	4.98 ± 0.90	3.14 ± 0.41	2.89 ± 0.36	3.10 ± 0.19	6.21 ± 0.79	3.87 ± 0.38
	IC <sub>75</sub>	11.0 ± 2.18	6.69 ± 0.80	6.35 ± 0.64	7.58 ± 0.35	12.8 ± 1.67	8.15 ± 0.83

The mononuclear complex **Cu1** is more efficient than dinuclear **Cu4**. As for the free ligands, higher efficiencies towards lung small cells is observed; For instance, **Cu4** is nine times more toxic for DMS53, compared to A549. Finally, it can also be noted that both complexes present lower IC<sub>50</sub> values than the reference molecules (Table 14).

In view of the remarkable results obtained with **Cu1** and **Cu4** with several cell lines (Table 13 and (Table 14), it was decided to investigate their efficiency against neuroblastoma, which is a rare but very aggressive cancer that affects children, mostly under the age of 5 years old. Neuroblastoma is an embryonic malignancy of early childhood and it is characterized as a solid, extracranial tumour. It is a cancer with very poor prognosis, especially for kids diagnosed between birth and 18 months of age.<sup>148</sup> This tumour oscillates from spontaneous regression to relentless progression regardless of rigorous multimodal treatments,<sup>149</sup> and has the highest metastatic rate. Usually, it can easily spread to liver, bone marrow, skin as well as several other organs.<sup>150-153</sup>

The antineoplastic drug SN38 (7-ethyl-10-hydroxy-camptothecin, Figure 52), which is used to treat neuroblastoma, was used as a reference compound.<sup>154-156</sup>

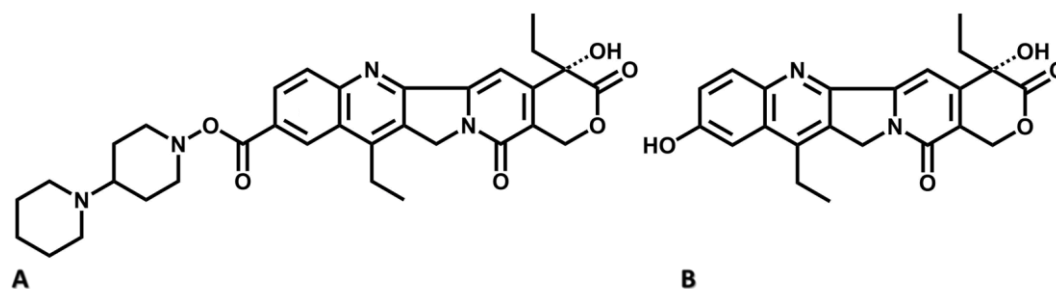


**Figure 37:** Representation of the chemical structures of A. irinotecan (CPT-11 or (4S)-4,11-diethyl-4-hydroxy-3,14-dioxo-3,4,12,14-tetrahydro-1H-pyrano[3',4':6,7]indolizino[1,2-b]quinolin-9-yl-1,4'-bipiperidine-1'-carboxylate) and its metabolite B. SN38 (7-ethyl-10-hydroxy-camptothecin).

SN38 is known to be the active metabolite of irinotecan ((4S)-4,11-diethyl-4-hydroxy-3,14-dioxo-3,4,12,14-tetrahydro-1H-pyrano[3',4':6,7]indolizino[1,2-b]quinolin-9-yl-1,4'-bipiperidine-1'-carboxylate), which is also an active compound used against neuroblastoma. Irinotecan is the synthetic derivative of camptothecin, an alkaloid found in a Chinese plant, which acts as an inhibitor of DNA topoisomerase I. This molecule has been used extensively in the treatment of several types of tumours. The hydrolysis of irinotecan produces SN38, which is 1000 times more active than its parent compound; however, it shows high toxicity and notable solubility issues.<sup>54,55</sup>

Two neuroblastoma cell lines were used for these additional studies, namely SK-N-BE(2) and CHLA-90. The results are summarized in Table 19 and Figure 53.

**Table 15:** IC<sub>25-75</sub> values (μM) of Cu1, Cu4 and the control compound SN38 for the neuroblastoma cell lines SK-N-BE(2) and CHLA-90, determined after an incubation time of 24 h. The data shown are means ± SD of three independent experiments.

SKNBE-2		
Cu1	Cu4	SN38
3.69 ± 0.20	2.76 ± 0.24	1.27 ± 0.14
6.43 ± 0.34	5.00 ± 0.41	7.57 ± 0.61
10.3 ± 0.47	8.81 ± 0.62	37.0 ± 1.65
CHLA90		
Cu1	Cu4	SN38
1.75 ± 0.10	2.21 ± 0.30	6.18 ± 0.53
3.78 ± 0.36	5.75 ± 0.78	12.7 ± 0.83
7.56 ± 0.81	12.0 ± 0.19	19.2 ± 1.81

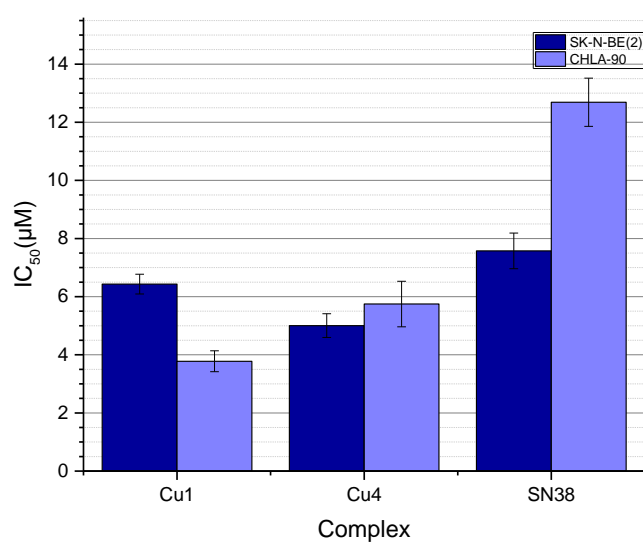


**Figure 38:** Graphical representation of the IC<sub>50</sub> values (in μM) for the Cu(II) complexes Cu1 and Cu4 and the reference compound SN38, in two neuroblastoma cell lines, namely SK-N- BE(2) and SCLA-90, determined after an incubation time of 24 h.

**Cu1** and **Cu4** exhibit comparable activities for both cell lines (Table 19). Compared to the reference compound SN38, The IC<sub>50</sub> values of the copper complexes are analogous against SK-N-BE(2) cells. For the CHLA90 cell line, **Cu1** and **Cu4** are respectively 3 and 2 times more active than SN38 (Table 19).

## Conclusions

Four new Schiff bases (**HL1–HL4**), inspired by the ligand Hpyrimol, were carefully designed, synthesized and fully characterized. Different copper(II) complexes were subsequently prepared with the idea to produce efficient chemical nucleases, as the parent compound  $[\text{Cu}^{\text{II}}(\text{pyrimol})\text{Cl}]$ . Hence, reaction of the ligands with various copper salts led to the generation of a series of mono (**Cu1** and **Cu2**), di (**Cu3** and **Cu4**) and polynuclear (**Cu5** and **Cu6**) complexes, which were structurally characterized by means of single-crystal X-ray diffraction studies.

The DNA-interacting properties of the six copper(II) complexes were accessed using complementary analytical techniques. Surprisingly, the results showed that **Cu1–Cu6** were not able to cleave the DNA strands through a redox process, contrary to the analogous complex  $[\text{Cu}^{\text{II}}(\text{pyrimol})\text{Cl}]$ , from which they were derived from. However, the copper compounds were capable of interacting with the biomolecule, mostly through groove binding. These strong interactions could induce intramolecular DNA coiling, as indicated by several techniques.

The cytotoxic behaviour of the complexes was then evaluated, and their  $\text{IC}_{25-75}$  values were determined for three murine cell types and eight human cancer cell lines. All complexes, except **Cu5**, showed outstanding cytotoxic properties, better than the reference compound cisplatin (under the same experimental conditions). The dinuclear complexes **Cu3** and **Cu4** present better  $\text{IC}_{50}$  values (about 10 times lower) than those of the mononuclear complexes **Cu1** and **Cu2**. Complex **Cu6** shows some selectivity towards L929 and EAT cells, with  $\text{IC}_{50}$  values in the range of those of **Cu1** and **Cu2**. The ligands **HL1** and **HL2** are less active than the corresponding copper compounds. However, **HL3** and **HL4** exhibit notable cytotoxic properties for the murine cell lines. The promising complexes **Cu1**, **Cu4** and the respective **HL1** and **HL4** were further tested against human cancer cell lines. The results revealed that **HL1** is more toxic than **HL4** and cisplatin, and shows higher selectivity against melanoma, breast and colorectal adenocarcinoma. Interestingly, **Cu4** and **HL4** are more selective against lung small cancer cells (DMS53) than the epithelial ones (A549). In general, the mononuclear complex **Cu1** is more efficient than dinuclear **Cu4**. Finally, both **Cu1** and **Cu4** showed remarkable cytotoxicity behaviours towards two neuroblastoma cell lines, in the range of a reference compound that is currently used clinically.

It can be pointed out here that the biodistribution and bioavailability of some of the complexes presented in this chapter are currently investigated in Poland. Polatom has prepared two complexes using radioactive copper and is performing biological studies with mice. Furthermore, the encapsulation of several compounds described in this chapter has been carried





out by Ecopol Tech; the use of polymeric capsules (as drug carriers) allows to have hydrophilic systems (the free compounds being poorly soluble in water), which can reach and enter the cells easier. These studies are currently being performed.

## References

- (1) Pfaender, S.; Grabrucker, A. M. *Metallomics* **2014**, *6*, 960.
- (2) Li, D. D.; Tian, J. L.; Gu, W.; Liu, X.; Zeng, H. H.; Yan, S. P. *J. Inorg. Biochem.* **2011**, *105*, 894.
- (3) van Rijt, S. H.; Sadler, P. J. *Drug Discov. Today* **2009**, *14*, 1089.
- (4) Marzano, C.; Pellei, M.; Tisato, F.; Santini, C. *Anticancer Agents Med. Chem.* **2009**, *9*, 185.
- (5) Tardito, S.; Marchio, L. *Curr. Med. Chem.* **2009**, *16*, 1325.
- (6) Denoyer, D.; Masaldan, S.; La Fontaine, S.; Cater, M. A. *Metallomics* **2015**, *7*, 1459.
- (7) Santini, C.; Pellei, M.; Gandin, V.; Porchia, M.; Tisato, F.; Marzano, C. *Chem. Rev.* **2014**, *114*, 815.
- (8) Farrell, N. *Transition metal complexes as drugs and chemotherapeutic agents*; Kluwer Academic Publishers: Dordrecht ; Boston, 1989.
- (9) Silva, J. J. R. F. d.; Williams, R. J. P. *The biological chemistry of the elements : The inorganic chemistry of life*; 2nd ed.; Oxford University Press: Oxford ; New York, 2001.
- (10) Wang, T.; Guo, Z. *Curr. Med. Chem.* **2006**, *13*, 525.
- (11) Brissos, R. F.; Caubet, A.; Gamez, P. *Eur. J. Inorg. Chem.* **2015**, *2015*, 2633.
- (12) Daniel, K. G.; Harbach, R. H.; Guida, W. C.; Dou, Q. P. *Front. Biosci.* **2004**, *9*, 2652.
- (13) Park, K. C.; Fouani, L.; Jansson, P. J.; Wooi, D.; Sahni, S.; Lane, D. J.; Palanimuthu, D.; Lok, H. C.; Kovacevic, Z.; Huang, M. L.; Kalinowski, D. S.; Richardson, D. R. *Metallomics* **2016**.
- (14) Brissos, R. F.; García, S.; Presa, A.; Gamez, P. *Comments Inorg. Chem.* **2011**, *32*, 219.
- (15) Cao, H.; Wang, Y. *Nucleic Acids Res.* **2007**, *35*, 4833.
- (16) Koppenol, W. H. *Redox Rep.* **2001**, *6*, 229.
- (17) Valko, M.; Rhodes, C. J.; Moncol, J.; Izakovic, M.; Mazur, M. *Chem. Biol. Interact.* **2006**, *160*, 1.
- (18) Arredondo, M.; Nunez, M. T. *Mol. Aspects Med.* **2005**, *26*, 313.
- (19) Turski, M. L.; Thiele, D. J. *J. Biol. Chem.* **2009**, *284*, 717.
- (20) Tisato, F.; Marzano, C.; Porchia, M.; Pellei, M.; Santini, C. *Med. Res. Rev.* **2010**, *30*, 708.
- (21) Wang, X.; Yan, M.; Wang, Q.; Wang, H.; Wang, Z.; Zhao, J.; Li, J.; Zhang, Z. *Molecules* **2017**, *22*.
- (22) Valko, M.; Morris, H.; Cronin, M. T. *Curr. Med. Chem.* **2005**, *12*, 1161.
- (23) Bowen, R. J.; Navarro, M.; Shearwood, A. M.; Healy, P. C.; Skelton, B. W.; Filipovska, A.; Berners-Price, S. J. *Dalton Trans.* **2009**, 10861.
- (24) Gandin, V.; Porchia, M.; Tisato, F.; Zanella, A.; Severin, E.; Dolmella, A.; Marzano, C. *J. Med. Chem.* **2013**, *56*, 7416.
- (25) Lopes, J.; Alves, D.; Morais, T. S.; Costa, P. J.; Piedade, M. F.; Marques, F.; Villa de Brito, M. J.; Helena Garcia, M. *J. Inorg. Biochem.* **2017**, *169*, 68.
- (26) Zanella, A.; Gandin, V.; Porchia, M.; Refosco, F.; Tisato, F.; Sorrentino, F.; Scutari, G.; Rigobello, M. P.; Marzano, C. *Invest. New Drugs* **2011**, *29*, 1213.
- (27) Dwyer, F. P.; Mayhew, E.; Roe, E. M.; Shulman, A. *Br. J. Cancer* **1965**, *19*, 195.
- (28) Sigman, D. S.; Graham, D. R.; D'Aurora, V.; Stern, A. M. *J. Biol. Chem.* **1979**, *254*, 12269.





- (29) Mazumder, A.; Sutton, C. L.; Sigman, D. S. *Inorg. Chem.* **1993**, *32*, 3516.
- (30) Sigman, D. S. *Acc. Chem. Res.* **1986**, *19*, 180.
- (31) de Hoog, P.; Louwerse, M. J.; Gamez, P.; Pitié, M.; Baerends, E. J.; Meunier, B.; Reedijk, J. *Eur. J. Inorg. Chem.* **2008**, *2008*, 612.
- (32) Grau, J.; Brissos, R. F.; Salinas-Uber, J.; Caballero, A. B.; Caubet, A.; Roubeau, O.; Korrodi-Gregorio, L.; Perez-Tomas, R.; Gamez, P. *Dalton Trans.* **2015**, *44*, 16061.
- (33) Hoog, P.; Boldron, C.; Gamez, P.; Sliedregt-Bol, K.; Roland, I.; Pitie, M.; Kiss, R.; Meunier, B.; Reedijk, J. *J. Med. Chem.* **2007**, *50*, 3148.
- (34) Meenongwa, A.; Brissos, R. F.; Soikum, C.; Chaveerach, P.; Gamez, P.; Trongpanich, Y.; Chaveerach, U. *New J. Chem.* **2015**, *39*, 664.
- (35) Pratumwieng, R.; Meenongwa, A.; Brissos, R. F.; Gamez, P.; Trongpanich, Y.; Chaveerach, U. *Transition Met. Chem.* **2017**, *1*.
- (36) McMillin, D. R.; McNett, K. M. *Chem. Rev.* **1998**, *98*, 1201.
- (37) Humphreys, K. J.; Karlin, K. D.; Rokita, S. E. *J. Am. Chem. Soc.* **2002**, *124*, 8055.
- (38) Selvakumar, B.; Rajendiran, V.; Uma Maheswari, P.; Stoeckli-Evans, H.; Palaniandavar, M. *J. Inorg. Biochem.* **2006**, *100*, 316.
- (39) Zhao, Y.; Zhu, J.; He, W.; Yang, Z.; Zhu, Y.; Li, Y.; Zhang, J.; Guo, Z. *Chem. Eur. J.* **2006**, *12*, 6621.
- (40) Cadoni, E.; Valletta, E.; Caddeo, G.; Isaia, F.; Cabiddu, M. G.; Vascellari, S.; Pivetta, T. *J. Inorg. Biochem.* **2017**, *173*, 126.
- (41) Pivetta, T.; Isaia, F.; Trudu, F.; Pani, A.; Manca, M.; Perra, D.; Amato, F.; Havel, J. *Talanta* **2013**, *115*, 84.
- (42) Tisato, F.; Marzano, C.; Porchia, M.; Pellei, M.; Santini, C. *Med. Res. Rev.* **2010**, *30*, 708.
- (43) Crim, J. A.; Petering, H. G. *Cancer Res.* **1967**, *27*, 1278.
- (44) Kilari, D.; Guancial, E.; Kim, E. S. *World J. Clin. Oncol.* **2016**, *7*, 106.
- (45) van der Steen, S.; de Hoog, P.; van der Schilden, K.; Gamez, P.; Pitie, M.; Kiss, R.; Reedijk, J. *Chem. Commun.* **2010**, *46*, 3568.
- (46) Palanimuthu, D.; Shinde, S. V.; Somasundaram, K.; Samuelson, A. G. *J. Med. Chem.* **2013**, *56*, 722.
- (47) Chauhan, M.; Banerjee, K.; Arjmand, F. *Inorg. Chem.* **2007**, *46*, 3072.
- (48) Zaidi, Y.; Arjmand, F.; Zaidi, N.; Usmani, J. A.; Zubair, H.; Akhtar, K.; Hossain, M.; Shadab, G. G. *Metallomics* **2014**, *6*, 1469.
- (49) Gamez, P.; Arends, I. W. C. E.; Reedijk, J.; Sheldon, R. A. *Chem. Commun.* **2003**, 2414.
- (50) Zhang, X.; Bi, C.; Fan, Y.; Cui, Q.; Chen, D.; Xiao, Y.; Dou, Q. P. *Int. J. Mol. Med.* **2008**, *22*, 677.
- (51) Zhang, Z.; Wang, H.; Yan, M.; Wang, H.; Zhang, C. *Mol. Med. Report.* **2017**, *15*, 3.
- (52) Lee, K. C.; Bramley, R. L.; Cowell, I. G.; Jackson, G. H.; Austin, C. A. *Biochem. Pharmacol.* **2016**, *103*, 29.
- (53) Dhar, S.; Nethaji, M.; Chakravarty, A. R. *Inorg. Chem.* **2006**, *45*, 11043.
- (54) An, Y.; Tong, M. L.; Ji, L. N.; Mao, Z. W. *Dalton Trans.* **2006**, 2066.
- (55) Qiao, X.; Ma, Z. Y.; Xie, C. Z.; Xue, F.; Zhang, Y. W.; Xu, J. Y.; Qiang, Z. Y.; Lou, J. S.; Chen, G. J.; Yan, S. P. *J. Inorg. Biochem.* **2011**, *105*, 728.
- (56) Li, D. D.; Huang, F. P.; Chen, G. J.; Gao, C. Y.; Tian, J. L.; Gu, W.; Liu, X.; Yan, S. P. *J. Inorg. Biochem.* **2010**, *104*, 431.

- (57) Tjioe, L.; Joshi, T.; Brugger, J.; Graham, B.; Spiccia, L. *Inorg. Chem.* **2011**, *50*, 621.
- (58) Ganguly, A.; Chakraborty, P.; Banerjee, K.; Choudhuri, S. K. *Eur. J. Pharm. Sci.* **2014**, *51*, 96.
- (59) Singh, K.; Barwa, M. S.; Tyagi, P. *Eur. J. Med. Chem.* **2006**, *41*, 147.
- (60) Tai, A. W.; Lien, E. J.; Lai, M. M.; Khwaja, T. A. *J. Med. Chem.* **1984**, *27*, 236.
- (61) Wang, P. H.; Keck, J. G.; Lien, E. J.; Lai, M. M. *J. Med. Chem.* **1990**, *33*, 608.
- (62) Shakir, M.; Abbasi, A.; Khan, A. U.; Khan, S. N. *Spectrochim. Acta A Mol. Biomol. Spectrosc.* **2011**, *78*, 29.
- (63) Spinu, C.; Kriza, A. *Acta Chem. Slov.* **2000**, *47*, 179.
- (64) Maheswari, P. U.; Roy, S.; den Dulk, H.; Barends, S.; van Wezel, G.; Kozlevcar, B.; Gamez, P.; Reedijk, J. *J. Am. Chem. Soc.* **2006**, *128*, 710.
- (65) Roy, S.; Maheswari, P. U.; Lutz, M.; Spek, A. L.; den Dulk, H.; Barends, S.; van Wezel, G. P.; Hartl, F.; Reedijk, J. *Dalton Trans.* **2009**, *0*, 10846.
- (66) de Hoog, P.; Pachon, L. D.; Gamez, P.; Lutz, M.; Spek, A. L.; Reedijk, J. *Dalton Trans.* **2004**, 2614.
- (67) Maheswari, P. U.; Barends, S.; Ozalp-Yaman, S.; de Hoog, P.; Casellas, H.; Teat, S. J.; Massera, C.; Lutz, M.; Spek, A. L.; van Wezel, G. P.; Gamez, P.; Reedijk, J. *Chem. Eur. J.* **2007**, *13*, 5213.
- (68) de Hoog, P.; Pachon, L. D.; Gamez, P.; Lutz, M.; Spek, A. L.; Reedijk, J. *Dalton Trans.* **2004**, 2614.
- (69) Jazdzewski, B. A.; Tolman, W. B. *Coord. Chem. Rev.* **2000**, *200*, 633.
- (70) Ozalp-Yaman, S.; de Hoog, P.; Maheswari, P. U.; Casellas, H.; Golobic, A.; Kozlevcar, B.; Gamez, P.; Reedijk, J. *Electrochim. Acta* **2010**, *55*, 8655.
- (71) Acilan, C.; Cevatemre, B.; Adiguzel, Z.; Karakas, D.; Ulukaya, E.; Ribeiro, N.; Correia, I.; Pessoa, J. C. *Biochim. Biophys. Acta* **2017**, *1861*, 218.
- (72) Maheswari, P. U.; Barends, S.; Ozalp-Yaman, S.; de Hoog, P.; Casellas, H.; Teat, S. J.; Massera, C.; Lutz, M.; Spek, A. L.; van Wezel, G. P.; Gamez, P.; Reedijk, J. *Chem.-Eur. J.* **2007**, *13*, 5213.
- (73) Koval, I. A.; Gamez, P.; Belle, C.; Selmecezi, K.; Reedijk, J. *Chem. Soc. Rev.* **2006**, *35*, 814.
- (74) Rolff, M.; Schottenheim, J.; Decker, H.; Tuzcek, F. *Chem. Soc. Rev.* **2011**, *40*, 4077.
- (75) Das, S.; Pal, S. *Inorg. Chim. Acta* **2010**, *363*, 3028.
- (76) Sadana, A. K.; Mirza, Y.; Aneja, K. R.; Prakash, O. *Eur. J. Med. Chem.* **2003**, *38*, 533.
- (77) Kumar, D.; Sekhar, K.; Dhillon, H.; Rao, V. S.; Varma, R. S. *Green Chem.* **2004**, *6*, 156.
- (78) Gibson, M. S. *Tetrahedron* **1963**, *19*, 1587.
- (79) Pollak, A.; Tisler, M. *Tetrahedron* **1966**, *22*, 2073.
- (80) Bourgeois, P.; Cantegril, R.; Chene, A.; Gelin, J.; Mortier, J.; Moyroud, J. *Synth. Commun.* **1993**, *23*, 3195.
- (81) Ciesielski, M.; Pufky, D.; Doring, M. *Tetrahedron* **2005**, *61*, 5942.
- (82) Chen, D.; Milacic, V.; Frezza, M.; Dou, Q. P. *Curr. Pharm. Des.* **2009**, *15*, 777.
- (83) Colotti, G.; Ilari, A.; Boffi, A.; Morea, V. *Mini Rev. Med. Chem.* **2013**, *13*, 211.





- (84) Frezza, M.; Hindo, S.; Chen, D.; Davenport, A.; Schmitt, S.; Tomco, D.; Ping Dou, Q. *Curr. Pharm. Des.* **2010**, *16*, 1813.
- (85) Iakovidis, I.; Delimaris, I.; Piperakis, S. M. *Mol. Biol. Int.* **2011**, *2011*, 594529.
- (86) Shahabadi, N.; Fatahi, P. *DNA Cell Biol.* **2012**, *31*, 1328.
- (87) Javed, F.; Altaf, A. A.; Badshah, A.; Tahir, M. N.; Siddiq, M.; Shah, A.; Ullah, S.; Lal, B. J. *Coord. Chem.* **2012**, *65*, 969.
- (88) Krishnamoorthy, P.; Sathyadevi, P.; Cowley, A. H.; Butorac, R. R.; Dharmaraj, N. *Eur. J. Med. Chem.* **2011**, *46*, 3376.
- (89) Pyle, A. M.; Rehmann, J. P.; Meshoyrer, R.; Kumar, C. V.; Turro, N. J.; Barton, J. K. *J. Am. Chem. Soc.* **1989**, *111*, 3051.
- (90) Shen, R.; Wang, P.; Tang, N. *J. Fluoresc.* **2009**, *19*, 1073.
- (91) Wang, Y.; Lin, G.-W.; Hong, J.; Li, L.; Yang, Y.-M.; Lu, T. *J. Coord. Chem.* **2010**, *63*, 3662.
- (92) Mishra, R. K.; Upadhyay, K. K.; Shukla, S.; Mishra, R. *Chem. Commun. (Camb)* **2012**, *48*, 4238.
- (93) Long, E. C.; Barton, J. K. *Accounts Chem. Res.* **1990**, *23*, 271.
- (94) Asadi, M.; Safaei, E.; Ranjbar, B.; Hasani, L. *New J. Chem.* **2004**, *28*, 1227.
- (95) Bradley, P. M.; Angeles-Boza, A. M.; Dunbar, K. R.; Turro, C. *Inorg. Chem.* **2004**, *43*, 2450.
- (96) Inclán, M.; Albelda, M. T.; Frias, J. C.; Blasco, S.; Verdejo, B.; Serena, C.; Salat-Canela, C.; Díaz, M. L.; García-España, A.; García-España, E. *J. Am. Chem. Soc.* **2012**, *134*, 9644.
- (97) Bhat, S. S.; Kumbhar, A. S.; Kumbhar, A. A.; Khan, A. *Chem.-Eur. J.* **2012**, *18*, 16383.
- (98) Kumar, C. V.; Asuncion, E. H. *J. Am. Chem. Soc.* **1993**, *115*, 8547.
- (99) Inclán, M.; Albelda, M. T.; Frías, J. C.; Blasco, S.; Verdejo, B.; Serena, C.; Salat-Canela, C.; Díaz, M. L.; García-España, A.; García-España, E. *J. Am. Chem. Soc.* **2012**, *134*, 9644.
- (100) Kashanian, S.; Javanmardi, S.; Chitsazan, A.; Omidfar, K.; Paknejad, M. *DNA Cell Biol.* **2012**, *31*, 1349.
- (101) Nordén, B.; Tjerneld, F.; Palm, E. *Biophys. Chem.* **1978**, *8*, 1.
- (102) Stokke, T.; Steen, H. B. *J. Histochem. Cytochem.* **1985**, *33*, 333.
- (103) Guan, Y.; Shi, R.; Li, X.; Zhao, M.; Li, Y. *J. Phys. Chem. B* **2007**, *111*, 7336.
- (104) Loontjens, F. G.; McLaughlin, L. W.; Diekmann, S.; Clegg, R. M. *Biochemistry* **1991**, *30*, 182.
- (105) Loontjens, F. G.; Regenfuss, P.; Zechel, A.; Dumortier, L.; Clegg, R. M. *Biochemistry* **1990**, *29*, 9029.
- (106) Fischer, B. E.; Haring, U. K.; Tribolet, R.; Sigel, H. *Eur J Biochem* **1979**, *94*, 523.
- (107) McPhail, D. B.; Goodman, B. A. *Biochem J* **1984**, *221*, 559.
- (108) Knapp, S.; Keenan, T. P.; Zhang, X.; Fikar, R.; Potenza, J. A.; Schugar, H. J. *J. Am. Chem. Soc.* **1990**, *112* (9), 3452.
- (109) Suresh, E.; Bhadbhade, M. M.; Srinivas, D. *Polyhedron* **1996**, *15*, 4133.
- (110) Albani, J. R. *Principles and applications of fluorescence spectroscopy*; Blackwell Science: Oxford ; Ames, Iowa, 2007.
- (111) Atherton, S. J.; Beaumont, P. C. *J. Phys. Chem. A* **1986**, *90*, 2252.
- (112) Meyer-Almes, F. J.; Porschke, D. *Biochemistry* **1993**, *32*, 4246.

- (113) Lepecq, J. B.; Paoletti, C. *J. Mol. Biol.* **1967**, *27*, 87.
- (114) Peberdy, J. C.; Malina, J.; Khalid, S.; Hannon, M. J.; Rodger, A. *J. Inorg. Biochem.* **2007**, *101*, 1937.
- (115) McCoubrey, A.; Latham, H. C.; Cook, P. R.; Rodger, A.; Lowe, G. *FEBS Lett.* **1996**, *380*, 73.
- (116) Lakowicz, J. R.; Weber, G. *Biochemistry* **1973**, *12*, 4161.
- (117) Rehman, S. U.; Sarwar, T.; Husain, M. A.; Ishqi, H. M.; Tabish, M. *Arch. Biochem. Biophys.* **2015**, *576*, 49.
- (118) Chaires, J. B. *Biopolymers* **1997**, *44*, 201.
- (119) Chaires, J. B. *Curr. Opin. Struct. Biol.* **1998**, *8*, 314.
- (120) Nelson, S. M.; Ferguson, L. R.; Denny, W. A. *Mutat. Res.* **2007**, *623*, 24.
- (121) Moravek, Z.; Neidle, S.; Schneider, B. *Nucleic Acids Res.* **2002**, *30*, 1182.
- (122) Neidle, S. *Nat. Prod. Rep.* **2001**, *18*, 291.
- (123) Neidle, S. *Nucleic acid structure and recognition*; Oxford University Press: Oxford ; New York, 2002.
- (124) Neidle, S. *Nat. Chem.* **2012**, *4*, 594.
- (125) Lauria, A.; Montalbano, A.; Barraja, P.; Dattolo, G.; Almerico, A. M. *Curr. Med. Chem.* **2007**, *14*, 2136.
- (126) Wang, H.; Laughton, C. A. *Phys. Chem. Chem. Phys.* **2009**, *11*, 10722.
- (127) Cosa, G.; Focsaneanu, K. S.; McLean, J. R. N.; McNamee, J. P.; Scaiano, J. C. *Photochem. Photobiol.* **2001**, *73*, 585.
- (128) Vega, M. C.; Garcia Saez, I.; Aymami, J.; Eritja, R.; Van der Marel, G. A.; Van Boom, J. H.; Rich, A.; Coll, M. *Eur. J. Biochem.* **1994**, *222*, 721.
- (129) Boffey, S. A. 1984; Vol. 2, p 43.
- (130) Tjioe, L.; Meininger, A.; Joshi, T.; Spiccia, L.; Graham, B. *Inorg. Chem.* **2011**, *50*, 4327.
- (131) Bertram, J. S. *Mol. Aspects Med.* **2000**, *21*, 167.
- (132) Roos, W. P.; Thomas, A. D.; Kaina, B. *Nat. Rev. Cancer* **2016**, *16*, 20.
- (133) Circu, M. L.; Aw, T. Y. *Free Radic. Biol. Med.* **2010**, *48*, 749.
- (134) Magder, S. *Crit. Care* **2006**, *10*, 208.
- (135) Pope, L. H.; Davies, M. C.; Laughton, C. A.; Roberts, C. J.; Tendler, S. J.; Williams, P. M. *J. Microsc.* **2000**, *199*, 68.
- (136) Eaton, P.; West, P. *Atomic force microscopy*; Oxford University Press: Oxford, 2010.
- (137) Engel, A.; Muller, D. J. *Nat. Struct. Mol. Biol.* **2000**, *7*, 715.
- (138) Hansma, H. G. *Annu. Rev. Phys. Chem.* **2001**, *52*, 71.
- (139) Gamba, I.; Salvado, I.; Brissos, R. F.; Gamez, P.; Brea, J.; Loza, M. I.; Vazquez, M. E.; Lopez, M. V. *Chem. Commun. (Camb.)* **2016**, *52*, 1234.
- (140) Gamba, I.; Salvado, I.; Rama, G.; Bertazzon, M.; Sanchez, M. I.; Sanchez-Pedregal, V. M.; Martinez-Costas, J.; Brissos, R. F.; Gamez, P.; Mascarenas, J. L.; Vazquez Lopez, M.; Vazquez, M. E. *Chem. Eur. J.* **2013**, *19*, 13369.
- (141) Escribano, E.; Font-Bardia, M.; Calvet, T.; Lorenzo, J.; Gamez, P.; Moreno, V. *Inorg. Chim. Acta* **2013**, *394*, 65.
- (142) Sebaugh, J. L. *Pharm. Stat.* **2011**, *10*, 128.
- (143) Sumantran, V. N. In *Cancer Cell Culture: Methods and Protocols*; Cree, I. A., Ed.; Humana Press: Totowa, NJ, 2011, p 219.
- (144) Mosmann, T. *J. Immunol. Methods* **1983**, *65*, 55.





- (145) Scudiero, D. A.; Shoemaker, R. H.; Paull, K. D.; Monks, A.; Tierney, S.; Nofziger, T. H.; Currens, M. J.; Seniff, D.; Boyd, M. R. *Cancer Res.* **1988**, *48*, 4827.
- (146) Riss, T. L.; Moravec, R. A.; Niles, A. L.; Duellman, S.; Benink, H. A.; Worzella, T. J.; Minor, L. In *Assay Guidance Manual*; Sittampalam, G. S., Coussens, N. P., Brimacombe, K., Grossman, A., Arkin, M., Auld, D., Austin, C., Baell, J., Bejcek, B., Chung, T. D. Y., Dahlin, J. L., Devanaryan, V., Foley, T. L., Glicksman, M., Hall, M. D., Hass, J. V., Inglese, J., Iversen, P. W., Kahl, S. D., Kales, S. C., Lal-Nag, M., Li, Z., McGee, J., McManus, O., Riss, T., Trask, O. J., Jr., Weidner, J. R., Xia, M., Xu, X., Eds. Bethesda (MD), 2004.
- (147) Stoddart, M. J. In *Mammalian Cell Viability: Methods and Protocols*; Stoddart, M. J., Ed.; Humana Press: Totowa, NJ, 2011, p 1.
- (148) Vistica, D. T.; Skehan, P.; Scudiero, D.; Monks, A.; Pittman, A.; Boyd, M. R. *Cancer Res.* **1991**, *51*, 2515.
- (149) Perumana, S. *Perspectives in cancer prevention-translational cancer research*; Springer: New York, 2013.
- (150) Mueller, S.; Matthay, K. K. *Curr. Oncol. Rep.* **2009**, *11*, 431.
- (151) Berlanga, P.; Canete, A.; Castel, V. *Expert Opin Emerg Drugs* **2017**, *22*, 63.
- (152) Wagner, L. In *Neuroblastoma: Diagnosis, Therapy, and Prognosis*; Hayat, M. A., Ed.; Springer Netherlands: Dordrecht, 2012, p 209.
- (153) Ferlay, J.; Soerjomataram, I.; Dikshit, R.; Eser, S.; Mathers, C.; Rebelo, M.; Parkin, D. M.; Forman, D.; Bray, F. *Int. J. Cancer* **2015**, *136*, E359.
- (154) Esposito, M. R.; Aveic, S.; Seydel, A.; Tonini, G. P. *J. Biomed. Sci.* **2017**, *24*, 14.
- (155) Matthay, K. K.; Maris, J. M.; Schleiermacher, G.; Nakagawara, A.; Mackall, C. L.; Diller, L.; Weiss, W. A. *Nat. Rev. Dis. Primers* **2016**, *2*, 16078.
- (156) Rothenberg, M. L. *Oncologist* **2001**, *6*, 66.
- (157) Xie, R.; Mathijssen, R. H.; Sparreboom, A.; Verweij, J.; Karlsson, M. *O. J. Clin. Oncol.* **2002**, *20*, 3293.
- (158) Chabot, G. G. *Clin. Pharmacokinet.* **1997**, *33*, 245.





## 2

# Targeting cancer with small molecules: Ruthenium complexes

---

*Ruthenium complexes have shown unique properties and it has been demonstrated that they can be potent and efficient therapeutic agents. Ruthenium-based compounds act not only as promising antitumor molecules but also as anti-metastatic agents and cell-growth inhibitors for different cancer-cell types.<sup>1-7</sup>*

*In this chapter, we assess the cytotoxic activity of a series of novel ruthenium complexes through cell-viability studies. The evaluation of their potential anti-metastatic activity was performed using a wound-healing assay.*

*Based on structure-activity relationship studies, new compounds were developed, which allowed to improve the activity significantly, and to establish that the nature of the ligands bound to the metal is crucial for the activity and cancer specificity of the drug.*

## Contents

---

PRELIMINARY DNA-INTERACTION STUDIES.....	83
CELL-VIABILITY ASSAYS .....	83
<i>Single-point assays</i> .....	83
<i>MTT Reduction Assay</i> .....	91
<i>Cell migration – Wound-healing assay</i> .....	98
CONCLUSIONS .....	103
REFERENCES .....	104

---





Over the last years, metal complexes have retained a firm place in medicinal chemistry, despite their relatively low clinical representation. In this category, it has been shown that ruthenium complexes can be effective as therapeutic agents.<sup>8</sup>

Their pharmacological relevance embrace a wide range of pathologies, from cancer to the treatment of Alzheimer's disease<sup>9,10</sup>, as well as nitric oxide scavengers<sup>11</sup>, among others.

The distinguishing chemical and biochemical proprieties of ruthenium complexes makes them promisingly candidates for medical use. The uniqueness of their available oxidation states under physiological conditions, namely Ru(II), Ru(III) and Ru(IV), can be exploited to adjust their biological activity; for instance, a drug may be administrated in its relatively inert Ru(III) form, which is reduced inside cells to an active Ru(II) state. All of them adopt a predominantly hexacoordinate centre with octahedral geometry. The coordination environment around the metallic centre plays a crucial role in the stabilization of the oxidation states and guides their inherent redox properties. These redox features confer unique mechanisms of action that differ from those of the classical platinum drugs.<sup>4,12</sup>

Another remarkable feature of ruthenium(II) systems is their interesting photophysical properties. Several complexes have been described as perfect candidates for their use as nucleic acid probes,<sup>13-16</sup> as DNA-mediated electron transfer agents,<sup>16-19</sup> in DNA footprinting,<sup>20-22</sup> DNA sequence-specific cleavage<sup>23-26</sup> and as anticancer drugs.<sup>6,8,27</sup>

Originally, ruthenium complexes were described to be DNA-targeting molecules, as observed for the platinum-related metallodrugs. However, after careful analysis and years of investigation, it has been demonstrated that ruthenium complexes differ on their mechanisms of action. Many Ru(II) and Ru(III) am(m)ine complexes exhibit selectivity towards the imine sites of biomolecules; they can also coordinate to the histidyl imidazole nitrogens on the surface of proteins or/and the N7 site on the imidazole ring of purine nucleotides.<sup>27</sup>

Nowadays, two main ruthenium families, *i.e.* the Ru(III)–indazole/imidazole and Ru(II)–arene complexes, have shown great therapeutic potential by displaying activity, not only, against primary tumours but also in metastatic tissues,<sup>3,22</sup> while presenting low toxicity and favourable clearance properties. A number of studies have demonstrated that ruthenium is able to mimic iron and bind some transporting proteins like transferrin, either in blood or in cells.<sup>28,29</sup>

As it is widely known, iron is an essential element that regulates, among other functions, cell growth and differentiation, and modulates cell-mediated immunity, which includes cytokine production. As one may expect, an intimate relationship between iron regulation and cancerous cells can be found. It is thoroughly described that there is an overexpression of most

of the iron-regulatory genes in tumorigenic cells.<sup>30,31</sup> The high expression of transferrin receptors in these type of cells can be an important factor regarding the selectivity of ruthenium for neoplastic masses rather than for normal tissues. Recent studies have demonstrated that, when treated with ruthenium-based compounds, there is a 2- to 12-fold increase in ruthenium concentration in cancer cells, compared with normal cells. Several ruthenium complexes have also been described to display a higher effectiveness against metastases than against primary tumours. Such complexes showing lower toxicity in primary tumours present potent anti-metastatic effects, arising from the inhibition of tumour cell detachment, invasion/migration, and re-adhesion.<sup>32-34</sup>

Due to their clinical low toxicity and remarkable results, some ruthenium compounds have successfully reached phase I or II clinical trials, stimulating anticancer research in this area.<sup>35-37</sup> It can be pointed out that although promising ruthenium agents are already in early phases of drug development, their molecular target(s) has(ve) not been unequivocally identified.

As stated earlier, ruthenium complexes differ from platinum ones not only on their biological targets but also on their reactivity. For instance, the inert character of ( $\eta^6$ -arene)Ru(II)  $\pi$ -bonds towards hydrolysis is worth mentioning. Hence, chlorido( $\eta^6$ -arene) ruthenium(II) complexes can be converted to their corresponding, much more reactive, aquated species. Arene ligands are known to stabilize Ru(II) species, providing an increasing hydrophobicity of the complex,<sup>38</sup> thus enhancing their recognition and transport through cell membranes. Such Ru(II)-arene complexes tend to bind preferentially to guanine residues of the double-helical DNA, inhibiting topoisomerase II and RNA polymerase, which are enzymes involved in cell division.<sup>39,40</sup>

Ruthenium(II) complexes containing biphenyl, dihydroanthracene, or tetrahydroanthracene ligands have a propensity to interact with the N7 position of guanine, *via* non-covalent, hydrophobic interactions between the arene part of the molecule and DNA, resulting in intercalation and/or minor groove binding. However, if the Ru(II) complex includes a bulky ring like a *p*-cymene moiety, these interactions are no longer possible. In fact, adducts of complexes containing a sterically hindered *p*-cymene ligand induce a distortion and a destabilization of the double-helical DNA.

Finally, it should also be pointed out that ruthenium complexes have a higher affinity to imidazolyl moieties on protein surfaces than to DNA guanines.<sup>41,42</sup>





Taking into account the favourable results found in literature for arene-based ruthenium(II) complexes,<sup>43</sup> it was decided to investigate the cytotoxic behaviour of a series of  $[\text{RuCl}_2(\eta^6\text{-arene})(\text{PR}_3)]$  compounds bearing bulky phosphane ligands.

### *Preliminary DNA-interaction studies*

The Ru(II)-arene complexes depicted in Figure 39 were synthesized in the research group of Prof. Guillermo Muller from the University of Barcelona.<sup>44,45</sup>

Preliminary studies by UV-Vis and fluorescence-dye displacement spectroscopy revealed that the complexes exhibited poor DNA-interacting properties. Their poor affinity towards the biomolecule was indeed reflected by the absence of spectral changes (Experimental section, Figure 92 to Figure 94).

Nevertheless, their toxicity profile and biologic activity against both cancerous and non-cancerous cell lines were subsequently examined.

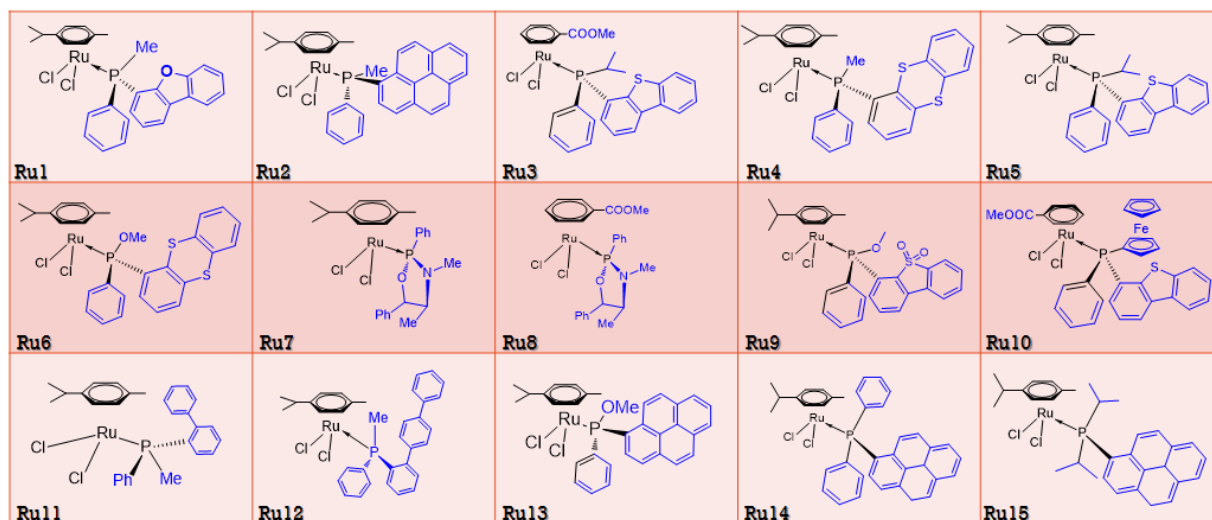


Figure 39: First series of Ru(II)-arene compounds used in the present study.<sup>44,45</sup>

### *Cell-viability assays*

Single-point assays were carried out for all compounds (**Ru1-Ru15**, Figure 39), with the objective to define the optimum conditions to determine the  $\text{IC}_{50}$  values.

### *Single-point assays*

The cytotoxic behaviour of the complexes was evaluated using two different complex concentrations, namely 10 and 50  $\mu\text{M}$ , against five cancer cell lines, that are A549 (lung adenocarcinoma), A375 (melanoma), MCF-7 (breast adenocarcinoma), SKOV3 (ovary adenocarcinoma) and SW620 (colorectal adenocarcinoma). The results obtained after an incubation time of 24 hours are shown in Figure 40 (10  $\mu\text{M}$ ; Table 16) and Figure 41 (50  $\mu\text{M}$ ; Table 17).

The cell viability was calculated as described in the experimental section, using the following equation:

$$viability (\%) = \frac{absorbance\ of\ the\ treated\ wells}{absorbance\ of\ the\ control\ wells} \times 100.$$

For [complex] = 10  $\mu$ M, complex **Ru2** clearly presents the highest cytotoxic behaviour, especially against the SW620 and A375 lines, with cell viabilities inferior to 5%; for the SKOV3, A549 and MCF-7 cell lines, viabilities below 50% are observed (Figure 40).

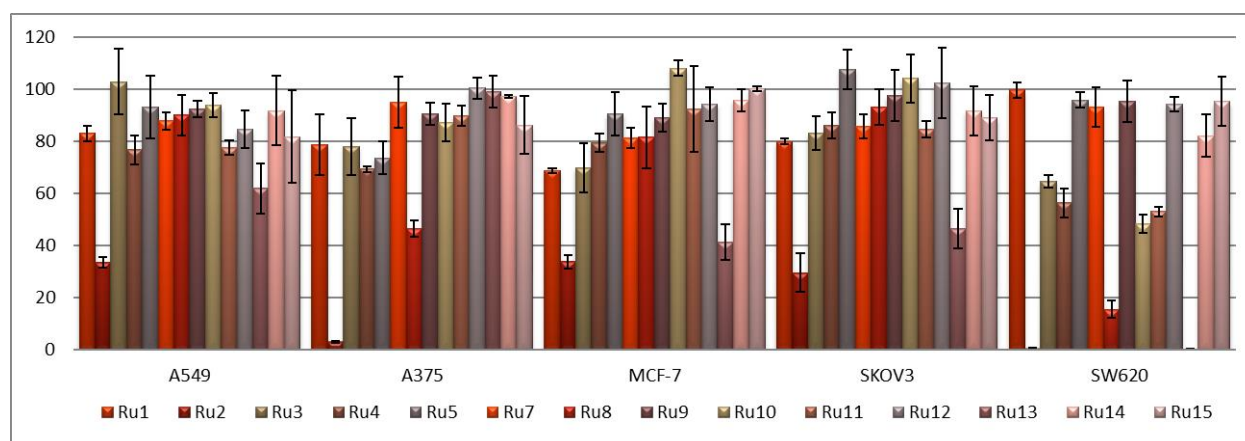


**Figure 40:** Cell-viability assays (single-point screening, % of cell viability) for Ru(II) complexes Ru1–Ru15, using different cancer-cell lines, namely A549 (lung adenocarcinoma), A375 (melanoma), MCF-7 (breast adenocarcinoma), SKOV3 (ovary adenocarcinoma) and SW620 (colorectal adenocarcinoma). [Complex] = 10  $\mu$ M; incubation time = 24 h. The results are means  $\pm$  SD of three independent experiments.

At this concentration, the specificity of complex **Ru8** and **Ru11** towards respectively, A375 and SW620, is also clearly evidenced (see Figure 40, Table 16). Furthermore, complex **Ru13** is highly cytotoxic towards SW620 cells, and shows mild antiproliferative properties towards MCF-7 and SKOV3 cells (viability below 50%).

For [complex] = 50  $\mu$ M, the great majority of the Ru(II) compounds exhibit considerable cytotoxic effects towards the selected cell lines, especially in SW620, followed by A375 and MCF-7 (Figure 41).

Complexes **Ru9** and **Ru12** show negligible toxicities against all cell lines, except for A375, for which a mild effect is observed. Comparatively, complex **Ru7** gives slightly better results, albeit not as remarkable as those of the other members of the series.





**Table 16:** Cell-viability assays (single-point screening, % cell viability) of Ru(II) complexes Ru1–Ru15 with different cancer-cell lines, namely A549 (lung adenocarcinoma), A375 (melanoma), MCF-7 (breast adenocarcinoma), SKOV3 (ovary adenocarcinoma) and SW620 (colorectal adenocarcinoma). Pre-set [complex] = 10  $\mu$ M (single-point assay); incubation time = 24 h. The data shown are means  $\pm$  SD of three independent experiments. Values in bold grey characterize a cell viability  $\leq$  50%; those in bold black a cell viability  $\leq$  25%.

	Cell Line				
	A549	A375	MCF-7	SW620	SKOV3
<b>Ru1</b>	83 $\pm$ 2.9	79 $\pm$ 11.5	69 $\pm$ 0.9	$\geq$ 100	80 $\pm$ 1.1
<b>Ru2</b>	<b>33</b> $\pm$ <b>2.1</b>	<b>3.0</b> $\pm$ <b>0.4</b>	<b>34</b> $\pm$ <b>2.6</b>	<b>0.6</b> $\pm$ <b>0.3</b>	<b>30</b> $\pm$ <b>7.4</b>
<b>Ru3</b>	$\geq$ 100	78 $\pm$ 11.0	70 $\pm$ 9.3	64 $\pm$ 2.5	83 $\pm$ 6.6
<b>Ru4</b>	77 $\pm$ 5.6	69 $\pm$ 1.2	79 $\pm$ 3.7	56 $\pm$ 5.5	86 $\pm$ 5.0
<b>Ru5</b>	93 $\pm$ 12.0	74 $\pm$ 6.4	91 $\pm$ 8.3	96 $\pm$ 2.9	107 $\pm$ 7.5
<b>Ru6</b>	78 $\pm$ 7.6	81 $\pm$ 12.0	86 $\pm$ 4.0	66 $\pm$ 1.9	91 $\pm$ 5.9
<b>Ru7</b>	88 $\pm$ 3.3	95 $\pm$ 9.9	81 $\pm$ 3.8	93 $\pm$ 7.5	86 $\pm$ 4.7
<b>Ru8</b>	90 $\pm$ 7.6	<b>46</b> $\pm$ <b>3.1</b>	81 $\pm$ 11.8	<b>15</b> $\pm$ <b>3.4</b>	93 $\pm$ 6.8
<b>Ru9</b>	92 $\pm$ 3.1	90 $\pm$ 4.4	89 $\pm$ 5.3	95 $\pm$ 7.8	97 $\pm$ 9.8
<b>Ru10</b>	94 $\pm$ 4.6	87 $\pm$ 7.2	$\geq$ 100	<b>48</b> $\pm$ <b>3.6</b>	$\geq$ 100
<b>Ru11</b>	78 $\pm$ 2.7	90 $\pm$ 3.9	92 $\pm$ 16.5	53 $\pm$ 2.0	84 $\pm$ 3.1
<b>Ru12</b>	84 $\pm$ 7.2	$\geq$ 100	94 $\pm$ 6.4	94 $\pm$ 2.8	$\geq$ 100
<b>Ru13</b>	62 $\pm$ 9.6	99 $\pm$ 6.2	<b>41</b> $\pm$ <b>6.8</b>	<b>0.3</b> $\pm$ <b>0.2</b>	<b>46</b> $\pm$ <b>7.5</b>
<b>Ru14</b>	92 $\pm$ 13.4	97 $\pm$ 0.6	96 $\pm$ 4.3	82 $\pm$ 8.2	92 $\pm$ 9.5
<b>Ru15</b>	82 $\pm$ 17.7	86 $\pm$ 11.0	$\geq$ 100	95 $\pm$ 9.4	89 $\pm$ 8.6

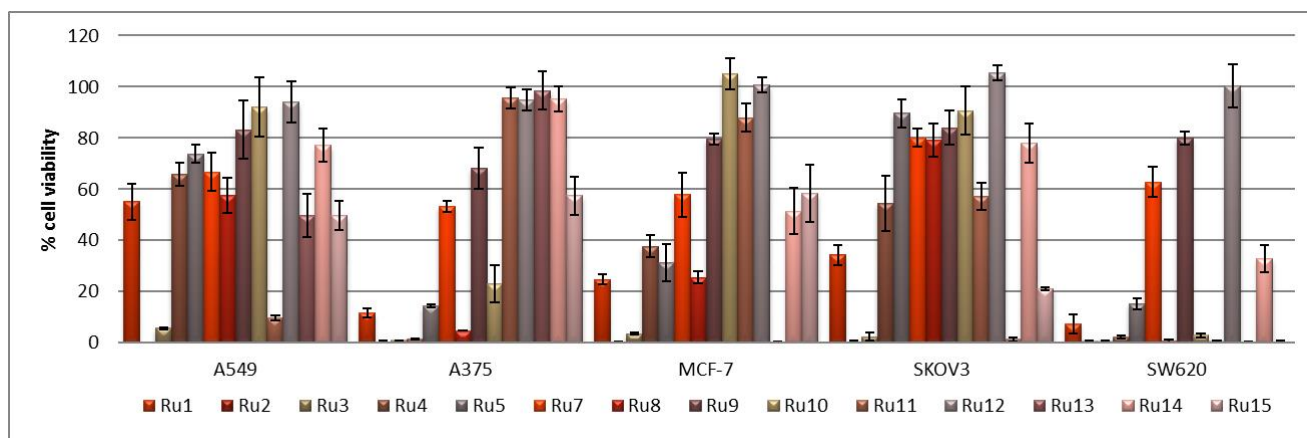


**Figure 41:** Cell-viability assays (single-point screening, % of cell viability) for Ru(II) complexes Ru1–Ru15, using different cancer cell lines, namely A549 (lung adenocarcinoma), A375 (melanoma), MCF-7 (breast adenocarcinoma), SKOV3 (ovary adenocarcinoma) and SW620 (colorectal adenocarcinoma). [Complex] = 50  $\mu$ M; incubation time = 24 h. The results are means  $\pm$  SD of three independent experiments.

In summary, the cell-viability results achieved with **Ru1–Ru15** revealed that they efficiently affect the growth of SW620 cells, following the sequence **Ru13** > **Ru2** > **Ru3**, **Ru11** > **Ru15** > **Ru8** > **Ru4** > **Ru10** > **Ru1** > **Ru5** > **Ru14** > **Ru6** > **Ru7**. An analogous classification can be made for A375 cells, namely **Ru2** > **Ru3** > **Ru4** > **Ru8** > **Ru1** > **Ru5** > **Ru10** > **Ru6** > **Ru7**. Finally, for the MCF-7 cell line, the activity sequence is **Ru2** > **Ru13** > **Ru3** > **Ru1** > **Ru8**

> **Ru5** > **Ru4** > **Ru7**, which clearly evidences that, for a complex concentration of 50  $\mu\text{M}$  and an incubation time of 24 hours, **Ru2** and **Ru13** are the most efficient compounds.

To better assess any structure-activity relationships, the data presented in Figure 41 (Table 17) were analysed further and rationally divided to generate several new charts based on specific structural features (Figure 42 to Figure 46).

Figure 42 gathers the cytotoxic profiles of the ruthenium complexes of the type  $[\text{RuCl}_2(\eta^6\text{-arene})(\text{PR}_3)]$ , whose arene ligand is a *p*-cymene (complexes **Ru2**, **Ru13-Ru15**; Figure 42). These complexes include a pyrene-containing phosphane ligand and two other substituents. The analysis of their cell-viability percentages shows clear differences.

The most cytotoxic complex (against all cell lines) is that with two isopropyl phosphane substituents (**Ru2**). **Ru13** containing a phenyl and a methoxy groups on the phosphane ligand is the second-best compound, particularly against adenocarcinomas, *i.e.* the MCF-7 and SW620 cell lines. Obviously, the nature of the phosphane ligand plays a key role in the cytotoxicity of the corresponding metal complexes.

**Table 17:** Cell-viability assays (single-point screening, % cell viability) of Ru(II) complexes **Ru1–Ru15** with different cancer cell lines, namely A549 (lung adenocarcinoma), A375 (melanoma), MCF-7 (breast adenocarcinoma), SKOV3 (ovary adenocarcinoma) and SW620 (colorectal adenocarcinoma). Pre-set [complex] = 50  $\mu\text{M}$  (single-point assay); incubation time = 24 h. The data shown are means  $\pm$  SD of three independent experiments. Values shown in bold grey characterize cell viabilities  $\leq 50\%$ ; those shown in bold black are for cell viabilities  $\leq 25\%$ .

	Cell Line				
	A549	A375	MCF-7	SW620	SKOV3
<b>Ru1</b>	55 $\pm$ 7.2	<b>12 <math>\pm</math> 1.7</b>	<b>25 <math>\pm</math> 2.0</b>	<b>7.5 <math>\pm</math> 1.1</b>	<b>34 <math>\pm</math> 3.8</b>
<b>Ru2</b>	<b>0.1 <math>\pm</math> 0.2</b>	<b>0.5 <math>\pm</math> 0.4</b>	<b>0.2 <math>\pm</math> 0.1</b>	<b>0.5 <math>\pm</math> 0.3</b>	<b>0.4 <math>\pm</math> 0.5</b>
<b>Ru3</b>	<b>5.8 <math>\pm</math> 0.4</b>	<b>0.9 <math>\pm</math> 0.1</b>	<b>3.5 <math>\pm</math> 0.4</b>	<b>0.6 <math>\pm</math> 0.3</b>	<b>2.4 <math>\pm</math> 1.6</b>
<b>Ru4</b>	66 $\pm$ 4.5	<b>1.6 <math>\pm</math> 0.2</b>	<b>38 <math>\pm</math> 4.3</b>	<b>2.2 <math>\pm</math> 0.6</b>	55 $\pm$ 10.7
<b>Ru5</b>	74 $\pm$ 3.5	<b>14 <math>\pm</math> 0.6</b>	<b>31 <math>\pm</math> 7.3</b>	<b>15 <math>\pm</math> 2.2</b>	90 $\pm$ 5.6
<b>Ru6</b>	68 $\pm$ 5.6	51 $\pm$ 10.4	81 $\pm$ 3.1	<b>46 <math>\pm</math> 1.1</b>	89 $\pm$ 6.7
<b>Ru7</b>	67 $\pm$ 7.5	53 $\pm$ 2.0	58 $\pm$ 8.6	63 $\pm$ 5.9	80 $\pm$ 3.5
<b>Ru8</b>	58 $\pm$ 6.9	<b>4.8 <math>\pm</math> 0.2</b>	<b>26 <math>\pm</math> 2.2</b>	<b>0.8 <math>\pm</math> 0.6</b>	79 $\pm$ 6.4
<b>Ru9</b>	83 $\pm$ 11.3	68 $\pm$ 8.2	80 $\pm$ 2.2	80 $\pm$ 2.6	84 $\pm$ 6.7
<b>Ru10</b>	92 $\pm$ 11.6	<b>23 <math>\pm</math> 7.1</b>	$\geq 100$	<b>2.9 <math>\pm</math> 0.7</b>	91 $\pm$ 9.4
<b>Ru11</b>	10 $\pm$ 0.9	96 $\pm$ 4.2	88 $\pm$ 5.4	<b>0.6 <math>\pm</math> 0.4</b>	57 $\pm$ 5.3
<b>Ru12</b>	94 $\pm$ 8.2	95 $\pm$ 4.0	$\geq 100$	$\geq 100$	$\geq 100$
<b>Ru13</b>	<b>50 <math>\pm</math> 8.4</b>	98 $\pm$ 7.5	<b>0.4 <math>\pm</math> 0.3</b>	<b>0.4 <math>\pm</math> 0.3</b>	<b>1.4 <math>\pm</math> 0.8</b>
<b>Ru14</b>	77 $\pm$ 6.6	95 $\pm$ 4.8	51 $\pm$ 9.1	33 $\pm$ 5.3	78 $\pm$ 7.6
<b>Ru15</b>	<b>50 <math>\pm</math> 5.7</b>	57 $\pm$ 7.6	58 $\pm$ 11.2	<b>0.7 <math>\pm</math> 0.5</b>	<b>21 <math>\pm</math> 0.5</b>



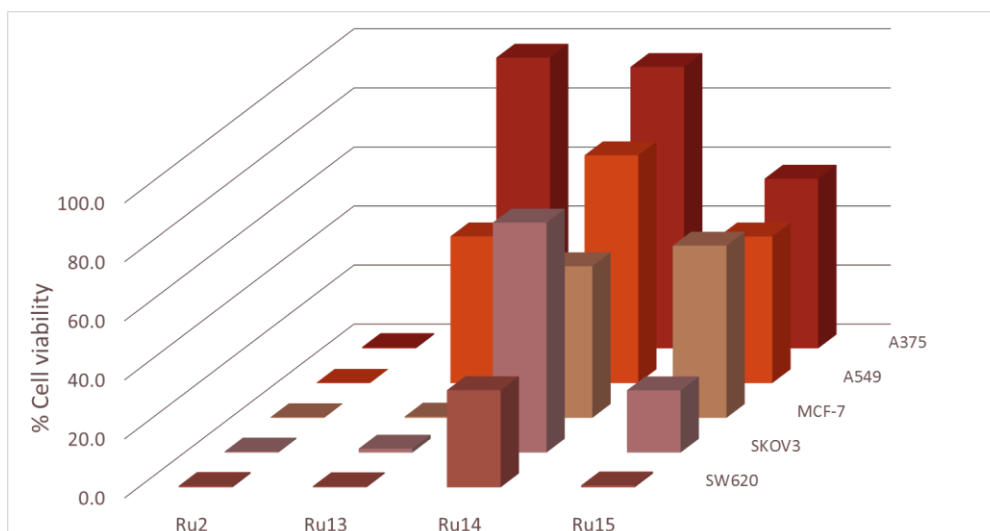


**Figure 42:** Cell-viability assays (single-point screening, % of cell viability) of Ru(II) complexes **Ru2**, **Ru13**–**Ru15** with different cancer cell lines, namely **A549** (lung adenocarcinoma), **A375** (melanoma), **MCF-7** (breast adenocarcinoma), **SKOV3** (ovary adenocarcinoma) and **SW620** (colorectal adenocarcinoma). [Complex] = 50  $\mu$ M; incubation time = 24 h.

Replacement of a methyl or a methoxy group by a phenyl moiety (respectively, **Ru2** to **Ru14** and **Ru13** to **Ru14**) leads to a general decrease of the cytotoxicity of the compound towards all cell lines. It can also be noted that **Ru13** is not efficient against **A549** and **A375** cells, in contrast to **Ru2**; these results suggest that electronic effects (methyl *versus* methoxy) can modify the biological activity of the complexes. Replacement of the two phenyl substituents (**Ru14**) by isopropyl groups (**Ru15**) generates a compound that is slightly more cytotoxic (clearly more cytotoxic in the case of **SW620**), although it is far less efficient than **Ru2** (and **Ru13**). Hence, it appears that steric hindrance (the isopropyl and phenyl groups being bulkier than the methyl or methoxy ones) also plays a significant role in the observed cytotoxicity.

The cytotoxic profiles of the ruthenium complexes of the type  $[\text{RuCl}_2(\eta^6\text{-arene})(\text{PR}_3)]$ , with methyl benzoate or *p*-cymene as arene ligand, are shown in Figure 43. Substitution of the methyl benzoate ring with a *p*-cymene group (**Ru3** to **Ru5**) produces a less efficient compound. It thus appears that the electron-withdrawing methyl benzoate ligand has a beneficial effect on the cytotoxic properties.

Remarkably, replacement of the isopropyl group of **Ru3** (a complex that is highly active in all cell lines; Figure 43) by a ferrocenyl unit generates complex **Ru10**, which is only highly active against **SW620** cells, and reasonably cytotoxic against **A375** cells.

Finally, complex **Ru9** is the less efficient compound of this series, further illustrating the critical role played by the ligands around the metal centre.

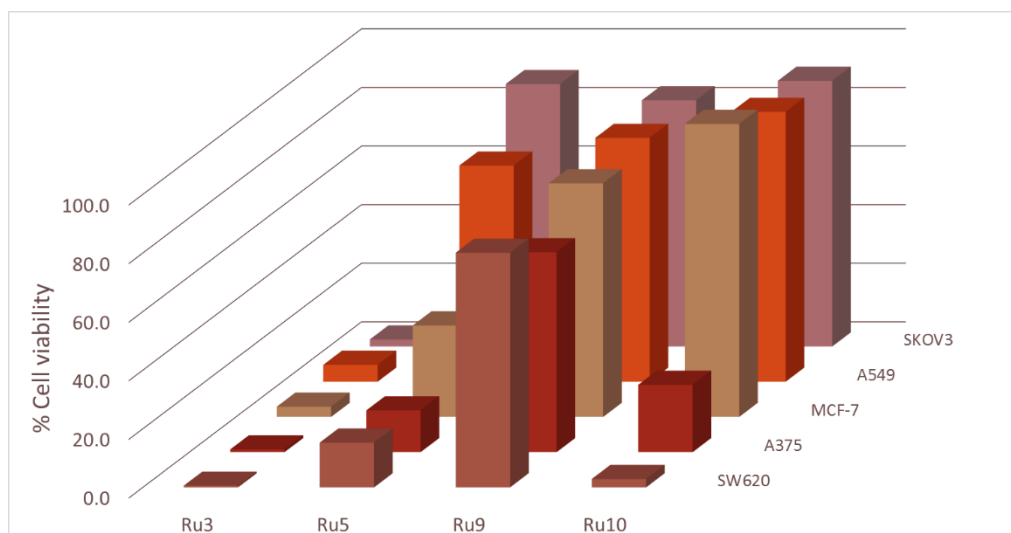


**Figure 43:** Cell-viability assays (single-point screening, % of cell viability) of Ru(II) complexes **Ru3**, **Ru5**, **Ru9** and **Ru10** with different cancer cell lines, namely **A549** (lung adenocarcinoma), **A375** (melanoma), **MCF-7** (breast adenocarcinoma), **SKOV3** (ovary adenocarcinoma) and **SW620** (colorectal adenocarcinoma). [Complex] = 50  $\mu$ M; incubation time = 24 h.

Complexes **Ru4** and **Ru6** only differ by a methyl (**Ru4**) or a methoxy (**Ru6**) on the phosphane ligand, which is characterized by the presence of a thianthrene group (Figure 44). Both complexes affect all the selected cell lines, **Ru4** being the most active, especially towards SW620 and A375 cells (with cell-viability percentages of 2.2% and 1.6%, respectively; Figure 44). As already noticed earlier (see **Ru2** and **Ru13**), replacement of a methyl substituent of the phosphane ligand by a methoxy group can significantly reduce the cytotoxic activity of the resulting metal complex.

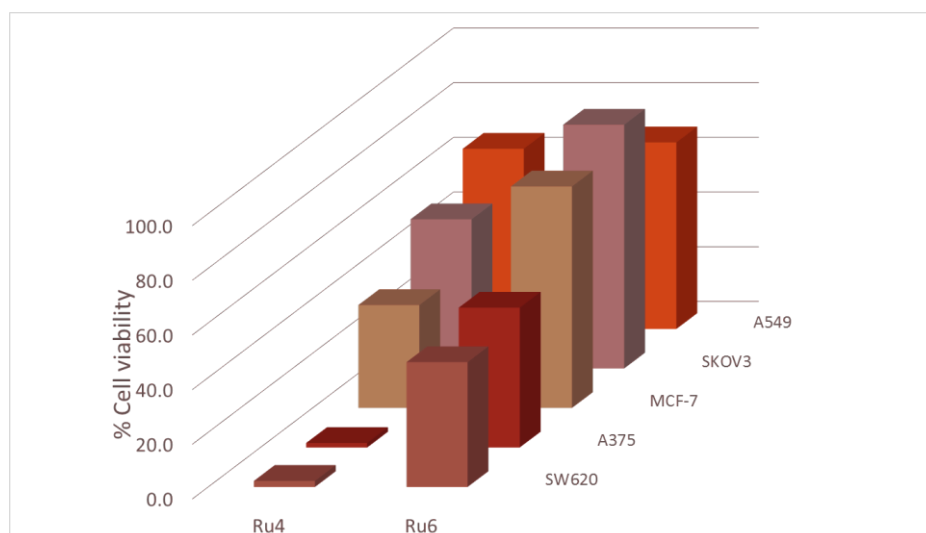


**Figure 44:** Cell-viability assays (single-point screening, % of cell viability) of Ru(II) complexes **Ru4** and **Ru6** with different cancer cell lines, namely **A549** (lung adenocarcinoma), **A375** (melanoma), **MCF-7** (breast adenocarcinoma), **SKOV3** (ovary adenocarcinoma) and **SW620** (colorectal adenocarcinoma). [Complex] = 50  $\mu$ M; incubation time = 24 h.





These thianthrene-containing complexes appear to be more specific for these two cell lines as the best activities of **Ru6** are also achieved with SW620 and A375. These last observations suggest that the cancer-cell specificity of such ruthenium(II) complexes may be fine-tuned by using/selecting different R groups on the PR<sub>3</sub> ligand; in other words, a complex of type [RuCl<sub>2</sub>(η<sup>6</sup>-arene)(PR<sub>3</sub>)] may be purposely (and rationally) designed for a particular cancer.

Complexes **Ru7** and **Ru8** are characterized by their PR<sub>3</sub> ligand containing an oxazaphospholidine moiety. These two complexes differ in their η<sup>6</sup>-arene ligand, which is a *p*-cymene for **Ru7** and a methyl benzoate for **Ru8**. As already observed (see for instance **Ru3** and **Ru5**), **Ru8**, including the methyl benzoate ring, is the most active complex (Figure 45), except for the cell lines A549 and SKOV3, for which the two compounds show similar (low) activities.

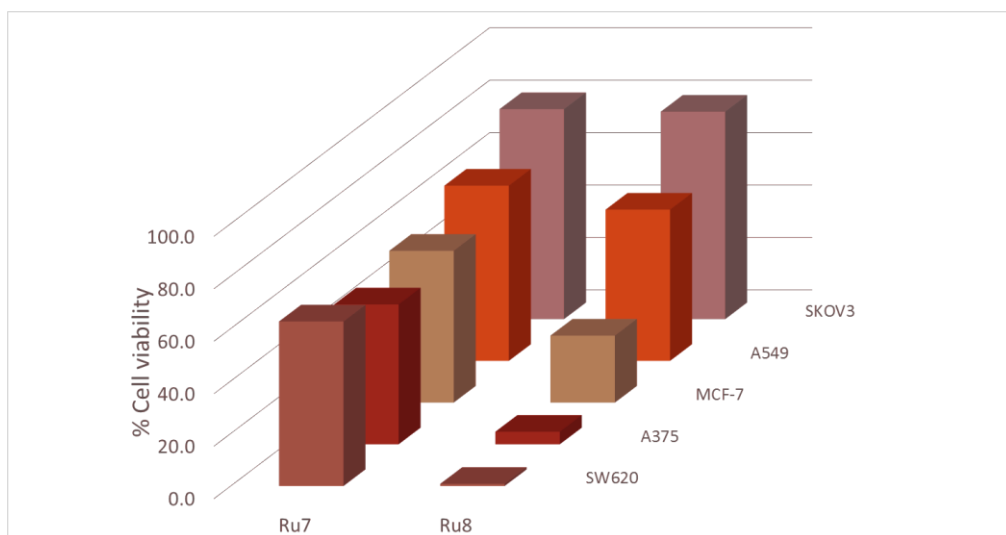


**Figure 45:** Cell-viability assays (single-point screening, % of cell viability) of Ru(II) complexes **Ru7** and **Ru8** with different cancer cell lines, namely A549 (lung adenocarcinoma), A375 (melanoma), MCF-7 (breast adenocarcinoma), SKOV3 (ovary adenocarcinoma) and SW620 (colorectal adenocarcinoma). [Complex] = 50 μM; incubation time = 24 h.

The related complexes **Ru11** and **Ru12** differ by one of the R groups of the PR<sub>3</sub> ligand; while **Ru11** has a phosphane diphenyl substituent, **Ru12** contains a longer polyphenyl group, namely a terphenyl group (Figure 46). **Ru11** is highly active towards the SW620 and A549 cell lines and exhibits some moderate cytotoxicity against SKOV3 cells (Figure 46). Clearly, the replacement of the diphenyl group by a terphenyl one (complex **Ru12**), results in a general loss of cytotoxic activity, which may be ascribed to the consequent increase of steric hindrance that may affect the interacting ability of the complex with biological targets, for instance DNA.

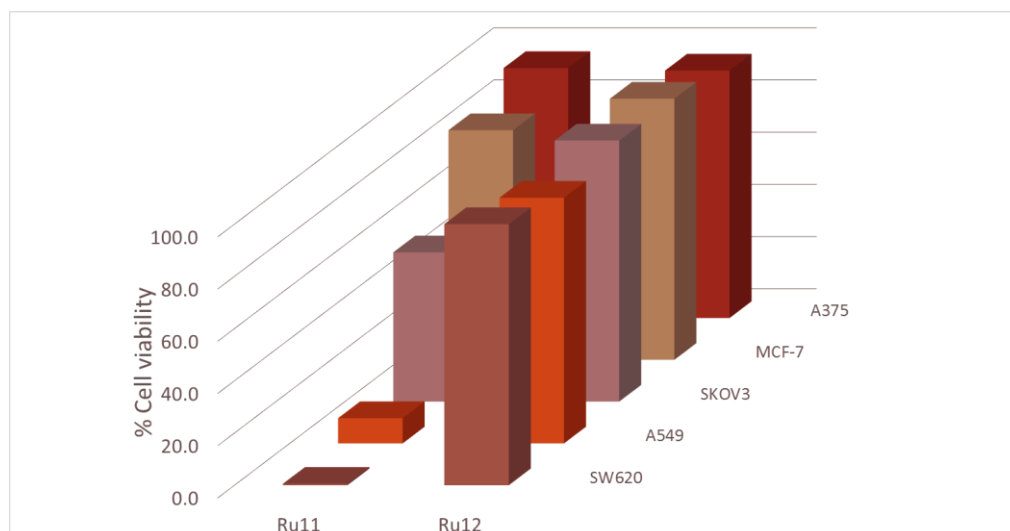


**Figure 46:** Cell-viability assays (single-point screening, % of cell viability) of Ru(II) complexes **Ru11** and **Ru12** with different cancer cell lines, namely **A549** (lung adenocarcinoma), **A375** (melanoma), **MCF-7** (breast adenocarcinoma), **SKOV3** (ovary adenocarcinoma) and **SW620** (colorectal adenocarcinoma). [Complex] = 50  $\mu$ M; incubation time = 24 h.

In summary, at a [complex] of 50  $\mu$ M and an incubation time of 24 hours, **Ru2** and **Ru13** are the compounds showing the most interesting cytotoxic behaviours. **Ru2** is highly cytotoxic against SW620, A375 with an effectiveness of 95%, followed by the cell lines SKOV3, A549 and MCF-7, with effectiveness superior to 50%. **Ru13** presents a remarkable cytotoxicity towards SW620 cells and is mildly cytotoxic against MCF-7 and SKOV3 cells (with an effectiveness superior to 50%). Most importantly, the data achieved with the series **Ru1-Ru15** clearly revealed a high versatility and great potential of this family of ruthenium(II) complexes; indeed, it has been shown that the biological activity (*i.e.*, cytotoxicity and cancer-cell specificity) of the  $[\text{RuCl}_2(\eta^6\text{-arene})(\text{PR}_3)]$  complexes depends on both the nature of the  $\eta^6$ -arene ligand and the  $\text{PR}_3$  phosphane. Therefore, it is anticipated that the activity of such compounds can be adjusted/fine-tuned through modification of these two ligands.

Based on the results obtained with **Ru1-Ru15**, a second series of  $[\text{RuCl}_2(\eta^6\text{-arene})(\text{PR}_3)]$  compounds, namely **Ru16-Ru19**, have been designed and prepared with the objective to improve the cytotoxic properties. The complexes of this second series all contain the pyrene substituent on the phosphane ligand (Figure 47), since it appears to be decisive for an efficient cytotoxic activity (see above). The  $\eta^6$ -arene ligand is also crucial for the cytotoxicity,<sup>46</sup> the methyl benzoate ring apparently leading to a more efficient system. Therefore, **Ru16-Ru18** contain this beneficial ligand, and **Ru19** includes the *p*-cymene moiety, for comparison purposes (for instance to compare the cytotoxicity of **Ru18** with that of **Ru19**).

As already mentioned, ruthenium(II) complexes with hydrophobic residues, such as polycyclic aromatic hydrocarbon substituents (*e.g.* a pyrene group), tend to be more stable.





This in turn can have a noteworthy enhancement of the biological-recognition processes and transport through the membranes, which can be reflected by a higher cytotoxicity of the complexes.<sup>47-49</sup>

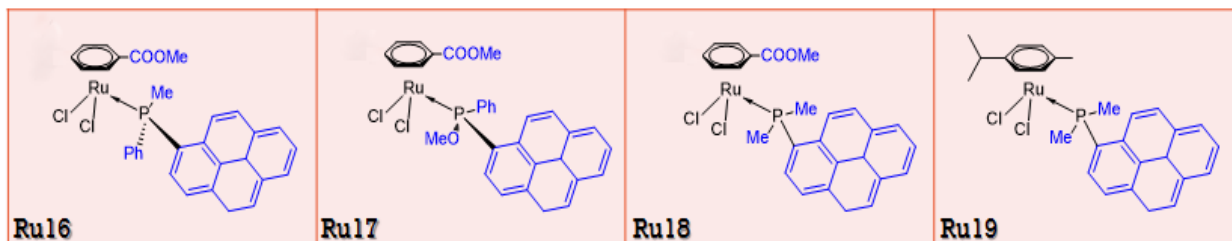


Figure 47: Second series of Ru(II)-arene compounds (Ru16-Ru19) used in the present study, whose design is based on the data collected with the first series (Ru1-Ru15).<sup>44,45</sup>

#### *MTT Reduction Assay*

Considering the results obtained by single-point studies at 24 hours (see above), the half-maximal inhibitory concentrations ( $IC_{50}$  values) of all complexes (from the two series) were determined with three types of cancer cells, *i.e.* colorectal adenocarcinoma (SW620), melanoma (A375) and breast adenocarcinoma (MCF-7), and a non-tumorigenic epithelial breast cell line, (MCF-10).

The  $IC_{50}$  values were obtained from the dose–response curves using GraphPad Prism V5.0 for windows (Graphpad Software, San Diego, CA, USA). All data are shown as the mean values  $\pm$  S.D. of three independent experiments.

The corresponding results, after an incubation time of 24 h, are summarized in Table 18, and the associated graphical representations are shown in Figure 48. Due to their very low activity in all cell lines selected, the  $IC_{50}$  values for complexes **Ru7**, **Ru9** and **Ru12** could not be determined. The results obtained for the remaining complexes corroborate the results achieved by the previous single-point screening measurements.

In general, the complexes present lower  $IC_{50}$  values than the reference inorganic molecule cisplatin. However, **Ru8** and **Ru13** do not affect A375 cells, and **Ru10** is inactive against both the tumorigenic (MCF-7) and non-tumorigenic (MCF-10) breast cell lines (Figure 48 and Figure 49).

**Table 18:** IC<sub>50</sub> values (μM) for different cell lines, namely SW620 (colorectal adenocarcinoma), A375 (melanoma), MCF-7 (breast adenocarcinoma) and MCF-10 (non-tumorigenic breast cell line), after 24 h of incubation. The data shown are means ± SD of three independent experiments. Values shown in bold grey characterize cell viabilities ≤ 50%; those shown in bold black are for cell viabilities ≤ 25%.

	IC <sub>50</sub> – 24 h (μM)			
	SW620	A375	MCF-7	MCF-10
<b>Ru1</b>	<b>23 ± 2.2</b>	<b>11 ± 1.0</b>	<b>13 ± 0.8</b>	<b>22 ± 2.3</b>
<b>Ru2</b>	<b>3.8 ± 0.7</b>	<b>3.1 ± 0.3</b>	<b>5.3 ± 0.9</b>	<b>10 ± 0.3</b>
<b>Ru3</b>	<b>13 ± 1.3</b>	<b>16 ± 1.5</b>	<b>19 ± 1.5</b>	<b>19 ± 1.4</b>
<b>Ru4</b>	<b>16 ± 1.0</b>	<b>16 ± 1.7</b>	<b>21 ± 1.1</b>	<b>12 ± 0.7</b>
<b>Ru5</b>	<b>29 ± 4.2</b>	<b>28 ± 2.9</b>	<b>24 ± 2.7</b>	<b>38 ± 6.7</b>
<b>Ru6</b>	<b>57 ± 5.2</b>	<b>34 ± 4.8</b>	<b>40 ± 5.6</b>	<b>41 ± 4.9</b>
<b>Ru8</b>	<b>14 ± 1.3</b>	> 100	<b>37 ± 2.3</b>	<b>32 ± 4.3</b>
<b>Ru10</b>	<b>20 ± 1.1</b>	<b>27 ± 4.6</b>	> 100	> 100
<b>Ru11</b>	<b>10 ± 0.7</b>	<b>30 ± 3.2</b>	<b>39 ± 2.1</b>	<b>23 ± 4.2</b>
<b>Ru13</b>	<b>5.0 ± 0.4</b>	> 100	<b>3.7 ± 0.3</b>	<b>4.2 ± 0.8</b>
<b>Ru14</b>	<b>28 ± 0.9</b>	<b>27 ± 2.2</b>	<b>39 ± 1.0</b>	<b>23 ± 3.1</b>
<b>Ru15</b>	<b>13 ± 0.4</b>	<b>21 ± 3.0</b>	<b>21 ± 2.8</b>	<b>5.5 ± 2.4</b>
<b>Ru16</b>	<b>1.7 ± 0.8</b>	<b>1.0 ± 0.1</b>	<b>7.2 ± 1.0</b>	<b>4.8 ± 0.8</b>
<b>Ru17</b>	<b>4.5 ± 0.5</b>	<b>2.4 ± 0.3</b>	<b>6.8 ± 1.3</b>	<b>4.9 ± 0.4</b>
<b>Ru18</b>	<b>0.7 ± 0.1</b>	<b>0.3 ± 0.1</b>	<b>0.8 ± 0.1</b>	<b>0.7 ± 0.1</b>
<b>Ru19</b>	<b>4.5 ± 0.7</b>	<b>3.9 ± 0.6</b>	<b>6.1 ± 0.6</b>	<b>7.1 ± 1.4</b>
<b>CisPt</b>	<b>85 ± 15</b>	<b>51 ± 5.4</b>	<b>82 ± 6.4</b>	<b>40 ± 4.5</b>

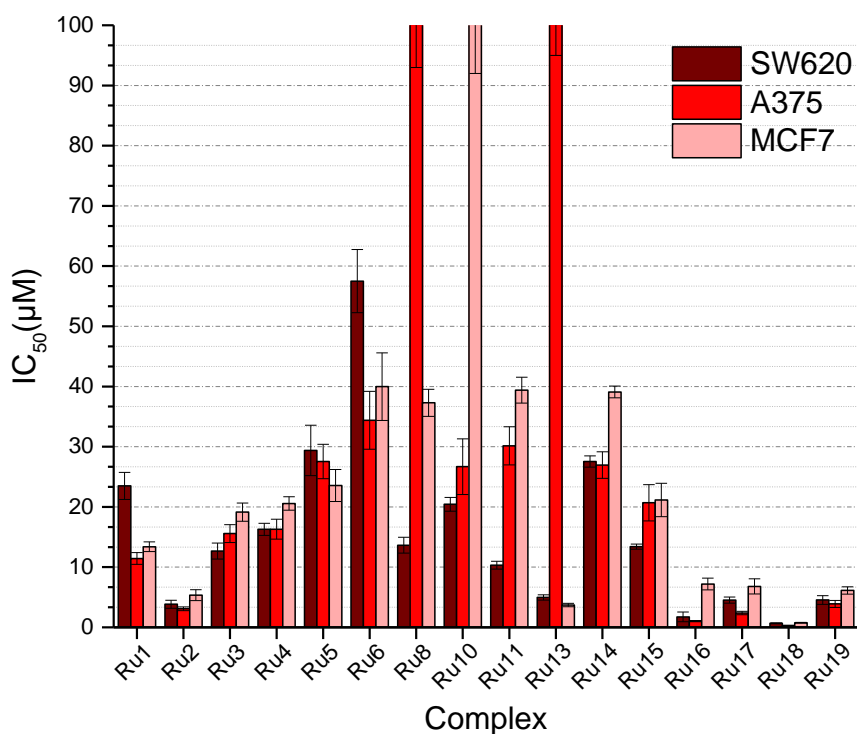


**Figure 48:** Graphical representation of the IC<sub>50</sub> values (in μM) for the Ru(II) complexes in different cancer cell lines, namely SW620 (colorectal adenocarcinoma), A375 (melanoma) and MCF-7 (breast adenocarcinoma), determined after an incubation time of 24 h.





**Ru18** is the most active complex in all cell lines, followed by **Ru16** (Figure 48). Importantly, these two compounds belong to the second series of  $[\text{RuCl}_2(\eta^6\text{-arene})(\text{PR}_3)]$  complexes, which have been designed on the basis of the structure-activity data achieved with the first series. **Ru16** and **Ru18** only differ by one R substituent on the  $\text{PR}_3$  ligand. Hence, the replacement of a phenyl group (**Ru16**) by a methyl group (**Ru18**) improves the cytotoxicity, which can be ascribed to steric or/and electronic issues.

The other complexes were divided in two groups. The first group is constituted of compounds **Ru1**, **Ru3**, **Ru4**, **Ru5**, **Ru6**, **Ru8**, **Ru10** and **Ru11**, which exhibit lower cytotoxicities, as already observed by single-point assays (see above).

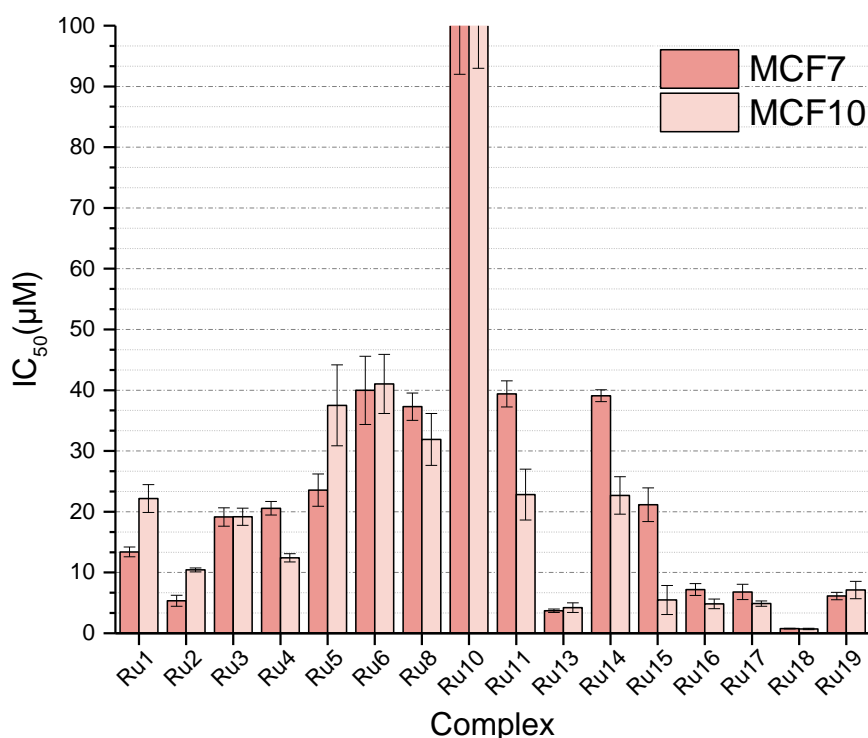
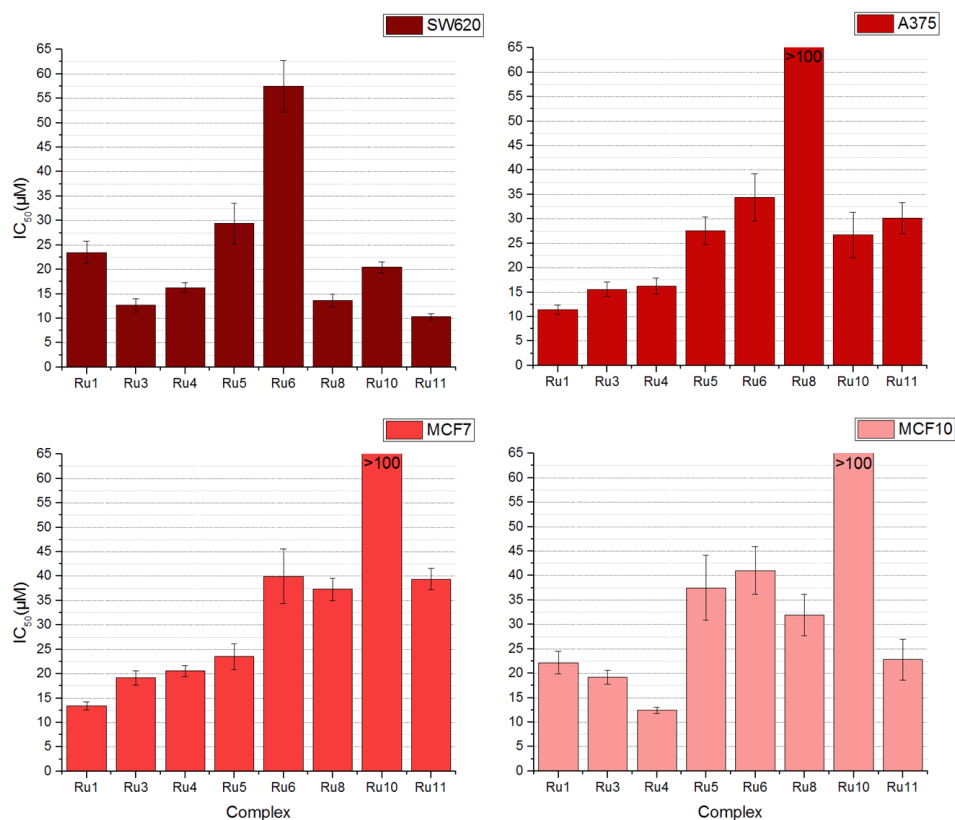


Figure 49: Graphical representation of the  $\text{IC}_{50}$  values (in  $\mu\text{M}$ ) for the  $\text{Ru}(\text{II})$  complexes in two different cell lines, namely MCF-7 (breast adenocarcinoma) and MCF-10 (non-tumorigenic breast cell line), determined after an incubation time of a 24 h.

Interestingly, the sole (a priori minor) difference between **Ru3** and **Ru5** is the arene ligand, *viz.* methyl benzoate for **Ru3** and *p*-cymene for **Ru5**; Nevertheless, **Ru3** presents a higher cytotoxicity than **Ru5**. Again, electronic effects (electron donating *versus* electron withdrawing effects) appear to have a clear effect on the cytotoxic behaviour. It can also be noticed that **Ru5** shows a higher selectivity towards the malignant breast cell line (MCF-7) compared with the non-tumorigenic one (MCF-10). **Ru10**, which holds the same (beneficial) arene substituent as **Ru3**, has no effect against the two breast cell lines ( $\text{IC}_{50} > 100 \mu\text{M}$ ), in contrast to **Ru3**. Thus, the ferrocenyl substituent on the  $\text{PR}_3$  ligand of **Ru10** has obviously, a negative effect on the cytotoxicity.

The importance of the R groups of the phosphane ligand on the cytotoxicity of the complex is further exemplified with **Ru4** and **Ru6**. Indeed, **Ru6** that has a phosphane methoxy substituent is less effective than the related methyl-substituted complex, *i.e.* **Ru4**. The IC<sub>50</sub> values of **Ru6** are approximately 3.5 times higher in SW620 and twice superior in A375 and MCF7 than those of **Ru4**. Similarly, differences are observed with **Ru1** and **Ru4**, which only vary by one phosphane R group. **Ru4** is slightly more active than **Ru1** against SW620 cells. However, for the cell lines A375 and MCF-7, **Ru1** is more active (1.5 times) than **Ru4** (Figure 48 and Figure 49); thus, the dibenzofuran (**Ru1**) and thianthrene (**Ru4**) substituents appear to have different cancer-cell specificities. Such a feature, already noticed by single-point assays (see above), opens the possibility to design potential, efficient drugs with cancer-specific properties (by playing with the arene ligand and the phosphane R groups).

**Ru8** presents a remarkable selectivity against SW620 cells (Figure 48 and Figure 50), but cannot differentiate healthy and tumorigenic breast cells (Figure 49). Finally, **Ru11** is highly active towards the cell line SW620; it is approximately 3 and 4 times more effective for this cell line than for A375 and MCF-7, respectively (Figure 48). Furthermore, **Ru11** is more cytotoxic to healthy breast cells (MCF-10) than to cancerous ones (MCF-7) (Figure 49).



**Figure 50:** Graphical representation of the IC<sub>50</sub> values (in μM) for Ru(II) complexes **Ru1**, **Ru3**-**Ru6**, **Ru8**, **Ru10** and **Ru11** in different cell lines, namely SW620 (colorectal adenocarcinoma), A375 (melanoma), MCF-7 (breast adenocarcinoma) and MCF-10 (non-tumorigenic breast cell line), determined after an incubation time of 24 h.





The second group of  $[\text{RuCl}_2(\eta^6\text{-arene})(\text{PR}_3)]$  complexes include compounds from the first and second series. This group of highly cytotoxic complexes (in the range 300 nM to 39  $\mu\text{M}$ ; Figure 51) is constituted of **Ru2** and **Ru13-Ru19**.

**Ru2** is highly cytotoxic against all selected cell lines ( $\text{IC}_{50}$  values in the range of 11 to 23  $\mu\text{M}$ ; Figure 51). It is more specific towards breast adenocarcinoma as it is twice more cytotoxic for MCF-7 than for MCF-10 cells (Figure 49).

**Ru13**, for which the methyl substituent of the  $\text{PR}_3$  ligand has been replaced with a methoxy one (Figure 51), is highly cytotoxic against MCF-7 and SW620 cells; nevertheless, it does not show specificity against tumorous cells (see MCF-7 *versus* MCF-10 cells Figure 49). As already aforementioned, replacement of the  $\text{PR}_3$  methoxy group with more hydrophobic groups, such as a phenyl or an isopropyl group, affects their activity towards colorectal adenocarcinoma (SW620). An increase in the hydrophobicity in this position results in a decrease of the activity of the corresponding complex; for instance, the cytotoxicity decreases 3-fold from **Ru13** to **Ru14**. Similarly, the biological activity decreases 10-fold from **Ru15** to **Ru2**.

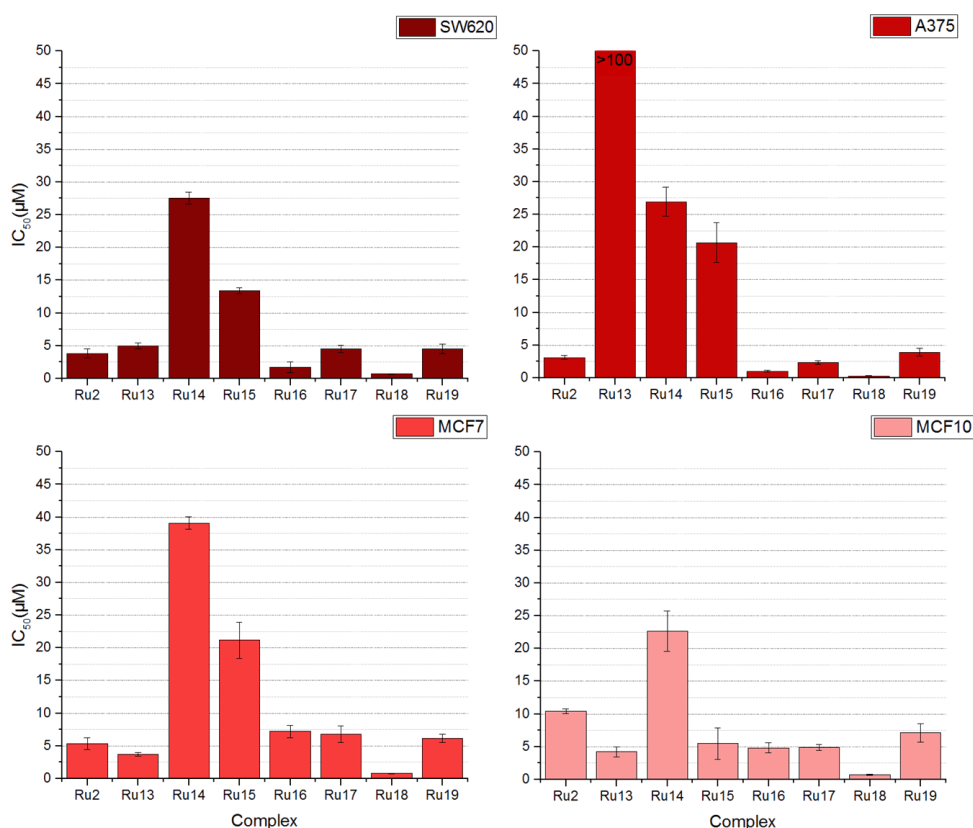


**Figure 51:** Graphical representation of the  $\text{IC}_{50}$  values (in  $\mu\text{M}$ ) for the Ru(II) complexes **Ru2**, **Ru13-Ru19** in different cell lines, namely SW620 (colorectal adenocarcinoma), A375 (melanoma), MCF-7 (breast adenocarcinoma) and MCF-10 (non-tumorigenic breast cell line), determined after an incubation time of 24 h.

**Ru18** is highly efficient, as reflected by its IC<sub>50</sub> values in the nM range (Figure 51). The analogous complexes **Ru16** and **Ru17** confirm the tendency observed with other members of the two series of compounds: replacement of one of the methyl substituents of PR<sub>3</sub> in **Ru18** by a phenyl (**Ru16**) or by a methoxy (**Ru17**) group gives rise to a clear decrease of the cytotoxic efficiency (Figure 51).

The effect of the arene ligand on the cytotoxic behaviour is nicely illustrated by complexes **Ru18** and **Ru19**. **Ru18**, which holds the methyl benzoate ring is 6 to 13 times more toxic than the *p*-cymene-containing one, namely **Ru19**. Comparison of the results achieved with compounds **Ru14**, **Ru15** and **Ru19** indicates that both electronic (phenyl *versus* methyl and phenyl *versus* isopropyl) and steric (phenyl *versus* methyl, isopropyl *versus* methyl and isopropyl *versus* phenyl) effects influence the cytotoxicity of the complexes.

This second series of [RuCl<sub>2</sub>(η<sup>6</sup>-arene)(PR<sub>3</sub>)] complexes does not show any cancer specificity, at least with the breast cell lines tested, namely the cancerous MCF-7 and healthy MCF-10 cells. Additional studies are definitively required with other non-tumorigenic cell lines to appraise whether **Ru16-Ru19** have some specificity for a particular type of cancer.

In view of the satisfactory results obtained with **Ru16-Ru19** for several cell lines (Table 18), their efficiency against neuroblastoma was investigated. Neuroblastoma is the most common embryonic malignancy of early childhood, which presents a poor prognosis for individuals diagnosed between birth and 18 months of age. It also has a disseminated disease as metastatic processes in liver, bone marrow, skin and several other organ.<sup>50</sup> The high metastatic rate and poor prognosis of the advanced disease, as well as their unique clinical features, stimulated research on neuroblastoma field.<sup>51-53</sup>

A well-known antineoplastic drug used against neuroblastoma, namely SN38 (7-ethyl-10-hydroxy-camptothecin), was used as positive control (Figure 52).<sup>54-56</sup> SN38 is the active metabolite of irinotecan ((4S)-4,11-diethyl-4-hydroxy-3,14-dioxo-3,4,12,14-tetrahydro-1H-pyrano[3',4':6,7]indolizino[1,2-b]quinolin-9-yl 1,4'-bipiperidine-1'-carboxylate), which is also acting against this disease (Figure 52).

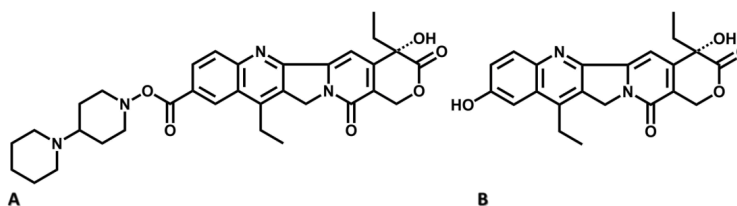


Figure 52: Representation of the chemical structures of A: irinotecan (CPT-11 or (4S)-4,11-diethyl-4-hydroxy-3,14-dioxo-3,4,12,14-tetrahydro-1H-pyrano[3',4':6,7]indolizino[1,2-b]quinolin-9-yl-1,4'-bipiperidine-1'-carboxylate) and its metabolite B:SN38 (7-ethyl-10-hydroxy-camptothecin).





Irinotecan is a synthetic derivative of camptothecin, an alkaloid found in a Chinese plant, which acts as an inhibitor of DNA topoisomerase I. It is widely used in the treatment of several types of tumours. SN38, which is obtained by hydrolysis of irinotecan, is 1000 times more active than its parent compound, but suffers from its high toxicity and solubility issues.<sup>54,55</sup>

**Ru16-Ru19** were thus tested against two neuroblastoma cell lines, namely SK-N-BE(2) and CHLA-90. The corresponding results are summarized in Table 19 and Figure 53.

**Table 19:** IC<sub>50</sub> values (μM) of Ru16-Ru19 for the neuroblastoma cell lines SK-N-BE(2) and CHLA-90, determined after an incubation time of 24 h. The data shown are means ± SD of three independent experiments. The values shown in bold grey are for cell viabilities ≤ 100 nM; those in bold black are for cell viabilities ≤ 5 μM.

	IC <sub>50</sub> – 24 h (μM)	
	SK-N-BE(2)	CHLA-90
<b>Ru16</b>	<b>0.9 ± 0.1</b>	<b>0.8 ± 0.02</b>
<b>Ru17</b>	<b>0.9 ± 0.1</b>	<b>1.2 ± 0.1</b>
<b>Ru18</b>	<b>0.5 ± 0.02</b>	<b>0.4 ± 0.05</b>
<b>Ru19</b>	<b>3.2 ± 0.4</b>	<b>3.0 ± 0.1</b>
<b>SN38</b>	7.6 ± 0.6	13 ± 0.8

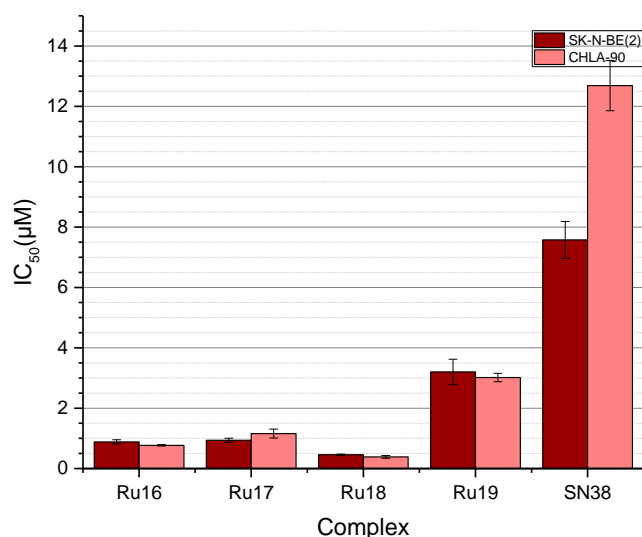


**Figure 53:** Graphical representation of the IC<sub>50</sub> values (in μM) for the Ru(II) complexes Ru16-Ru19 and SN38, in two neuroblastoma cell lines, namely SK-N-BE(2) and SCLA-90, determined after an incubation time of 24 h.

Again, the nature of the arene and PR<sub>3</sub> ligands drives the activity of the corresponding complexes, with the same tendency as that described earlier. The compounds with the methyl benzoate ring, *i.e.* **Ru16-Ru18**, are 6-times more active than **Ru19**, which contains a *p*-cymene ligand. The IC<sub>50</sub> values vary from 400 nM to 7.6 μM; as with the previous cell lines (see Figure

53), **Ru18** is the most efficient compound while **Ru19** is the least active against both neuroblastoma cell lines. Most interestingly, all the complexes are significantly more effective than the reference compound SN38 (Table 19).

#### *Cell migration – Wound-healing assay*

Metastasis is an intricate process that combines a series of sequential steps including the (i) invasion of adjacent tissues, (ii) intravasation, (iii) transport through the circulatory system, (iv) arrest at a secondary site, (v) extravasation and (vi) growth in a secondary organ. Metastases are the cause of 90% of human cancer deaths,<sup>57</sup> because the currently used treatment used are far from satisfactory: efficient antimetastatic drugs are still lacking.

Collective cell migration plays essential roles in a wide spectrum of biological processes and it has been described that ruthenium complexes may inhibit them. The wound-healing assay is a standard, *in vitro* technique, for probing collective cell migration in two dimensions. Using physical exclusion or removing the cells from an area through mechanical, thermal or chemical damage, a cell-free zone (*i.e.* a “wound”) can be created in a confluent monolayer. Subsequently, images are captured at the beginning and at regular time intervals during the cell migration closing the wound. Comparison of the images with and without the presence of a potential antimetastatic agent and quantification of the respective migration rate of the cells allow to investigate the (possible) effect of the compound on the “healing process” and to explore critical mechanisms of action involved in it.<sup>58-60</sup>

In this assay, only the cell lines HN4 (laryngeal squamous cell carcinoma), SK-N-BE(2) (neuroblastoma) and CHLA-90 (neuroblastoma) were used because limitations on either the technique or the conditions applied did not permit to employ all cells. Complexes **Ru2**, **Ru13** and **Ru16-Ru19** were tested and compared to a reference compound, *viz.* prodigiosine, known to inhibit cell migration.<sup>61,62,63</sup>

For these experiments, the cells were plated in 12-well microtiter cell-culture plates. When the cells have reached the desired confluence, an incision was made using a plastic pipette tip to produce a clean wound area. The images obtained for the cells with and without treatment with the metal-based compounds are shown in Figure 54 to Figure 54.

The calculated areas were plotted against time, allowing the determination of two different parameters, namely the time needed to close half of the wound, *i.e.*  $t_{1/2}$  (hours), and the migration velocity, *viz.*  $v_{\text{migration}}$  ( $\mu\text{m/h}$ ). All data obtained are listed in Table 20.





**Table 20:** Calculated  $t_{1/2}$  values (hours) and  $v_{\text{migration}}$  data ( $\mu\text{m/h}$ ) for complexes **Ru2**, **Ru13** and **Ru16-Ru19** with three different cell lines, namely **HN4** (laryngeal squamous cell carcinoma), **SK-N-BE(2)** (neuroblastoma) and **CHLA-90** (neuroblastoma), using various incubation times (up to 36 h). The data shown are means  $\pm$  SD of three independent experiments. The control was carried out with prodigiosine, a known cell-migration inhibitor.

	Cell Lines					
	HN4		SK-N-BE(2)		CHLA-90	
	$t_{1/2}$ (hours)	$v_{\text{migration}}$ ( $\mu\text{M}/\text{hour}$ )	$t_{1/2}$ (hours)	$v_{\text{migration}}$ ( $\mu\text{M}/\text{hour}$ )	$t_{1/2}$ (hours)	$v_{\text{migration}}$ ( $\mu\text{M}/\text{hour}$ )
<b>Control</b>	8.9 $\pm$ 0.72	21.4 $\pm$ 0.8	23.1 $\pm$ 4.35	7.8 $\pm$ 0.00	18.6 $\pm$ 4.3	7.8 $\pm$ 0.5
<b>Ru2</b>	8.7 $\pm$ 0.92	19.6 $\pm$ 4.1	30.1 $\pm$ 7.47	6.4 $\pm$ 1.65	20.1 $\pm$ 6.1	7.3 $\pm$ 0.9
<b>Ru13</b>	11.5 $\pm$ 0.86	16.2 $\pm$ 5.4	24.9 $\pm$ 2.72	6.8 $\pm$ 0.26	n.d.	n.d.
<b>Ru16</b>	8.1 $\pm$ 0.89	21.5 $\pm$ 2.3	24.2 $\pm$ 1.40	5.7 $\pm$ 1.59	22.5 $\pm$ 1.1	6.9 $\pm$ 0.7
<b>Ru17</b>	9.4 $\pm$ 0.43	16.9 $\pm$ 3.8	20.4 $\pm$ 1.93	8.8 $\pm$ 1.86	19.5 $\pm$ 2.0	8.1 $\pm$ 1.5
<b>Ru18</b>	11.4 $\pm$ 2.70	14.6 $\pm$ 4.4	37.2 $\pm$ 3.67	3.0 $\pm$ 0.27	21.1 $\pm$ 5.9	8.0 $\pm$ 0.9
<b>Ru19</b>	11.3 $\pm$ 1.34	18.2 $\pm$ 4.8	27.8 $\pm$ 0.52	7.6 $\pm$ 0.25	17.3 $\pm$ 2.0	8.9 $\pm$ 0.5

n.d.: in the conditions of the experiment it was not possible to determine the  $t_{1/2}$  values (hours) and  $v_{\text{migration}}$ ; the variations on the wound size were not significant.

The wound-healing data obtained revealed that some of the complexes could efficiently inhibit the migration of tumour cells *in vitro*. The most efficient compound for the three cell lines is **Ru18**, as reflected but its higher  $t_{1/2}$  values (characterizing the time required to close the wound) and associated lower migration velocities, especially when compared with those of the respective controls (Table 20). Remarkably, SK-N-BE(2) cells exposed to this complex migrate at approximately half of the velocity of that observed with the control that only contains cells in the buffered solution used for the assays (this buffer contains 2% of DMSO).

**Ru13**, **Ru17** and **Ru19** solely induce a positive effect on the cell line HN4 (Table 20), and **Ru2** only affects the migration of SK-N-BE(2) cells.

These preliminary results are very promising; hence, further investigation is clearly required to better understand the mode of action of this type of complexes. For instance, additional wound-healing experiments varying the complex concentrations are necessary, and more biological studies should definitively be performed to elucidate the mechanism of the observed complex-mediated inhibition of cell migration.

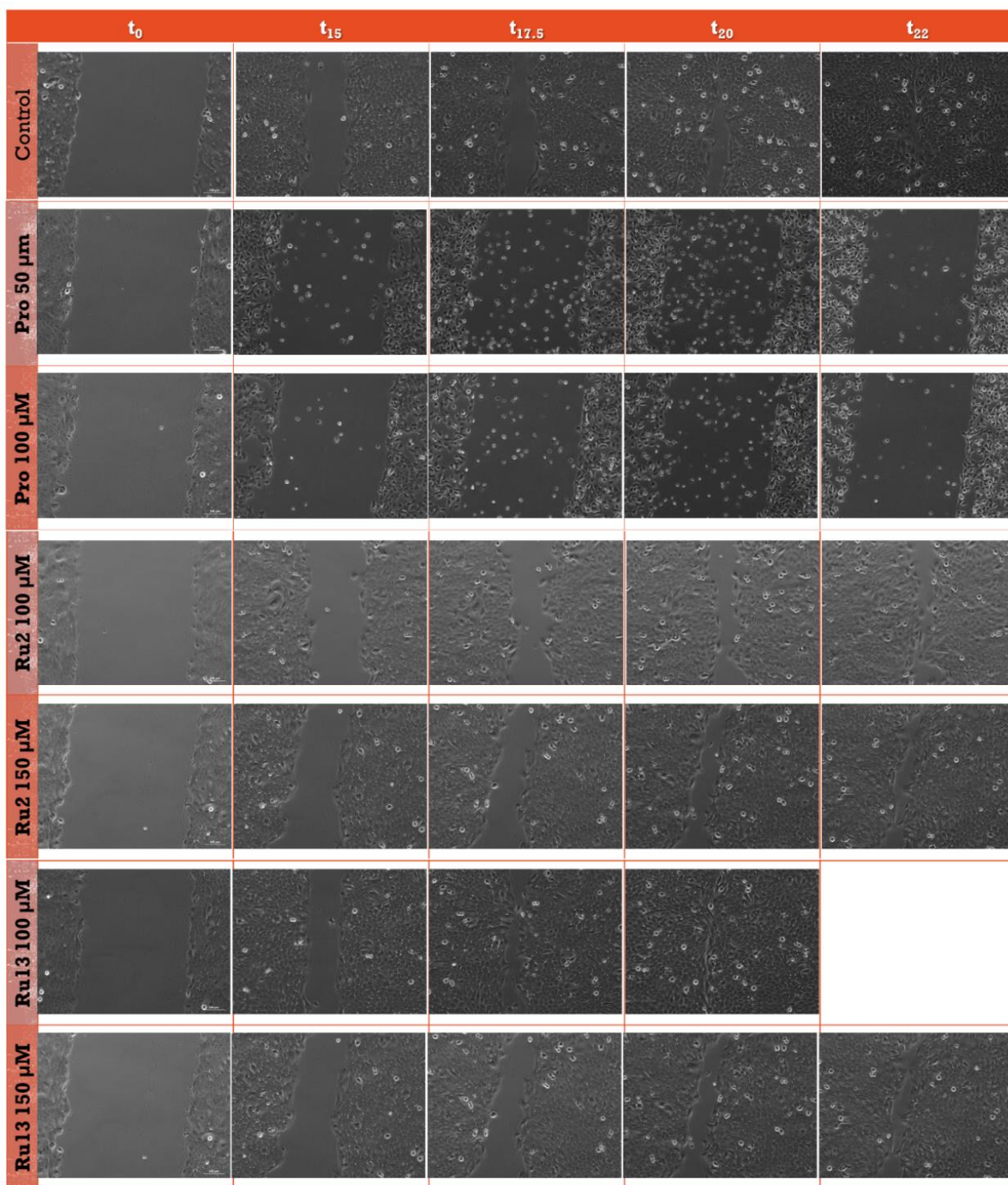
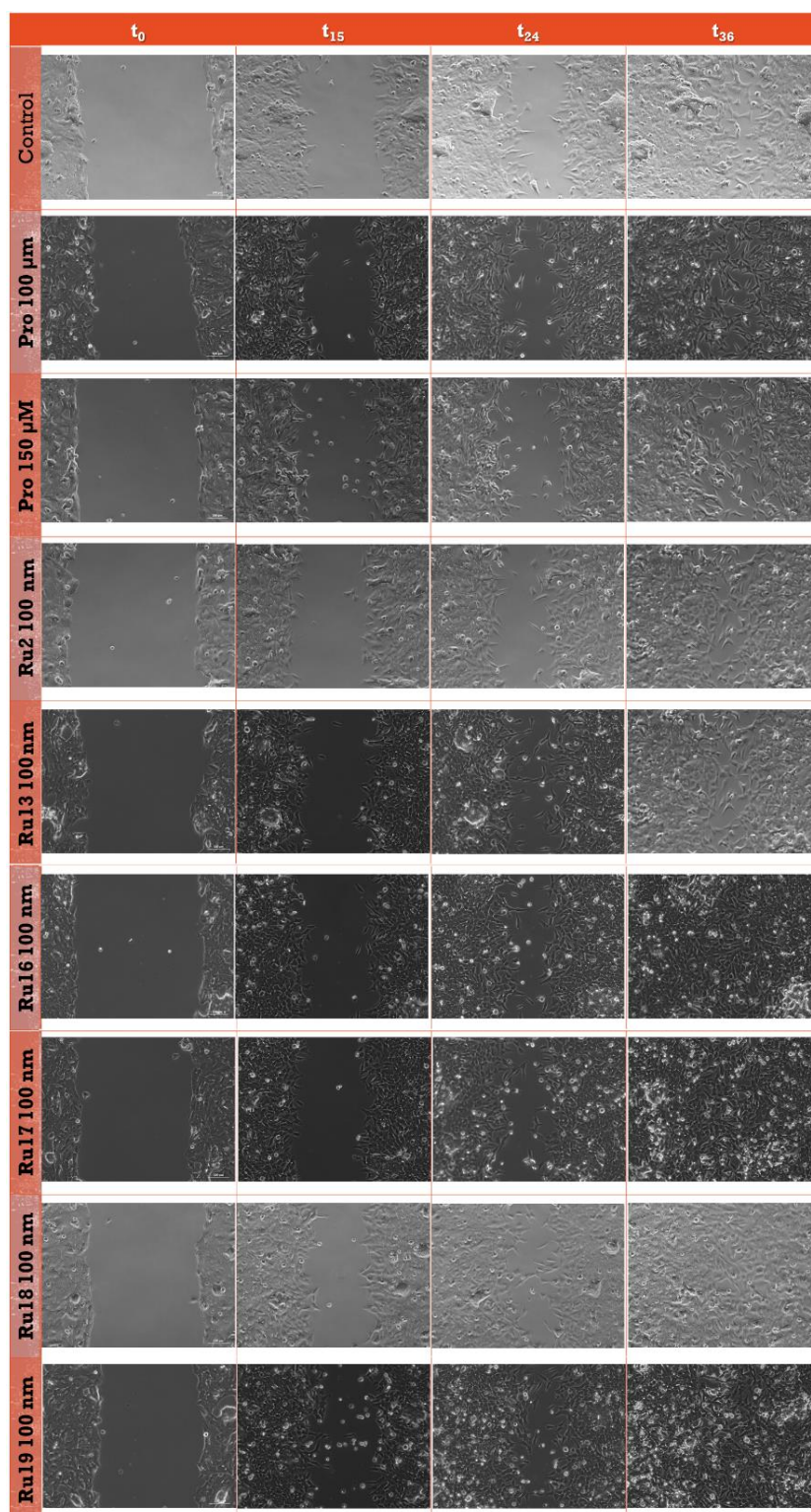


Figure 54: Representative bright-field images from a scratch-assay experiment at different time points and using different experimental conditions. The laryngeal squamous cell carcinoma cells (HN4) were plated and wounded with a p20 pipette tip, and subsequently imaged overnight using a microscope. The cells were incubated with different concentrations of the complexes Ru2 and Ru13. Controls were carried out with and without prodigiosine. Scale bar 100 nm.





**Figure 55:** Representative bright-field images from a scratch-assay experiment at different time points and different experimental conditions. The neuroblastoma cells (SK-N-BE(2)) were plated and wounded with a p20 pipette tip, and subsequently imaged overnight using a microscope. The cells were incubated with different concentrations of complexes Ru2, Ru13 and Ru16-Ru19. Controls were carried out with and without prodigiosine. Scale bar 100 nm.

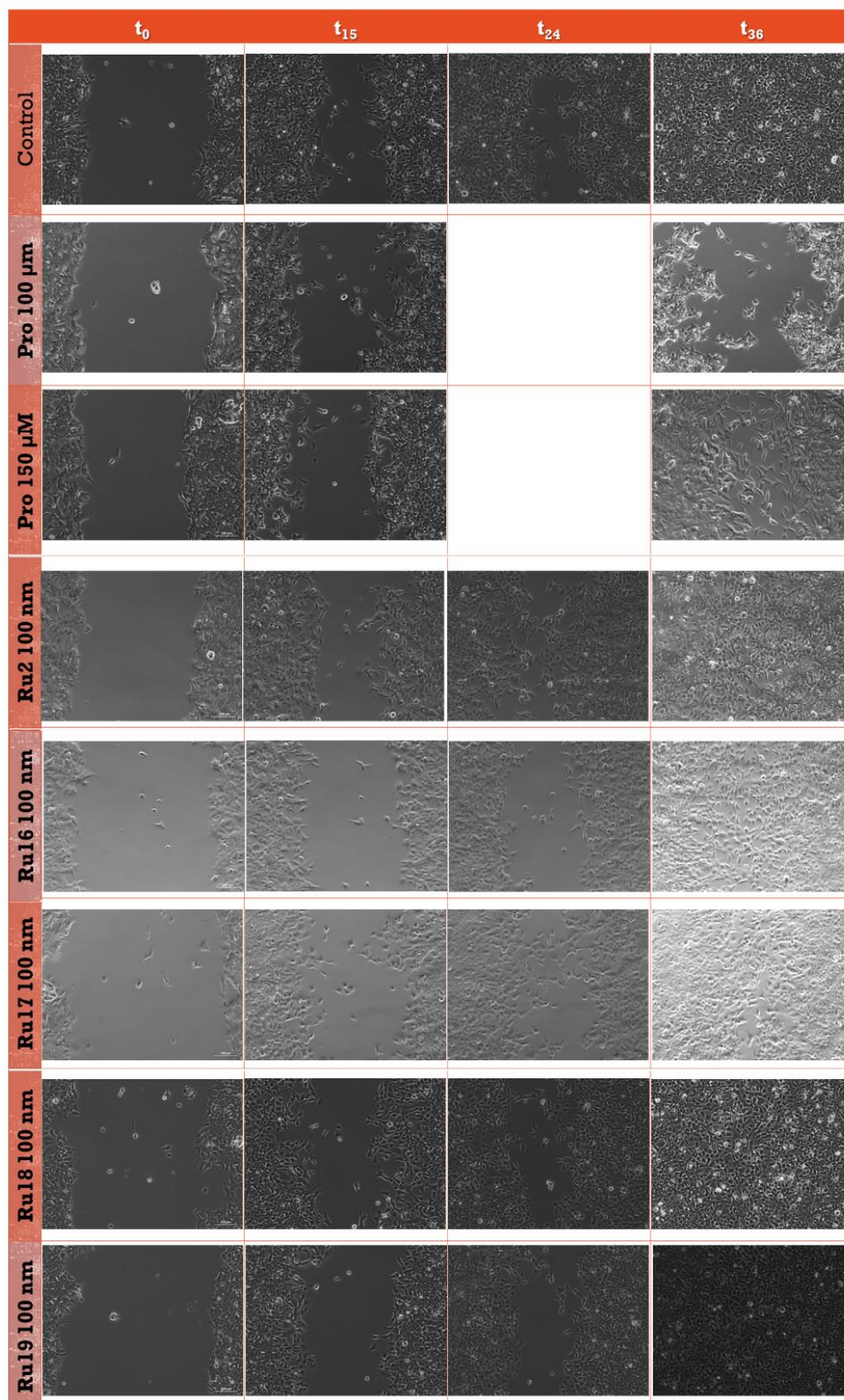


Figure 56: Representative bright-field images from scratch-assay experiments at different time points and different experimental conditions. The neuroblastoma cells (CHLA90) were plated and wounded with a p20 pipette tip, and subsequently imaged overnight using a microscope. The cells were incubated with different concentrations of complexes Ru2 and Ru16-Ru19. Controls were carried out with and without prodigiosine. Scale bar 100 nm.





### Conclusions

The cytotoxic behaviour of 19 new ruthenium(II) complexes of the type  $[\text{RuCl}_2(\eta^6\text{-arene})(\text{PR}_3)]$  was evaluated by means of single-point assays and the determination of the  $\text{IC}_{50}$  values with different cell lines. These studies revealed the great potential of such metal-based compounds, most of them being more active than the well-known reference molecule cisplatin. Only 3 out of the 19 complexes prepared exhibited poor cytotoxic behaviours under the experimental conditions used and for the cell lines selected. Examination of structure-activity relationship of the compounds allowed to show that the nature of the  $\eta^6\text{-arene}$  and phosphane ligands is crucial for their cytotoxic properties. Hence, steric, electronic and hydrophobic effects appear to play a vital role regarding their biological behaviour, both in terms of cytotoxic efficiency and cancer specificity. The data achieved disclosed the versatility of this family of ruthenium(II) complexes since numerous different R groups can be introduced in the  $\text{PR}_3$  ligand and various arene rings can be selected. It is therefore clear that the cytotoxic activity and/or cancer specific of such compounds can be fine-tuned through the appropriate choice of the two ligands around the metal centre.

The activity of the most efficient complexes was also investigated against two neuroblastoma cell lines, which resulted in cytotoxic activities in the nM range, far below the  $\text{IC}_{50}$  values reached with the drugs currently used for this disease, *i.e.* irinotecan and SN38.

Preliminary antimetastatic assays were also performed, which allowed to show that some of the ruthenium(II) compounds are capable of efficiently inhibiting cell migration. Further studies are needed to confirm these outstanding results and to try to fully understand the mechanism(s) of action such metal complexes, like for instance determining their potential cellular targets, which may unravel key cellular signalling pathways affected by their interaction.

## References

- (1) Han Ang, W.; Dyson, P. J. *Eur. J. Inorg. Chem.* **2006**, 2006, 4003.
- (2) Abid, M.; Shamsi, F.; Azam, A. *Mini Rev. Med. Chem.* **2015**.
- (3) Alessio, E.; Mestroni, G.; Bergamo, A.; Sava, G. *Curr. Top. Med. Chem.* **2004**, 4, 1525.
- (4) Antonarakis, E. S.; Emadi, A. *Cancer Chemother. Pharmacol.* **2010**, 66, 1.
- (5) Bergamo, A.; Gaiddon, C.; Schellens, J. H.; Beijnen, J. H.; Sava, G. *J. Inorg. Biochem.* **2012**, 106, 90.
- (6) Groessl, M.; Tsybin, Y. O.; Hartinger, C. G.; Keppler, B. K.; Dyson, P. J. *J. Biol. Inorg. Chem.* **2010**, 15, 677.
- (7) Iida, J.; Bell-Loncella, E. T.; Purazo, M. L.; Lu, Y.; Dorchak, J.; Clancy, R.; Slavik, J.; Cutler, M. L.; Shriver, C. D. *J. Transl. Med.* **2016**, 14, 1.
- (8) Su, W.; Tang, Z.; Li, P. *Mini Rev. Med. Chem.* **2016**, 16, 787.
- (9) Messori, L.; Camarri, M.; Ferraro, T.; Gabbiani, C.; Franceschini, D. *ACS Med. Chem. Lett.* **2013**, 4, 329.
- (10) Vyas, N. A.; Ramteke, S. N.; Kumbhar, A. S.; Kulkarni, P. P.; Jani, V.; Sonawane, U. B.; Joshi, R. R.; Joshi, B.; Erxleben, A. *Eur. J. Med. Chem.* **2016**, 121, 793.
- (11) Guo, Z.; Sadler, P. J. *Angew. Chem. Int. Ed. Engl.* **1999**, 38, 1512.
- (12) Brabec, V.; Novakova, O. *Drug. Resist. Updat.* **2006**, 9, 111.
- (13) Hall, J. P.; Keane, P. M.; Beer, H.; Buchner, K.; Winter, G.; Sorensen, T. L.; Cardin, D. J.; Brazier, J. A.; Cardin, C. J. *Nucleic Acids Res.* **2016**, 44, 9472.
- (14) Bahira, M.; McCauley, M. J.; Almaqwashi, A. A.; Lincoln, P.; Westerlund, F.; Rouzina, I.; Williams, M. C. *Nucleic Acids Res.* **2015**, 43, 8856.
- (15) Chao, H.; Ji, L. N. *Bioinorg. Chem. Appl.* **2005**, 15.
- (16) Wagenknecht, H. A.; Stemp, E. D.; Barton, J. K. *Biochemistry* **2000**, 39, 5483.
- (17) Augustyn, K. E.; Stemp, E. D.; Barton, J. K. *Inorg. Chem.* **2007**, 46, 9337.
- (18) Frank, N. L.; Meade, T. J. *Inorg. Chem.* **2003**, 42, 1039.
- (19) Wang, P.; Miller, J. E.; Henling, L. M.; Stern, C. L.; Frank, N. L.; Eckermann, A. L.; Meade, T. J. *Inorg. Chem.* **2007**, 46, 9853.
- (20) Jackson, B. A.; Barton, J. K. *Curr. Protoc. Nucleic Acid Chem.* **2001**, Chapter 6, Unit 6 2.
- (21) Chatterjee, B. D.; Mitra, A.; De, G. S. *Platinum Met. Rev.* **2006**, 50, 2.
- (22) Wu, B.; Ong, M. S.; Groessl, M.; Adhireksan, Z.; Hartinger, C. G.; Dyson, P. J.; Davey, C. A. *Chemistry (Easton)* **2011**, 17, 3562.
- (23) Brabec, V.; Pracharova, J.; Stepankova, J.; Sadler, P. J.; Kasparkova, J. *J. Inorg. Biochem.* **2015**.
- (24) van der Steen, S.; de Hoog, P.; van der Schilden, K.; Gamez, P.; Pitie, M.; Kiss, R.; Reedijk, J. *Chem. Commun. (Camb)* **2010**, 46, 3568.
- (25) Sun, Y.; Li, J.; Zhao, H.; Tan, L. *J. Inorg. Biochem.* **2016**, 163, 88.
- (26) Mohanraj, M.; Ayyannan, G.; Raja, G.; Jayabalakrishnan, C. *Mater. Sci. Eng. C Mater. Biol. Appl.* **2016**, 69, 1297.
- (27) Clarke, M. J. *Coord. Chem. Rev.* **2002**, 232, 69.
- (28) Sun, H.; Li, H.; Sadler, P. J. *Chem. Rev.* **1999**, 99, 2817.
- (29) Sava, G.; Bergamo, A. *Int. J. Oncol.* **2000**, 17, 353.
- (30) Fischer-Fodor, E.; Miklasova, N.; Berindan-Neagoe, I.; Saha, B. *Clujul Med.* **2015**, 88, 272.
- (31) Torti, S. V.; Torti, F. M. *Nat. Rev. Cancer* **2013**, 13, 342.





- (32) Bergamo, A.; Gagliardi, R.; Scarcia, V.; Furlani, A.; Alessio, E.; Mestroni, G.; Sava, G. *J. Pharmacol. Exp. Ther.* **1999**, 289, 559.
- (33) Bergamo, A.; Sava, G. *Dalton Trans.* **2007**, 1267.
- (34) Morris, R. E.; Aird, R. E.; Murdoch Pdel, S.; Chen, H.; Cummings, J.; Hughes, N. D. *J. Med. Chem.* **2001**, 44.
- (35) Lentz, F.; Drescher, A.; Lindauer, A.; Henke, M.; Hilger, R. A.; Hartinger, C. G.; Scheulen, M. E.; Dittrich, C.; Keppler, B. K.; Jaehde, U.; Central European Society for Anticancer Drug Research, E. *Anticancer Drugs* **2009**, 20, 97.
- (36) Kuhn, P. S.; Pichler, V.; Roller, A.; Hejl, M.; Jakupiec, M. A.; Kandiolle, W.; Keppler, B. K. *Dalton Trans.* **2015**, 44, 659.
- (37) Leijen, S.; Burgers, S. A.; Baas, P.; Pluim, D.; Tibben, M.; van Werkhoven, E.; Alessio, E.; Sava, G.; Beijnen, J. H.; Schellens, J. H. *Invest. New Drugs* **2015**, 33, 201.
- (38) Bugarcic, T.; Habtemariam, A.; Deeth, R. J.; Fabbiani, F. P.; Parsons, S.; Sadler, P. J. *Inorg. Chem.* **2009**, 48.
- (39) Gopal, Y. N.; Jayaraju, D.; Kondapi, A. K. *Biochemistry* **1999**, 38, 4382.
- (40) Chen, X.; Gao, F.; Yang, W. Y.; Zhou, Z. X.; Lin, J. Q.; Ji, L. N. *Chem. Biodivers.* **2013**, 10, 367.
- (41) Chen, H.; Parkinson, J. A.; Parsons, S.; Coxall, R. A.; Gould, R. O.; Sadler, P. J. *J. Am. Chem. Soc.* **2002**, 124, 3064.
- (42) Chen, H.; Parkinson, J. A.; Morris, R. E.; Sadler, P. J. *J. Am. Chem. Soc.* **2003**, 125, 173.
- (43) Martinez-Alonso, M.; Busto, N.; Jalon, F. A.; Manzano, B. R.; Leal, J. M.; Rodriguez, A. M.; Garcia, B.; Espino, G. *Inorg. Chem.* **2014**, 53, 11274.
- (44) Clavero, P.; Grabulosa, A.; Rocamora, M.; Muller, G.; Font-Bardia, M. *Dalton Trans.* **2016**, 45, 8513.
- (45) Navarro, M.; Vidal, D.; Clavero, P.; Grabulosa, A.; Muller, G. *Organometallics* **2015**, 34, 973.
- (46) Aird, R. E.; Cummings, J.; Ritchie, A. A.; Muir, M.; Morris, R. E.; Chen, H.; Sadler, P. J.; Jodrell, D. I. *Br. J. Cancer* **2002**, 86, 1652.
- (47) Ganeshpandian, M.; Loganathan, R.; Suresh, E.; Riyasdeen, A.; Akbarsha, M. A.; Palaniandavar, M. *Dalton Trans.* **2014**, 43, 1203.
- (48) Komatsu, H.; Yoshihara, K.; Yamada, H.; Kimura, Y.; Son, A.; Nishimoto, S.; Tanabe, K. *Chemistry (Easton)* **2013**, 19, 1971.
- (49) Peacock, A. F.; Sadler, P. J. *Chem. Asian J.* **2008**, 3, 1890.
- (50) Wagner, L. In *Neuroblastoma: Diagnosis, Therapy, and Prognosis*; Hayat, M. A., Ed.; Springer Netherlands: Dordrecht, 2012, p 209.
- (51) Ferlay, J.; Soerjomataram, I.; Dikshit, R.; Eser, S.; Mathers, C.; Rebelo, M.; Parkin, D. M.; Forman, D.; Bray, F. *Int. J. Cancer* **2015**, 136, E359.
- (52) Esposito, M. R.; Aveic, S.; Seydel, A.; Tonini, G. P. *J. Biomed. Sci.* **2017**, 24, 14.
- (53) Matthay, K. K.; Maris, J. M.; Schleiermacher, G.; Nakagawara, A.; Mackall, C. L.; Diller, L.; Weiss, W. A. *Nat. Rev. Dis. Primers* **2016**, 2, 16078.
- (54) Rothenberg, M. L. *Oncologist* **2001**, 6, 66.
- (55) Xie, R.; Mathijssen, R. H.; Sparreboom, A.; Verweij, J.; Karlsson, M. *O. J. Clin. Oncol.* **2002**, 20, 3293.
- (56) Chabot, G. G. *Clin. Pharmacokinet.* **1997**, 33, 245.
- (57) Hoon, D. S.; Ferris, R.; Tanaka, R.; Chong, K. K.; Alix-Panabieres, C.; Pantel, K. *J. Surg. Oncol.* **2011**, 103, 508.

- (58) Grada, A.; Otero-Vinas, M.; Prieto-Castrillo, F.; Obagi, Z.; Falanga, V. *J. Invest. Dermatol.* **2017**, *137*, e11.
- (59) Hulkower, K. I.; Herber, R. L. *Pharmaceutics* **2011**, *3*, 107.
- (60) Jonkman, J. E.; Cathcart, J. A.; Xu, F.; Bartolini, M. E.; Amon, J. E.; Stevens, K. M.; Colarusso, P. *Cell Adh. Migr.* **2014**, *8*, 440.
- (61) Perez-Tomas, R.; Montaner, B.; Llagostera, E.; Soto-Cerrato, V. *Biochem. Pharmacol.* **2003**, *66*, 1447.
- (62) Montaner, B.; Perez-Tomas, R. *Curr. Cancer. Drug Targets* **2003**, *3*, 57.
- (63) Perez-Tomas, R.; Vinas, M. *Curr. Med. Chem.* **2010**, *17*, 2222.





# 3

## Helices and Helicates – Supramolecular rational design

---

*Supramolecular chemistry allows to design and produce sophisticated self-assembled structures, for instance using organic ligands with different binding sites and metallic centres. Three-dimensional architectures may be generated applying this synthetic approach, and supramolecular complexes that can recognize and target unusual DNA structures, or even interfere with important biological functions leading to cell death, can be rationally prepared.*

*In this chapter, the design and preparation of a series of metallo-helicates is described. The thorough investigation of the interaction of these supramolecular compounds with DNA is subsequently reported. Finally, the evaluation of the cytotoxic properties of the complexes is described.*

### Contents

---

SYNTHESIS .....	110
<i>Design of dinucleating organic ligands – Poly-<math>\beta</math>-diketones</i> .....	110
Synthesis of 1,3-bis(3-oxo-3-(2-naphthyl)-propionyl)benzene (H <sub>2</sub> L1) .....	113
Ligands with H-acceptor groups, <i>i.e.</i> with pyridinyl substituents .....	113
Synthesis of 1,3-bis-(3-oxo-3-(2-pyridinyl)-propionyl)benzene (H <sub>2</sub> L2) .....	113
Synthesis of 1,3-bis-(3-oxo-3-(3-pyridinyl)-propionyl)benzene (H <sub>2</sub> L3) .....	113
Synthesis of 1,3-bis-(3-oxo-3-(4-pyridinyl)-propionyl)benzene (H <sub>2</sub> L4) .....	114
Ligands with H-donor groups, <i>i.e.</i> hydroxyl substituents .....	114
Synthesis of 1,3-bis-(3-oxo-3(2-hydroxyphenyl)propionyl)benzene (H <sub>4</sub> L5) .....	114
Synthesis of 1,3-bis-(3-oxo-3(3-hydroxyphenyl)propionyl)benzene (H <sub>4</sub> L6) .....	114
Synthesis of 1,3-bis-(3-oxo-3(4-hydroxyphenyl)propionyl)benzene (H <sub>4</sub> L7) .....	115

---

---

<i>General method for the preparation of the supramolecular complexes .....</i>	<i>115</i>
DNA-BINDING STUDIES.....	119
<i>UV-Vis Spectroscopy .....</i>	<i>119</i>
<i>Fluorescence-dye displacement.....</i>	<i>121</i>
<i>Circular Dichroism.....</i>	<i>124</i>
<i>Agarose-gel electrophoresis .....</i>	<i>125</i>
<i>Polyacrylamide-gel electrophoresis – DNA three-way junction binding.....</i>	<i>126</i>
<i>AFM experiments.....</i>	<i>129</i>
CELL-VIABILITY ASSAYS .....	131
<i>Single-point assays .....</i>	<i>131</i>
<i>MTT Reduction Assay.....</i>	<i>132</i>
<i>Fluorescence spectroscopy assays.....</i>	<i>133</i>
Immunofluorescence .....	133
Cell cycle .....	133
CONCLUSIONS .....	135
REFERENCES .....	137

---





Nature has its exceptional ways to take advantage of a unique selection of weak, non-covalent interactions, namely the hydrogen-bonding, donor-acceptor,  $\pi$ - $\pi$ , van der Waals, and hydrophilic/hydrophobic interactions, to generate highly complex and often symmetrical 3D architectures.<sup>1</sup> Initially described by Lehn in 1978, supramolecular chemistry was brilliantly defined as a ‘sort of molecular sociology’, in which non-covalent interactions and the individual properties of the molecules define the intermolecular bond.<sup>2</sup> This large branch of chemical research is hence devoted to the study of the complexity beyond individual molecules. The design of supramolecular structures started to gain more interest in the mid-1980s, following the crucial contribution of Lehn and co-workers in the field. Supramolecular self-assembly processes can be classified according to the main interactions involved, *viz.* hydrogen bonding, ion-ion, ion-dipole,  $\pi$ - $\pi$  stacking, cation- $\pi$ , van der Waals, or hydrophobic interactions, and also the strong and directional metal-ligand bonds.<sup>1</sup> The first artificial triple metallo-helical structure was described by Busch and co-workers in 1950.<sup>3</sup> However, Lehn was the first to propose the term ‘helicate’ for such assemblies. It can be pointed out here that potential applications of metallo-helicates as chemotherapeutics only emerged a few years ago.<sup>4-6</sup>

Vital biological processes, such as reproduction, signal transduction, biocatalysis, information storage and processing etc., are based on ‘simple’ self-assembly processes sustained by supramolecular interactions.<sup>7</sup> Thus, supramolecular frameworks like metallo-helicates may mimic biological structures, and therefore interfere with biological activities, for instance through recognition processes relying on the complementarity of noncovalent binding sites (hydrogen bonding and/or  $\pi$ - $\pi$  interactions).<sup>8</sup> It has been reported that metallo-helicates can mimic  $\alpha$ -helix protein motifs, owing to their similar size and shape.<sup>9,10</sup> Examples of supramolecular helical structures recognizing the major groove of DNA have been described in the literature.<sup>11-19</sup> It is well known that DNA recognition mostly occurs by interaction between the DNA major groove and specific protein-surface motifs like helix-turn-helix motifs, zinc fingers, zipper motifs,  $\beta$ -sheets and  $\beta$ -hairpins; hence, metallo-helicates may mimic such DNA-interacting systems. Therefore, specific gene expression may be controlled by developing supramolecular frameworks capable of mimicking either the structure or function of these biological DNA-binding molecules.<sup>20</sup>

Major-groove sequence recognition is an important aim in the field of anticancer drug design; as mentioned earlier, the major groove of DNA is one of the most important binding sites of proteins involved in either replication, transcription or recombination. Consequently,

molecules able to block natural recognition processes in the major groove will induce cell death.

Recognition in the major groove relies on specific H-bond donor and H-bond acceptor contacts to the edges of DNA base pairs, which makes them distinguishable from one another.<sup>21,22</sup> Thus, synthetic molecules should be perfectly designed to favour such supramolecular interactions and to have the perfect size to fit in the major groove but large enough to avoid minor-groove interaction.

Although such supramolecules show a real great potential in the area of anticancer drug design, their investigation is clearly marginal, most likely because it requires the design and synthesis of molecules with larger dimensions than the conventional ones.<sup>23</sup>

## ***Synthesis***

### ***Design of dinucleating organic ligands – Poly- $\beta$ -diketones***

The formation of metallo-supramolecular helicates is based on specific interactions between the organic ligands and the metal ions.<sup>24</sup> When coordinated to a metal centre, the ligand strands tend to create intramolecular attractive and/or repulsive interactions that lean towards helical conformations.<sup>25</sup> The organic ligands need to have several metal-binding domains along the strand, separated by spacers that will ensure the possible generation of helical arrays. These spacers should confer a sufficiently rigid environment to prevent the coordination of two binding units of the same ligand to the same metal ion, and, at the same time, flexible enough to wrap around the metal ions and produce a helical architecture. The folding is controlled by either the metal ion coordination or by other supramolecular interactions, such as hydrogen bonds or  $\pi$ -stacking contacts.<sup>25,26</sup> Metallo-helicates can be polymetallic double-, triple- or quadruple-stranded complexes. They are homostranded if the stands are equal and heterostranded if the strands are different.<sup>27</sup>

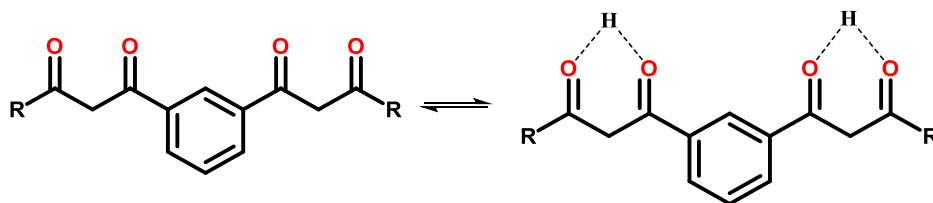
The design of the organic ligand is extremely important to achieve the desired helicity of the subsequent molecules. In the present study, the *Claisen condensation* between a ketone and an ester was used to produce a series of polydentate, dinucleating ligands. These poly- $\beta$ -diketones were prepared in a straightforward manner, through a one-step reaction from commercially-available reagents. Optimized reaction conditions have been applied, namely using strong bases such as sodium hydride or sodium amide, and solvents like 1,2-dimethoxyethane (DME).<sup>28</sup>





It can be stressed here that (poly-)β-diketones have been used extensively in coordination chemistry, generating elegant and extremely interesting families of supramolecular architectures, including homo- and heterometallic linear arrays, metallamacrocycles of different sizes, metallacoronates, triple-stranded helicates, or cage clusters of various nuclearities.<sup>28-33</sup> The outstanding flexibility and the concomitant straightforward synthesis of β-diketones promoted the appearance of numerous literature reports on coordination compounds based on them. Such elegant molecular architectures have found applications as light-emitting diodes, in quantum computing, as imaging agents, carriers, luminescent probes and sensors.<sup>34</sup>

Bis-β-diketones have two β-diketonato moieties separated by a spacer, which does not contain any additional donor groups, and that is connected at the position 1 or 2 of the β-diketone unit. In these systems, the two β-diketonate moieties can coordinate two metal ions, leading to dinuclear molecules. The two metal centres do not directly interact with each other, the only possible interaction being *via* the spacer group or through additional bridging ligands. The excellent binding properties of these chelating ligands is a consequence of their intrinsic chemical properties, determined by the keto-enol tautomerism (Scheme 8). Indeed, β-diketones possess an acidic proton and its removal gives rise to the formation of an efficient anionic ligand.



Scheme 8: Tautomerism of β-diketones.

During the past two decades, Hannon and co-workers have nicely shown that metallo-helicates based on nitrogen-containing ligands could efficiently stabilize specific DNA structures, namely DNA three-way junctions.<sup>9,18,35-39</sup> In the present investigation, new metallo-helicates were designed from oxygen-containing ligands, *viz.* from linear ligands containing two β-diketone units and H-donor or H-acceptor groups (Figure 57). The DNA-interacting and biological/cytotoxic properties of these supramolecular architectures were subsequently studied.

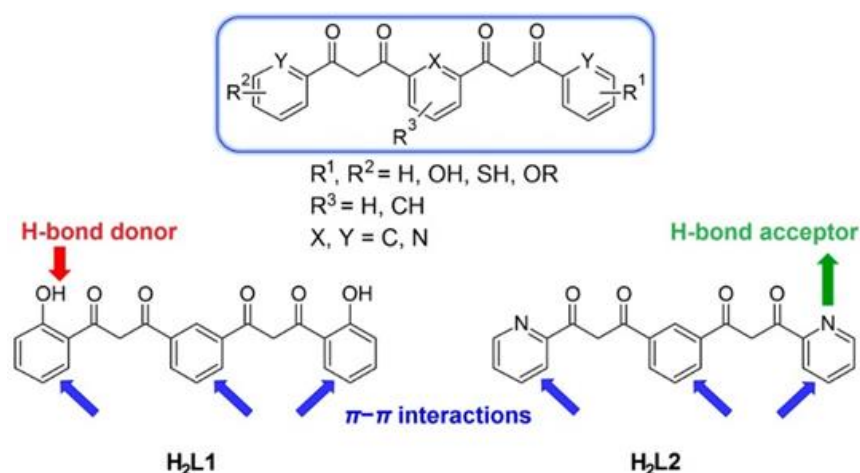
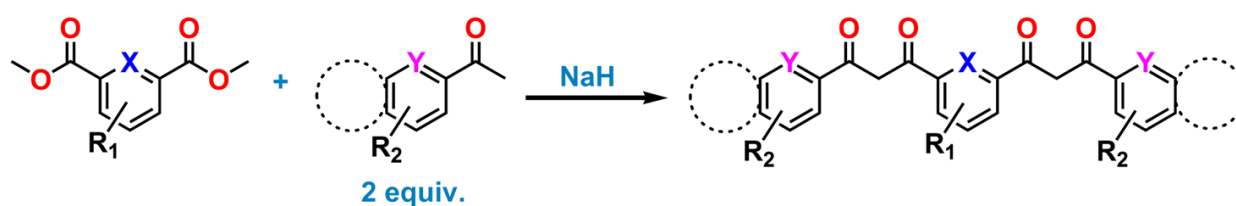


Figure S7: Illustration of the different bis- $\beta$ -diketones designed for the generation of metallo-helicates with distinct supramolecular properties.

Depending on the different functional groups introduced in the  $\beta$ -diketone ligands, distinct supramolecular properties can be achieved, which may give rise to different biological activities. For instance, ligand **H<sub>2</sub>L1** exhibits H-bond donor groups (phenol moieties) while ligand **H<sub>2</sub>L2** is an H-bond acceptor (pyridine rings). Furthermore, the position of the H-acceptor or H-donor group can be varied (see below); this allows to study the effect of the position of these groups on the DNA-interacting properties of the corresponding metallo-helicates.

The ligands were synthesized following the synthetic pathway depicted in Scheme 9. All ligands contain an aryl spacer, *viz.* a benzene ring, connected to two  $\beta$ -diketonate moieties including a naphthyl, phenolic, methoxyphenyl or pyridyl group.

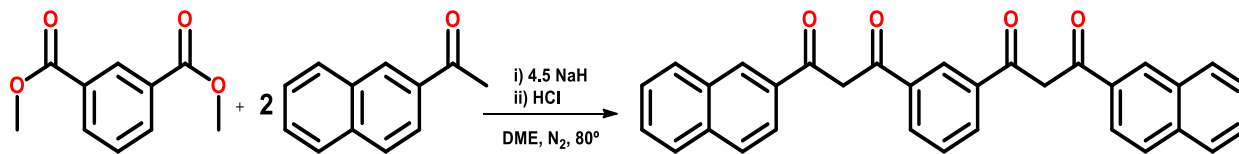


Scheme 9: Typical synthetic pathway for the preparation of bis- $\beta$ -diketone ligands. For example, **R1** and **R2** can be alkyl chains, aromatic groups, H-donor or H-acceptor units, charged moieties, etc. **X, Y** = carbon or nitrogen atom.



### Synthesis of 1,3-bis(3-oxo-3-(2-naphthyl)-propionyl)benzene (**H<sub>2</sub>L1**)

Ligand **H<sub>2</sub>L1** contains a benzyl spacer connecting two  $\beta$ -diketone units functionalized with naphthyl groups (Scheme 10). Hence, **H<sub>2</sub>L1** is hydrophobic and prompt to promote  $\pi$ - $\pi$  stacking interactions between its naphthyl units and nucleobases.



Scheme 10: Preparation of 1,3-bis(3-oxo-3-(2-naphthyl)-propionyl)benzene (**H<sub>2</sub>L1**).

**H<sub>2</sub>L1** is obtained by reaction of one equivalent of dimethyl isophthalate with two equivalents of 2-acetonaphthone, in the presence of 4.5 equivalents of sodium hydride used to generate the ketone enolate, which subsequently attacks the diester moiety (Scheme 3).

### Ligands with H-acceptor groups, *i.e.* with pyridinyl substituents

This series of ligands is characterized by a benzyl spacer and pyridine end groups, with various positions, *i.e.* ortho, meta, and para.

### Synthesis of 1,3-bis-(3-oxo-3-(2-pyridinyl)-propionyl)benzene (**H<sub>2</sub>L2**)

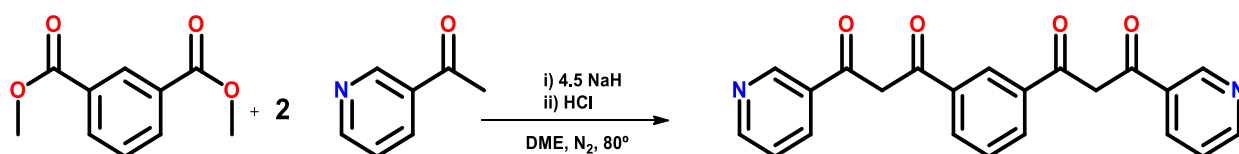
**H<sub>2</sub>L2** was synthesized by reaction of one equivalent of 1,3-diacetylbenzene with two equivalents of ethyl 2-picolinate, in the presence of 4.5 equivalents of sodium hydride in DME (Scheme 11).



Scheme 11: Preparation of 1,3-bis-(3-oxo-3-(2-pyridinyl)-propionyl)benzene (**H<sub>2</sub>L2**).

### Synthesis of 1,3-bis-(3-oxo-3-(3-pyridinyl)-propionyl)benzene (**H<sub>2</sub>L3**)

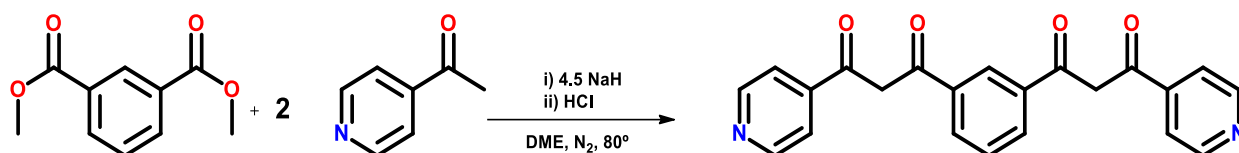
**H<sub>2</sub>L3** was obtained impure by the reaction of one equivalent of dimethyl isophthalate with two equivalents of 3-acetylpyridine, in the presence of 4.5 equivalents of sodium hydride in DME (Scheme 12).



Scheme 12: Preparation of 1,3-bis-(3-oxo-3-(3-pyridinyl)-propionyl)benzene (**H<sub>2</sub>L3**).

### Synthesis of 1,3-bis-(3-oxo-3-(4-pyridinyl)propionyl)benzene (**H<sub>2</sub>L4**)

This ligand was obtained impure using one equivalent of dimethyl isophthalate and two equivalents of 4-acetylpyridine, in the presence of 4.5 equivalents of sodium hydride in DME (Scheme 13).

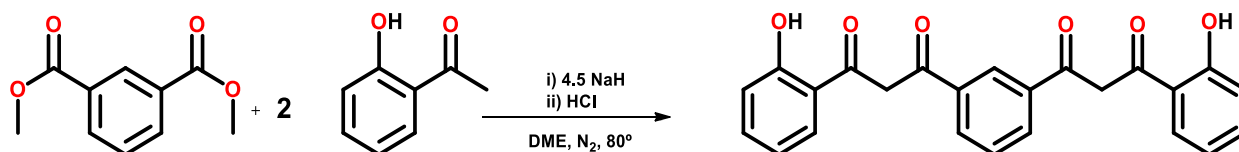


Scheme 13: Preparation of 1,3-bis-(3-oxo-3-(4-pyridinyl)propionyl)benzene (**H<sub>2</sub>L4**).

### Ligands with H-donor groups, *i.e.* hydroxyl substituents

The next series of bis- $\beta$ -diketone ligands is related to the previous one, the pyridine groups being replaced by phenol moieties. Consequently, this new series exhibits H-donor properties, in contrast with the previous ligands. Like for the pyridine-containing ligands (see above), the ortho, meta and para phenolic ligands were prepared.

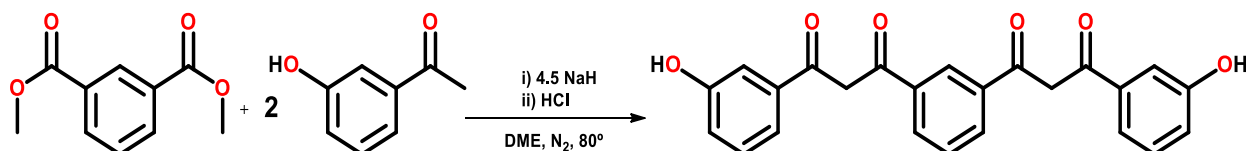
### Synthesis of 1,3-bis-(3-oxo-3(2-hydroxyphenyl)propionyl)benzene (**H<sub>4</sub>L5**)



Scheme 14: Preparation of 1,3-bis-(3-oxo-3(2-hydroxyphenyl)propionyl)benzene (**H<sub>4</sub>L5**).

The synthesis of this ligand has already been described in the literature.<sup>40</sup> Hence, **H<sub>4</sub>L5** was prepared by reaction of one equivalent of dimethyl isophthalate with two equivalents of 2'-hydroxyacetophenone, in the presence of 4.5 equivalents of sodium hydride in DME (Scheme 14).

### Synthesis of 1,3-bis-(3-oxo-3(3-hydroxyphenyl)propionyl)benzene (**H<sub>4</sub>L6**)

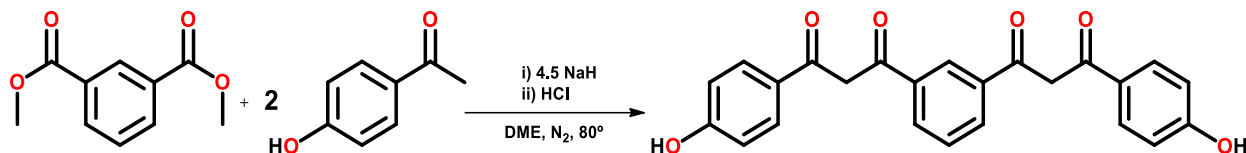


Scheme 15: Preparation of 1,3-bis-(3-oxo-3(3-hydroxyphenyl)propionyl)benzene (**H<sub>4</sub>L6**).



**H<sub>4</sub>L6** was synthesized by reaction of one equivalent of dimethyl isophthalate with two equivalents of 3'-hydroxyacetophenone, in the presence of 4.5 equivalents of sodium hydride in DME (Scheme 15).

#### Synthesis of 1,3-bis-(3-oxo-3(4-hydroxyphenyl)propionyl)benzene (**H<sub>4</sub>L7**)



Scheme 16: Preparation of 1,3-bis-(3-oxo-3(4-hydroxyphenyl)propionyl)benzene (**H<sub>4</sub>L7**).

Similarly, **H<sub>4</sub>L7** was obtained by reaction of one equivalent of dimethyl isophthalate with two equivalents of 4'-hydroxyacetophenone, in the presence of 4.5 equivalents of sodium hydride in DME (Scheme 16).

Lastly, two ligands (Figure 58) developed by the research group of Dr Guillem Aromí from the University of Barcelona<sup>29-31</sup> were included in the present study, because of their similarity with **H<sub>2</sub>L1–H<sub>4</sub>L7**.

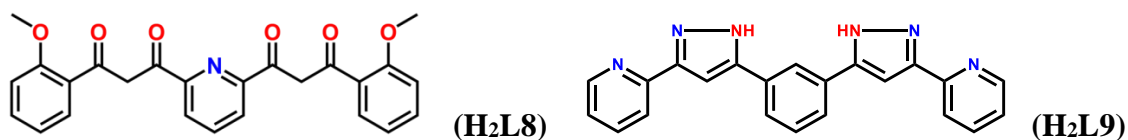


Figure 58: 1,3-Bis-(3-oxo-3(methoxyphenyl)propionyl)pyridine (**H<sub>2</sub>L8**) and 1,3-bis[1-(pyridine-2-yl)-pyrazol-3-yl]benzene (**H<sub>2</sub>L9**).

Ligand **H<sub>2</sub>L8** contain three H-acceptor groups provided by the central pyridine spacer and the external methoxyphenyl unit (Figure 58). Ligand **H<sub>2</sub>L9** is derived from a bis- $\beta$ -diketone; actually, it is obtained by one-pot reaction of ligand **H<sub>2</sub>L2** with hydrazine. As **H<sub>2</sub>L1–H<sub>4</sub>L7**, **H<sub>2</sub>L8** and **H<sub>2</sub>L9** were used to prepare metallo-helicates.

#### *General method for the preparation of the supramolecular complexes*

All bis- $\beta$ -diketones prepared were subsequently used to generate the metal complexes. Thus, reaction of three equivalents of each ligand with two equivalents of an iron(III) salt produced the corresponding neutral, triple-stranded metallo-helicates, as dark-red compounds. The reactions were carried out in the presence of  $\text{NaHCO}_3$ , required to deprotonate the O-donor ligands. Attempts to obtain single crystals of all metallo-helicates synthesized have only been

successful for three out of seven complexes. From these three compounds, two are new, *i.e.* those obtained from ligands **H<sub>2</sub>L1** and **H<sub>4</sub>L7**. The complex [Fe<sub>2</sub>(**L5**)<sub>3</sub>] has already been described in the literature.<sup>40</sup> X-ray diffraction studies of the new complexes revealed the expected triple-stranded helical structures, where two iron(III) ions are wrapped by three ligands, each metal centre being therefore coordinated by six oxygen atoms (Figure 59). The helical structure of [Fe<sub>2</sub>(**L1**)<sub>3</sub>] is shown in Figure 59 and Figure 60; crystallographic data and selected bond distances and angles are given in Table 21 and Table 22, respectively.

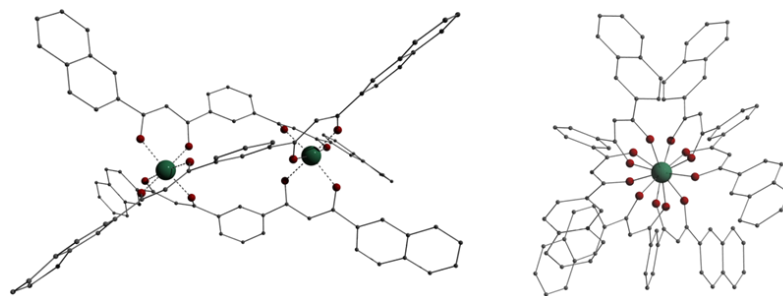


Figure 59: Representation of the crystal structure of Fe<sub>2</sub>(**L1**)<sub>3</sub>; left: front view and right: side view.

Table 21: Crystal data and structure refinement for [Fe<sub>2</sub>(**L1**)<sub>3</sub>]

Formula	C <sub>96</sub> H <sub>60</sub> Fe <sub>2</sub> O <sub>12</sub> , (C <sub>2</sub> H <sub>3</sub> N), 0.25(C <sub>4</sub> H <sub>8</sub> O)
Fw (g mol <sup>-1</sup> )	1576.22
Crystal system, space group	triclinic, <i>P</i> -1
a, b, c (Å)	15.300(2), 16.940(3), 17.496(3)
α, β, γ (°)	64.285(2), 72.373(2), 82.106(2)
V(Å <sup>3</sup> )	3893.6(11)
Z	2
μ (mm <sup>-1</sup> )	0.551
Temperature (K)	100
T <sub>min</sub> , T <sub>max</sub>	
No. f measured, independent and observed [I > 2σ(I)] reflections	
R[I > 2σ(I)], wR(I), S	
No. of parameters	

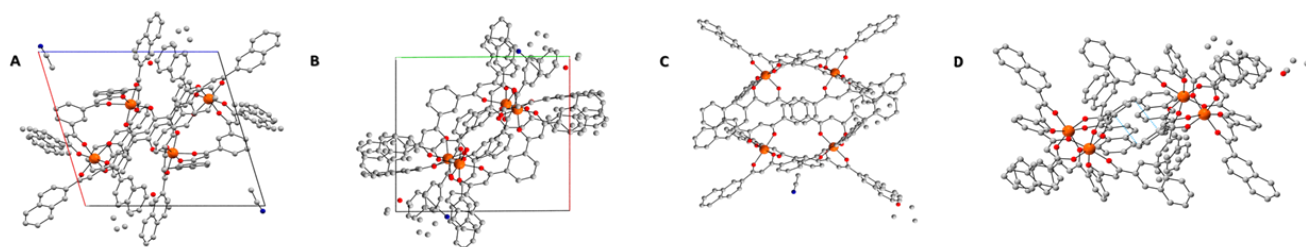
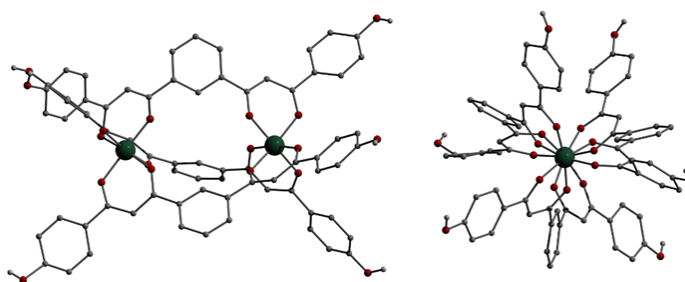
The X-ray structure of [Fe<sub>2</sub>(**H<sub>2</sub>L7**)<sub>3</sub>] shows a triple-stranded helicate structure (Figure 61). As previously, the two iron(III) ions are wrapped by three ligands, each metal centre being therefore coordinated by six oxygen atoms. The packing of [Fe<sub>2</sub>(**H<sub>2</sub>L7**)<sub>3</sub>] is illustrated in Figure 62. Crystallographic data and selected bond distances and angles are given in Table 23 and Table 24, respectively.

The coordination helicates whose DNA-interacting and cytotoxic/biological properties were investigated are listed in Figure 63. The metallo-helicates **H3–H6** and **H8** were provided by the group of Dr Guillem Aromí, from the University of Barcelona.



**Table 22: Coordination bond lengths (Å) and angles (°), and intermolecular contacts for [Fe<sub>2</sub>(L1)<sub>3</sub>]**

<i>Distances</i>					
Fe1 — O1	2.018(4)				
Fe1 — O2	2.000(4)				
Fe1 — O5	1.974(6)				
Fe1 — O6	2.001(4)				
Fe1 — O9	1.980(4)				
Fe1 — O10	1.966(6)				
Fe2 — O3	1.977(4)				
Fe2 — O4	1.988(5)				
Fe2 — O7	1.979(6)				
Fe2 — O8	1.978(4)				
Fe2 — O11	1.982(5)				
Fe2 — O12	1.970(6)				
<i>Angles</i>					
O1 — Fe1 — O2	85.6(2)	O3 — Fe2 — O4	87.0(2)	Fe1 — O1 — C11	129.7(5)
O1 — Fe1 — O5	87.4(2)	O3 — Fe2 — O7	85.4(2)	Fe1 — O2 — C13	131.6(5)
O1 — Fe1 — O6	166.1(2)	O3 — Fe2 — O8	169.7(2)	Fe2 — O3 — C20	127.6(5)
O1 — Fe1 — O9	94.3(2)	O3 — Fe2 — O11	88.7(2)	Fe2 — O4 — C22	128.2(5)
O1 — Fe1 — O10	99.3(2)	O3 — Fe2 — O12	98.5(2)	Fe1 — O5 — C43	130.4(5)
O2 — Fe1 — O5	97.5(2)	O4 — Fe2 — O7	95.8(2)	Fe1 — O6 — C45	127.9(4)
O2 — Fe1 — O6	83.6(2)	O4 — Fe2 — O8	87.6(2)	Fe2 — O7 — C52	130.0(5)
O2 — Fe1 — O9	173.8(2)	O4 — Fe2 — O11	174.7(2)	Fe2 — O8 — C54	131.9(6)
O2 — Fe1 — O10	87.9(2)	O4 — Fe2 — O12	90.7(2)	Fe1 — O9 — C75	130.5(5)
O5 — Fe1 — O6	85.4(2)	O7 — Fe2 — O8	86.5(2)	Fe1 — O10 — C77	129.3(4)
O5 — Fe1 — O9	88.6(2)	O7 — Fe2 — O11	86.9(2)	Fe2 — O11 — C84	130.1(5)
O5 — Fe1 — O10	171.7(2)	O7 — Fe2 — O12	172.6(2)	Fe2 — O12 — C86	130.9(5)
O6 — Fe1 — O9	97.4(2)	O8 — Fe2 — O11	97.1(2)		
O6 — Fe1 — O10	89.0(2)	O8 — Fe2 — O12	90.3(2)		
O9 — Fe1 — O10	86.0(2)	O11 — Fe2 — O12	86.9(2)		

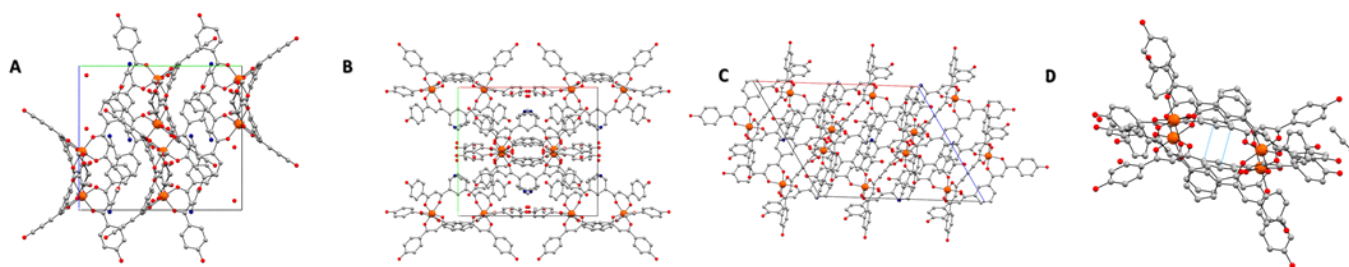
**Figure 60: Illustrations of the solid-state packing of [Fe<sub>2</sub>(L1)<sub>3</sub>].****Figure 61: Representation of the crystal structure of [Fe<sub>2</sub>(H<sub>2</sub>L7)<sub>3</sub>]; left: front view and right: side view.**

Formula	C <sub>72</sub> H <sub>48</sub> Fe <sub>2</sub> O <sub>18</sub> , 2(C <sub>2</sub> H <sub>3</sub> N), 2(H <sub>2</sub> O)
$\nu$ (g mol <sup>-1</sup> )	1430.94
Crystal system, space group	monoclinic, C2/c
a, b, c (Å)	23.016(4), 17.915(3), 18.590(6)
$\beta$ , $\gamma$ (°)	90, 121.900(2), 90
V (Å <sup>3</sup> )	6508(3)
Z	4
$\rho$ (mm <sup>-1</sup> )	0.551
Temperature (K)	100
$\lambda$ , $T_{\max}$	0.658, 0.747
No. of measured, independent and observed [ $I > 2\sigma(I)$ ] reflections	
[ $I > 2\sigma(I)$ ], $wR(I)$ , $S$	
No. of parameters	

Distances	
FE1 — O2	1.9702
FE1 — O3	1.9667
FE1 — O8	2.0101
FE1 — O9	1.9731
FE1 — O4	2.0209
FE1 — O5	2.0061
O4 — FE1	2.0209
O5 — FE1	2.0061
O8 — FE1	2.0101
O9 — C33	1.2776
O9 — FE1	1.9731

ngles							
O2	- O3	86.85	FE1 - O2 - C7	131.7	O8 - FE1 - O9	86.56	
O2 — FE1 — O8	88.31	FE1 — O3 — C9	130.27	O8 — FE1 — O2	88.31		
O2 — FE1 — O9	171.6	C16 — O4 — FE1	127.98	O8 — FE1 — O3	97.84		
O2 — FE1 — O4	99.89	C18 — O5 — FE1	128.95	O9 — FE1 — O2	171.6		
O2 — FE1 — O5	86.59	H7 — O7 — C25	109.09	O9 — FE1 — O3	87.27		
O3 — FE1 — O8	97.84	FE1 — O8 — C31	128.12	O2 — FE1 — O3	86.85		
O3 — FE1 — O9	87.27	FE1 — O9 — C33	127.51	H1 — O1 — C1	117.19		
O3 — FE1 — O4	86.85	O4 — FE1 — O5	84.94	FE1 — O2 — C7	131.7		
O3 — FE1 — O5	168.46	O4 — FE1 — O8	170.8	FE1 — O3 — C9	130.27		
O8 — FE1 — O9	86.56	O4 — FE1 — O9	85.76	FE1 — O4 — C16	127.98		
O8 — FE1 — O4	170.8	O4 — FE1 — O2	99.89	FE1 — O5 — C18	128.95		
O8 — FE1 — O5	91.45	O4 — FE1 — O3	86.85				
O9 — FE1 — O4	85.76	O5 — FE1 — O8	91.45				
O9 — FE1 — O5	100.18	O5 — FE1 — O9	100.18				
O4 — FE1 — O5	84.94	O5 — FE1 — O2	86.59				
H1 — O1 — C1	117.19	O5 — FE1 — O3	168.46				



118



Ligand	Metallo-Helicate
<b>H<sub>4</sub>L5</b>	[Fe <sub>2</sub> (L5) <sub>3</sub> ] (H1)
<b>H<sub>2</sub>L1</b>	[Fe <sub>2</sub> (L1) <sub>3</sub> ] (H2)
<b>H<sub>4</sub>L7</b>	[Fe <sub>2</sub> (H <sub>2</sub> L7) <sub>3</sub> ] (H6)
<b>H<sub>2</sub>L8</b>	[Fe <sub>2</sub> (L8) <sub>3</sub> ]KFeCl <sub>4</sub> (H3) [Fe <sub>2</sub> (L8) <sub>3</sub> ]NaClO <sub>4</sub> (H4) [Fe <sub>2</sub> (L8) <sub>3</sub> ]NaFeCl <sub>4</sub> (H5) [Fe <sub>2</sub> (L8) <sub>3</sub> ]KClO <sub>4</sub> (H6)
<b>H<sub>2</sub>L9</b>	[Fe <sub>2</sub> (L9) <sub>3</sub> ]Cl <sub>2</sub> (PF <sub>6</sub> ) <sub>2</sub> (H8)

Figure 63: Metallo-helicates with their respective labelling code that were used for the biological studies.

### DNA-binding studies

The interaction of some metallo-helicates with DNA has been described in the literature,<sup>3,41-44</sup> and it is believed that such compounds may allow to control and/or inhibit gene expression and important cellular processes. This type of molecules may thus act as efficient cytotoxic agents and find potential applications against cancer. The interaction of metallo-helicates **H1**–**H8** with DNA has been investigated using various complementary techniques.

### UV-Vis Spectroscopy

UV-Vis spectroscopy is an effective tool for the quantification of the binding strength of metal complexes to DNA.<sup>45</sup> In the present study, titration experiments were carried out to compare quantitatively the binding strength of the metallo-helicates. The potential binding of complexes **H1**–**H3**, **H6** and **H8** to *calf thymus* DNA (ct-DNA) was investigated, recording absorption spectra at a constant complex concentration, *i.e.* 15 μM, in the absence and presence of increasing amounts of ct-DNA (*i.e.* 0–25 μM). The spectra obtained for metallo-helicate **H1** are shown in Figure 64, which are representative of the other compounds (see Experimental section; Figure 95). For most helicates, the spectroscopic data could be fitted to equation (1), and the intrinsic binding constants  $K_b$  could be determined.<sup>46,47</sup> As explained in previous chapters,  $K_b$  is obtained from the ratio of the slope to the intercept.

$$\frac{[DNA]}{(\epsilon_a - \epsilon_f)} = \frac{[DNA]}{(\epsilon_b - \epsilon_f)} + \frac{1}{K_b(\epsilon_b - \epsilon_f)} \quad (1)$$

The results obtained for helicates **H1–H3**, **H6** and **H8** are summarized in Table 25.

**Table 25:** Intrinsic binding constants  $K_b$  determined for complexes **H1–H3**, **H6** and **H8**.

Complex	$K_b^{[a]}$ ( $10^5 \text{ M}^{-1}$ )	Log $K_b$
<b>H1</b>	$0.12 \pm 0.07$	4.09
<b>H2</b>	$1.13 \pm 0.13$	5.05
<b>H3</b>	$7.06 \pm 0.25$	5.85
<b>H6</b>	$1.65 \pm 0.25$	5.22
<b>H8</b>	$15.3 \pm 0.77$	6.18

<sup>[a]</sup> The uncertainties were determined from measurements in triplicate.

A linear fit of the absorption data to equation (1) could not be achieved for complexes **H4** and **H5**. Most likely, these compounds require longer incubation times with DNA. All experiments (*viz.* for all metallo-helicates) were however performed with the same incubation time of five minutes between each measurement.

All complexes show specific absorption bands, particularly around the region 275–450 nm. These bands correspond to  $\pi$ – $\pi^*$  transitions of the ligands (below 350 nm), and to metal-to-ligand charge transfer (MLCT) transitions in the range 350–450 nm. The latter ones were used to analyse the respective binding affinities of the metal complexes. Most spectroscopic data reveal an hypochromic effect without red shift, which is indicative of electrostatic interactions or groove binding.<sup>48</sup> For **H1**, a slight red shift is associated to the hypochromism (Figure 64), which suggests that this compound interacts through ligand intercalation.<sup>49,50</sup> In general, the data collected indicate that **H1–H3**, **H6** and **H8** act as DNA-groove binders.<sup>51</sup>

The helical complexes can be classified into three groups. The first group is composed of **H4** and **H5** that clearly interact with DNA, but for which the  $K_b$  values could not be determined. **H1**, **H2** and **H6** constitute the second group, which shows low binding constants, *i.e.*  $K_b$  varies from 0.1 to  $1.7 \times 10^5 \text{ M}^{-1}$ . The final group includes **H3** and **H8** that exhibit higher binding affinities than those of the helicates from the second group, as reflected by the respective  $K_b$  values of  $7 \times 10^5$  and  $15 \times 10^5 \text{ M}^{-1}$ .



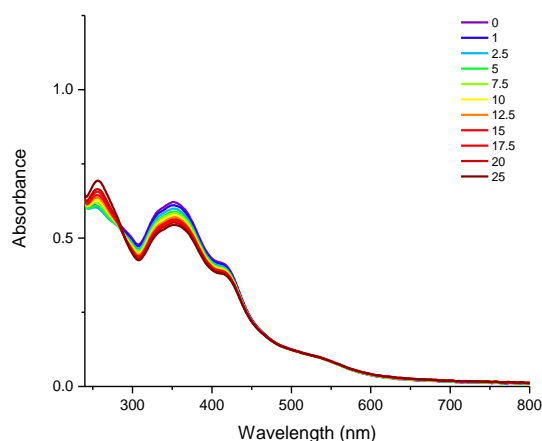


**Figure 64:** Absorption spectra of H1 in 10 mM sodium cacodylate, NaCl buffer upon addition of ct-DNA (0–22.5  $\mu\text{M}$ ). The inset shows an enlargement of the region 300–500 nm corresponding to metal-to-ligand charge-transfer (MLCT) transitions. The [ct-DNA] in base pairs was determined from its absorption intensity at 260 nm with a molar extinction coefficient of  $6600 \text{ M}^{-1}\text{cm}^{-1}$ .

Comparison of the  $K_b$  constants of the metallo-helicates with that of the efficient major-groove binder methyl green, which is around  $10^6 \text{ M}^{-1}$ ,<sup>52</sup> shows that **H8** may behave as this molecule. Comparing further the binding constants of the metallo-helicates with those of the minor groove binders Hoechst 33258 and DAPI, which are respectively around  $10^8$  and  $10^6$ ,<sup>53–56</sup> confirm that they interact in the DNA grooves; however, additional studies are necessary to verify whether they are more specific to the major groove or to the minor one.

#### *Fluorescence-dye displacement*

DNA intercalation and groove binding can be investigated using fluorescence spectroscopy. A specific dye, like for instance a minor groove binder or a DNA intercalator, can be used to assess the ability of a molecule to interact with DNA; this can be achieved by determining its aptitude to displace the dye, through the alterations of the dye fluorescence intensity. In the present study, ethidium bromide (EB) and Hoechst 33258 were used as *displaceable* dye.

EB is a DNA-intercalating agent that fluoresces when bound to the polynucleotide molecule. Its fluorescence intensity increases 20-fold when intercalated between DNA base pairs.<sup>57,58</sup> It should be stressed here that EB displacement by a molecule does not necessarily imply that it acts as an intercalator (like EB). In fact, electrostatic interactions or groove binding may be sufficient to alter significantly the conformation of the DNA double helix, inducing the release of EB.<sup>59,60</sup>

Fluorescence spectra were recorded at constant concentrations of ct-DNA and EB (*i.e.* 25 and 125  $\mu\text{M}$ , respectively), in the presence of increasing amounts of the complex

investigated. Representative emission spectra for EB in the presence of increasing quantities of **H1** are shown in Figure 65.

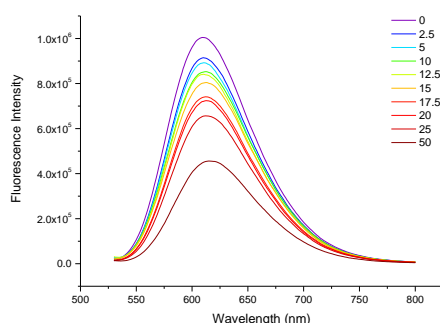


**Figure 65:** Emission spectra of the DNA–EB complex (obtained using [DNA] and [EB] of 25 and 125 μM, respectively) in 10 mM sodium cacodylate, 20 mM NaCl,  $\lambda_{\text{exc}} = 514$  nm,  $\lambda_{\text{em}} = 610$  nm, upon addition of increasing amounts of **H1** (2.5–50 μM).

In all cases, a clear and significant decrease in EB emission intensity was noticed, thus confirming the occurrence of strong interactions between the metallo-helicates and ct-DNA. To quantify the respective affinity of the different complexes for ct-DNA (compared to EB), their “quenching” efficiency was evaluated using the classical Stern-Volmer equation (2), which allows to determine the quenching constant,  $K_{\text{SV}}$ , by plotting  $I_0/I$  versus [complex].<sup>61</sup>

$$I_0/I = 1 + K_{\text{SV}}[\text{Q}] \quad (2)$$

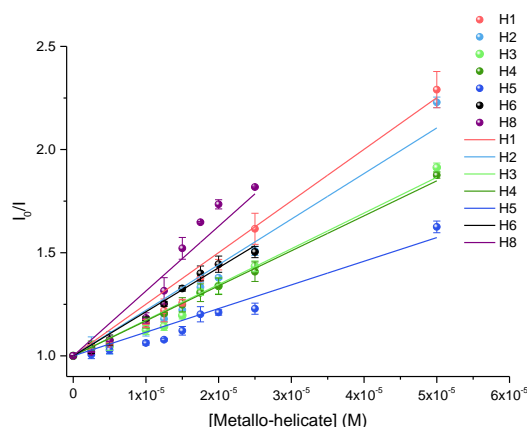


**Figure 66:** Plots of  $I_0/I$  vs. [complex] for the titration of DNA–EB with complexes **H1**–**H6** and **H8**, in 10 mM sodium cacodylate, 20 mM NaCl,  $\lambda_{\text{em}} = 610$  nm. Experimental data points and linear fitting of the data. [Metallo-helicates]: 0–50 μM; [DNA]: 25 μM; [EB]: 125 μM.

The  $K_{\text{SV}}$  value of **H7** could not be determined. For **H1**–**H6** and **H8**, the  $K_{\text{SV}}$  constants vary from  $1 \times 10^4$  to  $3 \times 10^4 \text{ M}^{-1}$  (see Figure 66 and Table 26), thus revealing a high aptitude of the complexes to displace EB. As already noticed by UV-Vis studies (see above), **H8** exhibits the strongest DNA interaction, as evidenced by its  $K_{\text{SV}}$  value.





Most likely, these large molecules interact with DNA through electrostatic contacts or/and groove binding,<sup>62-65</sup> which are sufficient to induce a strong alteration of the biomolecule structure, resulting in the release of EB. The higher effect induced by **H8** may be due to its pyrazole units (see Figure 63). Indeed, it has been reported that pyrrole groups can selectively target AT-rich regions of DNA, this recognition process being driven by hydrogen bonds, van der Waal contacts, and electrostatic interactions.<sup>66,67</sup> Thus, it is well possible that the N–H moieties of the pyrazole groups of the ligand **L9** in **H8** play a similar role, generating hydrogen bonds and van der Waal surface contacts, possibly in AT-rich regions within the DNA minor groove.

**Table 26:** Stern-Volmer constants  $K_{sv}$  determined for complexes **H1–H6** and **H8** using EB as dye.

Complex	$K_{sv}^{[a]} (10^5 \text{ M}^{-1})$		
<b>H1</b>	2.50	±	0.066
<b>H2</b>	2.21	±	0.12
<b>H3</b>	1.73	±	0.058
<b>H4</b>	1.70	±	0.019
<b>H5</b>	1.15	±	0.055
<b>H6</b>	2.14	±	0.051
<b>H8</b>	3.14	±	0.21

<sup>[a]</sup> The uncertainties were determined from measurements in triplicate.

Competitive binding studies were also performed with the minor-groove binder Hoechst 33258. This fluorescent dye has a high specificity for AT-rich sequences. Bound to ct-DNA, Hoechst 33258 fluoresces at  $\lambda_{em} = 458$  nm when excited at  $\lambda_{exc} = 349$  nm (for free Hoechst 33258,  $\lambda_{exc} = 337$  and  $\lambda_{em} = 508$  nm). The  $K_{SV}$  constants obtained for **H1–H6** with this dye vary from 1.50 to  $29.13 \times 10^4 \text{ M}^{-1}$  (see Table 27). The  $K_{SV}$  values for **H7** and **H8** could not be determined.

The data achieved show that **H1–H6** are all able to displace Hoechst 33258. Complexes **H2**, **H3** and **H6** exhibit the strongest DNA affinities (Table 27). The naphthyl groups of ligand **L2** in **H2** may be involved in stacking interactions in the minor groove.<sup>68-71</sup> The stronger DNA interaction of **H3** and **H6**, compared with that of the related compounds **H4** and **H5** (see Figure 63 and Table 27), may arise from the  $K^+$  ions; indeed, it is known that  $K^+$  has a higher propensity to bind in the minor groove of the DNA than  $Na^+$ .<sup>72</sup> This would explain the lower ability of **H4** and **H5**, which contain  $Na^+$  ions instead of  $K^+$  ones, for the DNA minor groove.

**Table 27:** Stern-Volmer constants  $K_{sv}$  determined for complexes **H1**–**H6** using Hoechst 33258 as fluorescent dye.

Complex	$K_{sv}^{[a]} (10^4 \text{ M}^{-1})$
<b>H1</b>	5.66 ± 0.28
<b>H2</b>	19.33 ± 1.25
<b>H3</b>	24.81 ± 2.38
<b>H4</b>	4.72 ± 0.71
<b>H5</b>	1.50 ± 0.16
<b>H6</b>	29.13 ± 1.44

<sup>[a]</sup> The uncertainties were determined from measurements in triplicate.

### *Circular Dichroism*

Circular dichroism (CD) spectroscopy is a very sensitive technique that can be used to detect changes occurring in the secondary structure of biomolecules (such as DNA) interacting with molecules.<sup>73,74</sup> Hence, it has extensively been used to analyse changes in the DNA backbone induced by the binding of a drug. Indeed, non-covalent DNA–drug interactions may affect the DNA structure, resulting in alterations of the CD signals.<sup>75</sup>

The CD spectrum of native ct-DNA has two major bands, one around 277 nm (positive), and another around 243 nm (negative). The positive band is due to base stacking, while helicity is responsible for the negative band; the value observed at 243 nm for ct-DNA is characteristic of a right-handed B form.<sup>76–79</sup> Both bands are extremely sensitive towards the interaction of small molecules with DNA.<sup>80,81</sup>

The CD spectra obtained for the interaction of metallo-helicates **H1**–**H6** with ct-DNA are displayed in Figure 11. Electrostatic interactions or minor-groove binding do not significantly alter the typical CD spectrum of ct-DNA, and this is observed with **H1**. DNA intercalation gives rise to significant CD spectral changes, both the positive and negative bands being altered. As evidenced in Figure 11, complexes **H1**–**H6** affect the two bands, thus suggesting that they may act as intercalators, in addition to groove binding (deduced from UV-Vis and fluorescence spectroscopy; see above). Finally, **H4** appears to strongly affect the helicity of the biomolecules, as revealed by the clear change of the negative part of the CD signal at a ratio of 1:2 (Figure 67).



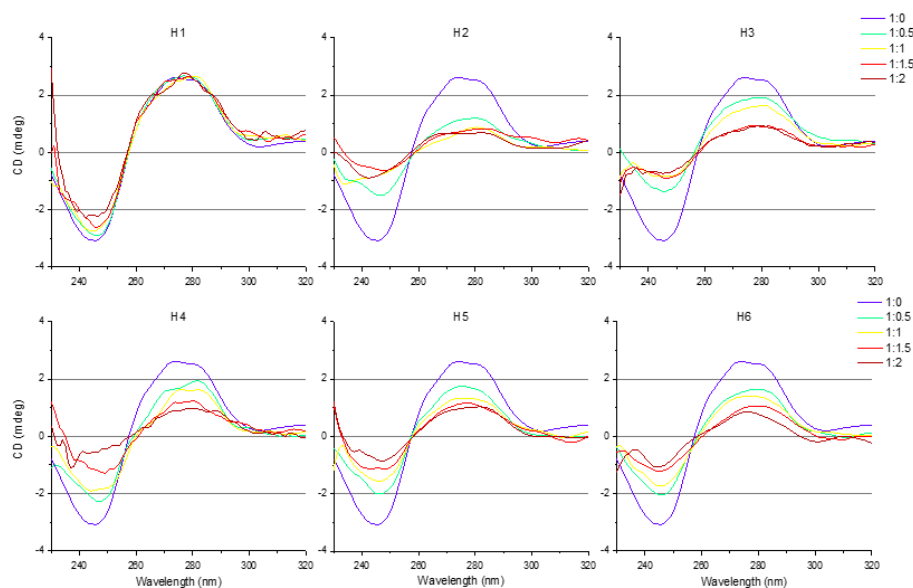


**Figure 67:** CD spectra of ct-DNA (2.5  $\mu\text{M}$ ) in 10 mM sodium cacodylate, 20 mM NaCl, upon addition of increasing amounts of metallo-helicates H1–H6 (12.5–100  $\mu\text{M}$ ).

In summary, ct-DNA maintains its B-conformation upon interaction with **H1–H6**. However, noticeable changes in the intensity of the CD signals take place when the concentration of the complexes is increased, which indicates that the secondary structure of DNA is perturbed by the interaction with the helicate.

### *Agarose-gel electrophoresis*

Agarose-gel electrophoresis is a simple technique that is commonly used to analyse biomolecules such as DNA, RNA and proteins, based on their size, charge or conformation.<sup>82</sup> This analytical method is usually carried out with pBR322 plasmid DNA, which is a double-stranded circular DNA that can be found in bacteria.

Herein, agarose-gel electrophoresis was essentially used to determine the ability of the metallo-helicates to unwind supercoiled plasmid DNA. For comparison purposes, gels were also performed with two well-known groove binders, namely methyl green and Hoechst 33258 (Figure 68). Increasing amounts of the different helicates (from 5 to 100  $\mu\text{M}$ ) were incubated with plasmid DNA for 24 hours, and subsequently electrophorized. The corresponding gel images obtained are shown in Figure 69.

Two different patterns are observed with the known groove binders (Figure 69). With the minor-groove binder Hoechst 33258, a progressive vanishing of the bands corresponding to DNA forms I and II is noticed when its concentration is increased (Figure 68, left). In the case of the major-groove binder methyl green, its interaction with DNA does not seem to affect

these bands, whose intensities are not altered with the increase of the dye concentration (Figure 68, right).

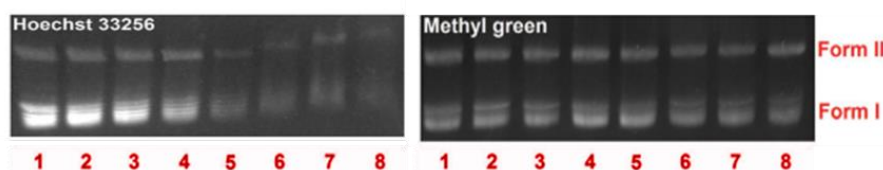


Figure 68: Agarose-gel electrophoresis images of pBR322 plasmid DNA incubated for 24 h at 37 °C with increasing concentrations of Hoechst 33258 (left) and methyl green (right). Hoechst 33258, lane 1: pure plasmid DNA; lane 2: [Hoechst] = 5  $\mu$ M; lane 3: [Hoechst] = 10  $\mu$ M; lane 4: [Hoechst] = 20  $\mu$ M; lane 5: [Hoechst] = 40  $\mu$ M; lane 6: [Hoechst] = 60  $\mu$ M; lane 7: [Hoechst] = 80  $\mu$ M; lane 8: [Hoechst] = 100  $\mu$ M. Methyl green, lane 1: pure plasmid DNA; lane 2: [methyl green] = 30  $\mu$ M; lane 3: [methyl green] = 60  $\mu$ M; lane 4: [methyl green] = 100  $\mu$ M; lane 5: [methyl green] = 150  $\mu$ M; lane 6: [methyl green] = 200  $\mu$ M; lane 7: [methyl green] = 300  $\mu$ M; lane 8: [methyl green] = 400  $\mu$ M. Each sample contains 200 ng of plasmid DNA.

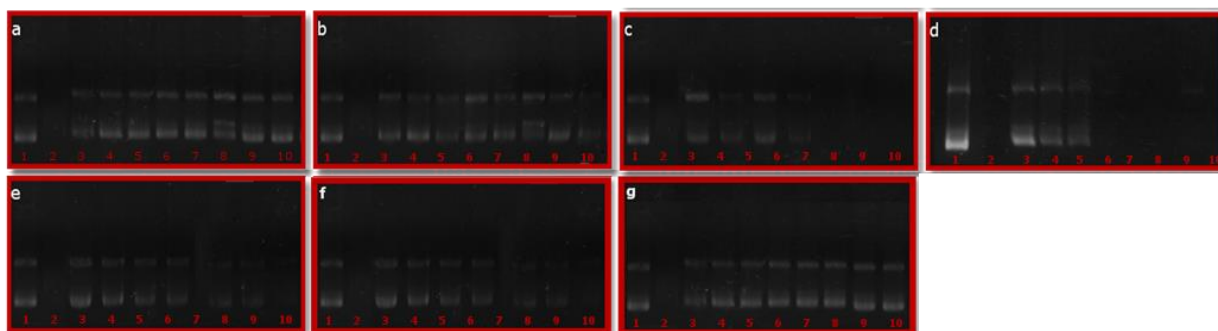


Figure 69: Agarose-gel electrophoresis images of pBR322 plasmid DNA incubated for 24 h at 37 °C with increasing concentrations of complexes H1–H6 and H8 (a to g, respectively). Lane 1: pure plasmid DNA; lane 2: [Hoechst] = 100  $\mu$ M; lane 3: [Methyl Green] = 100  $\mu$ M; lane 4: [complex] = 5  $\mu$ M; lane 5: [complex] = 10  $\mu$ M; lane 6: [complex] = 20  $\mu$ M; lane 7: [complex] = 40  $\mu$ M; lane 8: [complex] = 60  $\mu$ M; lane 9: [complex] = 80  $\mu$ M; lane 10: [complex] = 100  $\mu$ M. Each sample contains 200 ng of plasmid DNA.

The behaviour exhibited by Hoechst 33258 resembles that of complexes **H3–H6** (Figure 68-left and Figure 69c-f), suggesting that these helicates are acting as DNA minor-groove binders. On the other hand, compounds **H1**, **H2** and **H8** (Figure 69a,b,g) may interact with the major groove of the DNA double helix, since the corresponding gel data are comparable to those obtained with methyl green (Figure 68-right).

### *Polyacrylamide-gel electrophoresis – DNA three-way junction binding*

Gel-mobility-shift (gel-shift) assays are used to analyse the interaction between DNA and proteins or supramolecular drugs. Such assays can provide valuable information about the type of interactions, and allow to determine association, dissociation and affinity constants.<sup>83,84</sup>

DNA junctions play an important role in many biological processes; for instance, they have a key role as intermediates in homologous recombination. It is known that three-way





junctions (3WJs) are the simplest and most prevalent junctions, which are formed by three double-helical strands connected at the junction point. Helical junctions represent important nucleic acid structures in biology; in DNA, they act as intermediates in both homologous and site-specific recombination events (in the replication fork).<sup>85,86</sup> In RNA, 3WJs are important architectural elements that are essentially involved in splicing and translation.<sup>41,87-92</sup>

Hannon and co-workers described the first metallo-helicate (subsequently labelled **MH**, Figure 70) capable of binding to the major groove of DNA and of inducing intramolecular DNA coiling. Furthermore, it was observed that these structures were also able to stabilize DNA-3WJs. The positively charged helical molecule described by Hannon and co-workers, *i.e.* **MH**, interacts with the negatively charged sugar-phosphate backbone of the DNA *via* electrostatic interactions, and can stabilize a 3WJ through non-covalent interactions. It was shown that the phenyl rings of **MH** form  $\pi$ - $\pi$  stacking interactions with bases (adenine and the thymine) of the DNA strands forming the 3WJ.<sup>6,93-95</sup> It should be pointed out here that the stabilization of these structures can result in the interruption of the replication process, resulting in cell death.

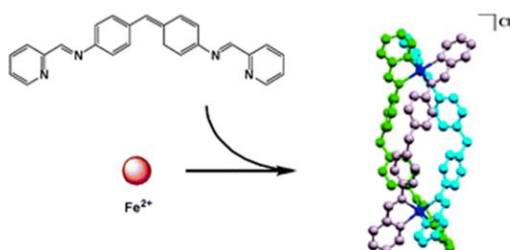


**Figure 70: Molecular structure of the tetracationic triple helical supramolecular helicate **MH**.**<sup>94</sup>

Iron(III) supramolecular structures, such as **MH**, having the right dimensions to fit in the hydrophobic cavity generated by the formation of a DNA 3WJ from complementary oligonucleotides may promote a shift in the mobility of the isolated oligonucleotides. Hence, the observation of such an effect may actually indicate the complex-driven formation and stabilization of a 3WJ. The ability of the metallo-helicates **H1–H8** to promote the formation of a 3WJ and stabilize it was evaluated by polyacrylamide gel electrophoresis technique (PAGE). This type of gel technique is used to analyse short DNA sequences. As explained in the experimental section, each complementary oligonucleotide strand was modified with a different fluorescent label (experimental section and Figure 70), thus allowing a very simple visualization of the gel. This new (unprecedented) procedure allows to perform faster, safer and more accurate experiments, compared with the radio-labelling method commonly described in literature.<sup>36</sup> Using this technique, in the absence of **MH** (lane 1 in Figure 70b),

The new PAGE procedure was subsequently used with metallo-helicates **H1–H8**, using **MH** as the reference compound (since it has been proven that it stabilizes 3WJs). The corresponding results obtained are shown in Figure 72. As expected, the reference compound **MH** is able to induce the formation of a 3WJ and stabilize it, as evidenced by the apparition of a new band in the gel (Figure 72a, lane 2 and Figure 72b, lane 2). Unfortunately, metallo-helicates **H1–H8** do not promote the formation of the 3WJ. This may be explained by electrostatic considerations; in order to self-assemble into a stabilized 3WJ, the four partners, *i.e.* the three complementary oligonucleotides and the metallo-helicate, should “find” each other in a highly-diluted solution. Thus, it is clear that electrostatic attraction between a positively charged metallo-helicate and the negatively charged oligonucleotide strands will favour the generation of the 3WJ. Tetracationic **MH** nicely promotes and stabilizes the 3WJ. However, the neutral metallo-helicates **H1–H7** (see Figure 72) clearly are not capable of inducing the formation of the 3WJ. This hypothesis was confirmed with consequent studies carried out by other members of the research group, using different (but related) highly charged metallo-helicates. Surprisingly, tetracationic **H8** (Figure 7) is also not able to form and stabilize

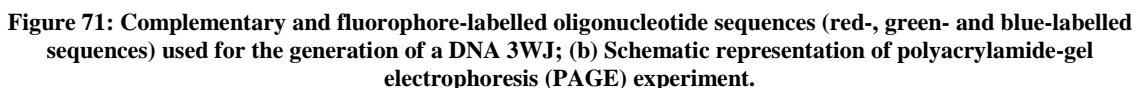


**Figure 71: Complementary and fluorophore-labelled oligonucleotide sequences (red-, green- and blue-labelled sequences) used for the generation of a DNA 3WJ; (b) Schematic representation of polyacrylamide-gel electrophoresis (PAGE) experiment.**

The new PAGE procedure was subsequently used with metallo-helicates **H1–H8**, using **MH** as the reference compound (since it has been proven that it stabilizes 3WJs). The corresponding results obtained are shown in Figure 72. As expected, the reference compound **MH** is able to induce the formation of a 3WJ and stabilize it, as evidenced by the apparition of a new band in the gel (Figure 72a, lane 2 and Figure 72b, lane 2). Unfortunately, metallo-helicates **H1–H8** do not promote the formation of the 3WJ. This may be explained by electrostatic considerations; in order to self-assemble into a stabilized 3WJ, the four partners, *i.e.* the three complementary oligonucleotides and the metallo-helicate, should “find” each other in a highly-diluted solution. Thus, it is clear that electrostatic attraction between a positively charged metallo-helicate and the negatively charged oligonucleotide strands will favour the generation of the 3WJ. Tetracationic **MH** nicely promotes and stabilizes the 3WJ. However, the neutral metallo-helicates **H1–H7** (see Figure 72) clearly are not capable of inducing the formation of the 3WJ. This hypothesis was confirmed with consequent studies carried out by other members of the research group, using different (but related) highly charged metallo-helicates. Surprisingly, tetracationic **H8** (Figure 7) is also not able to form and stabilize



the 3WJ. Since the structure of **H8** significantly differs from those of **MH** and **H1–H7**, a different cause should be found to explain its “non-activity”; in-depth studies are definitively required to better understand this behaviour.

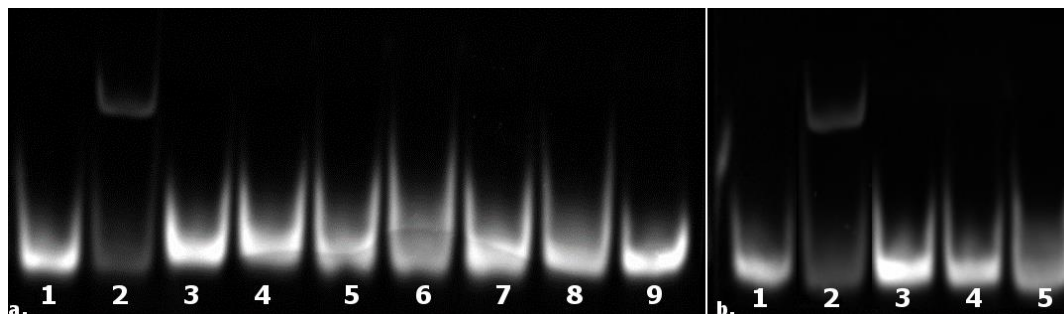


**Figure 72:** PAGE image of the complementary oligonucleotides incubated for 1 h at 37 °C, followed by incubation on ice for 15 minutes. The samples were analyzed by 15% polyacrylamide-gel electrophoresis for 1.50 hours at 6 V cm<sup>-1</sup> at room temperature. The incubation was made using constant concentration of metallo-helicate. a. Lane 1: Pure oligonucleotides; lane 2: MH; lane 3: Oligonucleotides with MgCl<sub>2</sub>; lane 4: H1; lane 5: H2; lane 6: H3; lane 7: H4; lane 8: H5; lane 9: H6; b. Lane 1: Pure oligonucleotides; lane 2: MH; lane 3: Oligonucleotides with MgCl<sub>2</sub>; lane 4: H7; lane 5: H8. Each sample contains a constant concentration of DNA and complex, in a [Metallo-helicate]:[DNA] ratio of 3:1.

### *AFM experiments*

Atomic force microscopy (AFM) is a powerful technique, which is becoming an essential tool for the visualization of biological interactions, as the result of its high resolution associated with simple sample preparation. Thus, this technique is ideally suited to the investigation of DNA structure and dynamics.<sup>96</sup> For instance, AFM allows to observe DNA-structural changes induced by its interaction with metal complexes. Hence, the interaction of **H1–H6** with pBR322 plasmid DNA has been investigated by AFM (Figure 73), using experimental conditions comparable to those applied for the agarose-gel electrophoresis studies, for a direct comparison of the results.

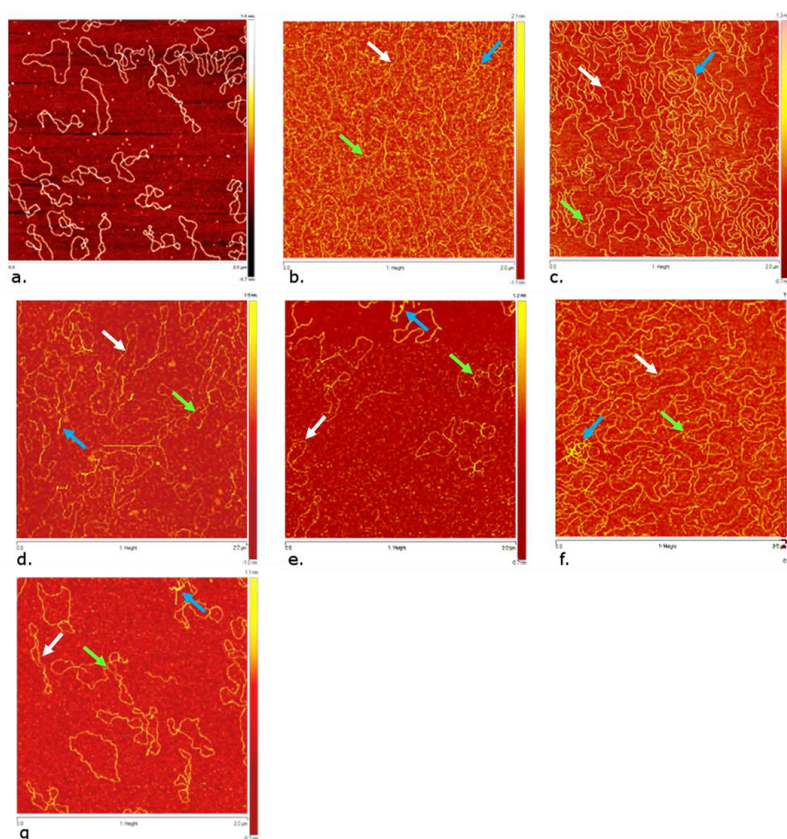


**Figure 73:** AFM images of (a) free pBR322 plasmid DNA; (b) plasmid DNA + H1 60  $\mu\text{M}$ ; (c) plasmid DNA + H2 60  $\mu\text{M}$ ; (d) plasmid DNA + H3 20  $\mu\text{M}$ ; (e) plasmid DNA + H4 60  $\mu\text{M}$ ; (f) plasmid DNA + H5 60  $\mu\text{M}$ ; (g) plasmid DNA + H6 60  $\mu\text{M}$ . Each sample contains 200 ng of DNA. The white arrows show supercoiling, the green arrows indicate crossing points, and the blue arrows show the initial formation of DNA globular aggregates.

As aforementioned (see electrophoresis section), plasmid DNA is formed by open circular structures and supercoiled structures; this morphological mixture is clearly seen in Figure 16a. Incubation of the plasmid DNA with compounds **H1–H6** obviously induces some morphological changes (see Figure 73b–g). All the metallo-helicates can promote intramolecular DNA (super)coiling (see white arrows in Figure 16), which corroborate results achieved by UV-Vis and fluorescence spectroscopy and gel electrophoresis (see above). This complex-induced supercoiling of DNA further generates crossing points between strands (green arrows), and the formation of DNA-complex aggregates (blue arrows) is detected, which is indicative of a strong interaction between the biomolecule and the metal-based compounds.





### Cell-viability assays

The cellular toxicity of the compounds was then examined using various *in-vitro* biological assays (see experimental section), the objective being to evaluate their possible use for the subsequent development of potential of anticancer agents.<sup>97</sup>

### Single-point assays

The cytotoxicity of **H1–H8** towards various cell lines was screened by means of single-point assays. For these assays, two complex concentrations, namely 10 and 50  $\mu\text{M}$ , were used with six cancer cell lines, *i.e.* A549 (lung adenocarcinoma), A375 (melanoma), MCF-7 (breast adenocarcinoma), SKOV3 (ovary adenocarcinoma), SW620 (colorectal adenocarcinoma) and PC3 (prostate adenocarcinoma). The cell viabilities were determined for each complex, after an incubation of 24 hours at 37 °C. The results obtained are shown in Figure 74, and listed in Table 28 and Table 29, for [metallo-helicate] = 10 and 50  $\mu\text{M}$ , respectively.

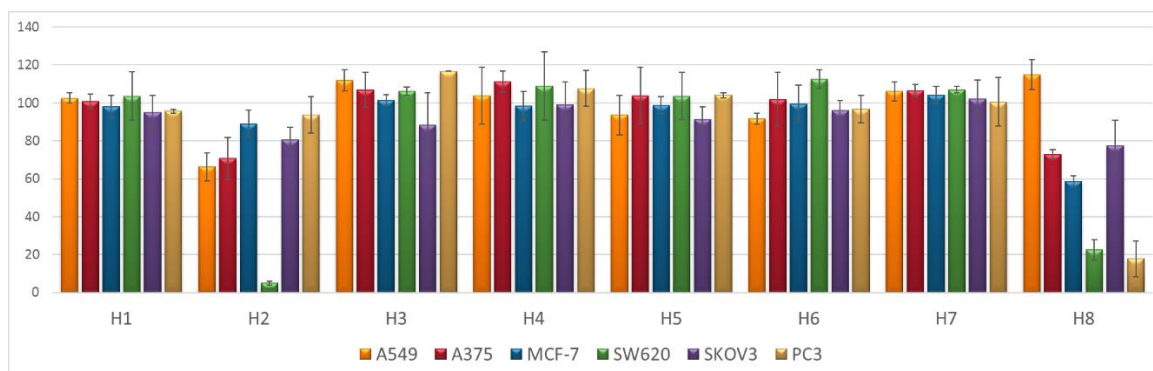


**Figure 74:** Cell-viability results for **H1–H8** with different cancer cell lines, namely A549 (lung adenocarcinoma), A375 (melanoma), MCF-7 (breast adenocarcinoma), PC3 (prostate adenocarcinoma), SKOV3 (ovary adenocarcinoma) and SW620 (colorectal adenocarcinoma). [Compound] = 10  $\mu\text{M}$ ; incubation time = 24 h. The results are means  $\pm$  SD of three separate experiments.

Surprisingly, **H1–H8** are mostly non-cytotoxic in the selected cell lines (Figure 74), contrasting their interesting DNA-interacting properties (see above). Nevertheless, the good activity of **H2** against SW620 cells (colorectal adenocarcinoma) should be stressed, so as that of **H8** against both SW620 and PC3 (prostate adenocarcinoma) cells.

The general lack of cytotoxicity exhibited by the metallo-helicates may be a consequence of their poor water solubility or of their non-aptitude to enter the cells. Thus, further studies would be required to increase their hydrophilicity and/or to develop carriers that would favour their cell internalization, which allow them to reach the nucleus.

**Table 28:** Cell-viability assays (single-point screening, % cell viability) for **H1–H8** with different cancer-cell lines, namely **A549** (lung adenocarcinoma), **A375** (melanoma), **MCF-7** (breast adenocarcinoma), **SKOV3** (ovary adenocarcinoma), **SW620** (colorectal adenocarcinoma) and **PC3** (prostate adenocarcinoma). Pre-set [complex] = 10  $\mu\text{M}$  (single-point assay); incubation time = 24 h. The data shown are means  $\pm$  SD of three independent experiments.

Cell-lines	Metallo-Helicate							
	H1	H2	H3	H4	H5	H6	H7	H8
A549	103 $\pm$ 2.76	66.3 $\pm$ 7.30	112 $\pm$ 5.66	104 $\pm$ 15	93.6 $\pm$ 11	91.7 $\pm$ 2.98	106 $\pm$ 5.15	115 $\pm$ 7.92
A375	101 $\pm$ 3.96	70.7 $\pm$ 11.0	107 $\pm$ 9.26	111 $\pm$ 5.5	104 $\pm$ 15	102 $\pm$ 14.2	107 $\pm$ 3.18	72.9 $\pm$ 2.46
MCF-7	98.1 $\pm$ 5.91	89.2 $\pm$ 7.19	101 $\pm$ 2.87	98.3 $\pm$ 7.8	98.6 $\pm$ 4.6	99.5 $\pm$ 9.76	104 $\pm$ 4.57	58.8 $\pm$ 2.86
SW620	104 $\pm$ 12.7	5.07 $\pm$ 0.97	106 $\pm$ 2.27	109 $\pm$ 18	104 $\pm$ 12	113 $\pm$ 4.83	107 $\pm$ 1.76	22.5 $\pm$ 5.34
SKOV3	95.1 $\pm$ 9.00	80.7 $\pm$ 6.53	88.4 $\pm$ 17.0	99.1 $\pm$ 12	91.4 $\pm$ 6.4	95.9 $\pm$ 5.53	102 $\pm$ 9.81	77.6 $\pm$ 13.3
PC3	95.6 $\pm$ 0.99	93.7 $\pm$ 9.45	117 $\pm$ 0.04	108 $\pm$ 9.4	104 $\pm$ 1.3	96.8 $\pm$ 7.31	101 $\pm$ 12.7	17.8 $\pm$ 9.45

**Table 29:** Cell-viability assays (single-point screening, % cell viability) for **H1–H8** with different cancer-cell lines, namely **A549** (lung adenocarcinoma), **A375** (melanoma), **MCF-7** (breast adenocarcinoma), **SKOV3** (ovary adenocarcinoma), **SW620** (colorectal adenocarcinoma) and **PC3** (prostate adenocarcinoma). Pre-set [complex] = 50  $\mu\text{M}$  (single-point assay); incubation time = 24 h.

Cell-lines	Metallo-Helicate							
	H1	H2	H3	H4	H5	H6	H7	H8
A549	97.9 $\pm$ 9.60	57.5 $\pm$ 5.96	117 $\pm$ 14.0	97.1 $\pm$ 6.48	89.2 $\pm$ 6.6	95.2 $\pm$ 11.18	92.1 $\pm$ 11.7	113 $\pm$ 7.92
A375	96.2 $\pm$ 6.82	50.1 $\pm$ 7.15	79.2 $\pm$ 9.38	110 $\pm$ 9.62	111 $\pm$ 5.5	106 $\pm$ 9.12	106 $\pm$ 8.88	31.1 $\pm$ 4.31
MCF-7	94.9 $\pm$ 6.61	84.2 $\pm$ 4.14	108 $\pm$ 5.76	100 $\pm$ 7.35	84.9 $\pm$ 12.0	98.2 $\pm$ 8.02	80.9 $\pm$ 12.2	34.3 $\pm$ 4.06
SW620	111 $\pm$ 9.70	5.28 $\pm$ 1.05	118 $\pm$ 1.65	118 $\pm$ 6.54	116 $\pm$ 12.0	128 $\pm$ 7.82	95.6 $\pm$ 18.0	9.6 $\pm$ 0.57
SKOV3	92.0 $\pm$ 5.20	61.9 $\pm$ 7.99	93.6 $\pm$ 19.0	98.5 $\pm$ 1.99	96.9 $\pm$ 3.62	99.0 $\pm$ 4.52	101 $\pm$ 5.77	47.4 $\pm$ 6.19
PC3	93.3 $\pm$ 0.78	93.7 $\pm$ 9.45	104 $\pm$ 18.5	104 $\pm$ 8.57	102 $\pm$ 23.5	106 $\pm$ 25.7	84.9 $\pm$ 26.5	15.1 $\pm$ 5.86

### MTT Reduction Assay

Considering the results achieved with the single-point assays (Figure 74, and listed in Table 28 and Table 29), the  $\text{IC}_{50}$  values were solely determined for **H2** and **H8** in the SW620 cell line, colorectal cancer being the third most commonly diagnosed cancer in male patients and the second one in female patients. The  $\text{IC}_{25-75}$  data obtained for these two complexes and two reference compounds, *i.e.* cisplatin and the metallo-helicate **MH**, after 24 h incubation, are listed in Table 30.

**Table 30:**  $\text{IC}_{25-75}$  values ( $\mu\text{M}$ ) of SW620 (colorectal adenocarcinoma), after 24 h of incubation. The data shown are means  $\pm$  SD of three independent experiments.

	SW620			
	H2 ( $\mu\text{M}$ )		H8 ( $\mu\text{M}$ )	cisPt ( $\mu\text{M}$ )
$\text{IC}_{25}$	4.4	$\pm$ 0.7	2.9	$\pm$ 0.8
$\text{IC}_{50}$	9.4	$\pm$ 1.4	11.0	$\pm$ 1.5
$\text{IC}_{75}$	23.0	$\pm$ 1.6	41.0	$\pm$ 5.3

Interestingly, **H2** and **H8** present lower  $\text{IC}_{50}$  values than the reference compounds (Table 30). Subsequently, the mechanism of cell death induced by **H2** and **H8** was somewhat investigated in some detail using fluorescence techniques.





### *Fluorescence spectroscopy assays*

Apoptosis is a highly regulated biological event and represents a vital process aimed at regulating crucial cellular activities involved in tissue growth, normal cell turnover, immune response, and tissue development (which are notable events when considering cancer). Several fluorescence techniques are used to study apoptosis. For instance, flow cytometry or confocal microscopy are very useful analytical means to investigate cell-death mechanism(s).<sup>98-101</sup>

### **Immunofluorescence**

An immunofluorescence assay was performed to assess the effect of **H2** and **H8** on SW620 cells, and particularly to check whether these compounds could trigger apoptosis. To this end, the nuclei were stained with a fluorescent dye allowing the detection of any detect cellular anomalies, like the formation/presence of apoptotic bodies or the deformation of the nuclei. The fluorescence microscopy images taken after 48 h incubation of the cells with the complexes are shown in Figure 75.

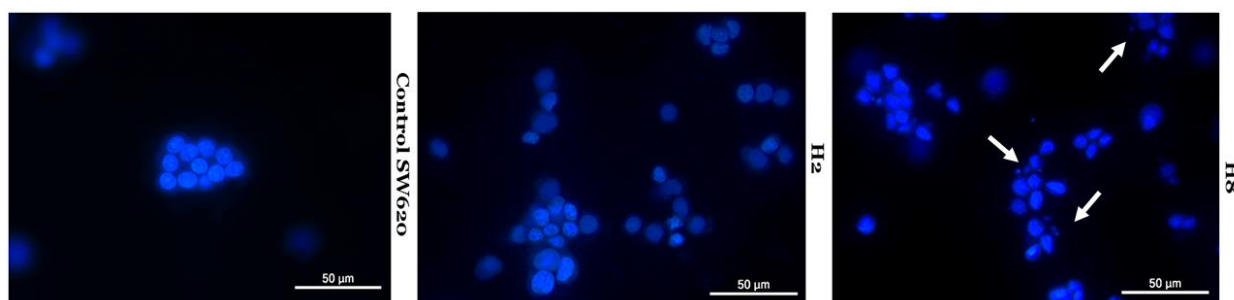


**Figure 75:** Fluorescence microscopy images showing SW620 cells incubated with the metallo-helicates **H2** and **H8**. [Compound] =  $1C_{25}$  (see Table 10); incubation time = 48 h. The nucleus was stained with TO-PRO™-3 (blue). Scale bar = 50  $\mu$ m. Images are representative of at least three independent experiments.

**H2** does not seem to significantly affect the nuclei of the SW620 cells (Figure 75, middle); therefore, more studies are required to determine the exact mechanism of **H2**-induced cell death. However, a very careful analysis of the images indicates that this complex may be able to somewhat disturb the cells nuclei, as it appears that, in some cases, swallowing is taking place. On the other hand, for **H8**, apoptotic bodies are clearly seen (white arrows).

### **Cell cycle**

To further analyse the previous results and verify whether **H2** and **H8** can effectively interact with DNA or/and affect any process related to cell growth and division, cell-cycle experiments were conducted. The cell cycle represents one of the most significant and fundamental processes in eukaryotic cells, which results in cell growth and division into two daughter cells.<sup>102</sup> The regulation of the cell cycle is critical to cell survival and defects in its

regulation is a common characteristic of tumour cells. The analysis of cell cycle has become increasingly important for both understanding the action of anti-cancer compounds and for studying mechanisms of cell division.<sup>103</sup> Such analysis allows to rapidly obtain quantitative information regarding the amounts (percentages) of cells in the G0/G1, S and G2/M phases of the cell cycle. Thus, SW620 cell suspensions were used in the presence of **H2** or **H8**, and the cell cycles were analysed. The results obtained are summarized in Figure 76.

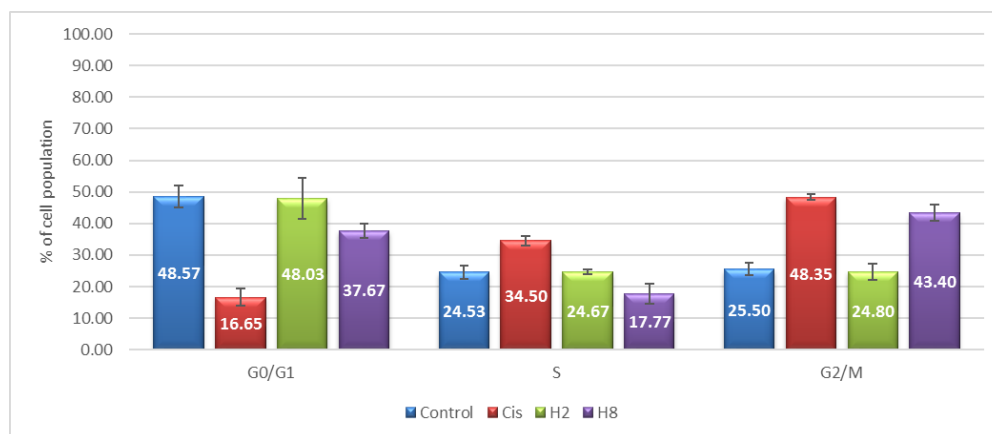


**Figure 76:** Cell-cycle experiments performed with the Muse™ Cell Cycle software for **H2** and **H8** with SW620 cells.  $2 \times 10^5$  cells mL<sup>-1</sup>; [compound] = 2  $\mu$ M; incubation time = 24 h. The results are representative of at least three independent experiments.

As already observed by fluorescence microscopy, **H2** does not significantly affect SW620 cells, as the cell cycle is not altered (green bars in Figure 76, which are comparable to those of the control, *i.e.* the blue bars). On the contrary, **H8** has a clear impact on the cell cycle, as it can stop the cycle in the G2/M phase (see purple bars in Figure 76), similarly to cisplatin (red bars in Figure 76). The G<sub>2</sub> phase corresponds to the moment when the cell division starts, and the G<sub>2</sub>/M phase marks the entrance of the cells into the M phase (mitosis); this G<sub>2</sub>/M phase has been associated with the resistance of tumour cells to chemotherapy. Upon G<sub>2</sub>/M arrest, the expression of some essential processes involved in the mitosis are altered, which cause an incomplete mitosis and mitotic catastrophe, leading to cell death.<sup>104</sup>





### Conclusions

Seven bis- $\beta$ -diketone ligands (**H<sub>2</sub>L1–H<sub>2</sub>L7**) containing various functional groups, such as H-bond donor or H-bond acceptor units, were prepared and fully characterized. These ligands were designed to generate metallo-helicates upon coordination with iron(III) ions, such supramolecular complexes being known to bind in the major groove of DNA or/and stabilize particular DNA structures, like three-way junctions (3WJs). Such DNA targets being relevant for the development of potential anticancer agents, attempts to obtain metallo-helicates from the new dinucleating O-donor ligands were made, which led to the generation of a series of helical compounds that were structurally characterized (by means of X-ray diffraction studies).

Subsequently, the DNA-interacting properties of eight new metallo-helicates (**H1–H8**) were evaluated using complementary analytical techniques. DNA binding studies revealed that all the complexes could interact and disturb the structure of the biomolecule, mostly through groove binding. It has also been shown that these strong interactions could induce intramolecular DNA coiling. From the series, **H8** has provided the most interesting results, its distinct behaviour most likely being due to its different structure (compared with those of **H1–H7**). Unfortunately, **H1–H8** are not capable of stabilizing 3WJs; however, a new and very simple procedure has been developed for the detection of 3WJs. Contrary to the commonly used method that involves  $^{32}\text{P}$ -labelled nucleotides, this unprecedented new procedure is performed with fluorophore-tagged oligonucleotides, and can therefore be applied in any lab, with no need to take particular safety precautions.

The cytotoxic properties of metallo-helicates **H1–H8** were then assessed by means of single-point assays and determining their  $\text{IC}_{25-75}$  values for different cancer cell lines. These studies revealed the great cytotoxic potential of two of these metal-based compounds, namely **H2** and **H8**, which exhibited lower  $\text{IC}_{50}$  values (against SW620 cells) than cisplatin and the metallo-helicate, *i.e.* **MH**, described by Hannon and co-workers. Preliminary fluorescence microscopy and cell-cycle studies revealed that **H8** can reach the nuclei and arrest the cell cycle at the G2/M phase, hence triggering apoptosis. Further in-depth studies are required to confirm these remarkable results achieved with **H8**, with the objective to better understand how such compounds are acting inside the cells. For instance, the observed cytotoxicity of **H2** against SW620 cells does not appear to be due to its interaction with DNA (as it does not affect the cell cycle); additional studies must be performed to unveil the cell-death mechanism(s) for this compound.

Finally, since all compounds prepared exhibited poor water solubility (which an important drawback considering their potential use for biological applications), ways to

increase their solubility in aqueous media should be investigated; for instance, the development of supramolecular nanocarriers (*e.g.* micelles) for the delivery of such compounds in the cells, allowing them to reach the nuclei, would definitely be an asset.





## References

- (1) Chakrabarty, R.; Mukherjee, P. S.; Stang, P. J. *Chem. Rev.* **2011**, *111*, 6810.
- (2) Lehn, J. M. *Supramolecular chemistry : concepts and perspectives*; VCH: Weinheim; New York, 1995.
- (3) Hannon, M. J.; Childs, L. J. *Supramol. Chem.* **2004**, *16*, 7.
- (4) Lehn, J. M.; Rigault, A.; Siegel, J.; Harrowfield, J.; Chevrier, B.; Moras, D. *Proc. Natl. Acad. Sci. U S A* **1987**, *84*, 2565.
- (5) Schoentjes, B.; Lehn, J.-M. *Helv. Chim. Acta* **1995**, *78*, 1.
- (6) J. Hannon, M.; L. Painting, C.; Jackson, A.; Hamblin, J.; Errington, W. *Chem. Commun.* **1997**, 1807.
- (7) Albrecht, M. *Naturwissenschaften* **2007**, *94*, 951.
- (8) Greig, L. M.; Philp, D. *Chem. Soc. Rev.* **2001**, *30*, 287.
- (9) Hannon, M. J. *Chem. Soc. Rev.* **2007**, *36*, 280.
- (10) Hannon, M. J.; Moreno, V.; Prieto, M. J.; Moldrheim, E.; Sletten, E.; Meistermann, I.; Isaac, C. J.; Sanders, K. J.; Rodger, A. *Angew. Chem. Int. Ed. Engl.* **2001**, *40*, 879.
- (11) Cerasino, L.; Hannon, M. J.; Sletten, E. *Inorg. Chem.* **2007**, *46*, 6245.
- (12) Ducani, C.; Leczkowska, A.; Hodges, N. J.; Hannon, M. J. *Angew. Chem. Int. Ed. Engl.* **2010**, *49*, 8942.
- (13) Hamblin, J.; Tuna, F.; Bunce, S.; Childs, L. J.; Jackson, A.; Errington, W.; Alcock, N. W.; Nierengarten, H.; Van Dorsselaer, A.; Leize-Wagner, E.; Hannon, M. J. *Chem. Eur. J.* **2007**, *13*, 9286.
- (14) Hotze, A. C.; Hodges, N. J.; Hayden, R. E.; Sanchez-Cano, C.; Paines, C.; Male, N.; Tse, M. K.; Bunce, C. M.; Chipman, J. K.; Hannon, M. J. *Chem. Biol.* **2008**, *15*, 1258.
- (15) Hotze, A. C.; Kariuki, B. M.; Hannon, M. J. *Angew. Chem. Int. Ed. Engl.* **2006**, *45*, 4839.
- (16) Khalid, S.; Hannon, M. J.; Rodger, A.; Rodger, P. M. *Chem. Eur. J.* **2006**, *12*, 3493.
- (17) Khalid, S.; Hannon, M. J.; Rodger, A.; Rodger, P. M. *J. Mol. Graph. Model.* **2007**, *25*, 794.
- (18) Malina, J.; Hannon, M. J.; Brabec, V. *Nucleic Acids Res.* **2008**, *36*, 3630.
- (19) Uerpmann, C.; Malina, J.; Pascu, M.; Clarkson, G. J.; Moreno, V.; Rodger, A.; Grandas, A.; Hannon, M. J. *Chem. Eur. J.* **2005**, *11*, 1750.
- (20) Cardo, L.; Hannon, M. J. *Inorg. Chim. Acta* **2009**, *362*, 784.
- (21) Lusby, P. J. *Annu. Rep. Prog. Chem., Sect A: Inorg. Chem.* **2010**, *106*, 319.
- (22) Hamilton, P. L.; Arya, D. P. *Nat. Prod. Rep.* **2012**, *29*, 134.
- (23) Childs, L. J.; Malina, J.; Rolfsnes, B. E.; Pascu, M.; Prieto, M. J.; Broome, M. J.; Rodger, P. M.; Sletten, E.; Moreno, V.; Rodger, A.; Hannon, M. J. *Chem. Eur. J.* **2006**, *12*, 4919.
- (24) Piguet, C.; Bernardinelli, G.; Hopfgartner, G. *Chem. Rev.* **1997**, *97*, 2005.
- (25) Berl, V.; Huc, I.; Khoury, R. G.; Lehn, J.-M. *Chem. Eur. J.* **2001**, *7*, 2798.
- (26) Geib, S. J.; Vicent, C.; Fan, E.; Hamilton, A. D. *Angew. Chem., Int. Ed.* **1993**, *32*, 119.
- (27) Hannon, M. J.; Childs, L. J. *Supramol. Chem.* **2004**, *16*, 7.
- (28) Aromí, G.; Gamez, P.; Reedijk, J. *Coord. Chem. Rev.* **2008**, *252*, 964.

- (29) Aromi, G.; Aguila, D.; Gamez, P.; Luis, F.; Roubeau, O. *Chem. Soc. Rev.* **2012**, *41*, 537.
- (30) Aromi, G.; Boldron, C.; Gamez, P.; Roubeau, O.; Kooijman, H.; Spek, A. L.; Stoeckli-Evans, H.; Ribas, J.; Reedijk, J. *Dalton Trans.* **2004**, 3586.
- (31) Darawsheh, M.; Barrios, L. A.; Roubeau, O.; Teat, S. J.; Aromi, G. *Chem. Eur. J.* **2016**, *22*, 8635.
- (32) Gamez, P.; Costa, J. S.; Quesada, M.; Aromi, G. *Dalton Trans.* **2009**, 7845.
- (33) Gonzalez-Fabra, J.; Bandeira, N. A.; Velasco, V.; Barrios, L. A.; Aguila, D.; Teat, S. J.; Roubeau, O.; Bo, C.; Aromi, G. *Chem. Eur. J.* **2017**.
- (34) Vigato, P. A.; Peruzzo, V.; Tamburini, S. *Coord. Chem. Rev.* **2009**, *253*, 1099.
- (35) Cardo, L.; Sadovnikova, V.; Phongtongpasuk, S.; Hodges, N. J.; Hannon, M. J. *Chem. Commun. (Camb)* **2011**, *47*, 6575.
- (36) Malina, J.; Hannon, M. J.; Brabec, V. *Chem. Eur. J.* **2007**, *13*, 3871.
- (37) Malina, J.; Hannon, M. J.; Brabec, V. *Chem. Eur. J.* **2008**, *14*, 10408.
- (38) Malina, J.; Hannon, M. J.; Brabec, V. *Chem. Eur. J.* **2015**, *21*, 11189.
- (39) Meistermann, I.; Moreno, V.; Prieto, M. J.; Moldrheim, E.; Sletten, E.; Khalid, S.; Rodger, P. M.; Peberdy, J. C.; Isaac, C. J.; Rodger, A.; Hannon, M. J. *Proc Natl Acad Sci U S A* **2002**, *99*, 5069.
- (40) Aromi, G.; Boldron, C.; Gamez, P.; Roubeau, O.; Kooijman, H.; Spek, A. L.; Stoeckli-Evans, H.; Ribas, J.; Reedijk, J. *Dalton Trans.* **2004**, 3586.
- (41) Muhuri, S.; Mimura, K.; Miyoshi, D.; Sugimoto, N. *J. Am. Chem. Soc.* **2009**, *131*, 9268.
- (42) Arya, D. P. *Acc. Chem. Res.* **2011**, *44*, 134.
- (43) Malina, J.; Scott, P.; Brabec, V. *Dalton Trans.* **2015**, *44*, 14656.
- (44) Malina, J.; Scott, P.; Brabec, V. *Nucleic Acids Res.* **2015**, *43*, 5297.
- (45) Javed, F.; Altaf, A. A.; Badshah, A.; Tahir, M. N.; Siddiq, M.; Shah, A.; Ullah, S.; Lal, B. *J. Coord. Chem.* **2012**, *65*, 969.
- (46) Krishnamoorthy, P.; Sathyadevi, P.; Cowley, A. H.; Butorac, R. R.; Dharmaraj, N. *Eur. J. Med. Chem.* **2011**, *46*, 3376.
- (47) Pyle, A. M.; Rehmann, J. P.; Meshoyrer, R.; Kumar, C. V.; Turro, N. J.; Barton, J. K. *J. Am. Chem. Soc.* **1989**, *111*, 3051.
- (48) Asadi, M.; Safaei, E.; Ranjbar, B.; Hasani, L. *New J. Chem.* **2004**, *28*, 1227.
- (49) Kumar, C. V.; Asuncion, E. H. *J. Am. Chem. Soc.* **1993**, *115*, 8547.
- (50) Inclán, M.; Albelda, M. T.; Frías, J. C.; Blasco, S.; Verdejo, B.; Serena, C.; Salat-Canela, C.; Díaz, M. L.; García-España, A.; García-España, E. *J. Am. Chem. Soc.* **2012**, *134*, 9644.
- (51) Kashanian, S.; Javanmardi, S.; Chitsazan, A.; Omidfar, K.; Paknejad, M. *DNA Cell Biol.* **2012**, *31*, 1349.
- (52) Nordén, B.; Tjerneld, F.; Palm, E. *Biophys. Chem.* **1978**, *8*, 1.
- (53) Stokke, T.; Steen, H. B. *J. Histochem. Cytochem.* **1985**, *33*, 333.
- (54) Guan, Y.; Shi, R.; Li, X.; Zhao, M.; Li, Y. *J. Phys. Chem. B* **2007**, *111*, 7336.
- (55) Loontjens, F. G.; McLaughlin, L. W.; Diekmann, S.; Clegg, R. M. *Biochemistry* **1991**, *30*, 182.
- (56) Loontjens, F. G.; Regenfuss, P.; Zechel, A.; Dumortier, L.; Clegg, R. M. *Biochemistry* **1990**, *29*, 9029.
- (57) Meyer-Almes, F. J.; Porschke, D. *Biochemistry* **1993**, *32*, 4246.





- (58) Lepecq, J. B.; Paoletti, C. *J. Mol. Biol.* **1967**, 27, 87.
- (59) Peberdy, J. C.; Malina, J.; Khalid, S.; Hannon, M. J.; Rodger, A. J. *Inorg. Biochem.* **2007**, 101, 1937.
- (60) McCoubrey, A.; Latham, H. C.; Cook, P. R.; Rodger, A.; Lowe, G. *FEBS Lett.* **1996**, 380, 73.
- (61) Lakowicz, J. R.; Weber, G. *Biochemistry* **1973**, 12, 4161.
- (62) Rehman, S. U.; Sarwar, T.; Husain, M. A.; Ishqi, H. M.; Tabish, M. *Arch. Biochem. Biophys.* **2015**, 576, 49.
- (63) Chaires, J. B. *Biopolymers* **1997**, 44, 201.
- (64) Chaires, J. B. *Curr. Opin. Struct. Biol.* **1998**, 8, 314.
- (65) Nelson, S. M.; Ferguson, L. R.; Denny, W. A. *Mutat. Res.* **2007**, 623, 24.
- (66) Dervan, P. B.; Edelson, B. S. *Curr. Opin. Struct. Biol.* **2003**, 13, 284.
- (67) Kielkopf, C. L.; Bremer, R. E.; White, S.; Szewczyk, J. W.; Turner, J. M.; Baird, E. E.; Dervan, P. B.; Rees, D. C. *J. Mol. Biol.* **2000**, 295, 557.
- (68) Albert, F. G.; Eckdahl, T. T.; Fitzgerald, D. J.; Anderson, J. N. *Biochemistry* **1999**, 38, 10135.
- (69) Cai, X.; Gray, P. J., Jr.; Von Hoff, D. D. *Cancer Treat. Rev.* **2009**, 35, 437.
- (70) Geierstanger, B. H.; Wemmer, D. E. *Annu. Rev. Biophys. Biomol. Struct.* **1995**, 24, 463.
- (71) Mi, R.; Bai, X.-T.; Tu, B.; Hu, Y.-J. *RSC Advances* **2015**, 5, 47367.
- (72) Reddy, B. S.; Sondhi, S. M.; Lown, J. W. *Pharmacol. Ther.* **1999**, 84, 1.
- (73) Martin, S. R.; Schilstra, M. J. In *Methods in Cell Biology*; Dr. John, J. C., Dr. H. William Detrich, III, Eds.; Academic Press: 2008; Vol. Volume 84, p 263.
- (74) Norden, B.; Kurucsev, T. *J. Mol. Recognit.* **1994**, 7, 141.
- (75) Kypr, J.; Kejnovska, I.; Renciuik, D.; Vorlickova, M. *Nucleic Acids Res.* **2009**, 37, 1713.
- (76) Ghosh, A.; Bansal, M. *Acta Crystallogr. D. Biol. Crystallogr.* **2003**, 59, 620.
- (77) Bishop, G. R.; Chaires, J. B. In *Current Protocols in Nucleic Acid Chemistry*; John Wiley & Sons, Inc.: 2001.
- (78) Doderio, V. I.; Quirolo, Z. B.; Sequeira, M. A. *Front. Biosci. (Landmark Ed)* **2011**, 16, 61.
- (79) Eriksson, M.; Norden, B. *Methods Enzymol.* **2001**, 340, 68.
- (80) Chang, Y. M.; Chen, C. K.; Hou, M. H. *Int. J. Mol. Sci.* **2012**, 13, 3394.
- (81) Vorlickova, M.; Kejnovska, I.; Bednarova, K.; Renciuik, D.; Kypr, J. *Chirality* **2012**, 24, 691.
- (82) Boffey, S. A. 1984; Vol. 2, p 43.
- (83) Yakhnin, A. V.; Yakhnin, H.; Babitzke, P. *Methods Mol. Biol.* **2012**, 905, 201.
- (84) Laniel, M. A.; Beliveau, A.; Guerin, S. L. *Methods Mol. Biol.* **2001**, 148, 13.
- (85) Singleton, M. R.; Scaife, S.; Wigley, D. B. *Cell* **2001**, 107, 79.
- (86) Masai, H.; Tanaka, T.; Kohda, D. *Bioessays* **2010**, 32, 687.
- (87) Lilley, D. M. *Q. Rev. Biophys.* **2000**, 33, 109.
- (88) Altona, C.; Pikkemaat, J. A.; Overmars, F. J. *Curr. Opin. Struct. Biol.* **1996**, 6, 305.
- (89) Arnott, S.; Chandrasekaran, R.; Hall, I. H.; Puigjaner, L. C.; Walker, J. K.; Wang, M. *Cold Spring Harb. Symp. Quant. Biol.* **1983**, 47 Pt 1, 53.

- (90) Assenberg, R.; Weston, A.; Cardy, D. L.; Fox, K. R. *Nucleic Acids Res.* **2002**, *30*, 5142.
- (91) Seemann, I. T.; Singh, V.; Azarkh, M.; Drescher, M.; Hartig, J. S. *J. Am. Chem. Soc.* **2011**, *133*, 4706.
- (92) Welch, J. B.; Duckett, D. R.; Lilley, D. M. *Nucleic Acids Res.* **1993**, *21*, 4548.
- (93) Moldrheim, E.; Hannon, M. J.; Meistermann, I.; Rodger, A.; Sletten, E. *J. Biol. Inorg. Chem.* **2002**, *7*, 770.
- (94) Oleksy, A.; Blanco, A. G.; Boer, R.; Uson, I.; Aymami, J.; Rodger, A.; Hannon, M. J.; Coll, M. *Angew. Chem. Int. Ed. Engl.* **2006**, *45*, 1227.
- (95) Pascu, M.; Clarkson, G. J.; Kariuki, B. M.; Hannon, M. J. *Dalton Trans.* **2006**, 2635.
- (96) Pope, L. H.; Davies, M. C.; Laughton, C. A.; Roberts, C. J.; Tendler, S. J.; Williams, P. M. *J. Microsc.* **2000**, *199*, 68.
- (97) Sebaugh, J. L. *Pharm. Stat.* **2011**, *10*.
- (98) Quiroz, M. M.; Khanal, G.; Pappas, D. In *Encyclopedia of Analytical Chemistry*; John Wiley & Sons, Ltd: 2006.
- (99) Elmore, S. *Toxicol. Pathol.* **2007**, *35*, 495.
- (100) Krysko, D. V.; Vanden Berghe, T.; Parthoens, E.; D'Herde, K.; Vandenabeele, P. *Methods Enzymol.* **2008**, *442*, 307.
- (101) Krysko, D. V.; Vanden Berghe, T.; D'Herde, K.; Vandenabeele, P. *Methods* **2008**, *44*, 205.
- (102) Benada, J.; Macurek, L. *Biomolecules* **2015**, *5*, 1912.
- (103) Bertram, J. S. *Mol. Aspects Med.* **2000**, *21*, 167.
- (104) Chen, T.; Stephens, P. A.; Middleton, F. K.; Curtin, N. J. *Drug Discov. Today* **2012**, *17*, 194.





# Conclusions

---





The present doctoral research project has led to the development of three unique families of metal-based cytotoxic compounds with distinct mechanisms of action, using distinct disciplines of (inorganic) chemistry, *viz.* coordination, organometallic and supramolecular chemistry.

Copper(II) **coordination** compounds from Schiff-base ligands have been designed, inspired from the efficient chemical nuclease  $[\text{Cu}^{\text{II}}(\text{pyrimol})\text{Cl}]$ . The DNA-interacting properties of the copper(II) complexes were accessed using complementary analytical techniques, which showed that they were not capable of cleaving the DNA strands, in contrast to the parent, model complex  $[\text{Cu}^{\text{II}}(\text{pyrimol})\text{Cl}]$ . However, the copper compounds can strongly interact with the biomolecule, mostly through groove binding. Almost all complexes showed remarkable cytotoxic properties, better than the reference compound cisplatin (under the same experimental conditions).

The biodistribution and bioavailability of some of the complexes are being investigated *in vivo* using radioactive copper. Moreover, the encapsulation of several of them is investigated by Ecolpol Tech; the use of drug carriers allows to have hydrophilic systems (the free compounds being poorly soluble in water) and to “control” their high toxicity (the compounds being only released inside cancer cells).

New **organometallic** ruthenium(II) compounds of the type  $[\text{RuCl}_2(\eta^6\text{-arene})(\text{PR}_3)]$  have been synthesized and fully characterized. Cell-toxicity studies revealed the enormous potential of such metal-based compounds, most of them being more active than the well-known reference molecule cisplatin. Examination of structure-activity relationship(s) of the compounds showed that the nature of the  $\eta^6\text{-arene}$  and phosphane ligands is crucial for their cytotoxic properties. Steric, electronic and hydrophobic effects play a vital role, both in terms of cytotoxic efficiency and cancer specificity. The results obtained illustrate the high versatility of such ruthenium(II) molecules that can be easily modified through the R groups of the  $\text{PR}_3$  ligand and the choice of  $\eta^6\text{-arene}$  rings. The cytotoxic activity and/or cancer specificity of such  $[\text{RuCl}_2(\eta^6\text{-arene})(\text{PR}_3)]$  compounds can be fine-tuned by appropriately selecting the two types of ligands around the metal centre, *viz.* the  $\pi\text{-arene}$  and the monophosphane.

Finally, preliminary antimetastatic assays revealed that some of the ruthenium(II) compounds prepared are capable of efficiently inhibiting cell migration. Further studies are clearly needed to confirm these very important results and to try to fully understand the exact mechanism(s) of action these organometallic compounds.

**Supramolecular** iron(III) metallohelicates have been designed and prepared from bis- $\beta$ -diketone ligands containing various functional groups, like H-bond donor or H-bond acceptor units. Such triple-stranded helical supramolecules are known to bind in the major groove of DNA or/and stabilize particular DNA structures, like three-way junctions (3WJs), which are relevant DNA targets for the development of potential anticancer agents.

The DNA-interacting properties of the new metallo-helicates obtained were evaluated, which revealed that all the supramolecular complexes could interact and disturb the structure of the biomolecule, mostly through groove binding. However, the metallohelicates are not able to stabilize 3WJs, as evidenced by a new and very simple procedure that has been developed during this work. This unprecedented technique is carried out with fluorophore-tagged oligonucleotides, and can therefore be applied in any lab, with no need to take particular safety precautions (the current applied procedure involves radioactive phosphorus).

Cytotoxicity studies revealed the great potential of two of these metal-based supramolecules, with lower  $IC_{50}$  values (against SW620 cells) than cisplatin and the metallohelicate of reference, described by Hannon and co-workers. Preliminary fluorescence microscopy and cell-cycle studies revealed that the most interesting metallohelicate can reach the nuclei and arrest the cell cycle at the G2/M phase, hence triggering apoptosis.





# Experimental section

## Contents

MATERIALS AND METHODS .....	CXLVII
<i>Synthesis</i> .....	<i>cxlvii</i>
<i>DNA-binding studies</i> .....	<i>cxlvii</i>
UV-Vis Spectroscopy .....	cxlviii
Fluorescence dye displacement .....	cl
Circular Dichroism .....	cliii
Gel electrophoresis .....	clv
AFM experiments .....	clviii
<i>Cell Culture</i> .....	<i>clx</i>
Viability assays - MTT Reduction Assay .....	clxi
Single point assays .....	clxii
IC <sub>50</sub> Determination .....	clxii
Fluorescence spectroscopy assays .....	clxii
Cell migration – Wound-Healing assay .....	clxiv
CHAPTER I – COPPER COMPLEXES .....	CLXVI
<i>Preparation of the Schiff bases</i> .....	<i>clxvi</i>
2- <i>tert</i> -butyl-6-(pyridin-2-ylhydrazonomethyl)phenol (HL1) .....	clxvi
2- <i>tert</i> -butyl-6-(quinolin-2-ylhydrazonomethyl)phenol (HL2) .....	clxvi
4- <i>tert</i> -butyl-2,6-bis-(pyridin-2-ylhydrazonomethyl)phenol (HL3) .....	clxvi
4- <i>tert</i> -butyl-2,6-bis-(quinolin-2-ylhydrazonomethyl)phenol (HL4) .....	clxvi
<i>Preparation of the complexes</i> .....	<i>clxvii</i>
[Cu(L1)Cl]·CH <sub>3</sub> OH (Cu1) .....	clxvii
[Cu(L2)NO <sub>3</sub> ] (Cu2) .....	clxvii
[Cu <sub>2</sub> (L3)(ClO <sub>4</sub> ) <sub>2</sub> (CH <sub>3</sub> O)(CH <sub>3</sub> OH)]·CH <sub>3</sub> OH (Cu3) .....	clxvii



[Cu <sub>2</sub> (L4)(ClO <sub>4</sub> )(OH)(CH <sub>3</sub> OH)]ClO <sub>4</sub> (Cu4) .....	clxvii
[Cu <sub>8</sub> (L3) <sub>4</sub> (NO <sub>3</sub> ) <sub>4</sub> (OH) <sub>5</sub> ](NO <sub>3</sub> ) <sub>3</sub> ·(CH <sub>3</sub> OH) <sub>5</sub> ·(H <sub>2</sub> O) <sub>8</sub> (Cu5) .....	clxvii
[Cu <sub>3</sub> (HL2') <sub>4</sub> Cl <sub>6</sub> ]·(CH <sub>3</sub> OH) <sub>6</sub> (Cu6) .....	clxvii
<i>DNA-Binding Studies</i> .....	clxviii
UV-Vis Spectroscopy .....	clxviii
ESI-MS and EPR spectroscopy .....	clxx
Fluorescence dye displacement .....	clxxii
Circular Dichroism .....	clxxiv
Gel electrophoresis .....	clxxiv
CHAPTER II - RUTHENIUM COMPLEXES .....	CLXXV
<i>Structure of the complexes</i> .....	clxxv
<i>DNA-Binding Studies</i> .....	clxxvi
Fluorescence dye displacement .....	clxxvii
CHAPTER III - HELICATES .....	CLXXX
<i>Preparation of the Poly-β-diketones</i> .....	clxxx
1,3-bis(3-oxo-3-(2-naphthyl)-propionyl)benzene (H <sub>2</sub> L1) .....	clxxx
1,3-bis-(3-oxo-3-(2-pyridinyl)-propionyl)benzene (H <sub>2</sub> L2) .....	clxxx
1,3-bis-(3-oxo-3-(3-pyridinyl)-propionyl)benzene (H <sub>2</sub> L3) .....	clxxx
1,3-bis-(3-oxo-3-(4-pyridinyl)-propionyl)benzene (H <sub>2</sub> L4) .....	clxxxi
Synthesis of 1,3-bis-(3-oxo-3(2-hydroxyphenyl)propionyl)benzene (H <sub>4</sub> L5) .....	clxxxi
1,3-bis-(3-oxo-3(3-hydroxyphenyl)propionyl)benzene (H <sub>4</sub> L6) .....	clxxxii
1,3-bis-(3-oxo-3(4-hydroxyphenyl)propionyl)benzene (H <sub>4</sub> L7) .....	clxxxii
<i>Preparation of the supramolecular complexes</i> .....	clxxxii
[Fe <sub>2</sub> (L1) <sub>3</sub> ] (H2): .....	clxxxiii
[Fe <sub>2</sub> (H <sub>2</sub> L7) <sub>3</sub> ] (H7): .....	clxxxiii
<i>DNA-Binding Studies</i> .....	clxxxiv
UV-Vis Spectroscopy .....	clxxxiv
Fluorescence dye displacement .....	clxxxiv
Circular Dichroism .....	clxxxvii
Gel electrophoresis .....	clxxxviii
<i>Cell Studies</i> .....	CXC
Single point .....	CXC
IC <sub>50</sub> Determination .....	CXCii
Immunofluorescence microscopy .....	CXCiv
Cell cycle .....	CXCvi
REFERENCES .....	CXCVIII





## **Materials and Methods**

### **Synthesis**

The preparation of the copper complexes was carried out under aerobic conditions. All the reagents and solvents were purchased from Aldrich, Acros Organics or TCI Europe and were used as received.

$^1\text{H}$  NMR spectra were recorded at room temperature with a Varian Unity 400 MHz spectrometer. Proton chemical shifts are expressed in parts per million (ppm,  $\delta$  scale) and are referenced to the solvent peak.

Infrared spectra (as KBr pellets) were recorded using a Nicolet-5700 FT-IR (in the range  $4000\text{--}400\text{ cm}^{-1}$ ), and data are represented as the frequency of absorption ( $\text{cm}^{-1}$ ).

Elemental analyses were performed by the Servei de Microanàlisi, Consejo Superior de Investigaciones Científicas (CSIC) of Barcelona.

Mass-spectrometry analyses (ESI) were performed at the Serveis Científicotècnics of the Universitat de Barcelona.

### **DNA-binding studies**

Ethidium bromide, sodium cacodylate, and *calf thymus* DNA were obtained from Sigma-Aldrich and were used as received. Ultrapure water was used to prepare all the buffers and sample solutions. The pH of the cacodylate (10 mM sodium cacodylate, 20 mM NaCl) and Tris-HCl (5 mM Tris-HCl–50 mM NaCl) buffer solutions was adjusted to 7.2 with an ultrapure aqueous solution of hydrochloric acid. Fluorescence, UV-Vis and circular dichroism spectra were collected in 1-cm pathlength quartz cuvettes. pBR322 DNA was purchased from Roche.

UV-Vis experiments were performed with a Varian Cary-100 spectrophotometer. The fluorescence measurements were carried out with a KONTRON SFM 25 spectrofluorometer. ESI mass spectroscopy was carried out at the Serveis Científicotècnics of the University of Barcelona, using a LC/MSD-TOF Spectrometer from Agilent Technologies, equipped with an electrospray ionization (ESI) source.

### **Buffers**

It should be pointed out that some buffers may interact with metal ions and/or can form radicals.<sup>1,2</sup> Therefore, it is extremely important to select an appropriate buffer to perform biological studies. It is known that Tris (2-amino-2-hydroxymethyl-propane-1,3-diol) binds divalent metal ions, with a higher affinity for copper compared with zinc.<sup>3-5</sup>



Calf thymus DNA (ct-DNA) is commonly used to study the interaction of double-helix DNA with small molecules. Fresh solutions of ct-DNA were prepared by dissolving lyophilized ct-DNA in the buffer at pH = 7.2. The concentration of ct-DNA was determined from its absorption intensity at 260 nm with a molar extinction coefficient of  $6600 \text{ M}^{-1}\text{cm}^{-1}$ . The DNA purity was assessed by determining the 260 nm/280 nm ratio. This ratio of the UV absorbance at 260 and 280 nm ( $A_{260}/A_{280}$ ) should be around 1.8–1.9 to indicate that the DNA used is sufficiently protein free.<sup>6-8</sup>

The stock solutions of ct-DNA were stored at 4 °C and were used within a maximum of 4 days.

### UV-Vis Spectroscopy

Ultraviolet (UV) and visible (vis) absorption spectroscopy is an effective tool to investigate the binding strength of compounds to DNA.<sup>9-11</sup> The molecules studied should preferably present a clear absorption band in the visible region, which may be used to estimate the magnitude of the drug-DNA interaction. Any absorption shift can provide valuable information regarding the nature of the DNA-binding properties of the molecule investigated. The magnitude of the shifting can be associated with the strength of the interaction.<sup>12,13</sup> A decrease of the absorption, accompanied with hypochromism and bathochromism (red shift) is indicative of intercalation. The stacking interaction between an aromatic chromophore and a DNA base pair results in a decrease of the  $\pi$ - $\pi^*$  transition energy. The magnitude of the hypochromism depends on the strength of the intercalative interaction. The decrease in strength is expected to be as the cube of the distance between the chromophore and the DNA bases.<sup>14-17</sup> Hypochromism occurs when a decrease of the distance between the intercalated compound (drug) and the DNA bases takes place.

A hyperchromic effect is observed when the interaction is purely electrostatic, which reflects changes in the DNA conformation and structure upon interaction with the compound. Base–base interactions can be reduced by those interactions, leading to an increase of the UV absorbance of DNA (because hydrogen bonds between bases are affected); up to 40% increase of the absorbance can be achieved.<sup>18</sup> The electrostatic interaction of cations with DNA (*via* electrostatic attraction to the phosphate backbone) will induce a contraction of DNA and thus an overall damage of its secondary structure.<sup>19-21</sup> Finally, hyperchromism can also stem from the uncoiling of the helical structure of DNA, which will expose the bases.<sup>22,23</sup>

The interaction(s) can be estimated calculating the binding constant/association constant ( $K_b$ ) of the drug, using the Benesi–Hildebrand equation (1):<sup>24</sup>





$$\frac{A_0}{(A-A_0)} = \frac{\epsilon_G}{(\epsilon_{H-G} - \epsilon_G)} + \frac{\epsilon_G}{(\epsilon_{H-G} - \epsilon_G)} \times \frac{1}{K_b[DNA]} \quad (1)$$

In this equation,  $K_b$  is the association/binding constant,  $A_0$  and  $A$  are respectively, the absorbances of the free compound and its complex with DNA.  $\epsilon_G$  and  $\epsilon_{H-G}$  are the absorption coefficients of the free compound and the compound–DNA complex, respectively. The association constant can be obtained from the intercept-to-slope ratios of  $A_0/(A - A_0)$  vs.  $1/[DNA]$  plots.  $K_b$  can also be determined from the intercept-to-slope ratios of the plot of  $[DNA]$  vs.  $[DNA]/\epsilon_a - \epsilon_f$ , where  $\epsilon_a$  (or  $\epsilon_G$ ) and  $\epsilon_f$  (or  $\epsilon_{H-G}$ ) are the absorption coefficients of the free compound and the compound–DNA complex, respectively. The simplified equation (2) below can be used:

$$\frac{[DNA]}{(\epsilon_a - \epsilon_f)} = \frac{[DNA]}{(\epsilon_b - \epsilon_f)} + \frac{1}{K_b(\epsilon_b - \epsilon_f)} \quad (2)$$

Titration experiments were thus performed to compare quantitatively the binding strength of different metal complexes to DNA. The experiments were carried out by maintaining a constant concentration of metal complex (25  $\mu$ M) and varying the DNA concentration (from 0 to 50  $\mu$ M) in a buffer solution. After each DNA addition, the resulting DNA-complex mixture was allowed to equilibrate for 5 min at 25 °C, after which the absorption spectra were recorded. The intrinsic binding constants,  $K_b$ , to ct-DNA were determined by monitoring the changes in the lower energy bands; in most cases, the results could be fitted using equation (2).<sup>10,25</sup> In equation (2),  $[DNA]$  is the concentration of DNA expressed in base pairs,  $\epsilon_a$  is the apparent extinction coefficient obtained from  $A_{obs}/[\text{complex}]$ ,  $\epsilon_f$  corresponds to the extinction coefficient of the DNA-free complex solution, and  $\epsilon_b$  refers to the extinction coefficient of the DNA-bound complex solution. Each set of data fitted with (2), gave a straight line with a slope of  $\frac{1}{(\epsilon_b - \epsilon_f)}$  and a y-intercept of  $\frac{1}{K_b(\epsilon_b - \epsilon_f)}$ ;  $K_b$  was determined from the ratio of the slope to the intercept.<sup>26-29</sup> The  $K_b$  values of well-known DNA-interacting molecules (Figure 77) are given in Table 31, where their respective mechanism of action is also mentioned.

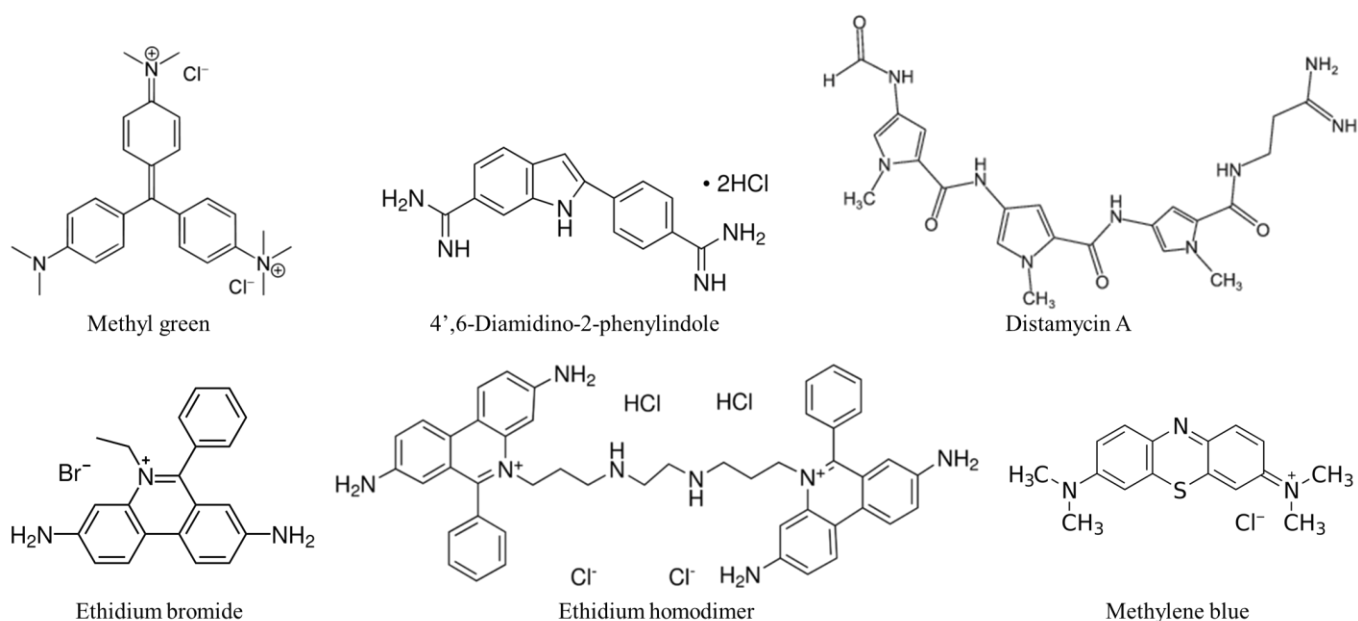


Figure 77: Structures of some well-known DNA-interacting molecules. Adapted from <sup>30</sup>

Table 31: Binding characteristics of common DNA-binding molecules (42% % G+C).  $K_b$ , binding constant.<sup>30</sup>

Ligand	Charge	Reference	Strongest mode	$K_b$ with $[\text{Na}^+]$ ( $\text{M}^{-1}$ )		Site size (bp)	Sequence selectivity
				50 mM	100 mM		
Methyl green	2+	31	Major groove	$1 \times 10^6$	$3 \times 10^5$	$\approx 5$	insignificant
4',6-Diamidino-2-phenylindole (DAPI)	2+	32,33	Minor groove	$5 \times 10^3$	$1 \times 10^5$	3–4	(AT) <sub>n</sub>
		34	Minor groove	$\approx 10^9$	$\approx 10^8$	4	[poly(dA-dT)] <sub>2</sub>
		34	Intercalation	$7 \times 10^5$	$2 \times 10^5$	2	[poly(dC-dC)] <sub>2</sub>
Distamycin A	1+	33,35	Minor groove	$8 \times 10^5$	$4 \times 10^5$	5	(A-T) <sub>n</sub>
Ethidium bromide	1+	36	Intercalation	$1 \times 10^6$	$5 \times 10^5$	2	insignificant
Ethidium homodimer	4+	37	Bis-intercalation (low salt)	$2 \times 10^4$	$4 \times 10^5$	2–3	insignificant
Methylene blue	1+	38,39	Intercalation (low salt)	—	—	—	(A-T) <sub>n</sub>
		38,39	Major groove (high salt)	—	—	—	(A-T) <sub>n</sub>

## Fluorescence dye displacement

Fluorescence spectroscopy is one of the most commonly used techniques to study host–guest binding dynamics. The routine applicability of this technique relies on its high sensitivity, large linear concentration range and selectivity.<sup>14,40</sup> Compounds that contain aromatic functional groups with low-energy  $p \rightarrow p^*$  transition levels usually show fluorescence properties. Aliphatic and alicyclic compounds with carbonyl function(s) or with highly conjugated double-bond structures may also present some fluorescence.<sup>41,42</sup>

Fluorescence quenching experiments are very useful to provide information regarding the localization and the mode of interaction of compounds with DNA.<sup>43</sup> Fluorescence



spectroscopy is a highly sensitive technique; small structural changes result in significant spectral shifts both in excitation and emission. For instance, intercalating molecules usually show a significant increase of their fluorescence when they stack between DNA base pairs.<sup>44</sup> This phenomenon can be explained by the impediment of the free rotation of the molecules (rotations that favour the deactivation of the excited states).<sup>45</sup> For groove-binding agents, for which electrostatic, hydrogen bonding or hydrophobic interactions drive their binding to the sugar-phosphate backbone, a decrease of the fluorescence intensity is observed.<sup>46</sup>

Fluorescence-dye displacement spectroscopy is a technique used to study the interaction of a complex with a highly fluorescent dye-DNA complex.<sup>47-49</sup> Displacement of the dye by the incoming molecule will result in a decrease of the emission intensity (since the free dye is poorly fluorescent). This fluorescence-quenching phenomenon allows to evaluate the DNA-binding ability of the molecule investigated. Thus, competitive binding experiments were performed for the complexes, maintaining a constant concentration of ct-DNA.<sup>28,50,51</sup> Apparent binding constants ( $K_{app}$ ) were calculated using the classical Stern-Volmer equation (3):<sup>52</sup>

$$\frac{I_0}{I} = 1 + K[Q] \quad (3)$$

To determine the quenching constant,  $K$ , plots of  $I_0/I$  *versus*  $[Q]$  are used, where  $I_0$  is the fluorescence intensity of the DNA bound to ethidium bromide and  $I$  is the fluorescence intensity upon addition of the quencher molecule,  $Q$ .<sup>52</sup>

### **Ethidium Bromide Displacement Assay**

Ethidium bromide (EB; Figure 77 and Figure 78) is a fluorophore that is commonly used as DNA intercalator. One of the main characteristics that distinguish this DNA binder is the fact that its fluorescence quantum yield is very low in buffer solution and increases dramatically when it is intercalated between adjacent base pairs of ct-DNA (Figure 78).<sup>53-55</sup>

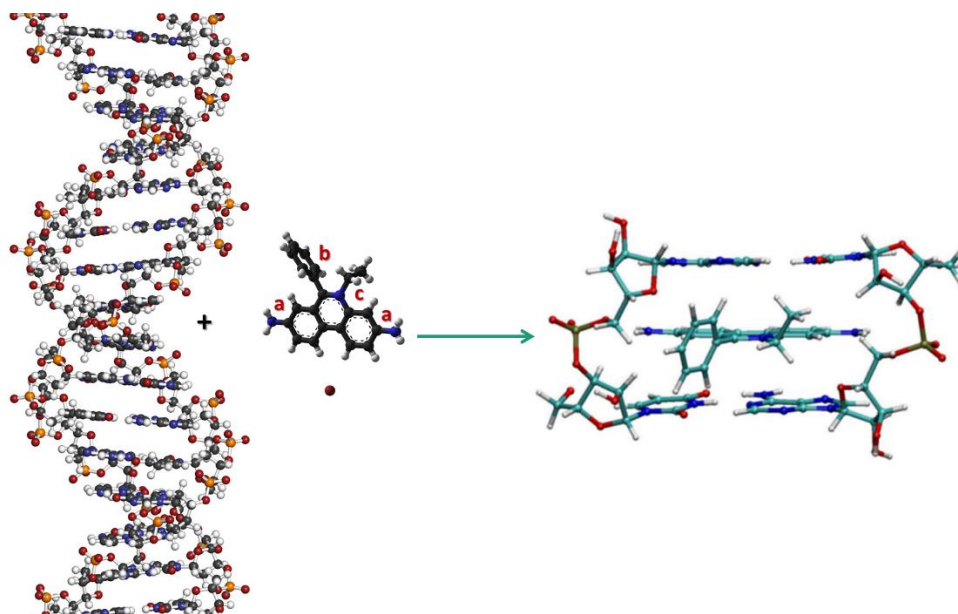


**Figure 78: Schematic representation of the intercalative binding mode of ethidium bromide; important functions of ethidium bromide: a) amino substituents responsible for the fluorescence increase upon intercalation; b) phenyl substituent for steric control; c) permanent positive charge for aqueous solubility and electrostatic attraction to the biomolecule phosphate backbone.**

Displacement of DNA-bound EB by an “incoming” molecule will result in fluorescence quenching, and therefore will allow the evaluation of its interacting/intercalating ability.<sup>56,57</sup> Two mechanisms have been proposed to explain the reduction of EB emission: (i) release of the fluorophore leading to free, non-fluorescent EB,<sup>25</sup> and/or (ii) electron transfer.<sup>29,50</sup>

Fluorescence spectra were recorded at room temperature buffers containing 20 to 50 mM NaCl in order to avoid secondary binding of EB to DNA. The excitation used was 514 nm and the emission was observed at about 610 nm. The experiments were performed with an EB–DNA solution obtained from 25  $\mu$ M ct-DNA and 125  $\mu$ M EB.<sup>58-60</sup>

The fluorescence-quenching effect caused by the interacting complexes, *i.e.* their quenching efficiency, was assessed by determining the corresponding Stern–Volmer constant  $K_{SV}$ , applying equation (3).

### **Hoechst Displacement Assay Procedure**

Hoechst 33258 is a molecule that selectively binds in the minor groove of DNA through van der Waals and hydrogen-bonding interactions. This molecule also interacts electrostatically with DNA and recognizes AT base pairs in the minor groove (Figure 29).<sup>61</sup> Like for EB, its quantum yield of emission as free molecule is very low while a significant increase of the emission intensity occurs when bound to DNA.<sup>42,43</sup>



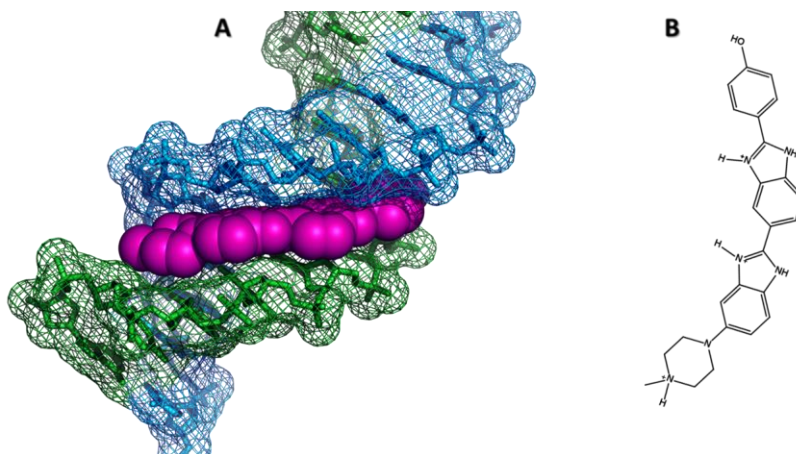


**Figure 79: A. Molecular structure of DNA A-tract dodecamer d(CGCAAATTTGCG) complexed with Hoechst 33258, determined by X-ray diffraction B. Structure of dicationic Hoechst 33258.<sup>62,63</sup>**

The procedure described by Matsuba and co-workers was applied.<sup>64</sup> The fluorescence spectra were recorded at room temperature with  $\lambda_{\text{exc}} = 350$  nm and  $\lambda_{\text{em}} = 450$  nm. The experiments were performed with Hoeschst–DNA solutions obtained from  $1.5 \times 10^{-5}$  M Hoeschst and  $1.9 \times 10^{-6}$  M ct-DNA.<sup>65,66</sup> Fluorescence quenching induced by the complexes investigated is indicative of their potential binding in the minor groove of DNA (since the quenching is due to the release of Hoechst molecules). The quenching constants ( $K_{\text{sv}}$ ) were determined using the classical Stern-Volmer equation (equation (3)).

### Circular Dichroism

Circular dichroism is a very sensitive technique that can be used to detect alterations of the secondary structure of biomolecules (proteins, DNA, etc.) upon interaction with molecules.<sup>67,68</sup> This spectroscopic technique is based, on the differences in absorption of left- and right- circularly polarised light passing through a chiral sample.<sup>69</sup> It can be noted that induced chirality may occur in non-chiral molecules interacting with chiral molecules (*e.g.* small chiral molecules that binding to a supramolecule), giving a characteristic CD signal.

A CD signal results from the differences in magnitude of the vectors corresponding to left and right lights. This difference gives rise to an overall vector, an elliptically polarized beam (that is obtained from the superposition of the two opposite circularly polarized beams that have passed through the sample). Ellipticity is the unit of CD and is defined as the angle whose tangent is the minor elliptical axis divided by the major elliptical axis.

As mentioned before, the structure of the DNA is formed by nucleosides with chiral sugars presenting an intrinsic asymmetry. The interaction of the strong  $\pi \rightarrow \pi^*$  transitions of the chromophoric bases with the higher energy in the sugars produces a characteristic low-intensity CD signal. The circular dichroism of nucleic acids mainly relies on the stacking

geometry of the bases.<sup>67,70</sup> The CD spectrum of native calf thymus DNA has two major bands, namely a positive long wavelength band at 260–300 nm and a negative one around 245 nm. The positive band is due to base stacking, while helicity is responsible for the negative band; the value of 245 nm for this negative band characterises a right-handed B-DNA (Figure 80a).<sup>71-74</sup> Both bands are extremely sensitive to the interaction of molecules with DNA.<sup>75,76</sup> A-DNA is a right-handed,  $\alpha$ -helical double helix (Figure 80b), which exhibits a relatively smaller and more compact helical structure than B-DNA. The CD spectrum of this DNA structure is characterized by a dominant positive band around 240 nm and a fairly small negative band at 215 nm. Z-form DNA is a left-handed helix with a zigzag phosphate backbone (Figure 80c), with grooves of comparable width. The CD spectrum of Z-DNA displays a wide and extremely deep negative band at 220-290 nm and a minor positive band above 290 nm.<sup>75</sup>

Non-covalent interactions between DNA and a potential drug may affect the helical structure, which in turn will modify the CD response.<sup>77</sup> When the interactions are mainly electrostatic binding or occur in the minor groove, very little changes are observed. If intercalation is taking place, both the positive and negative bands can be affected significantly. Changes in the position and intensity of the bands can also be informative. For example, when B-DNA converts to A-DNA, the positive band shows an increase in intensity while the negative band shows a significant intensity decrease associated with a shift towards a higher wavelength.

A decrease in intensity of both bands upon interaction with a molecule may suggest that this interacting compound is capable of (i) promoting alterations in the base stacking (positive band) and (ii) unwinding the DNA helix reflected by a loss of its helicity (negative band).<sup>51,78</sup>



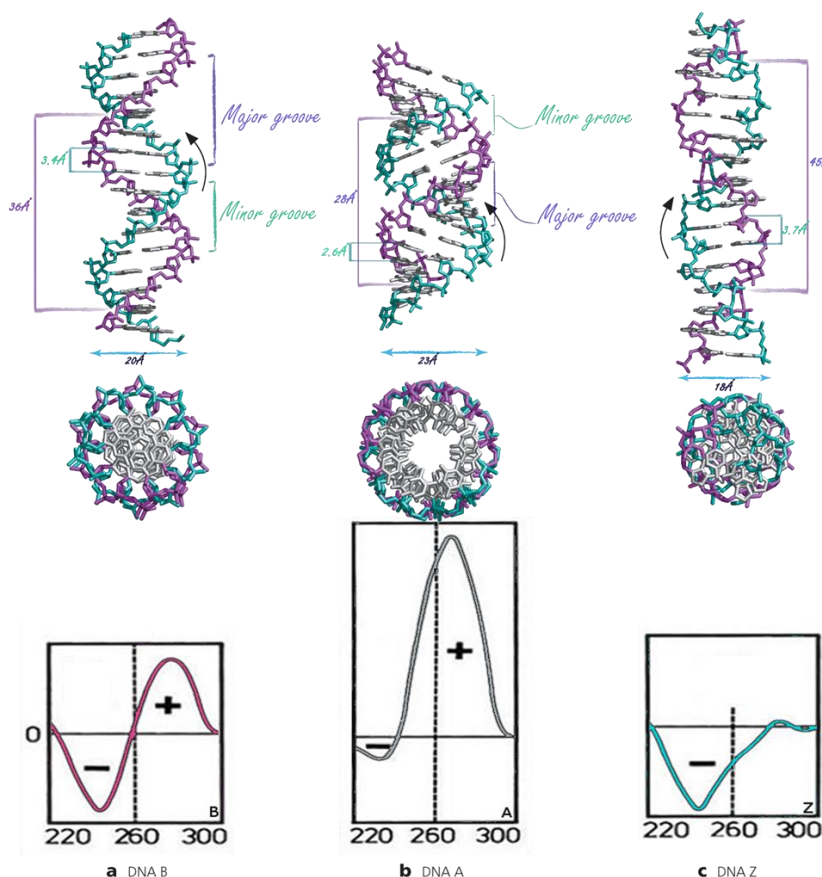


Figure 80: Schematic structures of B-, A- and Z-DNA and their corresponding CD spectra.<sup>73</sup>

## Gel electrophoresis

### Agarose Gel electrophoresis

Electrophoresis is a simple technique that analyses the migration of a charged particle under the influence of an electric field. Many biomolecules possess ionisable groups and are therefore electrically charged species in solution, either as cations (+) or anions (-). Under the influence of an electric field, these charged molecules will migrate either to the cathode or to the anode, depending on the nature of their net charge. Agarose forms gels through a network of hydrogen bonds, whose pore size depends on the agarose concentration used to prepare them. DNA will migrate through a gel under the influence of an electric field at a speed that will depend on its size (conformation). Therefore, the way in which a molecule interacts with DNA can be studied by agarose gel electrophoresis.<sup>79,80</sup> As already mentioned above, the electrophoretic mobility of the DNA depends on its conformation/size; for instance, the supercoiled form of plasmid pBR322 (form I) will have a relatively fast migration speed. If DNA scission occurs on one strand (nicking), the generated open circular form (form II) will have a lower electrophoretic mobility. If both strands are cleaved, a linear form (Form III) is produced that migrates in between form I and form II. A schematic representation of these three forms and their relative electrophoretic migration are depicted in Figure 81. Using this

technique, the formation of form II and/or III, so as the disappearance of form I can be visualized (Figure 81). Qualitative information is usually obtained; however, quantitative data may also be achieved using curve-fitting approaches.

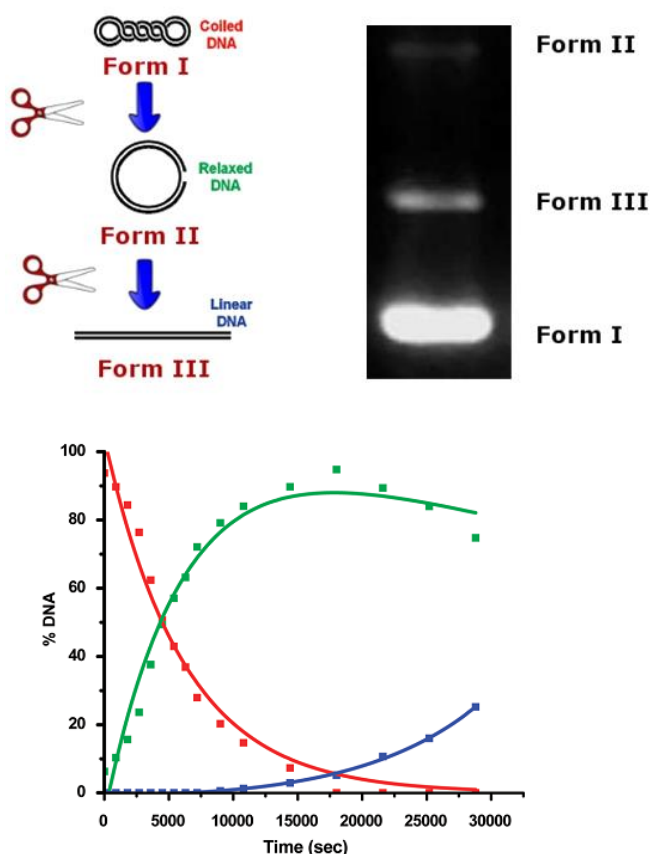


**Figure 81: Schematic representation of DNA forms I, II and III and their respective electrophoretic migration. Plots illustrating the disappearance of form I and consequent in-time generation of forms II and III (Adapted from <sup>81</sup>).**

All stock solutions of the complexes (5 mM) were freshly prepared in milli-Q water with 2% DMSO. Before electrophoresis, the reactions were quenched by the addition of 4  $\mu$ L of loading buffer (5 mM xylene cyanol and 4 mM glycerol). Then, the samples were electrophoretized on agarose gel (1% a in 0.5 M TBE-Buffer for 5 h at  $1.5 \text{ V.cm}^{-1}$ ). Finally, the DNA was stained with SYBR<sup>®</sup> and pictures were taken on a BioRad Gel Doc EZ Imager.



## **Gel Mobility Shift Assays to Study Three-Way Junctions:**

The electrophoretic mobility shift (also known as gel shift) assay (EMSA) is an informative and versatile method commonly used to analyse the interaction between DNA and proteins; it can be applied to determine association, dissociation and affinity constants.<sup>82,83</sup> This gel shift assay may also be used to obtain information on interactions between DNA and drugs.

Native polyacrylamide gel electrophoresis (PAGE) can be utilised to evaluate the ability of metal complexes to interact with important DNA such as three- and four-way junctions, bulges (palindromic sequences like hairpins or cruciforms), RNA:DNA hybrids, Holliday junctions and G-Quadruplexes.

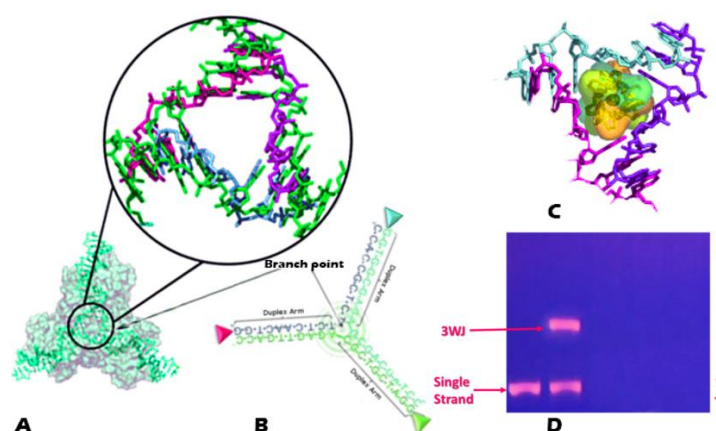


**Figure 82:** A. Side-view of a 3WJ and zoom into the branch point. B. Schematic representation of a 3WJ constituted of complementary and fluorophore-labelled oligonucleotide sequences (S1, S2 and S3, red-, green- and blue-labelled sequences, respectively). C. Crystallographic side-view of the complex formed between a 3WJ and a triple helicate complex reported by Hannon and co-workers (PBD Id: 2ET0). D. Example of polyacrylamide-gel electrophoresis (PAGE) experiment. Adapted from<sup>84</sup>.

Three-way junctions (3WJs) are helical junctions that represent important nucleic acid structures since they act as intermediates in both homologous and site-specific recombination events (in the replication fork).<sup>85,86</sup> In RNA, 3WJs are important architectural elements essentially involved in splicing and translation.<sup>87,88</sup>

The formation of 3WJs can be visualised by PAGE; hence, their formation and stabilization mediated by complexes can be demonstrated using this technique. PAGE experiments were carried out using 15% native polyacrylamide in 1×TB buffer pH 8.3, obtained from 89 mM tris(hydroxymethyl)aminomethane and 89 mM boric acid. The complementary oligonucleotides were custom made by Genecust Europe. Stoichiometric amounts of each single-stranded oligonucleotide (0.4 μM) were incubated with the different complexes in TBN buffer, prepared from 89 mM tris(hydroxymethyl) amino methane, 89 mM boric acid and 100 μM NaCl. The solutions were incubated at room temperature for 1 hour, followed by 15 minutes incubation on ice, and loaded on the freshly prepared polyacrylamide

gel. Electrophoresis was performed during 1.50 hours at  $6 \text{ Vcm}^{-1}$  and room temperature. The gels were pictured using a BioRad Gel Doc EZ Imager.

### AFM experiments

Atomic force microscopy is a technique that has experienced a tremendous development during recent years.<sup>89-93</sup> Its low cost and simple manipulation makes a very good tool to visualize biological structures and their dynamics.<sup>94</sup>

This analytical technique allows to obtain “topographic” images through the reflection of a laser beam that moves through the surface of a sample. The image is collected based on the interaction between the sample and a tip at the end of a cantilever. This tip fluctuates with respect to the surface features of the sample, as the result of attractive and repulsive forces with the sample. These deflection movements are measured through a laser beam reflected off the cantilever into an array of photodetectors, allowing the generation of a topographical image (Figure 83).<sup>95</sup>

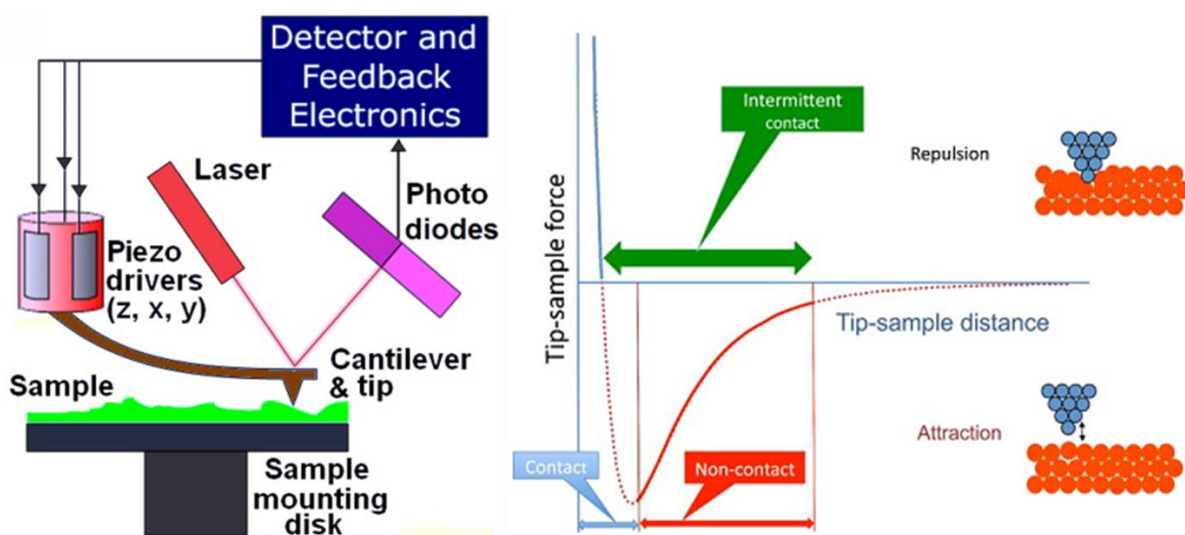
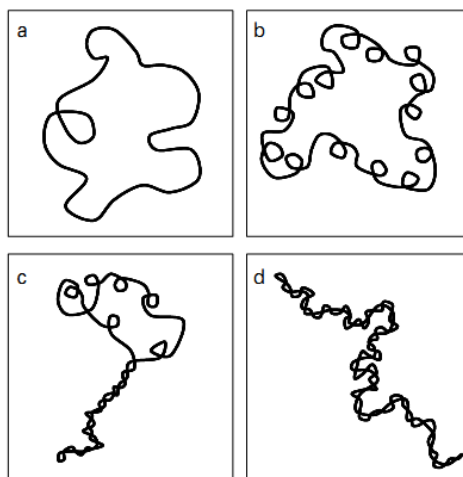


Figure 83: Principles of the AFM. Left: AFM tip (brown triangle) that “scans” the surface profile of the sample (shown in green). The position of the tip relative to the sample is controlled by a piezoelectric scanner. Right: schematic representation of the tapping mode (Adapted from <sup>96</sup>).

The tapping mode is commonly used with biomolecules. It allows intermittent contacts between the silicon tip and the sample, therefore decreasing the error caused by the damage that would be observed upon constant screening of the sample. In this mode, a cantilever is deliberately vibrated at a frequency close to its resonant frequency, thanks to a piezoelectric modulator with very small amplitude. As the tip approaches the surface, van der Waals attractive forces between the tip and the sample alter both the amplitude and the phase of the cantilever vibration. These changes are monitored by a Z-servo system feed-back loop to control the tip-sample distance.<sup>96</sup>



The binding of molecules to DNA leads to structural distortions, whose extent depends on the physical and chemical characteristics of the interacting molecules, and the forces between DNA and these molecules. AFM can be used to observe different morphologies of DNA, some of them, for instance, being caused by its interaction/binding with molecules. The appearance of kinks and compactions in the tertiary structure of plasmidic DNA can easily be identified using AFM. The common distinct tertiary structures that can be observed with this technique are schematically depicted in Figure 84.



**Figure 84:** Illustration of different tertiary structures of plasmid DNA: (a) predominantly relaxed; (b) toroidally supercoiled; (c) mixed toroidal and plectonemic supercoils; (d) complete plectonemic supercoiling. Adapted from <sup>94</sup>.

In the present work, pBR322 plasmid DNA was heated just before use at 60 °C for 10 min to obtain a homogeneous distribution of topoisomers. Buffered solutions of metal complexes were freshly prepared and filtered through 0.2 nm FP030/3 filters (Scheicher and Schuell, Germany). The stock solutions of the complexes, plasmid DNA, and the reaction samples were prepared as for the gel electrophoresis (see above).

The AFM samples were prepared by casting a 5  $\mu$ L drop of the sample solution onto freshly cleaved Muscovite mica disks as the support. The drop was allowed to stand undisturbed for 3 minutes at room temperature to favour the adsorbate/substrate interaction. Each DNA-laden disk was rinsed for 10 s in a jet of Milli-Q water and was blown dry with clean compressed argon gas directed normal to the disk surface. The samples were stored over silica prior to AFM imaging. The AFM images were obtained with a Multimode 8 AFM with electronic Nanoscope V scanning probe microscope from Bruker AXS, using the PEAK FORCE tapping mode. Commercial Si-tip on Nitride lever cantilevers (SNL, Bruker) with force constant of 0.4 N/m were used. The samples were deposited on mica disks (PELCO Mica Discs, 9.9 mm diameter; Ted Pella, Inc.), and dried before visualization.

### *Cell Culture*

Part of the cell cytotoxicity studies presented in this thesis (*viz.* those described in Chapter 1) was done in collaboration with Prof. Elisângela de Paula Silveira-Lacerda and co-workers.

Murine breast cancer (Ehrlich ascites tumour; ATCC<sup>®</sup> CCL-77<sup>TM</sup>) and murine sarcoma 180 tumour cells (S180; ATCC<sup>®</sup> TIB-66<sup>TM</sup>) were cultured in RPMI 1640 medium (pH 7.2 – 7.4) (Sigma Chemical Co., MO). The murine fibroblast normal cells (L929; ATCC<sup>®</sup> CCL-1<sup>TM</sup>) (Sigma Chemical Co., MO) were cultured in DMEM medium (pH 7.2 – 7.4). The cells were maintained in a humidified atmosphere (Thermo Scientific) at 37 °C containing 5% CO<sub>2</sub>. Both media were supplemented with 10% fetal calf serum, 100 UI mL<sup>-1</sup> penicillin G, 100 µg mL<sup>-1</sup> streptomycin (all reagents were obtained from Gibco<sup>®</sup>, Invitrogen, Carlsbad, CA, USA).<sup>97</sup>

Human melanoma (A375; ATCC<sup>®</sup> CRL-1619<sup>TM</sup>) lung (A549; ATCC<sup>®</sup> CCL-185<sup>TM</sup>), breast (MCF-7; ATCC<sup>®</sup> HTB-22<sup>TM</sup>), prostate (PC-3; ATCC<sup>®</sup> CRL-1435<sup>TM</sup>), ovary (SK-OV-3; ATCC<sup>®</sup> HTB-77<sup>TM</sup>), colorectal (SW-620; ATCC<sup>®</sup> CCL-227DQ<sup>TM</sup>) adenocarcinoma, small-cell lung (DM S53; ATCC<sup>®</sup> CRL-2062<sup>TM</sup>), head and neck (NH4; ATCC<sup>®</sup> CVCL-IS30<sup>TM</sup>), human neuroblastoma (SK-N-BE(2); ATCC<sup>®</sup> CRL-2271<sup>TM</sup>), human neuroblastoma (CHLA-90; ATCC<sup>®</sup> CVCL-6610<sup>TM</sup>) and mammary epithelial (MCF-10A; ATCC<sup>®</sup> CRL-10317<sup>TM</sup>) cell lines were purchased from the American Type Culture Collection (ATCC, Manassas, VA, USA). The cell lines A549, A375, SK-OV-3, SW-620 and NH4 were cultured in DMEM medium, PC-3 in F12 medium, DM S53 in RPMI 1640 medium and MCF-10A in DMEM:F12 media.

All media were supplemented with 10% heat-inactivated fetal bovine serum (FBS; Life Technologies, Carlsbad, CA, USA), 100 U mL<sup>-1</sup> penicillin, 100 µg mL<sup>-1</sup> streptomycin, and 2 mM L-glutamine. The MCF-7 cell line was cultured in DMEM–F12 (HAM) media (1:1) supplemented with 5% horse serum (Life Technologies), 100 µM sodium pyruvate (Sigma-Aldrich Chemical Co., St. Louis, MO, USA), 10 µg mL<sup>-1</sup> insulin (Sigma-Aldrich), 100 U mL<sup>-1</sup> penicillin, 100 µg mL<sup>-1</sup> streptomycin, and 2 mM L-glutamine. The MCF-10 cell line was cultured in RPMI 1640 supplemented with 5% horse serum (Life Technologies), 20 ng mL<sup>-1</sup> EGF, 0.5 µg/mL Hydrocortisone, 100 ng mL<sup>-1</sup> Cholera toxin, 10 µg/mL insulin all from Sigma-Aldrich and 100 U/mL penicillin, 100 µg mL<sup>-1</sup> streptomycin, and 2 mM glutamine (Biological Industries). The DMEM–F12 (HAM) medium (1:1) was supplemented with 5% horse serum (Life Technologies), 100 µM sodium pyruvate (Sigma-Aldrich Chemical Co., St. Louis, MO, USA), 10 µg mL<sup>-1</sup> insulin (Sigma-Aldrich), 100 U mL<sup>-1</sup> penicillin, 100 µg mL<sup>-1</sup> streptomycin, and 2 mM glutamine. The media and supplements whenever not stated were bought from





Biological Industries, Beit Haemek, Israel. Cells were grown at 37 °C under a 5% CO<sub>2</sub> atmosphere.

Cisplatin (*cis*-diamminedichloridoplatinum(II)) was purchased from Sigma, dissolved in water prior to use. 3-(4,5-Dimethylthiazol-2-yl)-2,5-diphenyltetrazolium bromide (MTT) was purchased from Sigma. Prodigiosin (2-methyl-3-pentyl-6-methoxyprodigiosene) was provided by Dr. R.J. Schultz of the National Cancer Drug Synthesis and Chemistry Branch Chemotherapeutic Agents Repository (Bethesda, MD).

### Viability assays - MTT Reduction Assay

The number of healthy cells in a sample defines the cell viability. Hence, the cell viability of a sample in normal growth conditions and in the presence of a specific studied compound was determined. Cell viability methods can be categorised into those that analyse whole populations and those that are based on the analysis of individual cells. The population analysis is a fast method, but gives less detailed results compared with viability measurements at the single-cell level.<sup>98</sup> Several dyes have been developed that rely on the metabolic activity of cells, which can be used with adherent cells and therefore allow high-throughput analyses. Typically, a plate reader is employed for the measurements, with one of the most used metabolic dyes, *viz.* 3-(4,5-dimethylthiazol-2-yl)-2,5-diphenyltetrazolium bromide (MTT). This assay is based on the cellular reduction of soluble tetrazolium into insoluble blue formazan needle-like crystals. The analysis is thus associated with the color change of MTT upon metabolic reduction.<sup>99,100</sup>

The cytotoxic properties of all copper(II) coordination compounds were evaluated applying the MTT assay with murine cell lines.<sup>99</sup> Thus,  $1 \times 10^5$  S180 and EAT and  $2 \times 10^4$  L929 cells were plated in 96-well tissue culture plates and subsequently treated with different concentrations of the copper(II) compounds (in the range 0.2-200  $\mu$ M), with an incubation time of 48 h. After treatment, 10  $\mu$ L of MTT (5 mg mL<sup>-1</sup>) (Sigma-Aldrich, St. Louis, MO, USA) were added to each well, and the plates were incubated at 37 °C for another 3 h. The purple formazan crystals were dissolved in 50  $\mu$ L SDS, and the plates were kept in the dark overnight. The absorbance was measured at 545 nm using a Stat Fax 2100 microplate reader (Awareness Technology, Palm City, FL, USA).

For the Ru(II) compounds and the metallohelicates, the cells ( $1 \times 10^5$  cells per mL) were seeded in 96-well plates and allowed to grow for 24 h. After treatment, 10  $\mu$ M of MTT (Sigma-Aldrich) were added to each well, and the cells were incubated for an additional 4 h. DMSO (Amresco Inc., Cleveland, OH, USA) was added in control cells. Afterwards, the media

was aspirated, and the blue formazan precipitate was dissolved in 100  $\mu$ L of DMSO. The absorbance at 570 nm was measured on a multi-well plate reader (Multiskan FC, Thermo Scientific). The cell viability was calculated according to equation (4).

$$Viability (\%) = \frac{Absorbance\ of\ the\ treated\ wells}{Absorbance\ of\ the\ control\ wells} \times 100 \quad (4)$$

The cell viability was expressed as the percentage of control cells, and data are shown as the mean value  $\pm$  S.D. of three independent experiments.<sup>101</sup>

### Single point assays

Single-point experiments allow to rapidly determine the range of effectiveness of compounds. In the present work, two concentrations were used, namely 10 and 50  $\mu$ M, with incubation times of 24 and 48 h. The cell viability is expressed as a percentage compared to control cells, and the data are shown as the mean value  $\pm$  S.D. of three independent experiments.

### IC<sub>50</sub> Determination

IC<sub>50</sub>s (inhibitory concentrations) were determined for each studied compound in the cell line(s) in which it was the most efficient.<sup>98,101</sup> To obtain dose–response curves, the cells were treated with increasing concentrations of the different compounds; from these plots, the concentrations required for 50% inhibition (IC<sub>50</sub> values) were calculated using GraphPad Prism V5.0 for windows (Graphpad Software, San Diego, CA, USA). The IC<sub>50</sub>s (in  $\mu$ M) are shown as the mean value  $\pm$  S.D. of three independent experiments.

### Fluorescence spectroscopy assays

#### Immunofluorescence technique

SW620 cells ( $2 \times 10^5$  cells mL<sup>-1</sup>) were cultured in a 12-well plate containing glass coverslips and were incubated for 24 and 48 h, with IC<sub>25</sub> concentrations of the compounds investigated. The cells were then washed with 1  $\times$  PBS and fixed with 4% paraformaldehyde in PBS, during 20 minutes at room temperature. The fixed cells were permeabilized with 0.2% Triton™ X-100; then, the coverslips were washed twice with 1  $\times$  PBS and treated for 2 h at RT with blocking solution (PBS-Tween-20 0.1%, 0.1% Bovine Serum Albumin, and 10% normal goat serum). The cells were incubated for 1 h with the nuclear marker TO-PRO™-3 iodide (1:400, Cat T3605, Molecular Probes). Afterwards, the coverslips were washed with PBS and placed on slides with Mowiol (Sigma-Aldrich, St. Louis, MO, USA). The immunofluorescence





images were captured using a Leica TCS-SL filter-free spectral confocal microscope (Leica Microsystems). Independent experiments were performed, and the fluorescence intensities ( $n = 30/\text{condition}$ ) were normalized and quantified using the ImageJ software.

All reagents were from Sigma-Aldrich apart from TO-PRO<sup>®</sup>-3 iodide (Molecular Probes, Invitrogen AG, Basel, Switzerland).

### **Flow Cytometry**

The cell cycle represents one of the most significant and fundamental processes in eukaryotic cells, which results in cell growth and division. The regulation of the cell cycle is critical to cell survival, as it manages the repair of genetic damage as well as the prevention of uncontrolled cell division. A largely described feature of carcinogenic cells is the fact that they present defects in their cell-cycle regulation, which leads to mutations in genes involved in cell-cycle control. One of the techniques that became increasingly popular is the cell-cycle analysis. This technique is very useful to study the mechanism of action of potential anti-cancer compounds, so as to investigate cell-division mechanisms. Flow cytometry allows rapid quantitative measurements of the percentage of cells in the G0/G1, S, and G2/M phases of the cell cycle.<sup>102</sup>

Fluorescent propidium iodide (PI) was used to classify the cells and to assign them to different phases of the cell cycle; this discrimination is based on the distinct DNA contents of the cell at the different phases. It is known that resting cells (G0/G1) contain two copies of each chromosome. As the cells undergo cell division, they start to synthesize chromosomal DNA (S phase). Consequently, the fluorescence intensity of PI increases, the maximum intensity being reached when the quantity of DNA has doubled (G2/M phase). As a matter of fact, the fluorescence intensity of G2/M cells is twice that of G0/G1 cells. The G2/M cells eventually divide into two cells. The histogram obtained reflects the percentage of cells at the distinct stages of the cycle, *i.e.* G, S, and G/M phases.

SW620 cells ( $2 \times 10^5$  cells/mL) were cultured in a 6-well and were incubated for 24 h with IC<sub>50</sub> concentrations of the studied compounds. The cells were subsequently trypsinized, collected and centrifuged at 300 x g for 5 minutes. The supernatant was discarded without disturbing the cell pellets. An appropriated volume of PBS was added to each tube to obtain a concentration of  $1 \times 10^6$  cells mL<sup>-1</sup>. The cells were centrifuged at 300 x g for 5 minutes. The supernatant was removed and discarded without disturbing the cell pellets. Approximately 50 µL of PBS per  $1 \times 10^6$  cells were added and the pellets were resuspended. The resuspended cells were added drop-wise into a tube containing 1 mL of ice-cold ethanol (70%), while

vortexing at medium speed. The samples were then freeze-dried at  $-20\text{ }^{\circ}\text{C}$  for at least 3 hours prior to staining. 200  $\mu\text{L}$  of ethanol-fixed cells were recovered and centrifuged at  $300 \times g$  for 5 minutes at room temperature. The supernatant was removed and discarded without disturbing the cell pellets. Approximately 250  $\mu\text{L}$  of PBS were added to obtain a cell concentration of around  $5 \times 10^5\text{ cells mL}^{-1}$ . This step was repeated to eliminate all the fixing solution. The cell pellets were resuspended in 200  $\mu\text{L}$  of Muse™ Cell Cycle Reagent and incubated for 30 minutes at room temperature, protected from light. The suspension was transferred into a 1.5-mL microcentrifuge tube prior to analysis with a Muse™ Cell Analyzer.

The results are expressed as the mean  $\pm$  SEM of at least three independent experiments. One-way ANOVAs were carried out with the Statgraphics centurion statistical package and post-hoc Tukey analyses were performed.

### **Cell migration – Wound-Healing assay**

The movement of individual cells, cell sheets and clusters from one location to another is defined as cell migration.<sup>103</sup> Cell invasion is defined as the 3-dimensional migration of cells penetrating an extracellular matrix (ECM).<sup>104</sup> Migration in a wound-healing process is highly regulated; it is achieved by different cell types including keratinocytes, fibroblasts, endothelial cells and macrophages, and involves a variety of growth factors, used as stimulants to facilitate wound healing. In cancer, metastasis is a multistep process employed by cancer cells to spread. Since metastatic carcinomas are the leading cause of high mortality of patients with cancer, their regulators represent targets of choice for the development of anti-metastatic therapies.<sup>105,106</sup>

The wound-healing assay allows to study cell migration and cell-to-cell interactions, and to assess the effect of compounds on them.<sup>107</sup>

The cell-migration activity was thus evaluated using wound-healing experiments. The cells ( $1 \times 10^5\text{ cells/mL}$ ) were seeded in a 12-well plate and allowed to grow for 24 h. Cell division (proliferation) was blocked by adding 10  $\mu\text{g/mL}$  mitomycin C. After 24 h, the cells reached a density of approximately 80%; subsequently, an incision was made using a plastic pipette tip to produce a clean wound area (schematically represented in Figure 85). The cells were then treated with each compound using concentrations of 100 and 150  $\mu\text{M}$ , and images were regularly taken during 36 h. The images were observed under an inverted phase contrast microscope (Axio Observer Z1, Gottingen, Germany). The area closure was quantified using the MRI Wound Healing Tool macro for ImageJ ([http://dev.mri.cnrs.fr/projects/imagej-macros/wiki/Wound\\_Healing\\_Tool](http://dev.mri.cnrs.fr/projects/imagej-macros/wiki/Wound_Healing_Tool)).



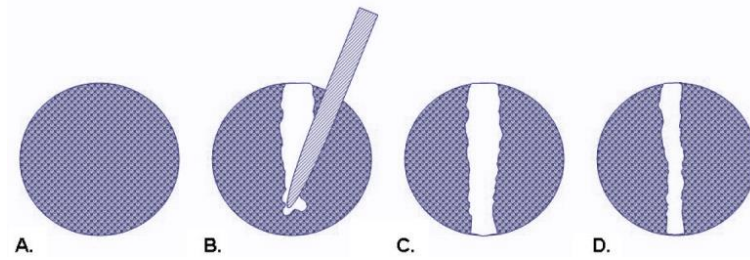


**Figure 85: Scratch Assay.** A wound is introduced into a confluent monolayer of cells (A) by drawing a tip across the cell layer (B). The denuded area is imaged to measure the boundary of the wound at pre-migration (C), and after cells have migrated inward to fill the void (D).

The results are expressed as the mean  $\pm$  SEM of at least three independent experiments. One-way ANOVAs were carried out with the Statgraphics centurion statistical package and post-hoc Tukey analyses were performed.

## Chapter I – Copper Complexes

### Preparation of the Schiff bases

The ligands were obtained through a condensation reaction between a hydrazinyl derivative and a monoaldehyde or a dialdehyde in refluxing methanol. After four hours, the pure precipitated ligands were collected by filtration and dried under reduced pressure.

#### **2-tert-butyl-6-(pyridin-2-ylhydrazonomethyl)phenol (HL1)**

Yield = 1.78 g (6.6 mmol, 66%).  $^1\text{H}$  NMR ( $[\text{D}_6]$ DMSO):  $\delta$  = 12.00 (s, OH), 11.48 (s, 1H), 8.23 (s, 1H), 8.19 (d, 1H,  $J$  = 8 Hz), 7.70 (t, 1H,  $J$  = 8 Hz), 7.19 (t, 2H,  $J$  = 8 Hz), 6.84 (m, 3H), 1.40 (s, 9 H) ppm; IR (KBr):  $\bar{\nu}$  = 3452, 3200, 3047, 3000, 3000, 2869, 1950, 1700, 1600, 1578, 1439  $\text{cm}^{-1}$ ; elemental analysis calculated for  $\text{C}_{16}\text{H}_{19}\text{N}_3\text{O}$  (269.35): C 71.35, H 7.11, N 15.60; found: C 71.66, H 7.22, N 15.64.

#### **2-tert-butyl-6-(quinolin-2-ylhydrazonomethyl)phenol (HL2)**

Yield = 2.71 g (8.5 mmol, 85%).  $^1\text{H}$  NMR ( $[\text{D}_6]$ DMSO):  $\delta$  = 12.00 (s, OH), 11.48 (s, 1H), 8.31 (s, 1H), 8.82 (d, 1H,  $J$  = 8 Hz), 7.79 (d, 1H,  $J$  = 8 Hz), 7.63 (m, 3H), 7.30 (t, 1H,  $J$  = 8 Hz), 7.22 (d, 2H,  $J$  = 8 Hz), 7.18 (d, 1H,  $J$  = 8 Hz), 6.86 (t, 1H,  $J$  = 8 Hz), 1.43 (s, 9H) ppm; IR (KBr):  $\bar{\nu}$  = 3439, 3334, 3047, 3004, 2947, 2665, 1950, 1700, 1600, 1508, 1430  $\text{cm}^{-1}$ ; elemental analysis calculated for  $\text{C}_{20}\text{H}_{21}\text{N}_3\text{O}$  (319.41): C 75.21, H 6.63, N 13.16; found: C 75.13, H 6.71, N 13.14.

#### **4-tert-butyl-2,6-bis-(pyridin-2-ylhydrazonomethyl)phenol (HL3)**

Yield = 1.77 g (4.6 mmol, 91%).  $^1\text{H}$  NMR ( $[\text{D}_6]$ DMSO):  $\delta$  = 12.00 (OH), 11.48 (s, 2H), 8.35 (s, 2H), 8.18 (d, 2H,  $J$  = 8 Hz), 7.68 (t, 2H,  $J$  = 8 Hz), 7.61 (s, 2H), 7.07 (d, 2H,  $J$  = 8 Hz), 6.79 (t, 2H,  $J$  = 8 Hz), 1.32 (s, 9H) ppm; IR (KBr):  $\bar{\nu}$  = 3434, 3191, 3104, 2952, 2852, 1950, 1700, 1600, 1565, 1434  $\text{cm}^{-1}$ ; elemental analysis calculated for  $\text{C}_{22}\text{H}_{24}\text{N}_6\text{O}$  (388.48): C 68.02, H 6.23, N 21.63; found: C 67.99, H 6.37, N 21.63.

#### **4-tert-butyl-2,6-bis-(quinolin-2-ylhydrazonomethyl)phenol (HL4)**

Yield = 1.95 g (4.0 mmol, 80%).  $^1\text{H}$  NMR ( $[\text{D}_6]$ DMSO):  $\delta$  = 12.00 (s, OH), 11.48 (s, 2H), 8.47 (s, 1H), 8.20 (d, 1H,  $J$  = 8 Hz), 7.79 (d, 1H,  $J$  = 8 Hz), 7.60 (m, 3H), 7.43 (d, 1H,  $J$  = 8 Hz), 7.29 (t, 1H,  $J$  = 8 Hz), 1.35 (s, 9H) ppm; IR (KBr):  $\bar{\nu}$  = 3421, 3203, 3042, 2951, 2846, 1950, 1700, 1613, 1504, 1434  $\text{cm}^{-1}$ ; elemental analysis calculated for  $\text{C}_{30}\text{H}_{28}\text{N}_6\text{O}$  (488.60): C 73.75, H 5.78, N 17.20; found: C 73.65, H 5.72, N 16.84.





### *Preparation of the complexes*

As perchlorate salts are potentially explosive, all the reactions bellow were handled with extreme care.<sup>108</sup>

#### **[Cu(L1)Cl]·CH<sub>3</sub>OH (Cu1)**

Yield = 62% (92 mg, 0.23 mmol, based on HL1). IR (KBr):  $\bar{\nu}$  = 3439, 3195, 3121, 3039, 2860, 1950, 1700, 1617 cm<sup>-1</sup>; elemental analysis calculated for C<sub>17</sub>H<sub>22</sub>ClCuN<sub>3</sub>O<sub>2</sub> (399.37): C 51.13, H 5.55, N 10.52; found: C 52.28, H 5.01, N 11.35.

#### **[Cu(L2)NO<sub>3</sub>] (Cu2)**

Yield = 44% (61 mg, 0.14 mmol, based on HL2). IR (KBr):  $\bar{\nu}$  = 3386, 2956, 2865, 2782, 2413, 1950, 1700, 1621 cm<sup>-1</sup>; elemental analysis calculated for C<sub>20</sub>H<sub>20</sub>CuN<sub>4</sub>O<sub>4</sub> (443.95): C 54.14, H 4.54, N 12.62; found: C 53.88, H 4.62, N 12.33.

#### **[Cu<sub>2</sub>(L3)(ClO<sub>4</sub>)<sub>2</sub>(CH<sub>3</sub>O)(CH<sub>3</sub>OH)]·CH<sub>3</sub>OH (Cu3)**

Yield = 71% (177 mg, 0.22 mmol, based on HL3). IR (KBr):  $\bar{\nu}$  = 3404, 2965, 2865, 2765, 2421, 1950, 1700, 1630 cm<sup>-1</sup>; elemental analysis calculated for C<sub>25</sub>H<sub>34</sub>Cl<sub>2</sub>Cu<sub>2</sub>N<sub>6</sub>O<sub>12</sub> (808.58): C 37.14, H 4.24, N 10.39; found: C 36.70, H 4.12, N 10.20.

#### **[Cu<sub>2</sub>(L4)(ClO<sub>4</sub>)(OH)(CH<sub>3</sub>OH)]ClO<sub>4</sub> (Cu4)**

Yield = 63% (114 mg, 0.13 mmol, based on HL4). IR (KBr):  $\bar{\nu}$  = 3439, 3217, 3060, 2960, 2600, 1950, 1700, 1626 cm<sup>-1</sup>; elemental analysis calculated for C<sub>31</sub>H<sub>32</sub>Cl<sub>2</sub>Cu<sub>2</sub>N<sub>6</sub>O<sub>11</sub> (862.63): C 43.16, H 3.74, N 9.74; found: C 42.98, H 3.53, N 9.74.

#### **[Cu<sub>8</sub>(L3)<sub>4</sub>(NO<sub>3</sub>)<sub>4</sub>(OH)<sub>5</sub>](NO<sub>3</sub>)<sub>3</sub>·(CH<sub>3</sub>OH)<sub>5</sub>·(H<sub>2</sub>O)<sub>8</sub> (Cu5)**

Yield = 53% (99 mg, 0.03 mmol, based on HL3). IR (KBr):  $\bar{\nu}$  = 3452, 3226, 2952, 2865, 2352, 1950, 1700, 1617 cm<sup>-1</sup>; elemental analysis calculated for [Cu<sub>5</sub> – 3 CH<sub>3</sub>OH + 7 H<sub>2</sub>O], C<sub>90</sub>H<sub>127</sub>Cu<sub>8</sub>N<sub>31</sub>O<sub>47</sub> (2887.55): C 37.23, H 4.41, N 14.95; found: C 36.70, H 4.12, N 15.20.

#### **[Cu<sub>3</sub>(HL2')<sub>4</sub>Cl<sub>6</sub>]·(CH<sub>3</sub>OH)<sub>6</sub> (Cu6)**

Yield = 55% (84 mg, 0.045 mmol, based on HL2). IR (KBr):  $\bar{\nu}$  = 3460, 3239, 3100, 2952, 2800, 1950, 1700, 1621 cm<sup>-1</sup>; elemental analysis calcd for [Cu<sub>6</sub> – 6 CH<sub>3</sub>OH + 6 H<sub>2</sub>O], C<sub>80</sub>H<sub>88</sub>Cl<sub>6</sub>Cu<sub>3</sub>N<sub>12</sub>O<sub>10</sub> (1781.01.18): C 53.95, H 4.98, N 9.44; found: C 53.40, H 4.80, N 9.40.

**X-ray crystallography:** Data for compounds **Cu1**, **Cu2**, **Cu4** and **Cu6** were obtained at 100(2) K with a Bruker APEX II CCD diffractometer on the Advanced Light Source beamline 11.3.1 at Lawrence Berkeley National Laboratory, from a silicon 111 monochromater ( $\lambda$  = 0.7749 Å). Data for compounds **Cu3** and **Cu5** were recorded at 190(2) K on a Bruker

APEX II equipped with a CCD area detector and a graphite monochromator (MoK $\alpha$  radiation  $\lambda = 0.71073$  Å). Data reduction and absorption corrections were performed with SAINT and SADABS, respectively. The structures were solved with SIR92 (**Cu1**, **Cu2**, **Cu4**, **Cu6**)<sup>109</sup> and SIR97 (**Cu3**, **Cu5**),<sup>110</sup> and refined on  $F^2$  with SHELXTL (**Cu1**, **Cu2**, **Cu4**, **Cu6**) and SHELX97 (**Cu3**, **Cu5**).<sup>111,112</sup> The PLATON SQUEEZE procedure<sup>113</sup> was used for compound **Cu5** to treat regions of diffuse solvent, which could not be sensibly modelled in terms of atomic sites. Their contribution to the diffraction pattern was removed and modified  $F_o^2$  written to a new HKL file. The number of electrons thus located, 150 per unit cell, were included in the formula, formula weight, calculated density,  $\mu$  and  $F(000)$ . This residual electron density was assigned to eight methanol molecules per unit cell.

Crystallographic and refinement parameters, selected bond distances and angles are summarized in the previous chapters. The CIFs can be obtained free of charge from The Cambridge Crystallographic Data Centre via [www.ccdc.cam.ac.uk/data\\_request/cif](http://www.ccdc.cam.ac.uk/data_request/cif) in CIF format with CCDC numbers 964834–964839.

### *DNA-Binding Studies*

#### **UV-Vis Spectroscopy**

The spectroscopic data were fitted to equation (1), and the intrinsic binding constants  $K_b$  were subsequently determined.<sup>10,25</sup>



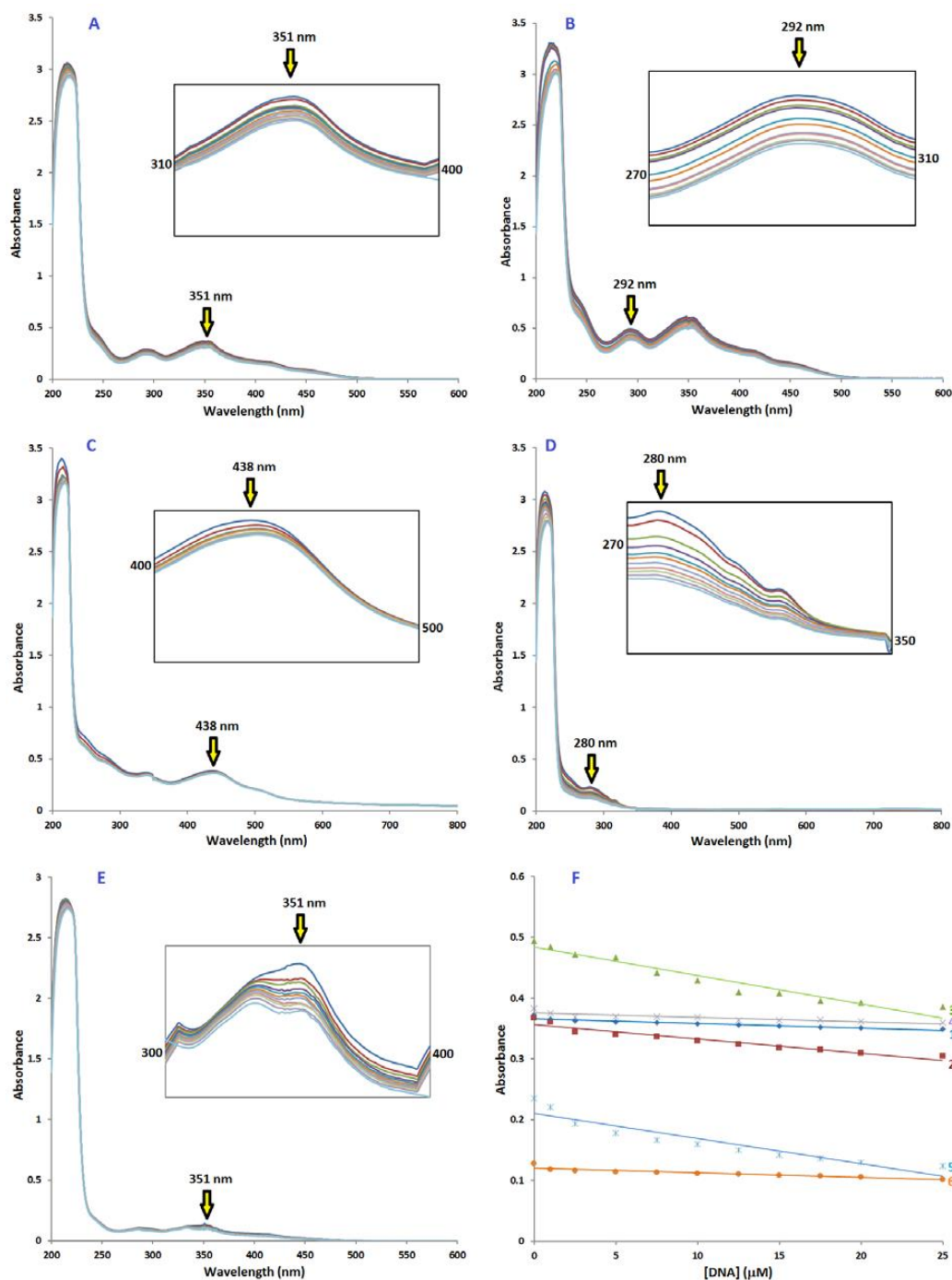


Figure 86: A to E. Absorption spectra of complexes Cu<sub>2</sub> to Cu<sub>6</sub> in 5 mM Tris-HCl–50 mM NaCl (pH = 7.2) upon addition of ct-DNA ([DNA]: 0–25 μM) at a constant concentration of complex (25 μM); F. Absorbance vs. [DNA] plots for Cu<sub>1</sub> to Cu<sub>6</sub>.

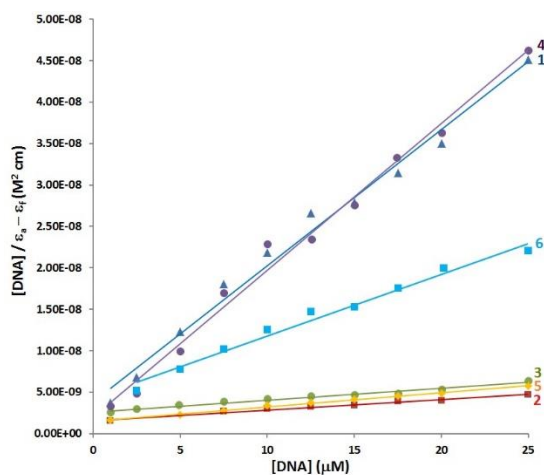


Figure 87: Plots of  $[DNA] / \epsilon_a - \epsilon_f$  vs.  $[DNA]$  for the titration of ct-DNA with complexes Cu1 to Cu6 at the corresponding wavelengths indicated by yellow arrows in Figure 88 (see above).

### ESI-MS and EPR spectroscopy

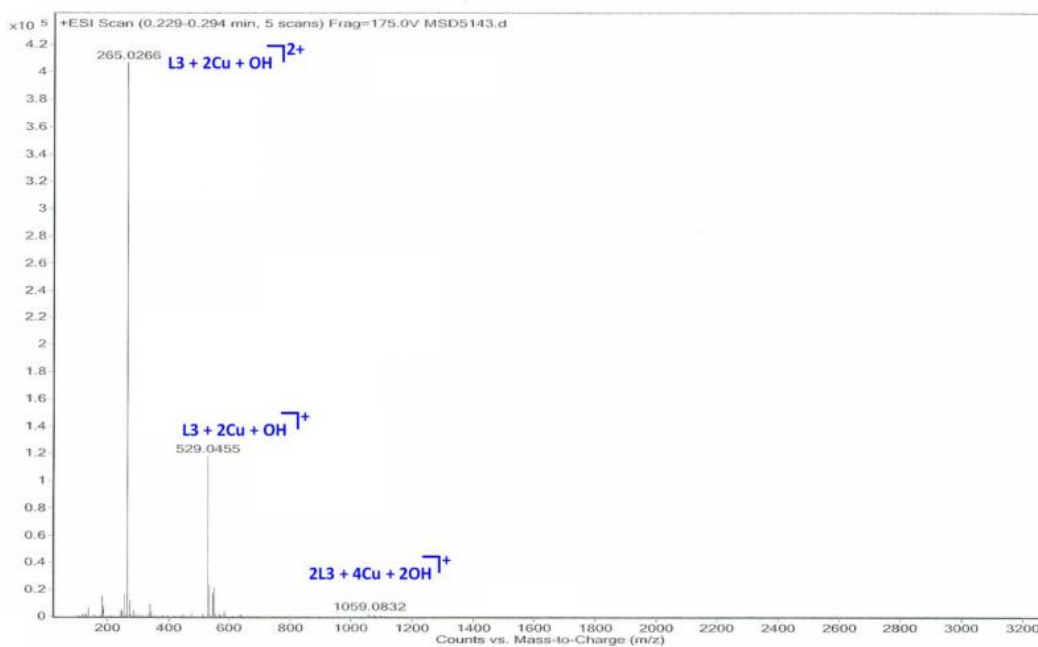


Figure 88: ESI-MS spectrum for compound Cu5 ( $m/z$  range 0–3200).



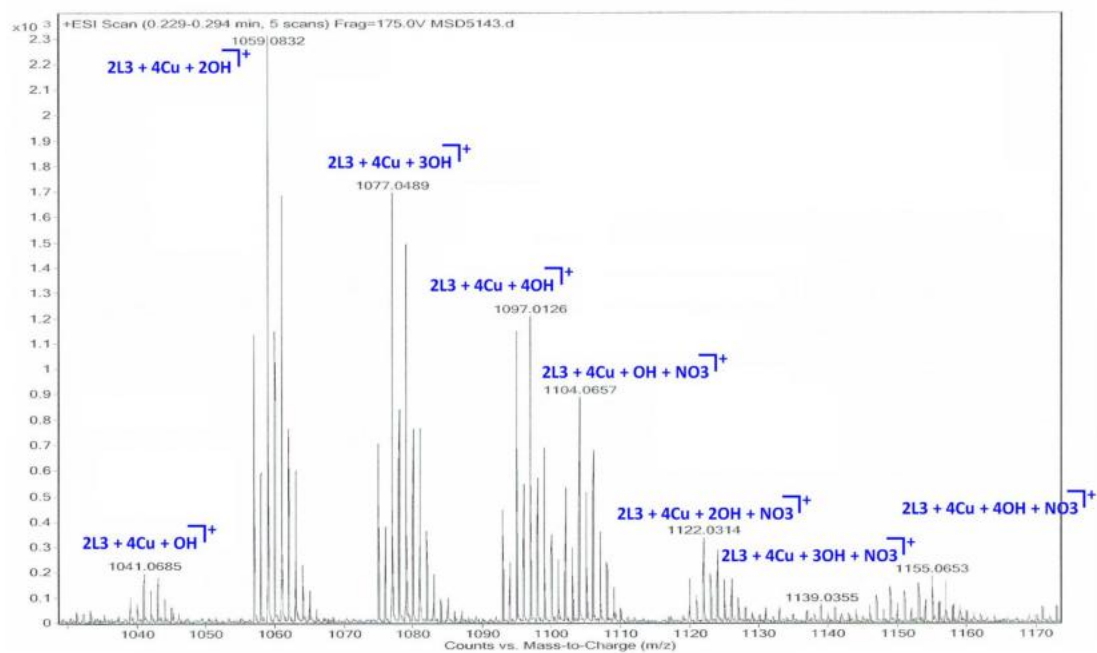


Figure 89: ESI-MS spectrum for compound Cu5 (m/z range 1030–1170).

## Fluorescence dye displacement

### Ethidium Bromide Displacement Assay

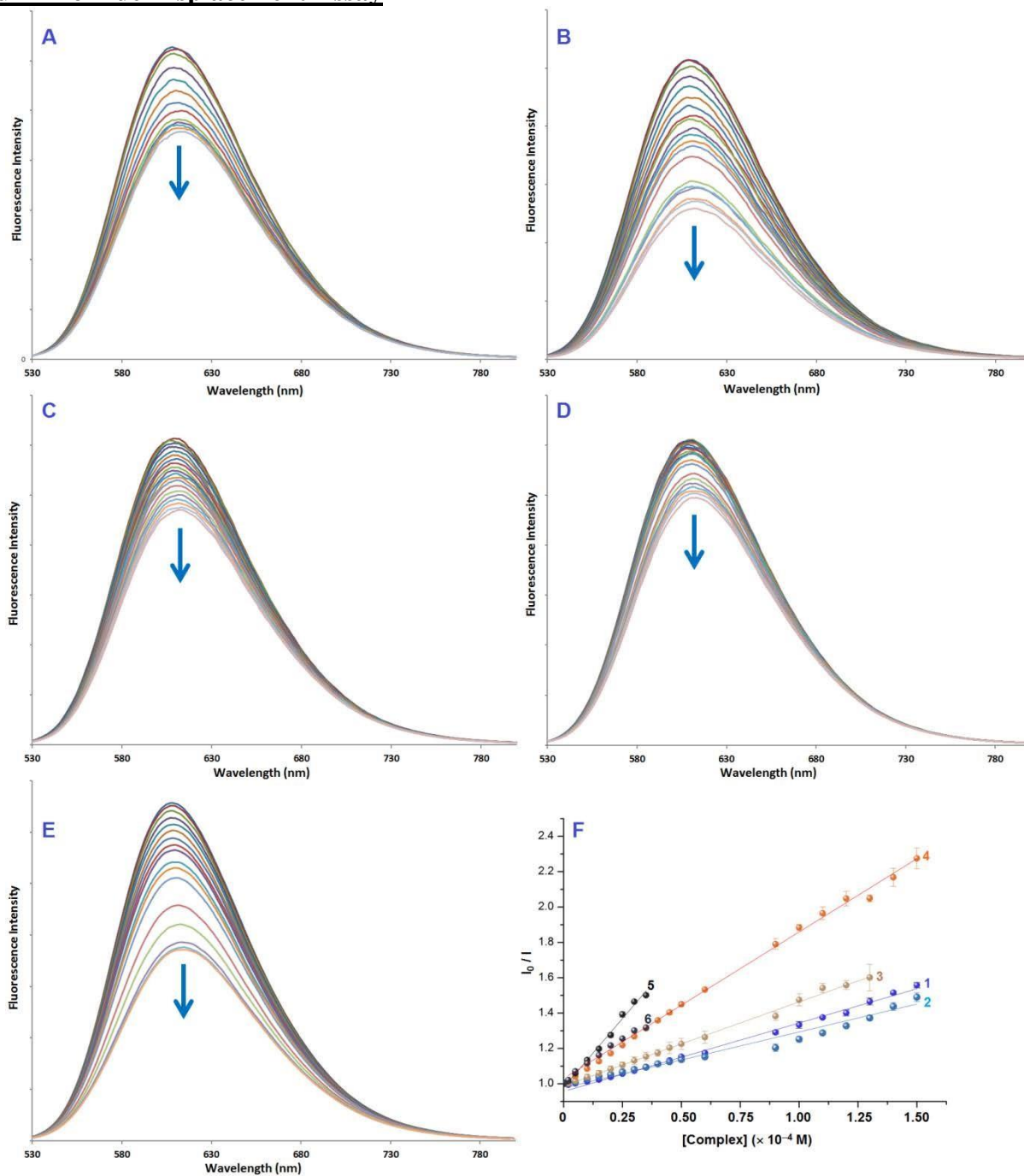
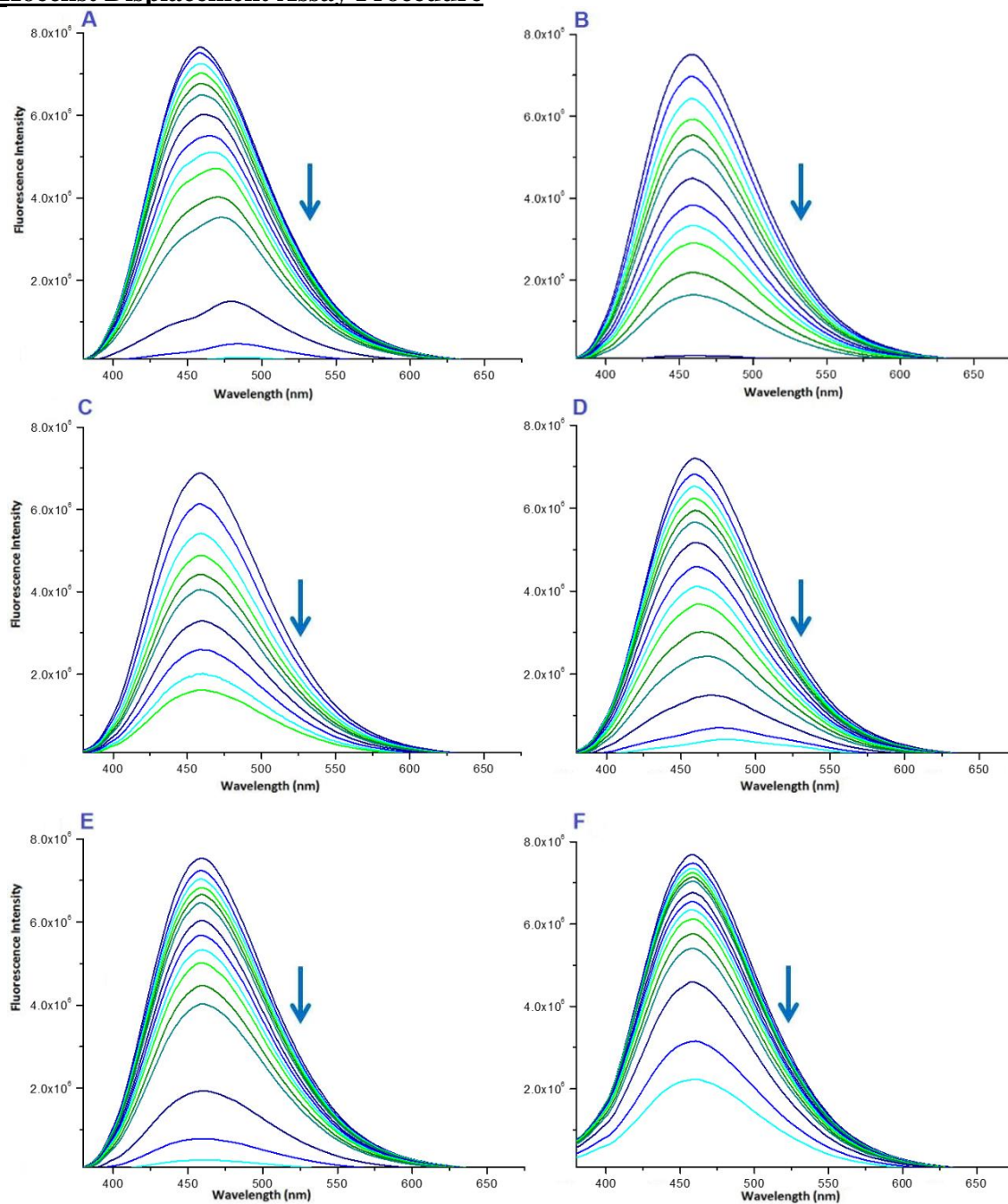


Figure 90: A to E. Emission spectra of the DNA-EB complex (2.5 and 12.5  $\mu\text{M}$ ),  $\lambda_{\text{exc}} = 514 \text{ nm}$ ,  $\lambda_{\text{em}} = 610 \text{ nm}$ , upon addition of increasing amounts of complexes Cu2 to Cu6 (2–150  $\mu\text{M}$ ). The arrows show the diminution of the emission intensity with the increase of complex concentration. F.  $I_0/I$  vs. [complex] plots for the titration of DNA-EB with complexes Cu1 to Cu6 at  $\lambda_{\text{exc}} = 514 \text{ nm}$  and  $\lambda_{\text{em}} = 610 \text{ nm}$ . Concentrations of complex: 2 to 150  $\mu\text{M}$ ; [DNA]: 2.5  $\mu\text{M}$ ; [EB]: 12.5  $\mu\text{M}$ .



### Hoechst Displacement Assay Procedure



**Figure 91: A to F.** Emission spectra of the DNA-Hoechst complex (0.19 and 15  $\mu\text{M}$ ),  $\lambda_{\text{exc}} = 350 \text{ nm}$ ,  $\lambda_{\text{em}} = 450 \text{ nm}$ , upon addition of increasing amounts of complexes Cu1 to Cu6 (12.5  $\mu\text{M}$ , 2–150  $\mu\text{M}$ ). The arrows show the diminution of the emission intensity with the increase of complex concentration.

### **Circular Dichroism**

Stock solutions of the copper(II) compounds were prepared in 40 mM HEPES/10 mM MgCl<sub>2</sub> buffer (pH = 7.2) containing 2% DMSO.

### **Gel electrophoresis**

#### **Agarose Gel electrophoresis**

Gel electrophoresis experiments: Stock solutions of the copper(II) compounds were prepared in 40 mM HEPES/10 mM MgCl<sub>2</sub> buffer (pH = 7.2) containing 2% DMSO. pBR322 plasmid DNA aliquots (0.2 µg mL<sup>-1</sup>) in 40 mM HEPES/10 mM MgCl<sub>2</sub> buffer were incubated with the complexes for 24 h at 37°C. Subsequently, ascorbic acid (100 µM in 40 mM HEPES/10 mM MgCl<sub>2</sub> buffer) was added and the resulting mixture (containing 200 ng of DNA in a 100 µM solution of complex) was incubated at 37 °C for an additional hour. Next, the reaction samples were quenched with 4 µL of xylene cyanol and subsequently electrophoretized on agarose gel (1% in TAE buffer, tris-acetate-EDTA) for 2 h at 1.5 V cm<sup>-1</sup>, using a BIORAD horizontal tank connected to a PHARMACIA GPS 200/400 variable potential power supply. Samples of free DNA and DNA in presence of ascorbic acid were used as controls. Afterwards, the DNA was stained with SYBR<sup>®</sup> safe and the gel was photographed with a BIORAD Gel Doc<sup>TM</sup> EZ Imager.





## Chapter II - Ruthenium Complexes

### Structure of the complexes

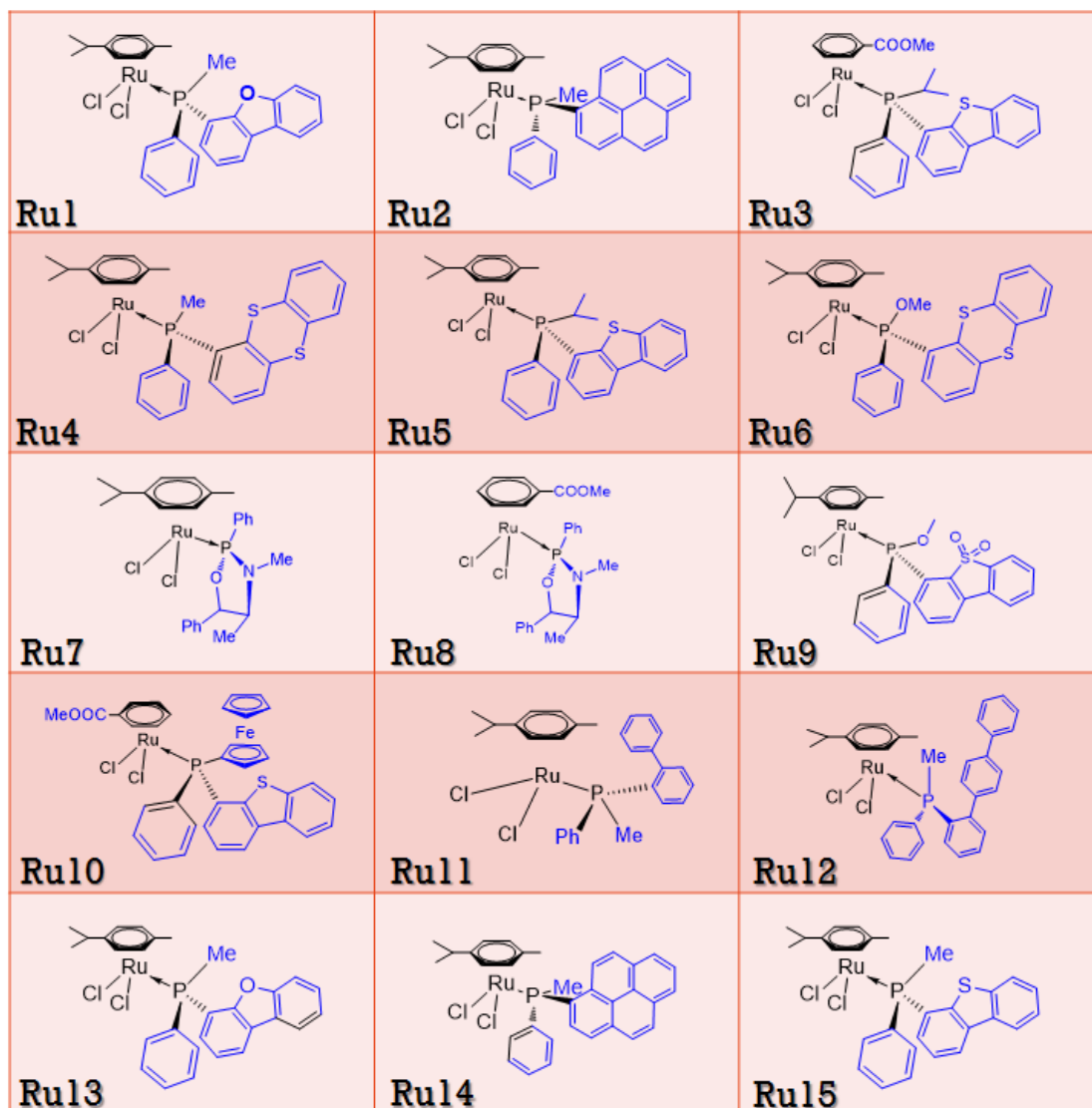


Figure 32: First series of Ru(II)-arene compounds used in the present study.<sup>114,115</sup>

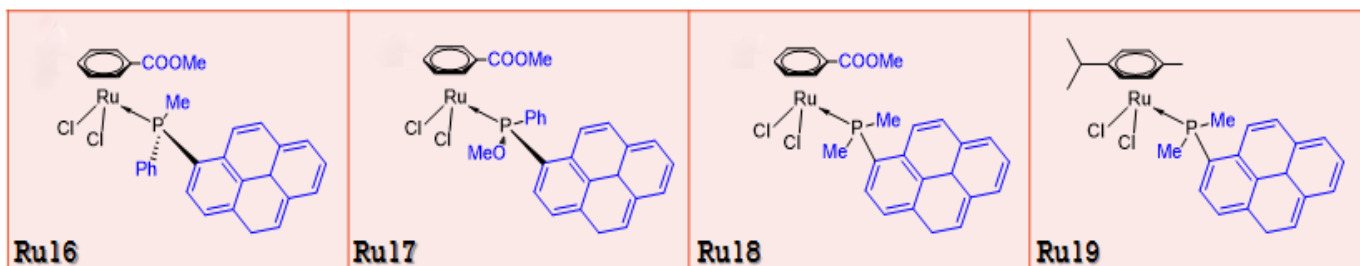


Figure 33: Second series of Ru(II)-arene compounds (Ru16-Ru19) used in the present study, whose design is based on the data collected with the first series (Ru1-Ru15).<sup>114,115</sup>

### ***DNA-Binding Studies***

The UV-Vis data could not be fitted to equation (1); therefore, the intrinsic binding constants  $K_b$  for the ruthenium complexes could not be determined.<sup>10,25</sup>





## Fluorescence dye displacement

### Ethidium Bromide Displacement Assay

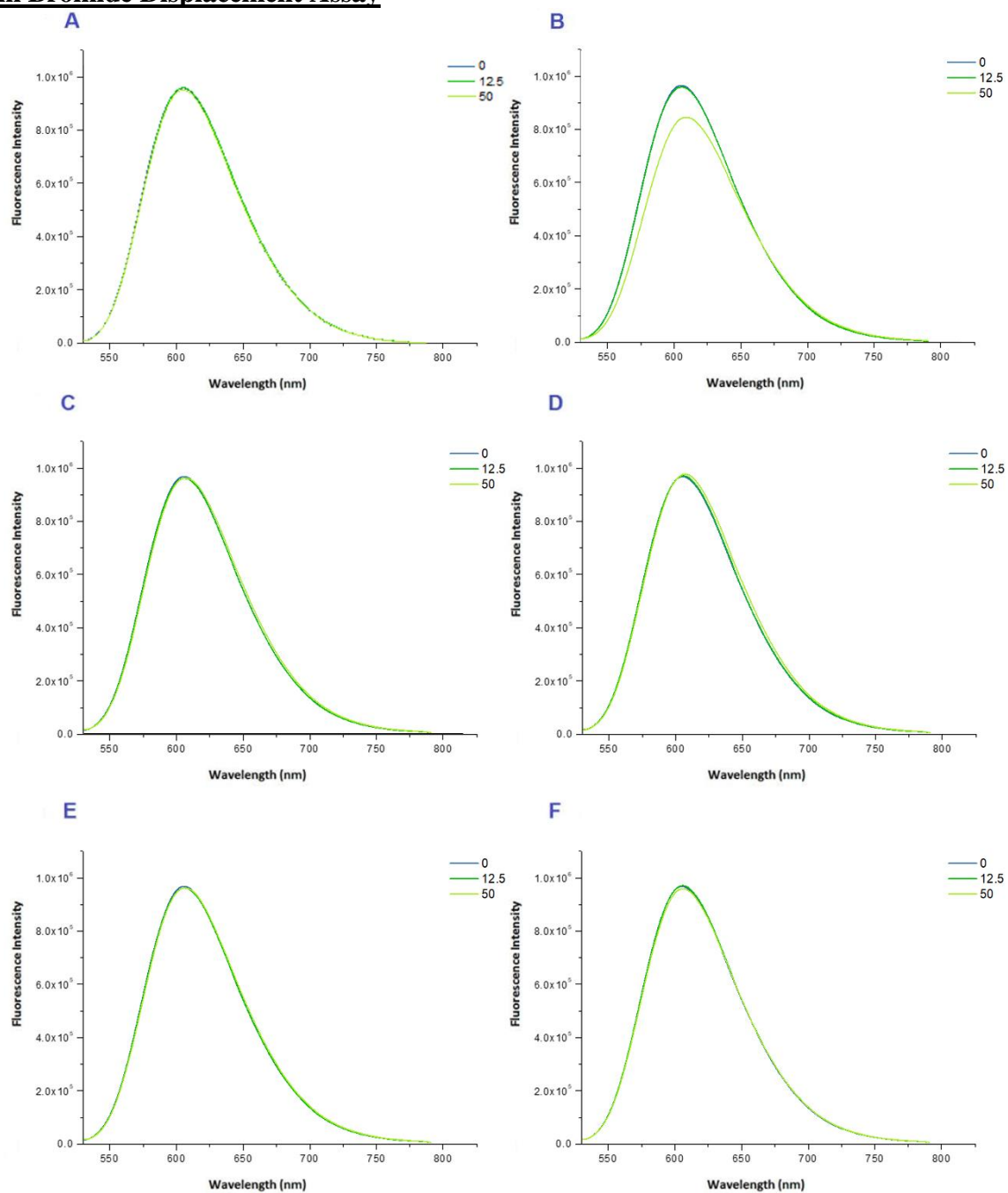


**Figure 92: A to E.** Emission spectra of the DNA-EB complex (2.5 and 12.5  $\mu\text{M}$ ) upon addition of increasing amounts of complexes Ru1 to Ru6 (12.5 and 50  $\mu\text{M}$ ) at  $\lambda_{\text{exc}} = 514 \text{ nm}$  and  $\lambda_{\text{em}} = 610 \text{ nm}$ . Concentrations of complex: 12.5 and 50  $\mu\text{M}$ ; [DNA]: 2.5  $\mu\text{M}$ ; [EB]: 12.5  $\mu\text{M}$ .

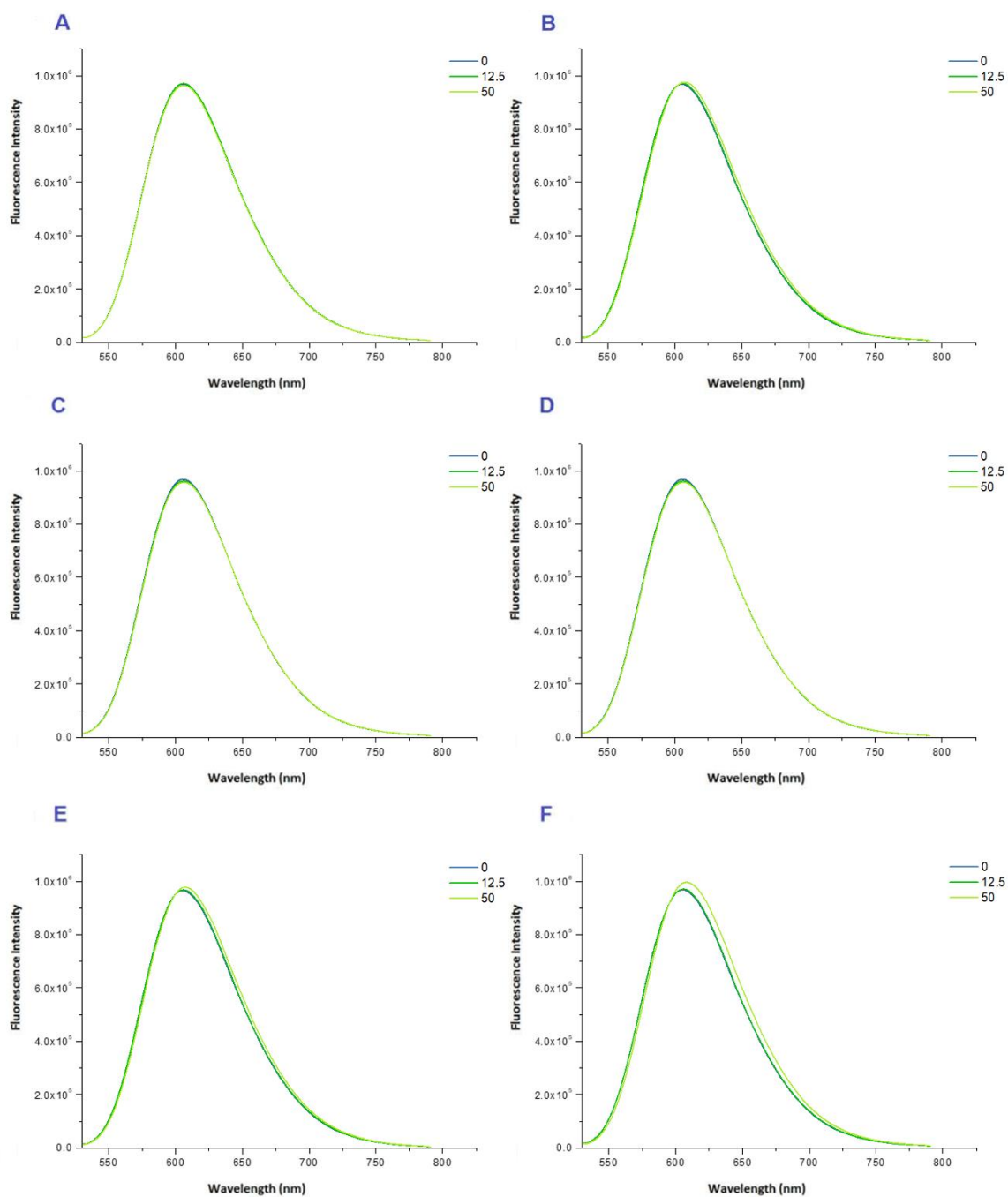


**Figure 93: A to E.** Emission spectra of the DNA-EB complex (2.5 and 12.5  $\mu\text{M}$ ) upon addition of increasing amounts of complexes Ru7 to Ru12 (12.5 and 50  $\mu\text{M}$ ) at  $\lambda_{\text{exc}} = 514 \text{ nm}$  and  $\lambda_{\text{em}} = 610 \text{ nm}$ . Concentrations of complex: 12.5 and 50  $\mu\text{M}$ ; [DNA]: 2.5  $\mu\text{M}$ ; [EB]: 12.5  $\mu\text{M}$ .

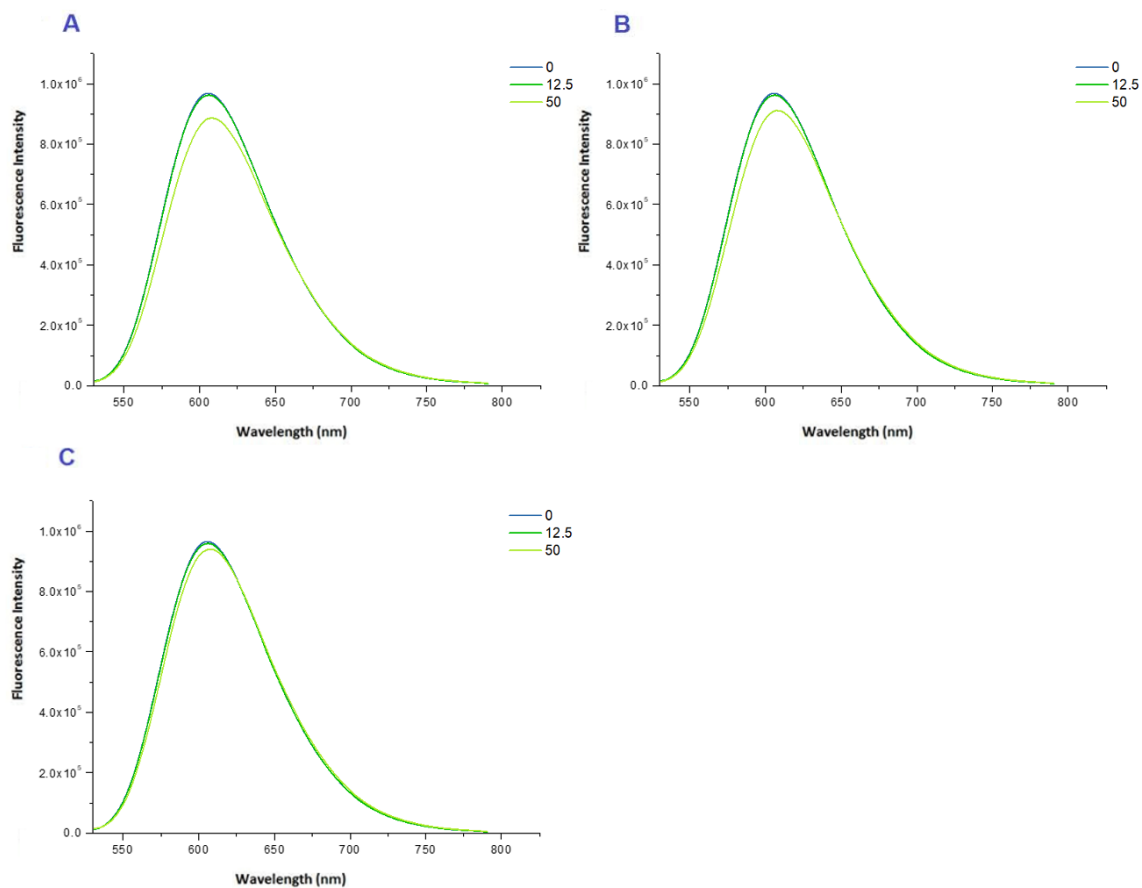


**Figure 94: A to E.** Emission spectra of the DNA-EB complex (2.5 and 12.5  $\mu\text{M}$ ) upon addition of increasing amounts of complexes Ru13 to Ru15 (12.5 and 50  $\mu\text{M}$ ) at  $\lambda_{\text{exc}} = 514$  nm and  $\lambda_{\text{em}} = 610$  nm. Concentrations of complex: 12.5 and 50  $\mu\text{M}$ ; [DNA]: 2.5  $\mu\text{M}$ ; [EB]: 12.5  $\mu\text{M}$ .

### **Chapter III - Helicates**

#### **Preparation of the Poly- $\beta$ -diketones**

The bis- $\beta$ -diketones were prepared through a Claisen condensation between a ketone and an ester, as reported by Dr. Aromí and co-workers.<sup>116</sup>

##### **1,3-bis(3-oxo-3-(2-naphthyl)-propionyl)benzene (H<sub>2</sub>L1)**

To a suspension of 60 % NaH (oil dispersion, 5 g, 132 mmol) in DME (150 mL), dimethyl isophthalate (2.9 g, 15 mmol) was added and the mixture was stirred for 15 min. Then 2-acetonaphthone (5 g, 29 mmol) in DME (50 mL) was added dropwise, and the mixture was heated under reflux for 4 h. A yellow-mustard suspension was formed, which was quenched by addition of EtOH (5 mL), and the resulting solid was then collected by filtration. The solid was suspended in H<sub>2</sub>O (150 mL), the pH was adjusted to 2–3 using 12 % HCl, and the mixture was left for 30 min under stirring. The yellow solid was collected by filtration, washed with water, and dried under vacuum. Yield = 5.47 g (77 %); <sup>1</sup>H NMR (300 MHz, CDCl<sub>3</sub>):  $\delta$ =8.67 (td, H), 8.24 (dd, 2 H), 8.08 (m, 2 H), 7.97 (m, 2 H), 7.91 (d, 2 H), 7.68 (dd, 2 H), 7.62 (m, 2 H), 4.01 (s, 2 H), ppm; Elemental analysis calculated for C<sub>32</sub>H<sub>24</sub>O<sub>4</sub>, C, 81.34; H, 5.12; Found C, 75.91; H, 6.44; (MS (ESI<sup>+</sup>):  $m/z$ : 471.15 [ $M+H$ ]<sup>+</sup>).

##### **1,3-bis-(3-oxo-3-(2-pyridinyl)-propionyl)benzene (H<sub>2</sub>L2)**

To a suspension of 60 % NaH (oil dispersion, 2 g, 50 mmol) in DME (150 mL), 1,3-diacetylbenzene (2 g, 12.3 mmol) was added and the mixture was stirred for 15 min. Then 2-ethylpicolinate (3.4 mL, 24.7 mmol) in DME (50 mL) was added dropwise, and the mixture was heated under reflux overnight. A mustard-green suspension was formed, which was quenched by addition of EtOH (5 mL), and the resulting solid was then collected by filtration. The solid was suspended in H<sub>2</sub>O (150 mL), the pH was adjusted to 2–3 using 12 % HCl, and the mixture was left for 30 min under stirring. The yellow solid was collected by filtration, washed with water, and dried under vacuum. Yield = 2.7 g (59 %); <sup>1</sup>H NMR (300 MHz, CDCl<sub>3</sub>):  $\delta$ =7.43 (m, 2 H), 7.56 (m, 2 H), 7.66 (s, 2 H), 7.86 (t, 2 H), 8.16 (d, 2 H), 8.21 (dd, 2 H), 8.69 (m, 2 H), 16.45 ppm (br s, 2 H); Elemental analysis calculated for (). MS (ESI<sup>+</sup>):  $m/z$ : 373.12 [ $M+H$ ]<sup>+</sup>.

##### **1,3-bis-(3-oxo-3-(3-pyridinyl)-propionyl)benzene (H<sub>2</sub>L3)**

To a suspension of 60 % NaH (oil dispersion, 2 g, 50 mmol) in DME (150 mL), dimethyl isophthalate (5 g, 26 mmol) was added and the mixture was stirred for 15 min. Then 3-acetylpyridine (5.6 mL, 52 mmol) in DME (50 mL) was added dropwise, and the mixture





was heated under reflux for 4 h. A pale-yellow suspension was formed, which was quenched by addition of EtOH (5 mL) and the resulting solid was then collected by filtration. The solid was suspended in H<sub>2</sub>O (150 mL), the pH was adjusted to 2–3 using 12 % HCl, and the mixture was left for 30 min under stirring. The yellow solid was collected by filtration, washed with water, and dried under vacuum. The solid obtained was analysed by <sup>1</sup>H NMR and MS (ESI<sup>+</sup>), which revealed that the expected compound was not produced.

#### **1,3-bis-(3-oxo-3-(4-pyridinyl)–propionyl)benzene (H<sub>2</sub>L4)**

To a suspension of 60 % NaH (oil dispersion, 2 g, 50 mmol) in DME (150 mL), dimethyl isophthalate (5 g, 26 mmol) was added and the mixture was stirred for 15 min. Then 4-acetylpyridine (5.6 mL, 52 mmol) in DME (50 mL) was added dropwise, and the mixture was heated under reflux for 4 h. A pale-yellow suspension was formed, which was quenched by addition of EtOH (5 mL), and the resulting solid was then collected by filtration. The solid was suspended in H<sub>2</sub>O (150 mL), the pH was adjusted to 2–3 using 12 % HCl, and the mixture was left for 30 min under stirring. The yellow solid was collected by filtration, washed with water, and dried under vacuum. The solid was obtained analysed by <sup>1</sup>H NMR and MS (ESI<sup>+</sup>), which revealed that **H<sub>2</sub>L4** was not produced.

#### **Synthesis of 1,3-bis-(3-oxo-3(2-hydroxyphenyl)propionyl)benzene (H<sub>4</sub>L5)**

To a suspension of 60 % NaH (oil dispersion, 2 g, 50 mmol) in DME (150 mL), dimethyl isophthalate (5 g, 26 mmol) was added and the mixture was stirred for 15 min. Then 2'-hydroxyacetophenone (6.14 mL, 52 mmol) in DME (50 mL) was added dropwise, and the mixture was heated under reflux overnight. A yellow suspension formed, which was filtered out. This solid material was stirred in a mixture of 0.1 M HCl (200 mL) and dichloromethane (DCM; 200 mL) for 1 h; the organic phase was then collected using a separating funnel. The aqueous phase was further extracted twice with DCM (2 × 200 mL). The combined organic layers were dried over Na<sub>2</sub>SO<sub>4</sub>, filtered and evaporated under reduced pressure. The remaining residue was redissolved in refluxing EtOH. Upon cooling, a yellow precipitate formed, which was filtered and dried under vacuum. Yield = 5.9 g (56%); <sup>1</sup>H NMR (CDCl<sub>3</sub>, 300 MHz): δ 15.58 (s, 2 H), 12.02 (s, 2 H), 8.48 (s, 1 H), 8.10 (d, 2 H), 7.82 (d, 2 H), 7.63 (t, 1 H), 7.50 (t, 2 H), 7.26 (d, 2 H, J = 8 Hz), 6.96 (t, 2 H), 6.91 (s, 2 H) ppm. Elemental analysis calculated for C<sub>24</sub>H<sub>24</sub>O<sub>6</sub>, C, 70.57; H, 5.92; Found C, 69.68; H, 6.76; MS (ESI<sup>+</sup>): *m/z*: 401.0 [MH]<sup>+</sup>.

### **1,3-bis-(3-oxo-3(3-hydroxyphenyl)propionyl)benzene (H<sub>4</sub>L6)**

To a suspension of 60 % NaH (oil dispersion, 2 g, 50 mmol) in DME (150 mL), dimethyl isophthalate (5 g, 26 mmol) was added and the mixture was stirred for 15 min. Then 2'-hydroxyacetophenone (6.14 mL, 52 mmol) in DME (50 mL) was added dropwise, and the mixture was heated under reflux overnight. A yellow suspension formed, which was filtered. This solid material was stirred in a mixture of 0.1 M HCl (200 mL) and dichloromethane (DCM; 200 mL) for 1 h; the organic phase was then collected using a separating funnel. The aqueous phase was further extracted twice with DCM (2 × 200 mL). The combined organic layers were dried over Na<sub>2</sub>SO<sub>4</sub>, filtered and evaporated. The remaining residue was redissolved in refluxing EtOH. Upon cooling, a yellow precipitate formed, which was filtered and dried under vacuum. Yield = 4.3 g (41%); <sup>1</sup>H NMR (CDCl<sub>3</sub>, 300 MHz): 9.85 (s, 2 H), 8.70 (s, 1 H), 8.13 (d, 2 H), 7.83 (d, 2 H), 7.66 (t, 1 H), 7.50 (s, 2 H), 7.30 (t, 2 H), 3.34 (s, 2 H) ppm. Elemental analysis calculated for C<sub>24</sub>H<sub>24</sub>O<sub>6</sub>, C, 70.57; H, 5.92; Found C, 69.53; H, 6.84; MS (ESI<sup>+</sup>): *m/z*: 403.12 [MH]<sup>+</sup>.

### **1,3-bis-(3-oxo-3(4-hydroxyphenyl)propionyl)benzene (H<sub>4</sub>L7)**

To a suspension of 60 % NaH (oil dispersion, 2 g, 50 mmol) in DME (150 mL), dimethyl isophthalate (5 g, 26 mmol) was added and the mixture was stirred for 15 min. Then 2'-hydroxyacetophenone (6.14 mL, 52 mmol) in DME (50 mL) was added dropwise, and the mixture was heated under reflux overnight. A yellow suspension formed, which was filtered. This solid material was stirred in a mixture of 0.1 M HCl (200 mL) and dichloromethane (DCM; 200 mL) for 1 h; the organic phase was then collected using a separating funnel. The aqueous phase was further extracted twice with DCM (2 × 200 mL). The combined organic layers were dried over Na<sub>2</sub>SO<sub>4</sub>, filtered and evaporated. The remaining residue was redissolved in refluxing EtOH. Upon cooling, a yellow precipitate formed, which was filtered and dried under vacuum. Yield = 6.7 g (63%); <sup>1</sup>H NMR (CDCl<sub>3</sub>, 300 MHz): 9.73 (s, 2 H), 8.22 (d, 2 H), 7.79 (t, 1 H), 7.73 (d, 2 H), 7.56 (t, 2 H), 6.85 (d, 2 H), 3.75 (s, 2 H) ppm; Elemental analysis calculated for C<sub>24</sub>H<sub>24</sub>O<sub>6</sub>, C, 70.57; H, 5.92; Found C, 70.36; H, 6.87; MS (ESI<sup>+</sup>): *m/z*: 403.11 [MH]<sup>+</sup>.

### ***Preparation of the supramolecular complexes***

Six equivalents of NaHCO<sub>3</sub> were slowly added to a solution of three equivalents of the ligand dissolved in THF (30 mL). Then, a solution of 2 equivalents of FeCl<sub>3</sub>·4H<sub>2</sub>O in THF (20 mL) was slowly added. The resulting reaction mixture was refluxed for 45 minutes. Afterwards, the resulting dark red solution was filtered and used for crystallization attempts.





Single crystals were obtained for complexes with ligands **H<sub>2</sub>L1** and **H<sub>4</sub>L7**. The dark-red needle-like crystals were analysed by X-ray diffraction.

**[Fe<sub>2</sub>(L1)<sub>3</sub>] (H2):**

[Fe<sub>2</sub>(L1)<sub>3</sub>]·C<sub>2</sub>H<sub>3</sub>N·0.25×C<sub>4</sub>H<sub>8</sub>O; Yield = 62% (104 mg, 0.066 mmol, based on H<sub>2</sub>L1). Elemental analysis calculated for C<sub>99</sub>H<sub>65</sub>Fe<sub>2</sub>NO<sub>12.25</sub> (1576.22 g mol<sup>-1</sup>) C 75.44, H 4.16, N 0.89; found: C 67.94, H 7.47, N 3.12.

**[Fe<sub>2</sub>(H<sub>2</sub>L7)<sub>3</sub>] (H7):**

[Fe<sub>2</sub>(L7)<sub>3</sub>]·2×C<sub>2</sub>H<sub>3</sub>N·2×H<sub>2</sub>O (**H7**); Yield = 38% (135 mg, 0.094 mmol, based on H<sub>4</sub>L7). Elemental analysis calculated for C<sub>76</sub>H<sub>58</sub>Fe<sub>2</sub>N<sub>2</sub>O<sub>20</sub> (1430.94 g mol<sup>-1</sup>) C 65.37, H 4.42, N 1.96; found: C 68.91, H 6.13, N 1.45.

## DNA-Binding Studies

### UV-Vis Spectroscopy

The spectroscopic data could be fitted to equation (1), allowing to determine the corresponding intrinsic binding constants  $K_b$ .<sup>10,25</sup>

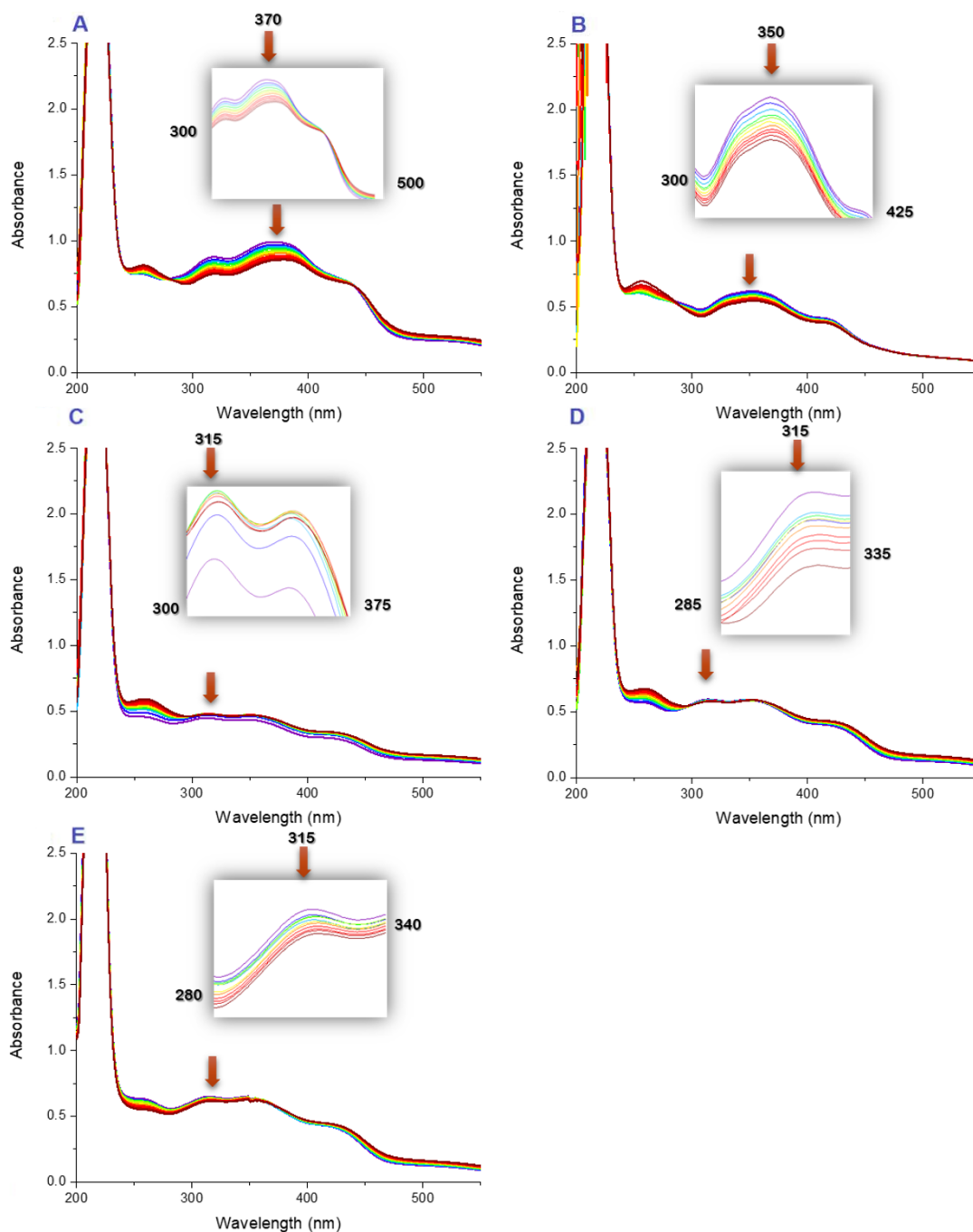
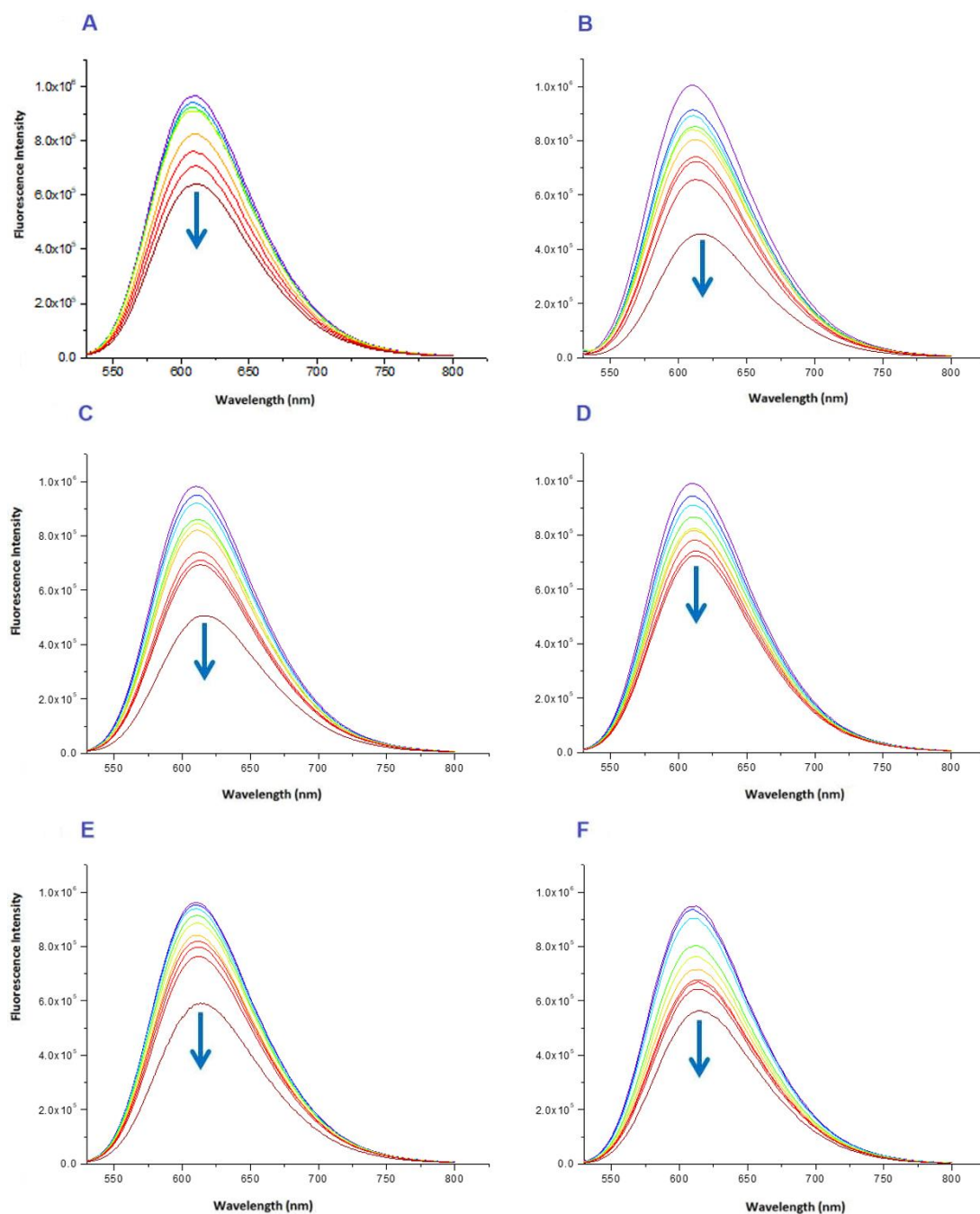


Figure 95: A to E. Absorption spectra of complexes H1, H2, H3, H6 and H8 in 10 mM sodium cacodylate, 20 mM NaCl buffer (pH = 7.2) upon addition of ct-DNA (0–22.5  $\mu$ M) at a constant concentration of complex (10  $\mu$ M).

### Fluorescence dye displacement

#### Ethidium Bromide Displacement Assay



**Figure 96: A to E.** Emission spectra of the DNA-EB complex (2.5 and 12.5  $\mu\text{M}$ ),  $\lambda_{\text{exc}} = 514 \text{ nm}$ ,  $\lambda_{\text{em}} = 610 \text{ nm}$ , upon addition of increasing amounts of complexes H1 to H6 (2–150  $\mu\text{M}$ ). The arrows show the diminution of the emission intensity with the increase of the complex concentration. Concentrations of complex: 2 to 150  $\mu\text{M}$ ; [DNA]: 2.5  $\mu\text{M}$ ; [EB]: 12.5  $\mu\text{M}$ .

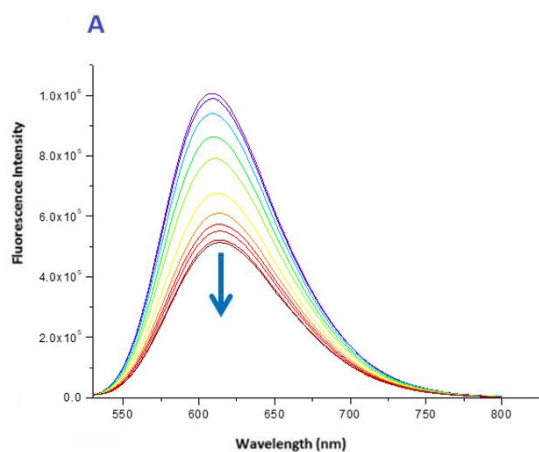


**Figure 97: A. Emission spectra of the DNA-EB complex (2.5 and 12.5  $\mu\text{M}$ ),  $\lambda_{\text{exc}} = 514 \text{ nm}$ ,  $\lambda_{\text{em}} = 610 \text{ nm}$ , upon addition of increasing amounts of complexes H8. The arrows show the diminution of the emission intensity with the increase of the increase of the complex concentration. Concentrations of complex: 2 to 150  $\mu\text{M}$ ; [DNA]: 2.5  $\mu\text{M}$ ; [EB]: 12.5  $\mu\text{M}$ .**





## Hoechst Displacement Assay Procedure

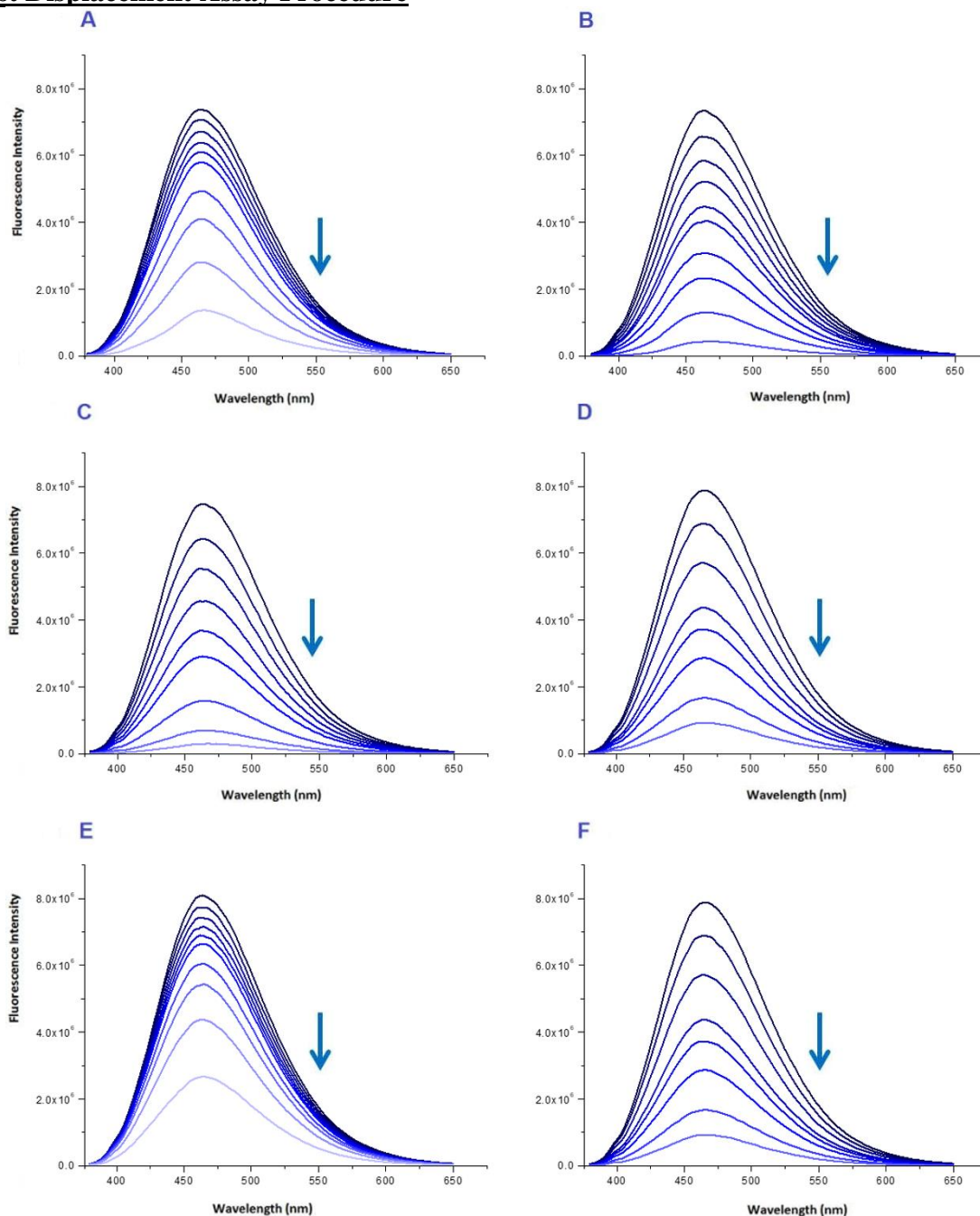


Figure 98: A to F. Emission spectra of the DNA-Hoechst complex (0.19 and 15  $\mu\text{M}$ ),  $\lambda_{\text{exc}} = 350 \text{ nm}$ ,  $\lambda_{\text{em}} = 450 \text{ nm}$ , upon addition of increasing amounts of complexes H1 to H6 (12.5  $\mu\text{M}$ . 2–150  $\mu\text{M}$ ). The arrows show the diminution of the emission intensity with the increase of the complex concentration.

## Circular Dichroism

Stock solutions of the iron(III) metallo-helicates were prepared in 40 mM HEPES/10 mM  $\text{MgCl}_2$  buffer (pH = 7.2) containing 2% DMSO.

## **Gel electrophoresis**

### **Agarose Gel electrophoresis**

Gel electrophoresis experiments: Stock solutions of the iron(III) metallo-helicates were prepared in 40 mM HEPES/10 mM MgCl<sub>2</sub> buffer (pH = 7.2) containing 2% DMSO. pBR322 plasmid DNA aliquots (0.2 µg mL<sup>-1</sup>) in 40 mM HEPES/10 mM MgCl<sub>2</sub> buffer were incubated with the complexes for 24 h at 37 °C. Next, the reaction samples (containing 200 ng of DNA in a 100 µM solution of complex) were quenched with 4 µL of xylene cyanol and subsequently electrophoretized on agarose gel (1% in TAE buffer, tris-acetate-EDTA) for 2 h at 1.5 V cm<sup>-1</sup>, using a BIORAD horizontal tank connected to a PHARMACIA GPS 200/400 variable potential power supply. Samples of free DNA were used as controls. Afterwards, the DNA was stained with SYBR<sup>®</sup> safe and the gel was photographed with a BIORAD Gel Doc<sup>TM</sup> EZ Imager.



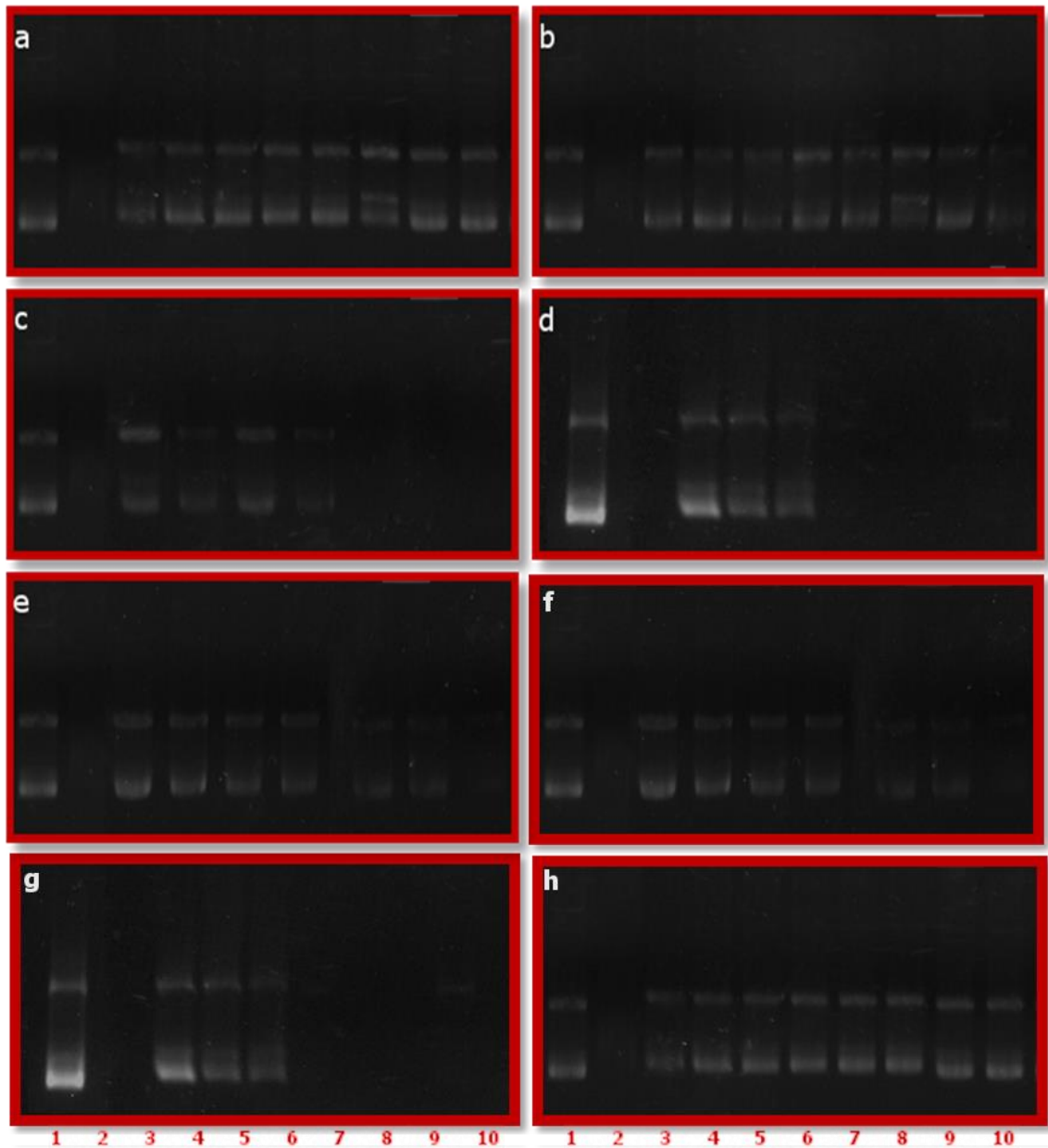


**Figure 99:** Agarose-gel electrophoresis images of pBR322 plasmid DNA incubated for 24 h at 37 °C with increasing concentrations of complexes H1–H6 and H8 (a to h, respectively). Lane 1: pure plasmid DNA; lane 2: [Hoechst] = 100  $\mu$ M; lane 3: [Methyl Green] = 100  $\mu$ M; lane 4: [complex] = 5  $\mu$ M; lane 5: [complex] = 10  $\mu$ M; lane 6: [complex] = 20  $\mu$ M; lane 7: [complex] = 40  $\mu$ M; lane 8: [complex] = 60  $\mu$ M; lane 9: [complex] = 80  $\mu$ M; lane 10: [complex] = 100  $\mu$ M. Each sample contains 200 ng of plasmid DNA.

## Cell Studies

### Single point

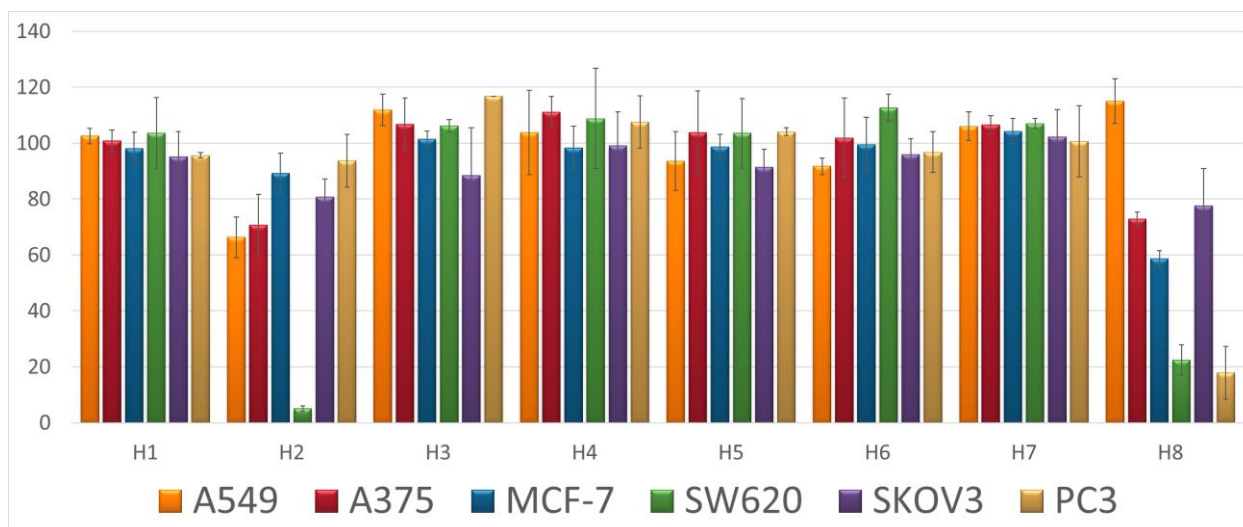


**Figure 100:** Cell-viability results for H1-H8 with different cancer cell lines, namely A549 (lung adenocarcinoma), A375 (melanoma), MCF-7 (breast adenocarcinoma), PC3 (prostate adenocarcinoma), SKOV3 (ovary adenocarcinoma) and SW620 (colorectal adenocarcinoma). [Compound] = 10 µM; incubation time = 24 h. The results are means  $\pm$  SD of three independent experiments.

**Table 34:** Cell-viability assays (single-point screening, % cell viability) for H1–H8 with different cancer-cell lines, namely A549 (lung adenocarcinoma), A375 (melanoma), MCF-7 (breast adenocarcinoma), SKOV3 (ovary adenocarcinoma), SW620 (colorectal adenocarcinoma) and PC3 (prostate adenocarcinoma). [Complex] = 10 µM (single-point assay); incubation time = 24 h. The data shown are means  $\pm$  SD of three independent experiments.

Cell-lines	Metallo-Helicate							
	H1	H2	H3	H4	H5	H6	H7	H8
A549	103 $\pm$ 2.76	66.3 $\pm$ 7.30	112 $\pm$ 5.66	104 $\pm$ 15	93.6 $\pm$ 11	91.7 $\pm$ 2.98	106 $\pm$ 5.15	115 $\pm$ 7.92
A375	101 $\pm$ 3.96	70.7 $\pm$ 11.0	107 $\pm$ 9.26	111 $\pm$ 5.5	104 $\pm$ 15	102 $\pm$ 14.2	107 $\pm$ 3.18	72.9 $\pm$ 2.46
MCF-7	98.1 $\pm$ 5.91	89.2 $\pm$ 7.19	101 $\pm$ 2.87	98.3 $\pm$ 7.8	98.6 $\pm$ 4.6	99.5 $\pm$ 9.76	104 $\pm$ 4.57	58.8 $\pm$ 2.86
SW620	104 $\pm$ 12.7	5.07 $\pm$ 0.97	106 $\pm$ 2.27	109 $\pm$ 18	104 $\pm$ 12	113 $\pm$ 4.83	107 $\pm$ 1.76	22.5 $\pm$ 5.34
SKOV3	95.1 $\pm$ 9.00	80.7 $\pm$ 6.53	88.4 $\pm$ 17.0	99.1 $\pm$ 12	91.4 $\pm$ 6.4	95.9 $\pm$ 5.53	102 $\pm$ 9.81	77.6 $\pm$ 13.3
PC3	95.6 $\pm$ 0.99	93.7 $\pm$ 9.45	117 $\pm$ 0.04	108 $\pm$ 9.4	104 $\pm$ 1.3	96.8 $\pm$ 7.31	101 $\pm$ 12.7	17.8 $\pm$ 9.45

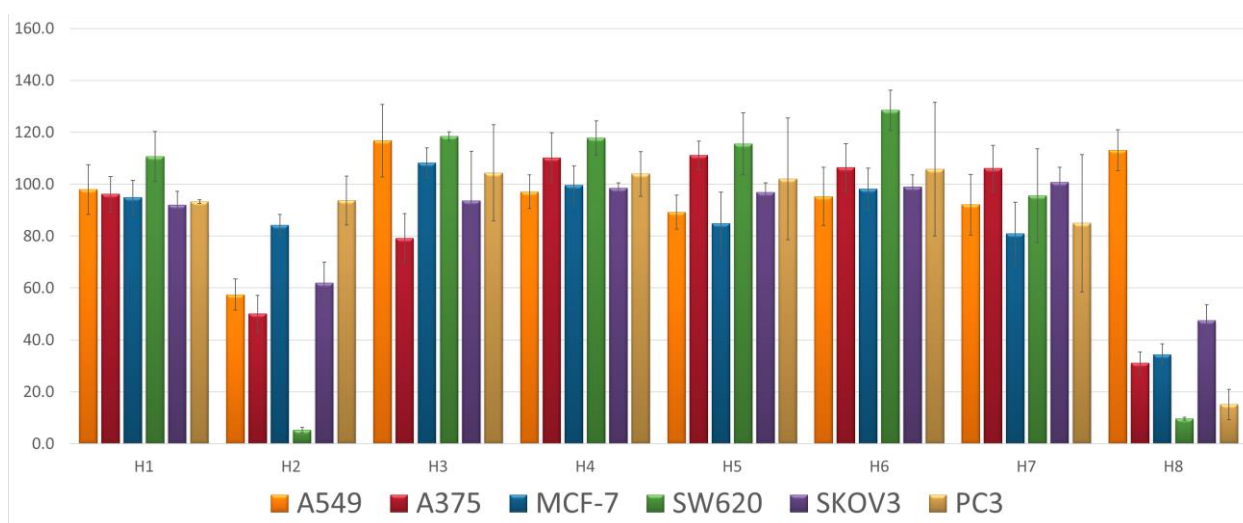


**Figure 101:** Cell-viability results for H1-H8 with different cancer cell lines, namely A549 (lung adenocarcinoma), A375 (melanoma), MCF-7 (breast adenocarcinoma), PC3 (prostate adenocarcinoma), SKOV3 (ovary adenocarcinoma) and SW620 (colorectal adenocarcinoma). [Compound] = 50 µM; incubation time = 24 h. The results are means  $\pm$  SD of three independent experiments.





**Table 35: Cell-viability assays (single-point screening, % cell viability) for H1–H8 with different cancer-cell lines, namely A549 (lung adenocarcinoma), A375 (melanoma), MCF-7 (breast adenocarcinoma), SKOV3 (ovary adenocarcinoma), SW620 (colorectal adenocarcinoma) and PC3 (prostate adenocarcinoma). [Complex] = 50  $\mu$ M (single-point assay); incubation time = 24 h.**

Cell-lines	Metallo-Helicate							
	H1	H2	H3	H4	H5	H6	H7	H8
A549	97.9 $\pm$ 9.60	57.5 $\pm$ 5.96	117 $\pm$ 14.0	97.1 $\pm$ 6.48	89.2 $\pm$ 6.6	95.2 $\pm$ 11.18	92.1 $\pm$ 11.7	113 $\pm$ 7.92
A375	96.2 $\pm$ 6.82	50.1 $\pm$ 7.15	79.2 $\pm$ 9.38	110 $\pm$ 9.62	111 $\pm$ 5.5	106 $\pm$ 9.12	106 $\pm$ 8.88	31.1 $\pm$ 4.31
MCF-7	94.9 $\pm$ 6.61	84.2 $\pm$ 4.14	108 $\pm$ 5.76	100 $\pm$ 7.35	84.9 $\pm$ 12.0	98.2 $\pm$ 8.02	80.9 $\pm$ 12.2	34.3 $\pm$ 4.06
SW620	111 $\pm$ 9.70	5.28 $\pm$ 1.05	118 $\pm$ 1.65	118 $\pm$ 6.54	116 $\pm$ 12.0	128 $\pm$ 7.82	95.6 $\pm$ 18.0	9.6 $\pm$ 0.57
SKOV3	92.0 $\pm$ 5.20	61.9 $\pm$ 7.99	93.6 $\pm$ 19.0	98.5 $\pm$ 1.99	96.9 $\pm$ 3.62	99.0 $\pm$ 4.52	101 $\pm$ 5.77	47.4 $\pm$ 6.19
PC3	93.3 $\pm$ 0.78	93.7 $\pm$ 9.45	104 $\pm$ 18.5	104 $\pm$ 8.57	102 $\pm$ 23.5	106 $\pm$ 25.7	84.9 $\pm$ 26.5	15.1 $\pm$ 5.86

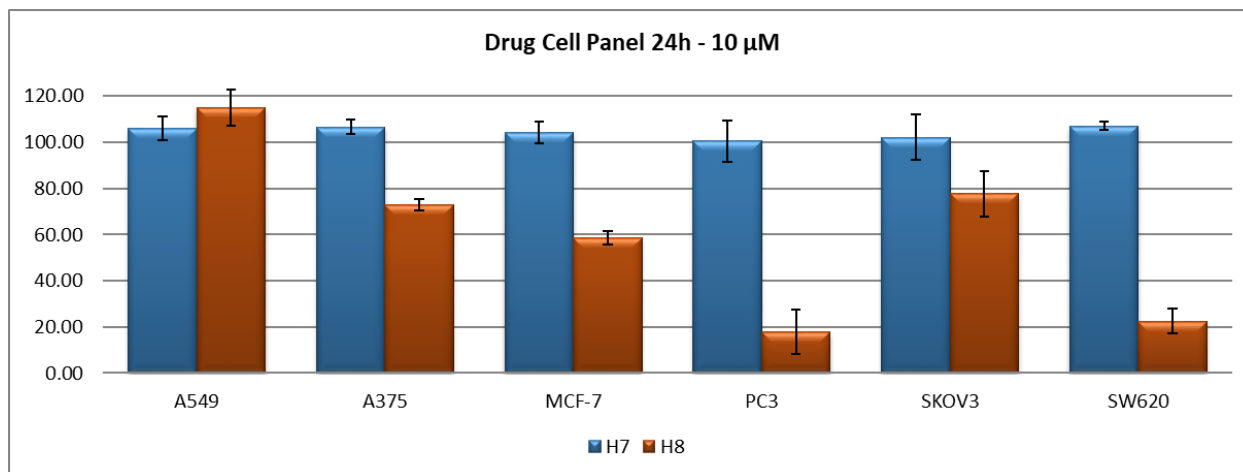


**Figure 102: Cell-viability results for H7 and H8 with different cancer cell lines, namely A549 (lung adenocarcinoma), A375 (melanoma), MCF-7 (breast adenocarcinoma), PC3 (prostate adenocarcinoma), SKOV3 (ovary adenocarcinoma) and SW620 (colorectal adenocarcinoma). [Compound] = 10  $\mu$ M; incubation time = 24 h. The results are means  $\pm$  SD of three independent experiments.**

**Table 36: Cell-viability assays (single-point screening, % cell viability) for H7 and H8 with different cancer-cell lines, namely A549 (lung adenocarcinoma), A375 (melanoma), MCF-7 (breast adenocarcinoma), SKOV3 (ovary adenocarcinoma), SW620 (colorectal adenocarcinoma) and PC3 (prostate adenocarcinoma). [Complex] = 10  $\mu$ M (single-point assay)**

	H7	H8
	% cell viability	% cell viability
A549	106.06 $\pm$ 5.15	115.05 $\pm$ 7.92
A375	106.55 $\pm$ 3.18	72.87 $\pm$ 2.46
MCF-7	104.25 $\pm$ 4.57	58.75 $\pm$ 2.86
PC3	100.61 $\pm$ 8.93	17.85 $\pm$ 9.45
SKOV3	102.14 $\pm$ 9.81	77.63 $\pm$ 9.80
SW620	106.99 $\pm$ 1.76	22.48 $\pm$ 5.34

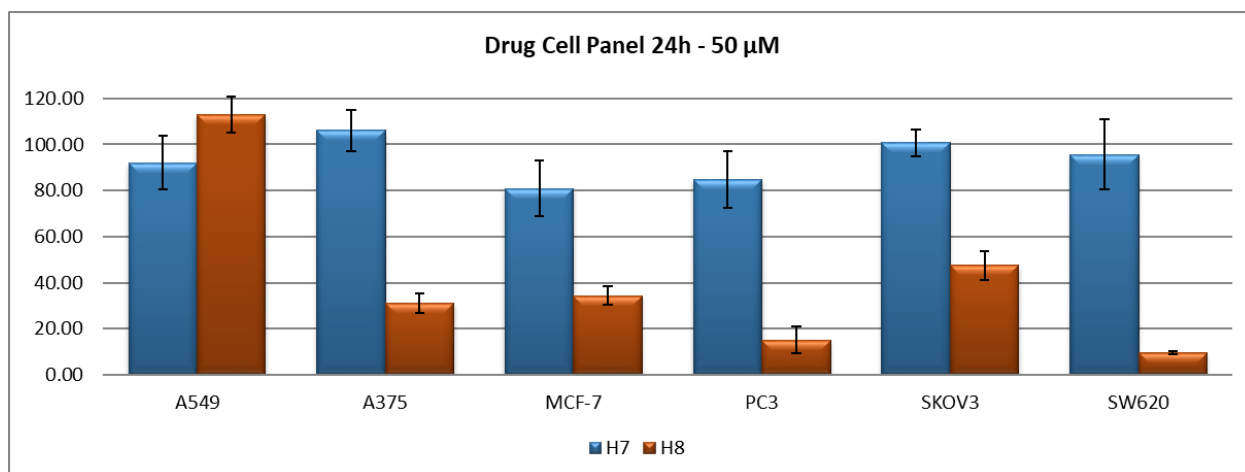


**Figure 103:** Cell-viability results for H7 and H8 with different cancer cell lines, namely A549 (lung adenocarcinoma), A375 (melanoma), MCF-7 (breast adenocarcinoma), PC3 (prostate adenocarcinoma), SKOV3 (ovary adenocarcinoma) and SW620 (colorectal adenocarcinoma). [Compound] = 50  $\mu$ M; incubation time = 24 h. The results are means  $\pm$  SD of three independent experiments.

**Table 37:** Cell-viability assays (single-point screening, % cell viability) for H7 and H8 with different cancer-cell lines, namely A549 (lung adenocarcinoma), A375 (melanoma), MCF-7 (breast adenocarcinoma), SKOV3 (ovary adenocarcinoma), SW620 (colorectal adenocarcinoma) and PC3 (prostate adenocarcinoma). [Complex] = 50  $\mu$ M (single-point assay).

	H7	H8
	% cell viability	% cell viability
A549	92.07 $\pm$ 11.72	113.04 $\pm$ 7.92
A375	106.09 $\pm$ 8.88	31.12 $\pm$ 4.31
MCF-7	80.88 $\pm$ 12.21	34.33 $\pm$ 4.06
PC3	84.93 $\pm$ 12.30	15.12 $\pm$ 5.86
SKOV3	100.81 $\pm$ 5.77	47.45 $\pm$ 6.19
SW620	95.61 $\pm$ 15.17	9.64 $\pm$ 0.57

### IC<sub>50</sub> Determination

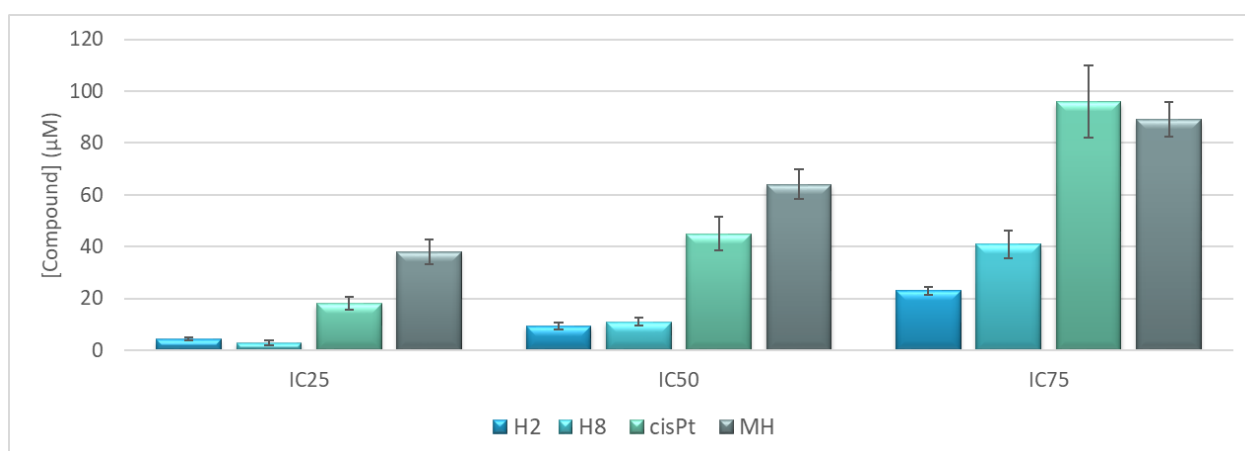


**Figure 104:** IC<sub>25-75</sub> values ( $\mu$ M) for H7, H8, cisPt and MH with SW620 cells. [Compound] = 10  $\mu$ M; incubation time = 24 h. The results are means  $\pm$  SD of three separate experiments.





**Table 38: IC<sub>25-75</sub> values (μM) for H7, H8, cisPt and MH after 24 h of incubation with SW620 (colorectal adenocarcinoma). The data shown are means ± SD of three independent experiments.**

	SW620											
	H2 (μM)			H8 (μM)			cisPt (μM)			MH (μM)		
IC <sub>25</sub>	4.4	±	0.7	2.9	±	0.8	18.0	±	2.5	38.0	±	4.6
IC <sub>50</sub>	9.4	±	1.4	11.0	±	1.5	45.0	±	6.4	64.0	±	5.7
IC <sub>75</sub>	23.0	±	1.6	41.0	±	5.3	96	±	14	89.0	±	6.7

## Immunofluorescence microscopy

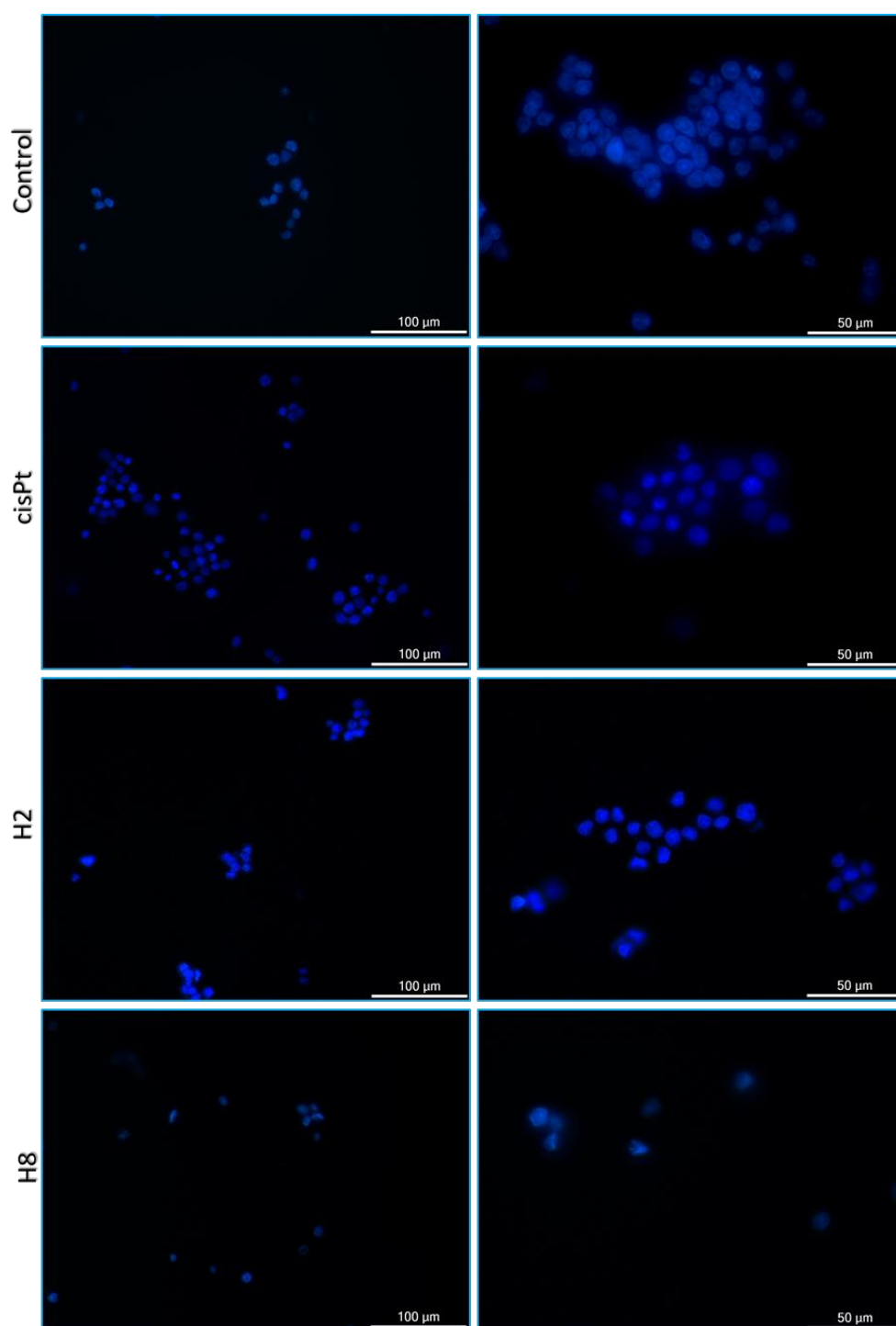


**Figure 105:** Fluorescence microscopy images showing SW620 cells and SW620 cells incubated with CisPt, H2 and H8. [Compound] =  $IC_{50}$  (see Table 38 above); incubation time = 24 h. The nucleus was stained with TO-PRO™-3 (blue). Scale bar = 50  $\mu m$ . The images are representative of at least three independent experiments.

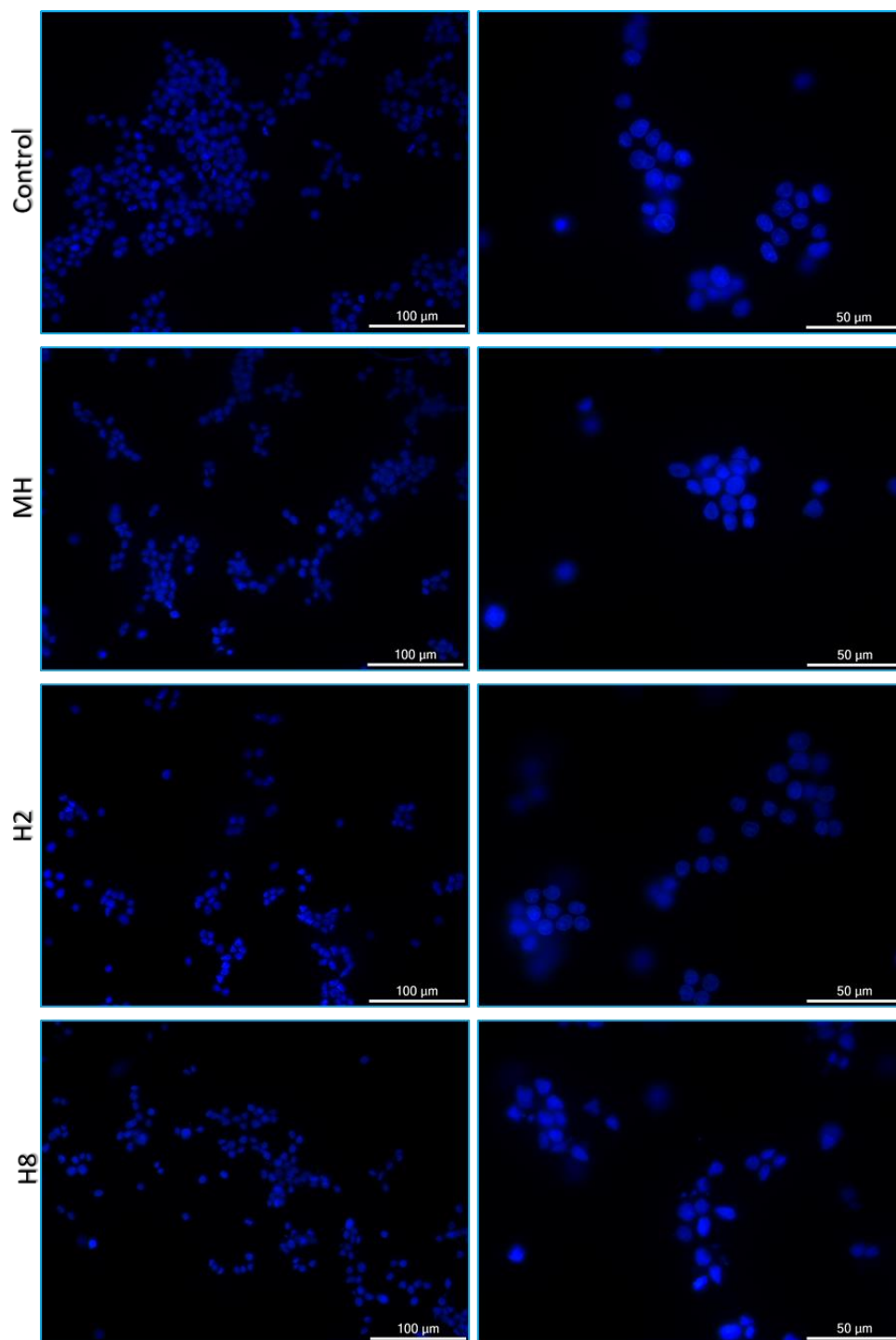


Figure 106: Fluorescence microscopy images showing SW620 cells and SW620 cells incubated with MH, H2 and H8. [Compound] =  $IC_{50}$  (see Table 38 above); incubation time = 48 h. The nucleus was stained with TO-PRO™-3 (blue). Scale bar = 50  $\mu m$ . The images are representative of at least three independent experiments.

## Cell cycle

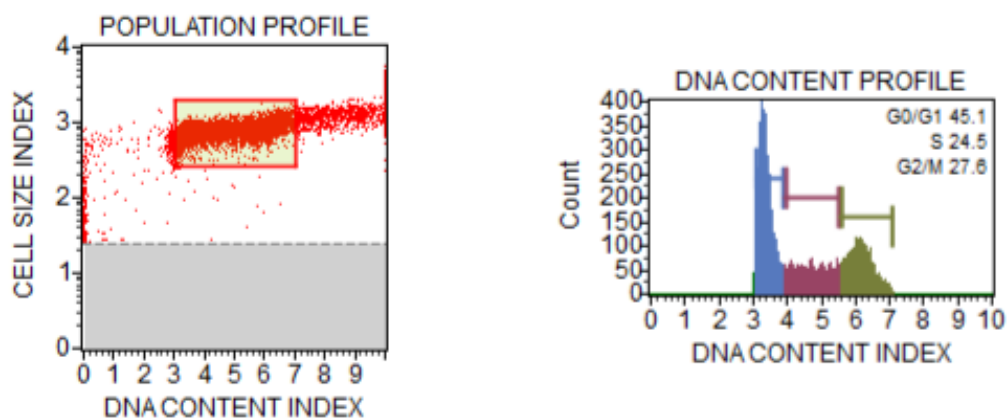


Figure 107: Control (DMSO) Cell-cycle experiments performed with the Muse™ Cell Cycle software for SW620 cells with DMSO.  $2 \times 10^5$  cells  $\text{mL}^{-1}$ ; incubation time = 24 h.

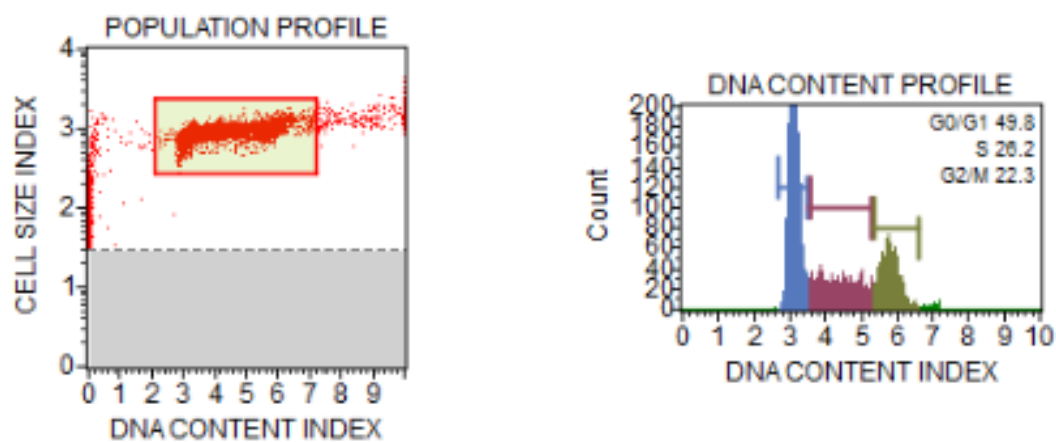


Figure 108: Cell-cycle experiments performed with the Muse™ Cell Cycle software for SW620 cells incubated with H2.  $2 \times 10^5$  cells  $\text{mL}^{-1}$ ; [compound] = 2  $\mu\text{M}$ ; incubation time = 24 h.

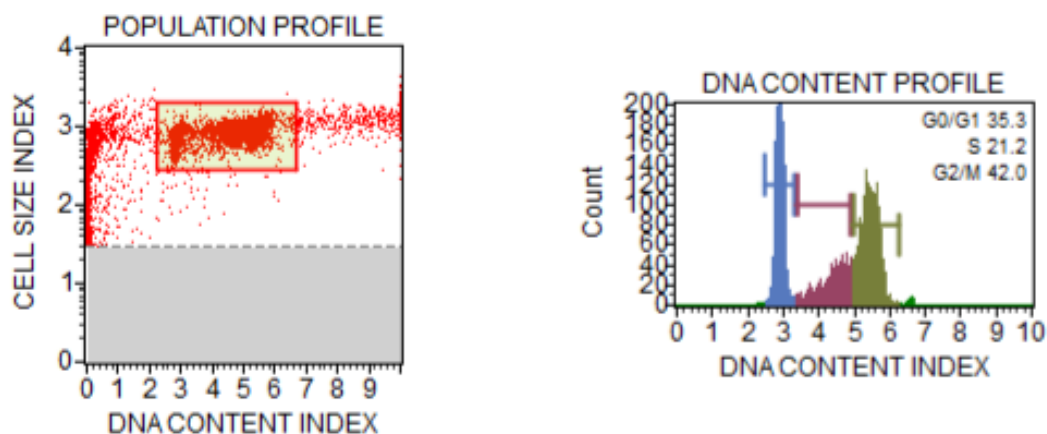
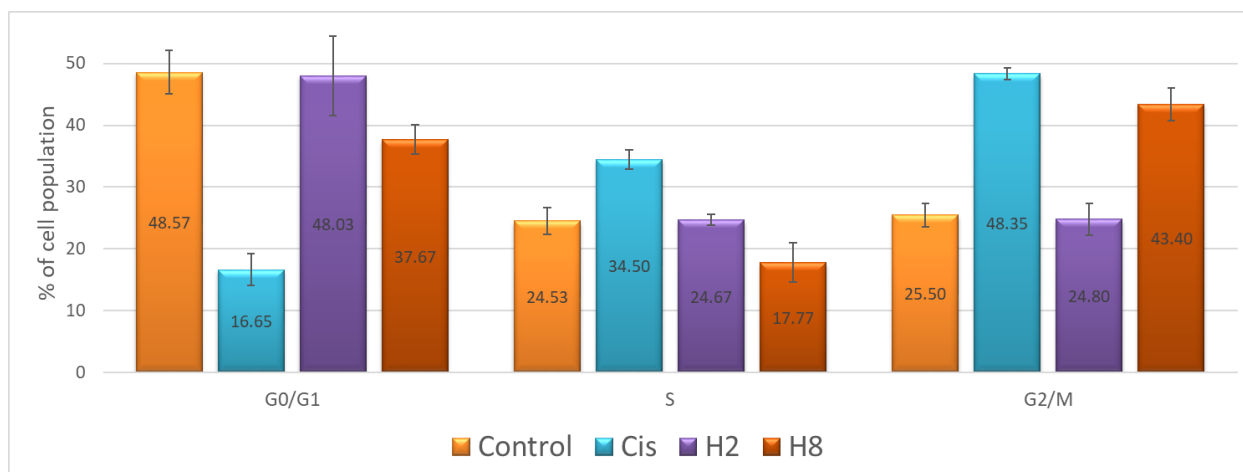


Figure 109: Cell-cycle experiments performed with the Muse™ Cell Cycle software for SW620 cells incubated with H2.  $2 \times 10^5$  cells  $\text{mL}^{-1}$ ; [compound] = 2  $\mu\text{M}$ ; incubation time = 24 h.



**Figure 110:** Cell-cycle experiments performed with the Muse™ Cell Cycle software for H2 and H8 with SW620 cells.  $2 \times 10^5$  cells  $\text{mL}^{-1}$ ; [compound] = 2  $\mu\text{M}$ ; incubation time = 24 h. The results are representative of at least three independent experiments.

## References

- (1) Fischer, B. E.; Haring, U. K.; Tribolet, R.; Sigel, H. *Eur J Biochem* **1979**, *94*, 523.
- (2) McPhail, D. B.; Goodman, B. A. *Biochem J* **1984**, *221*, 559.
- (3) Azab, H. A.; Orabi, A. S.; El-Salam, E. T. A. *J. Chem. Eng. Data* **2001**, *46*, 346.
- (4) Magyar, J. S.; Godwin, H. A. *Anal Biochem* **2003**, *320*, 39.
- (5) Yu, Q.; Kandegedara, A.; Xu, Y.; Rorabacher, D. B. *Anal. Biochem.* **1997**, *253*, 50.
- (6) Marmur, J. *J. Mol. Biol.* **1961**, *3*, 208.
- (7) Wang, H.; Shen, R.; Wu, J.; Tang, N. *Chem. Pharm. Bull. (Tokyo)* **2009**, *57*, 814.
- (8) Kelly, J. M.; Murphy, M. J.; McConnell, D. J.; OhUigin, C. *Nucleic Acids Res.* **1985**, *13*, 167.
- (9) Shahabadi, N.; Fatahi, P. *DNA Cell Biol.* **2012**, *31*, 1328.
- (10) Pyle, A. M.; Rehmann, J. P.; Meshoyrer, R.; Kumar, C. V.; Turro, N. J.; Barton, J. K. *J. Am. Chem. Soc.* **1989**, *111*, 3051.
- (11) Javed, F.; Altaf, A. A.; Badshah, A.; Tahir, M. N.; Siddiq, M.; Shah, A.; Ullah, S.; Lal, B. *J. Coord. Chem.* **2012**, *65*, 969.
- (12) Graves, D. E. 2000; Vol. 95, p 161.
- (13) Neidle, S. *Nucleic acid structure and recognition*; Oxford University Press: Oxford ; New York, 2002.
- (14) Long, E. C.; Barton, J. K. *Acc. Chem. Res.* **1990**, *23*, 271.
- (15) Ghosh, A.; Das, P.; Gill, M. R.; Kar, P.; Walker, M. G.; Thomas, J. A.; Das, A. *Chem. Eur. J.* **2011**, *17*, 2089.
- (16) Brissos, R. F.; Torrents, E.; dos Santos Mello, F. M.; Carvalho Pires, W.; Silveira-Lacerda Ede, P.; Caballero, A. B.; Caubet, A.; Massera, C.; Roubeau, O.; Teat, S. J.; Gamez, P. *Metallomics* **2014**, *6*, 1853.
- (17) Kashanian, S.; Javanmardi, S.; Chitsazan, A.; Omidfar, K.; Paknejad, M. *DNA Cell Biol.* **2012**, *31*, 1349.
- (18) Hammes, G. G. *Spectroscopy for the biological sciences*; Wiley-Interscience: Hoboken, N.J., 2005.
- (19) Pratviel, G.; Bernadou, J.; Meunier, B. In *Adv. Inorg. Chem.*; Sykes, A. G., Ed.; Academic Press: 1998; Vol. 45, p 251.
- (20) Shahabadi, N.; Shiri, F. *Nucleosides Nucleotides Nucleic Acids* **2017**, *36*, 83.
- (21) Sirajuddin, M.; Ali, S.; Badshah, A. *J. Photochem. Photobiol. B* **2013**, *124*, 1.
- (22) Rehman, S. U.; Sarwar, T.; Husain, M. A.; Ishqi, H. M.; Tabish, M. *Arch. Biochem. Biophys.* **2015**, *576*, 49.
- (23) Ghosh, S.; Salsbury, F. R., Jr.; Horita, D. A.; Gmeiner, W. H. *Nucleic Acids Res.* **2011**, *39*, 4490.
- (24) Benesi, H. A.; Hildebrand, J. H. *J. Am. Chem. Soc.* **1949**, *71*, 2703.
- (25) Krishnamoorthy, P.; Sathyadevi, P.; Cowley, A. H.; Butorac, R. R.; Dharmaraj, N. *Eur. J. Med. Chem.* **2011**, *46*, 3376.
- (26) Mishra, R. K.; Upadhyay, K. K.; Shukla, S.; Mishra, R. *Chem. Commun. (Camb)* **2012**, *48*, 4238.
- (27) Shen, R.; Wang, P.; Tang, N. *J. Fluoresc.* **2009**, *19*, 1073.
- (28) Wang, Y.; Lin, G.-W.; Hong, J.; Li, L.; Yang, Y.-M.; Lu, T. *J. Coord. Chem.* **2010**, *63*, 3662





- (29) Li, D. D.; Tian, J. L.; Gu, W.; Liu, X.; Zeng, H. H.; Yan, S. P. *J. Inorg. Biochem.* **2011**, *105*, 894.
- (30) Tuite, E.; Sehlstedt, U.; Hagmar, P.; Norden, B.; Takahashi, M. *Eur. J. Biochem.* **1997**, *243*, 482.
- (31) Nordén, B.; Tjerneld, F.; Palm, E. *Biophys. Chem.* **1978**, *8*, 1.
- (32) Kubista, M.; Akerman, B.; Norden, B. *Biochemistry* **1987**, *26*, 4545.
- (33) Jeppesen, C.; Nielsen, P. E. *Eur J Biochem* **1989**, *182*, 437.
- (34) Wilson, W. D.; Tanious, F. A.; Barton, H. J.; Jones, R. L.; Fox, K.; Wydra, R. L.; Strekowski, L. *Biochemistry* **1990**, *29*, 8452.
- (35) Lee, M.; Rhodes, A. L.; Wyatt, M. D.; Forrow, S.; Hartley, J. A. *Biochemistry* **1993**, *32*, 4237.
- (36) Bresloff, J. L.; Crothers, D. M. *Biochemistry* **1981**, *20*, 3547.
- (37) Becker, M. M.; Dervan, P. B. *J. Am. Chem. Soc.* **1979**, *101*, 3664.
- (38) Tuite, E.; Kelly, J. M. *Biopolymers* **1995**, *35*, 419.
- (39) Tuite, E.; Norden, B. *J. Am. Chem. Soc.* **1994**, *116*, 7548.
- (40) Albani, J. R. *Principles and applications of fluorescence spectroscopy*; Blackwell Science: Oxford ; Ames, Iowa, 2007.
- (41) Lakowicz, J. R. *Principles of fluorescence spectroscopy*; 3rd ed.; Springer: New York, 2006.
- (42) Sauer, M.; Hofkens, J.; Enderlein, J. *Handbook of fluorescence spectroscopy and imaging : from single molecules to ensembles*; Wiley-VCH: Weinheim, 2011.
- (43) González-Ruiz, V.; Olives, A.; Martin, M. A.; Ribelles, P.; Ramos, M.; Menendez, J. C. *An Overview of Analytical Techniques Employed to Evidence Drug-DNA Interactions. Applications to the Design of Genosensors*, 2011.
- (44) Suh, D.; Chaires, J. B. *Bioorg. Med. Chem.* **1995**, *3*, 723.
- (45) Olmsted, J., 3rd; Kearns, D. R. *Biochemistry* **1977**, *16*, 3647.
- (46) Li, W.-Y.; Xu, J.-G.; Guo, X.-Q.; Zhu, Q.-Z.; Zhao, Y.-B. *Spectrochimica Acta Part A: Molecular and Biomolecular Spectroscopy* **1997**, *53*, 781.
- (47) Pace, T. C. S.; Bohne, C. In *Adv. Phys. Org. Chem.*; Richard, J. P., Ed.; Academic Press: 2007; Vol. 42, p 167.
- (48) Larijani, B.; Rosser, C. A.; Woscholski, R. *Chemical biology : applications and techniques*; John Wiley & Sons: Chichester, 2006.
- (49) Hadjiliadis, N. D.; Sletten, E. *Metal complex - DNA interactions*; 1st ed.; Wiley: Chichester, West Sussex, U.K., 2009.
- (50) Baguley, B. C.; Le Bret, M. *Biochemistry* **1984**, *23*, 937.
- (51) Zhao, Y.; Zhu, J.; He, W.; Yang, Z.; Zhu, Y.; Li, Y.; Zhang, J.; Guo, Z. *Chem. Eur. J.* **2006**, *12*, 6621.
- (52) Lakowicz, J. R.; Weber, G. *Biochemistry* **1973**, *12*, 4161.
- (53) Waring, M. J. *J. Mol. Biol.* **1965**, *13*, 269.
- (54) Jain, S. C.; Sobell, H. M. *J. Biomol. Struct. Dyn.* **1984**, *1*, 1179.
- (55) Kubař, T.; Hanus, M.; Ryjáček, F.; Hobza, P. *Chem. Eur. J.* **2006**, *12*, 280.
- (56) Meyer-Almes, F. J.; Porschke, D. *Biochemistry* **1993**, *32*, 4246.
- (57) Nejat Dehkordi, M.; Lincoln, P. *J. Fluoresc.* **2013**, *23*, 813.
- (58) Novakova, O.; Chen, H.; Vrana, O.; Rodger, A.; Sadler, P. J.; Brabec, V. *Biochemistry* **2003**, *42*, 11544.
- (59) Butour, J. L.; Macquet, J. P. *Eur. J. Biochem.* **1977**, *78*, 455.
- (60) Butour, J. L.; Alvinerie, P.; Souchard, J. P.; Colson, P.; Houssier, C.; Johnson, N. P. *Eur. J. Biochem.* **1991**, *202*, 975.
- (61) Kakkar, R.; Garg, R.; Suruchi *Theochem* **2002**, *584*, 37.

- (62) Vega, M. C.; Garcia Saez, I.; Aymami, J.; Eritja, R.; Van der Marel, G. A.; Van Boom, J. H.; Rich, A.; Coll, M. *Eur. J. Biochem.* **1994**, 222, 721.
- (63) Wang, H.; Laughton, C. A. *Phys. Chem. Chem. Phys.* **2009**, 11, 10722.
- (64) Matsuba, Y.; Edatsugi, H.; Mita, I.; Matsunaga, A.; Nakanishi, O. *Cancer Chemother. Pharmacol.* **2000**, 46, 1.
- (65) Shahabadi, N.; Hadidi, S. *Spectrochim. Acta. A Mol. Biomol. Spectrosc.* **2012**, 96, 278.
- (66) Shahabadi, N.; Heidari, L. *Spectrochim. Acta. A Mol. Biomol. Spectrosc.* **2012**, 97, 406.
- (67) Martin, S. R.; Schilstra, M. J. In *Methods Cell Biol.*; Dr. John, J. C., Dr. H. William Detrich, III, Eds.; Academic Press: 2008; Vol. Volume 84, p 263.
- (68) Norden, B.; Kurucsev, T. *J. Mol. Recognit.* **1994**, 7, 141.
- (69) Wilson, K.; Walker, J. *Principles and techniques of biochemistry and molecular biology*; 7th ed.; Cambridge University Press: Cambridge, 2010.
- (70) Ranjbar, B.; Gill, P. *Chem. Biol. Drug Des.* **2009**, 74, 101.
- (71) Ghosh, A.; Bansal, M. *Acta Crystallogr. D. Biol. Crystallogr.* **2003**, 59, 620.
- (72) Bishop, G. R.; Chaires, J. B. In *Curr. Protoc. Nucleic Acid Chem.*; John Wiley & Sons, Inc.: 2001.
- (73) Doderio, V. I.; Quirolo, Z. B.; Sequeira, M. A. *Front. Biosci. (Landmark Ed)* **2011**, 16, 61.
- (74) Eriksson, M.; Norden, B. *Methods Enzymol.* **2001**, 340, 68.
- (75) Chang, Y. M.; Chen, C. K.; Hou, M. H. *Int. J. Mol. Sci.* **2012**, 13, 3394.
- (76) Vorlickova, M.; Kejnovska, I.; Bednarova, K.; Renciuik, D.; Kypr, J. *Chirality* **2012**, 24, 691.
- (77) Kypr, J.; Kejnovska, I.; Renciuik, D.; Vorlickova, M. *Nucleic Acids Res.* **2009**, 37, 1713.
- (78) Karidi, K.; Garoufis, A.; Hadjiliadis, N.; Reedijk, J. *Dalton Trans.* **2005**, 728.
- (79) Arbuse, A.; Font, M.; Martinez, M. A.; Fontrodona, X.; Prieto, M. J.; Moreno, V.; Sala, X.; Llobet, A. *Inorg. Chem.* **2009**, 48, 11098.
- (80) Maheswari, P. U.; Barends, S.; Ozalp-Yaman, S.; de Hoog, P.; Casellas, H.; Teat, S. J.; Massera, C.; Lutz, M.; Spek, A. L.; van Wezel, G. P.; Gamez, P.; Reedijk, J. *Chem. Eur. J.* **2007**, 13, 5213.
- (81) Tjioe, L.; Meininger, A.; Joshi, T.; Spiccia, L.; Graham, B. *Inorg. Chem.* **2011**, 50, 4327.
- (82) Yakhnin, A. V.; Yakhnin, H.; Babitzke, P. *Methods Mol. Biol.* **2012**, 905, 201.
- (83) Laniel, M. A.; Beliveau, A.; Guerin, S. L. *Methods Mol. Biol.* **2001**, 148, 13.
- (84) Vuong, S.; Stefan, L.; Lejault, P.; Rousselin, Y.; Denat, F.; Monchaud, D. *Biochimie* **2012**, 94, 442.
- (85) Singleton, M. R.; Scaife, S.; Wigley, D. B. *Cell* **2001**, 107, 79.
- (86) Masai, H.; Tanaka, T.; Kohda, D. *Bioessays* **2010**, 32, 687.
- (87) Lilley, D. M. *Q. Rev. Biophys.* **2000**, 33, 109.
- (88) Muhuri, S.; Mimura, K.; Miyoshi, D.; Sugimoto, N. *J. Am. Chem. Soc.* **2009**, 131, 9268.
- (89) Binnig, G.; Quate, C. F.; Gerber, C. *Phys. Rev. Lett.* **1986**, 56, 930.
- (90) Qin, G.-G.; Li, W.-H.; Xu, J.-C.; Kou, X.-L.; Zhao, R.; Luo, F.; Fang, X.-H. *Chinese Journal of Analytical Chemistry* **2017**, 45, 1813.
- (91) Maver, U.; Velnar, T.; Gaberšček, M.; Planinšek, O.; Finšgar, M. *TrAC, Trends Anal. Chem.* **2016**, 80, 96.
- (92) Jandt, K. D. *Surf. Sci.* **2001**, 491, 303.
- (93) Tseng, A. A. *Nano Today* **2011**, 6, 493.





- (94) Pope, L. H.; Davies, M. C.; Laughton, C. A.; Roberts, C. J.; Tendler, S. J.; Williams, P. M. *J. Microsc.* **2000**, *199*, 68.
- (95) Eaton, P.; West, P. *Atomic force microscopy*; Oxford University Press: Oxford, 2010.
- (96) Lyubchenko, Y. L. *Micron.* **2011**, *42*, 196.
- (97) Menezes, C. S.; de Paula Costa, L. C.; de Melo Rodrigues Avila, V.; Ferreira, M. J.; Vieira, C. U.; Pavanin, L. A.; Homsí-Brandeburgo, M. I.; Hamaguchi, A.; de Paula Silveira-Lacerda, E. *Chem. Biol. Interact.* **2007**, *167*, 116.
- (98) Stoddart, M. J. In *Mammalian Cell Viability: Methods and Protocols*; Stoddart, M. J., Ed.; Humana Press: Totowa, NJ, 2011, p 1.
- (99) Mosmann, T. *J. Immunol. Methods* **1983**, *65*, 55.
- (100) Liu, Y.; Peterson, D. A.; Kimura, H.; Schubert, D. *J Neurochem* **1997**, *69*, 581.
- (101) Sebaugh, J. L. *Pharm. Stat.* **2011**, *10*, 128.
- (102) Hawley, T. S.; Hawley, R. G.; SpringerLink (Online service) In *Methods in molecular biology* 263; 2nd ed ed.; Humana Press Inc.: Totowa, NJ, 2004, p p.
- (103) Voet, D.; Voet, J. G. *Biochemistry*; 3rd ed.; J. Wiley & Sons: New York, 2004.
- (104) Hoon, D. S.; Ferris, R.; Tanaka, R.; Chong, K. K.; Alix-Panabieres, C.; Pantel, K. *J. Surg. Oncol.* **2011**, *103*, 508.
- (105) Biname, F.; Pawlak, G.; Roux, P.; Hibner, U. *Mol. Biosyst.* **2010**, *6*, 648.
- (106) Kam, Y.; Guess, C.; Estrada, L.; Weidow, B.; Quaranta, V. *BMC Cancer* **2008**, *8*, 198.
- (107) Hulkower, K. I.; Herber, R. L. *Pharmaceutics* **2011**, *3*, 107.
- (108) Zettler, M. W. In *Encyclopedia of Reagents for Organic Synthesis*; John Wiley & Sons, Ltd: 2001.
- (109) Altomare, A.; Cascarano, G.; Giacovazzo, C.; Guagliardi, A. *J. Appl. Crystallogr.* **1993**, *26*, 343.
- (110) Altomare, A.; Burla, M. C.; Camalli, M.; Cascarano, G. L.; Giacovazzo, C.; Guagliardi, A.; Moliterni, A. G. G.; Polidori, G.; Spagna, R. *J. Appl. Crystallogr.* **1999**, *32*, 115.
- (111) Sheldrick, G. M. In *SHELXTL, Bruker AXS Inc., Madison, Wisconsin, USA*.
- (112) Sheldrick, G. M. *Acta Crystallogr. A* **2008**, *64*, 112.
- (113) van der Sluis, P.; Spek, A. L. *Acta Crystallographica Section A* **1990**, *46*, 194.
- (114) Navarro, M.; Vidal, D.; Clavero, P.; Grabulosa, A.; Muller, G. *Organometallics* **2015**, *34*, 973.
- (115) Clavero, P.; Grabulosa, A.; Rocamora, M.; Muller, G.; Font-Bardia, M. *Dalton Trans.* **2016**, *45*, 8513.
- (116) Aromí, G.; Gamez, P.; Reedijk, J. *Coord. Chem. Rev.* **2008**, *252*, 964.